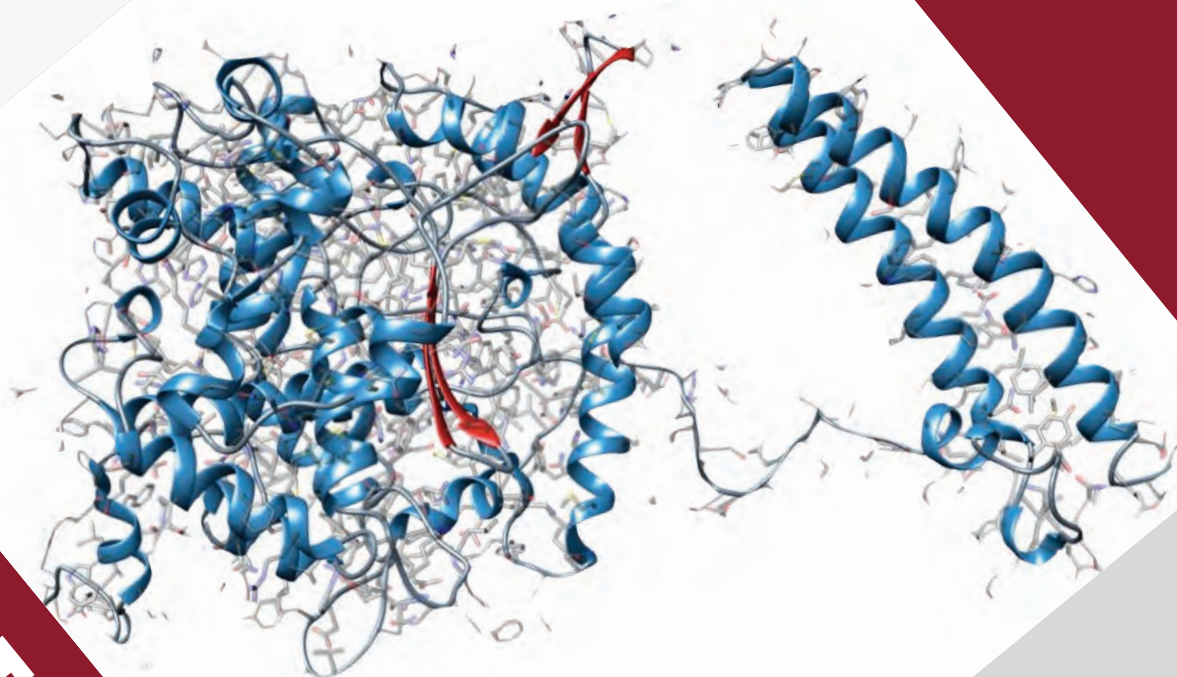




Trento Institute for
Fundamental Physics
and Applications



ACTIVITY REPORT 2020



TIFPA Activity Report 2020

TIFPA
Activity Report 2020



Typeset in the Bitstream Charter typeface using the $\text{\LaTeX} 2_{\epsilon}$ document formatting system and markup language

Editor: Piero Spinnato (TIFPA)

Cover and overall graphics design: Francesca Cuicchio (Ufficio Comunicazione INFN, Rome)

Cover image: Intermediate folding state of the ACE2 protein, the cellular receptor of SARS-COV2, simulated by Sibylla Biotech using computing power provided by INFN (15 million CPU-hours), in the context of a screening research aimed at identifying drugs able to prevent the ACE2 folding. The bonding pockets used in the screening campaign are highlighted in red. See p. 48 for further details. Image courtesy of Sibylla Biotech.

First print, June 2021

Printed and bound at Rotooffset Paganella, Trento

www.rotooffset.it

Contents

Foreword	1	PANDORA_Gr3	41
INFN Experiments	5	Theoretical Physics	43
Particle Physics	7	BELL	45
ATLAS	9	BIOPHYS	47
FASE2_ATLAS	11	FBS	50
Astroparticle Physics	13	FLAG	51
ADHD	15	MANYBODY	53
AMS	17	NEMESYS	55
DarkSide	19	Teongrav	57
FISH	21	Activities starting in 2021	59
HUMOR	23	NUCSYS	59
Limadou	25	Technological Research	61
LISA Pathfinder e LISA	27	3D SIAM	63
Quax	29	ARCADIA	65
Virgo	31	ASAP	67
Activities starting in 2021	33	DRAGoN	69
ET_ITALIA	33	FIRE	71
XRO	33	GLARE-X	72
Nuclear Physics	35	Isolpharm_EIRA	74
AEgIS	37	MADAM	76
FOOT	39	MoVe IT	78
Activities starting in 2021	41	NEPTUNE	80

Simp	82	FOOT-ECC	97
THEEOM-RD	84	GSM²	99
TIMESPOT	86	MoVe IT-TLD	101
Activities starting in 2021	88	GSI-O_DEPL	103
DART WARS	88	SIRMIO	105
MICROBE_IT	88	SPYRO	107
NanoEnHanCeMent	89	SUN_MEYER	109
XpCalib	90	TIFPA Publications	113
BOLAS_NEXT	91	Seminars	141
Proton Beam-based R&D	93		
FBK-SiPM	95		



Foreword

Giuseppe Battistoni

Direttore,
TIFPA

The 2020 Annual Report of the Trento Institute for Fundamental Physics and Applications (TIFPA) has indeed an importance which goes beyond the mere scientific interest. It testifies the capability of our research center to achieve many important goals for all the planned projects, notwithstanding the very difficult situation and the unavoidable limitations caused by the COVID-19 pandemics. Therefore, we are proud to present the summary review of all the scientific and technological activity that has been carried out at TIFPA in the last year.

All the partners of TIFPA, the Italian National Institute for Nuclear Physics (INFN), Trento University (UniTn), Bruno Kessler Foundation (FBK) and the Health-care Agency of Trento (APSS), have contributed to these achievements, together with all our external collaborators and users. As usual, this has been made possible thanks to the efforts of all staff and associates. Beyond the the strong commitment of TIFPA partners, the fundamental support from the government of Trento Province has to be recognized.

This is also my last contribute, since at the end of this year I will complete my mandate and another Director will be appointed for TIFPA. It is therefore an opportunity for me to express my gratitude for the beautiful and significant experience of serving as TIFPA Director. My work was made possible by the strong support of my direct collaborators of the administrative and technical services, to whom I wish to express again my sincere gratitude.

I wish to recognize to Dr. Piero Spinnato the merit for editing this document.

A handwritten signature in blue ink that reads "Giuseppe Battistoni". The signature is written in a cursive style.



Trento Institute for
Fundamental Physics
and Applications

TIFPA is a National Centre of INFN (Istituto Nazionale di Fisica Nucleare), which carries out scientific and technological research in the areas of Particle and Astroparticle Physics, Nuclear Physics, Theoretical Physics, Applications of Particle Physics in Medicine and Biological Sciences, development of sensors and detectors for Particle Physics.

TIFPA was founded in 2013, building on a large variety of scientific activities in Trento:

- the presence at the Department of Physics of the University of Trento of a large community of researchers in Particle Physics-related topics, active at the time within the "Gruppo Collegato" to the INFN section of Padua,
- the consolidated collaboration of INFN with FBK (Fondazione Bruno Kessler) for the development and production of sensors for Particle Physics detectors,
- the realisation in Trento of the APSS (Azienda Provinciale per i Servizi Sanitari) Centre for Protontherapy, with a beamline dedicated to research.

INFN, University of Trento, FBK and APSS formalised an agreement to collaborate within TIFPA for carrying out common research projects. A committee chaired by the TIFPA Director and composed by a delegate for each partner, called CPR (*Comitato Permanente di Raccordo*), has the mandate of coordinating the activities of the TIFPA partners for the fulfilment of the common research goals.

The TIFPA Director is elected by the INFN Board (*Consiglio Direttivo*) and is appointed for four years. Research activities within TIFPA are organised according to the INFN structure, which consists of five research lines, each one supervised by a CSN (*Commissione Scientifica Nazionale*). TIFPA is active in all INFN research lines, as illustrated in the research reports presented in this publication, yet it is officially present with its representatives in CSN2 (Astroparticle Physics), CSN4 (Theoretical Physics), and CSN5 (Applied and Technological Research); for CSN1 (Particle Physics) and CSN3 (Nuclear Physics) FTEs are currently not sufficient, according to INFN rules, for the election of a coordinator to represent the group within the CSN.

In order to pursue specific goals for the transfer of knowledge in particular areas of interest, three Virtual Labs (*Settori Tecnologici*) have been defined, in the topics of Medical Technologies, Sensors and Detectors, and Space Research. Support for research activities is organised in two services, SIGEA (*Servizio Integrato di Gestione ed Amministrazione*), which is in charge of all the administrative tasks of the Centre, and STAR (*Servizio di supporto Tecnico-logistico alle Attività di Ricerca*), which is in charge of all technical support activities.

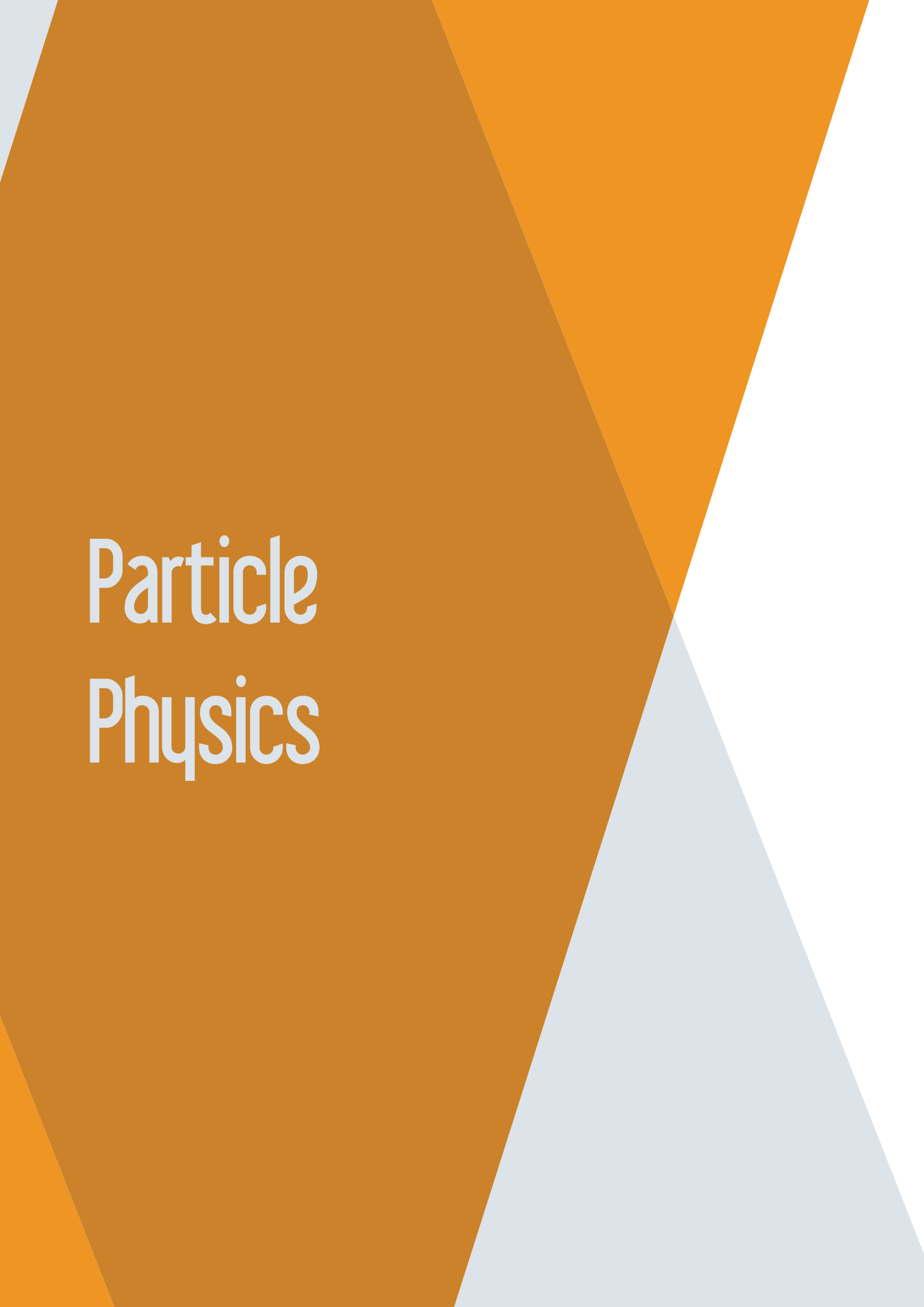
As of June 2021, TIFPA personnel includes:

Research	SIGEA	STAR
Elettra Bellinzona	Marta Perucci (head)	Piero Spinnato (head)
Ruggero Caravita	Isabella Martire	Alberto Franzoi
Constantinos Constantinou	Giuliana Pellizzari (on borrowed agreement from PAT)	Christian Manea
Francesco Dimiccoli	Irene Sartini (on long-term leave)	Enrico Verroi
Oleksii Gryniuk		
Alessandro Lovato (on long-term leave)		
Coralie Neubüser		
Francesco Nozzoli		
Edna Carolina Pinilla Beltran		
Irina Rashevskaya		
Emanuele Scifoni		
Sushil Sharma		

TIFPA research associates, grouped according to their area of activity, are listed in the following table. Senior associates (*Incaricati di Ricerca*) are marked as (IR). CSN coordinators are senior associates who locally coordinate the activities of the group and represent TIFPA at the meetings of the National Committee:

CSN1	Andrea Miani	Alessandro Casalino	Massimo Cazzanelli
Gian-Franco Dalla Betta (IR)	Martina Muratore	Francesco Giovanni Celiberto	Riccardo Checchetto
Roberto Iuppa (IR)	Giovanni Paternoster	Adolfo Renè Cisterna Roa	Alessandro Cian
Marco Cristoforetti	Alessio Perinelli	Elena Filandri	Thomas Corradino
Andrea Di Luca	Alessio Recati	Giovanni Garberoglio	Pablo De Vera Gomis
David Macii	Ester Ricci	Danial Ghamari	Emanuele Enrico
Daniela Mascione	Giuliana Russano	Riccardo Ghiloni	Paolo Farace
Arif Abdulla Md Samy	Francesco Salemi	Samuel Andrea Giuliani	Matteo Favaro
Giovanni Verzellesi	Sandro Stringari	Marco Giulini	Lorenza Ferrario
CSN2	Paolo Tosi	Piero Luchi	Andrea Ficorella
Rita Dolesi (coord.)	Michele Valentini	Giovanni Mattiotti	Francesco Ficorella
Roberto Battiston (IR)	Daniele Vetrugno	Sonia Mazzucchi	Francesco Fracchiolla
Antonio Perreca (IR)	Louise Wolswijk	Valter Moretti	Damiano Giubertoni
Giovanni Andrea Prodi (IR)	Alessandro Zenesini	Davide Pastorello	Stefano Lorentini
Stefano Vitale (IR)	CSN3	Alessandro Perotti	Devid Maniglio
William Weber (IR)	Roberto Sennen Brusa (IR)	Lorenzo Petrolli	Benno Margesin
Paolo Zuccon (IR)	Sebastiano Mariazzi (IR)	Raffaello Potestio	Renato Mezzena
Fabio Acerbi	Francesco Tommasino (IR)	Marta Rigoli	Marta Missiaggia
Anna Rita Altamura	Giorgio Cartechini	Samuele Marco Silveravalle	Antonella Motta
Damiano Avi	Maurizio Dapor	Luca Tubiana	Carlotta Mozzi
Sophie Bini	Luca Penasa	Michele Turelli	Viviana Mulloni
Michele Bonaldi	Luca Povolo	Francesco Turro	Luca Oberto
Giacomo Borghi	Simone Taioli	Christiaan J. Farielda van de Ven	Lucio Pancheri
Antonio Lorenzo Borrielli	Paolo Emilio Trevisanutto	Silvia Vicentini	Giancarlo Pepponi
Daniele Bortoluzzi	Marco Volponi	Luigi Zanovello	Matteo Perenzoni
William Jerome Burger	CSN4	CSN5	Antonino Picciotto
Iacopo Carusotto	Francesco Pederiva (coord.)	Alberto Quaranta (coord.)	Enrico Pierobon
Davide Dal Bosco	Pietro Faccioli (IR)	Paolo Falferi (IR)	Leonardo Ricci
Abhinandan Dass	Gianluca Lattanzi (IR)	Chiara La Tessa (IR)	Roberto Righetto
Arturo Farolfi	Winfried Leidemann (IR)	Lucio Pancheri (IR)	Sabina Ronchin
Gabriele Ferrari	Giuseppe Nardelli (IR)	Marco Schwarz (IR)	Marina Scarpa
Valerio Ferroni	Giuseppina Orlandini (IR)	Artem Arkhangelskiy	Enrico Serra
Francesco Maria Follega	Albino Perego (IR)	Giacomo Baldi	Alberto Taffelli
Giuseppe Gebbia	Massimiliano Rinaldi (IR)	Pietro Battocchio	Jacopo Terragni
Alberto Giacomo Gola	Luciano Vanzo (IR)	Nicola Bazzanella	Andrea Vinante
Andrea Grimaldi	Valentina Amitrano	Pierluigi Bellutti	Nicola Zorzi
Giacomo Lamporesi	Enrico Blanzieri	Alessandra Bisio	off-CSN
Alberto Mazzi	Simon Boudet	Maurizio Boscardin	Gianluigi Casse
Stefano Merzi	Ylenia Capitani	Davide Brunelli	Michele Kirchner

INFN Experiments



Particle Physics

ATLAS

Marco Cristoforetti, Andrea Di Luca, Francesco Maria Follega, Gian-Franco Dalla Betta, Roberto Iuppa,[†] Daniela Mascione

Three years after the start of the deepPP initiative (DEEP-learning for Particle Physics, <https://www.deeppp.eu>), Trento's ATLAS group made significant progress towards the inclusion of its ideas and solutions in the stream of jet-flavour tagging developments for Run3. The analysis of Higgs decays into b -pairs in association with a large p_T jet also progressed, coming to satisfactory results and presentations at international conferences. We notice here that b -jet physics is intended to play a major role in the short and mid-term future. Either in $H \rightarrow bb$ decays or in processes involving top quarks, corrections from beyond Standard Model effects are thought to be visible primarily by measuring b -quarks. Even in case no evidence of New Physics will come from Run3, particular attention is devoted to online b -tagging and fast b -jet analysis in the framework of High-Luminosity LHC. In this view, the deepPP initiative has been focussed on feature selections for efficient implementations of online tools for b -tagging: as much as FPGAs and fast electronics may progress in the next five years, the full information available from calorimeters cannot be inputted to firmwares to take online trigger decisions. Which are the most important observables for online tagging? Which price do we pay when dropping a few of them to make our algorithm deployable? Is there a way to find the best tradeoff between speed and efficiency?

$H \rightarrow bb$ analysis. The study of boosted Higgs bosons decaying to b -pairs in association with a jet is a powerful tool to probe Beyond Standard Model effects causing anomalous production at high transverse momentum (p_T). The signature consists of two high p_T jets, recoiling against each other, where one jet contains the bb system, very collimated because of the large Lorentz boost. The most important deliverable of this analysis is the differential measure-

ment of the Higgs signal strength in p_T bins. The results of the analysis using a dataset of 136 fb^{-1} collected by the ATLAS detector were shown recently at the Moriond EW 2021 (Shope 2021) (ATLAS Collaboration 2021) conference. Fig. 1 shows how the differential signal strength is consistent with Standard Model expectations within uncertainties even if a rising trend in p_T is present.

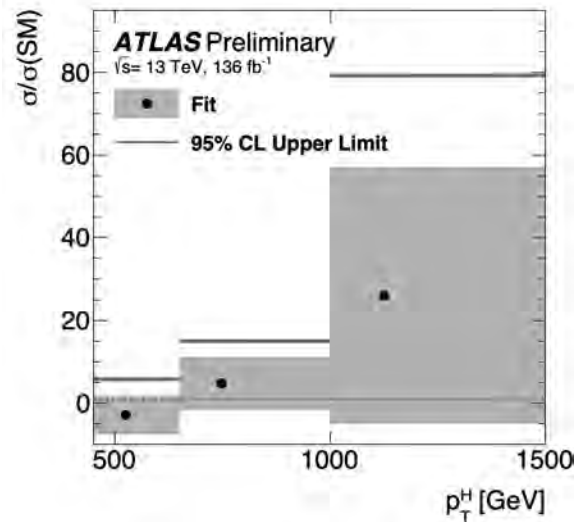


Figure 1: A summary of the signal strengths measured in the various p_T bins is shown.

B-tagging using deep neural networks. The task of identifying jets that contain b -hadrons (b -tagging) with respect to jets originated by lighter quarks is very important because of the abundance of interesting processes that contain b -hadrons in their final state at the LHC. Different kinds of information, both coming from the detector and developed by physicists, can be combined together to solve this task. A new high-level tagger based on a Deep Neural network and called DL1 was deployed last year. We conducted a detailed performance study to evaluate the possibility to reduce the

[†]Contact Author: roberto.iuppa@unitn.it

number of input variables to avoid undesired redundancy that could affect DL1 performance. We conducted also a detailed reproducibility study devoted to quoting additional uncertainties to take into account DL1 performance random fluctuations.

Data/Monte Carlo comparison in ATLAS. The TIFPA group developed a framework for algorithm validation to allow quick data/MC comparisons of new tagger trainings. This will permit the study of new training schemes to help mitigate calibration systematics uncertainties at training time. The software based on the analysis framework of the ATLAS collaboration, leverages on the infrastructure used in the calibration analyses, allowing for running ML based taggers within the validation code without the need to create new dedicated datasets. This will serve as a first cross check on new taggers to ensure that no major mismodellings are observed before running the full derivation campaigns needed for calibration.

Automated feature selection. Machine learning techniques are the new standard in high energy physics analyses to improve selection performances. We developed a possible approach to reduce the dimensionality and the correlation in classification problems

that involve machine learning techniques by ranking the relative importance of all available features in an automated process based on boosted decision tree algorithms. We tested the procedure with the selection of events at hadron colliders that contain highly boosted dijet resonances decaying to two b quarks, to be selected against an overwhelming QCD background. Fig. 2 shows that the ROC curves for different models. The model trained using the first 19 variables from the automated feature selection has performance comparable with the model trained on all the features within 5%.

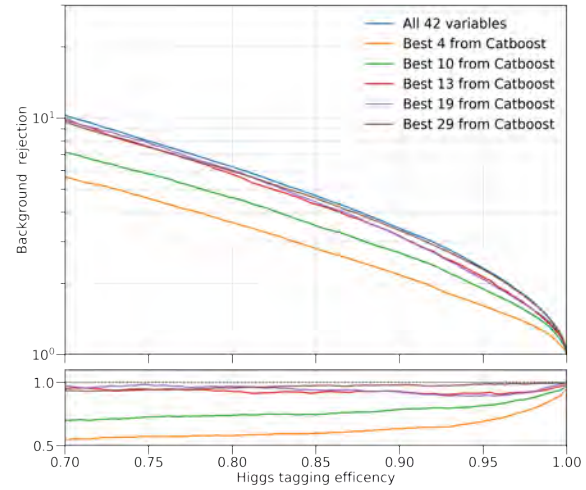


Figure 2: ROC representing the performance of models using different numbers of input variables.

Selected Papers

ATLAS Collaboration (2021). *Study of Higgs-boson production with large transverse momentum using the $H \rightarrow b\bar{b}$ decay with the ATLAS detector.* All figures including auxiliary figures are available at <https://atlas.web.cern.ch/Atlas/GROUPS/PHYSICS/CONFNOTES/ATLAS-CONF-2021-010>.

Shope, D. R., ATLAS Collaboration (2021). *Higgs Simplified Template and Differential Cross Sections.* <https://cds.cern.ch/record/2759461>.

FASE2_ATLAS

Gian-Franco Dalla Betta,[†] Giacomo Baldi, Maurizio Boscardin, Francesco Ficorella, Roberto Iuppa, David Macii, Roberto Mendicino, Giulio Monaco, Giovanni Paternoster, Irina Rachevskaya, Ester Ricci, Sabina Ronchin, Md Arif Abdulla Samy, Giovanni Verzellesi, Nicola Zorzi

The project is aimed at completing the R&D activities previously started in the RD-FASE2 project, with a more focused approach aimed at solving some specific remaining issues in view of the construction of the new ATLAS detector for High-Luminosity LHC. Within the Inner Tracker sub-project (ITk), TIFPA is responsible for the development and optimisation of 3D pixel sensors for the innermost layer. This application requires very high hit-rate capabilities, increased pixel granularity (e.g., 50×50 or $25\times 100\ \mu\text{m}^2$ pixel size) and extreme radiation hardness (up to $2\times 10^{16}\ \text{n}_{eq}\ \text{cm}^{-2}$ fluence). New 3D sensors are made at FBK with a single-sided process with thin active regions ($150\ \mu\text{m}$), narrow columnar electrodes ($\sim 5\ \mu\text{m}$) with reduced inter-electrode spacing ($\sim 30\ \mu\text{m}$), and very slim edges ($\sim 100\ \mu\text{m}$).

The activity carried out in 2020 was dealing with the characterization of sensors and modules from previous years, including tests on irradiated samples, and on the design and fabrication of new batches of sensors. The main results of both these activities are summarized in the following.

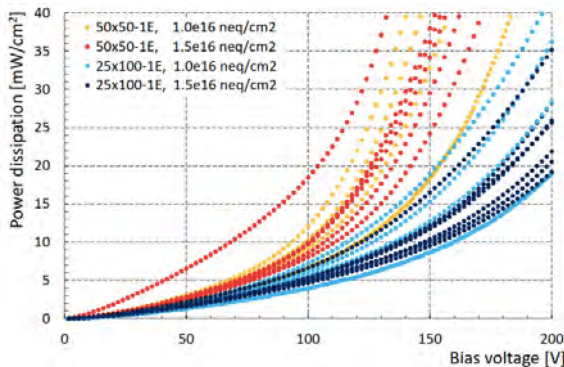


Figure 1: Power dissipation at $-25\ ^\circ\text{C}$ of diodes of 50×50 and $25\times 100\ \mu\text{m}^2$ geometry irradiated to two different fluences.

The results from the beam tests carried out

[†]Contact Author: gianfranco.dallabetta@unitn.it

in 2019 on irradiated RD53A pixel modules made with sensors from the third batch were analysed, and confirmed the high hit efficiency to be larger than 97% after a fluence of $1\times 10^{16}\ \text{n}_{eq}\ \text{cm}^{-2}$ (Garcia-Alonso et al. 2020). Due to the Covid-19 pandemic, the module irradiation campaigns to larger fluences and further beam tests were hindered, and the activity had to be extended to 2021.

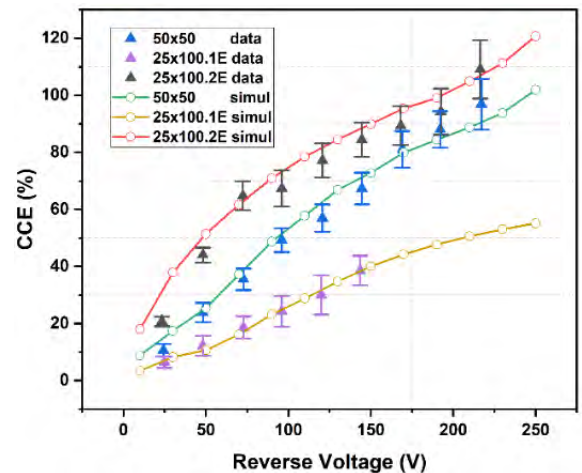


Figure 2: Comparison of measured and simulated charge collection efficiency in 3D diodes of different geometry irradiated with neutrons at $2\times 10^{16}\ \text{n}_{eq}\ \text{cm}^{-2}$.

Further tests were carried out on irradiated diodes to study the power dissipation. Small-area devices ($\sim 2\ \text{mm}^2$) of different pixel geometries were irradiated with reactor neutrons at two fluences, $1\times 10^{16}\ \text{n}_{eq}\ \text{cm}^{-2}$ and $1.5\times 10^{16}\ \text{n}_{eq}\ \text{cm}^{-2}$. The current-voltage characteristics were measured at $-25\ ^\circ\text{C}$ in a climatic chamber. The power dissipation was calculated multiplying the bias voltage and the measured current. Fig. 1 shows the results for different sets of diodes. Taking into account the ITk power limit of $40\ \text{mW}/\text{cm}^2$ for Layer0, it can be seen that devices can be safely operated within ranges of voltage (from 130 V to 180 V for the 50×50

samples, and even higher for the 25×100 ones) that allow for a high hit efficiency.

TCAD simulations by Synopsys Sentaurus, incorporating advanced radiation damage models, have been used to investigate the charge collection efficiency (CCE) of irradiated 3D sensors. As an example, Fig. 2 shows the experimental and simulated CCE of 3D diodes of different geometries irradiated with reactor neutrons at $2 \times 10^{16} \text{ n}_{eq} \text{ cm}^{-2}$ and measured with a position sensitive IR laser setup. Simulations yield a good agreement with experimental data, correctly predicting also the onset of charge multiplication effects observed in the measurements of sensors with the smaller inter-electrode distances at high voltage.

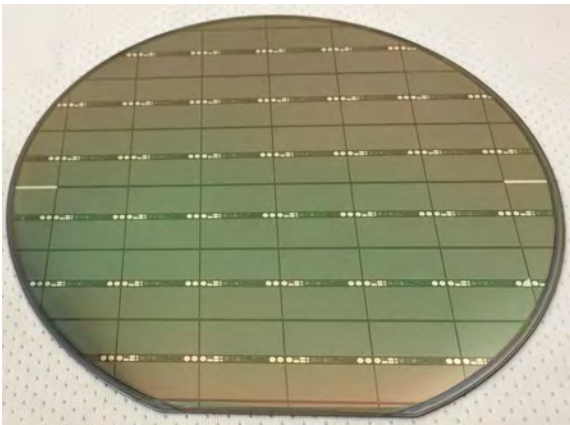


Figure 3: Photograph of a wafer from batch 4 fabricated with stepper lithography.

Levering the encouraging results from the third batch, the first made with stepper lithography, a fourth batch was designed in 2019 and submitted to FBK for fabrication. The wafer layout of the fourth batch was designed to comprise 52 sensors compatible with the RD53A

readout chip with two different pixel versions, i.e., 50×50 and $25 \times 100 \mu\text{m}^2$ (26 sensors for each), and test structures at the periphery (see Fig. 3). The batch was completed at FBK in July 2020. From the electrical tests carried out at wafer level using the temporary metal, it was possible to appreciate the good quality of the sensors. As an example, Fig. 4 shows the I-V plots of all sensors from wafer 5. It can be seen that a large fraction of the sensors has low leakage current and breakdown voltage larger than 80 V (the maximum bias applied). Based on the electrical characterisation results, the three best wafers from batch 4 were sent for bump bonding to IZM.

Mean time, decisions on the production of 3D sensors for ATLAS ITk have been taken. FBK has been assigned the production of half of the 50×50 which will equip the rings of Layer0. The layout of the sensors, compatible with the RD53B read-out chip, has been designed at UniTN, and the fabrication of the pre-production batch at FBK has just been completed in March 2021.

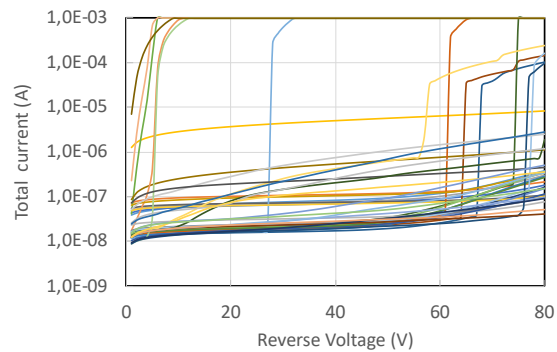
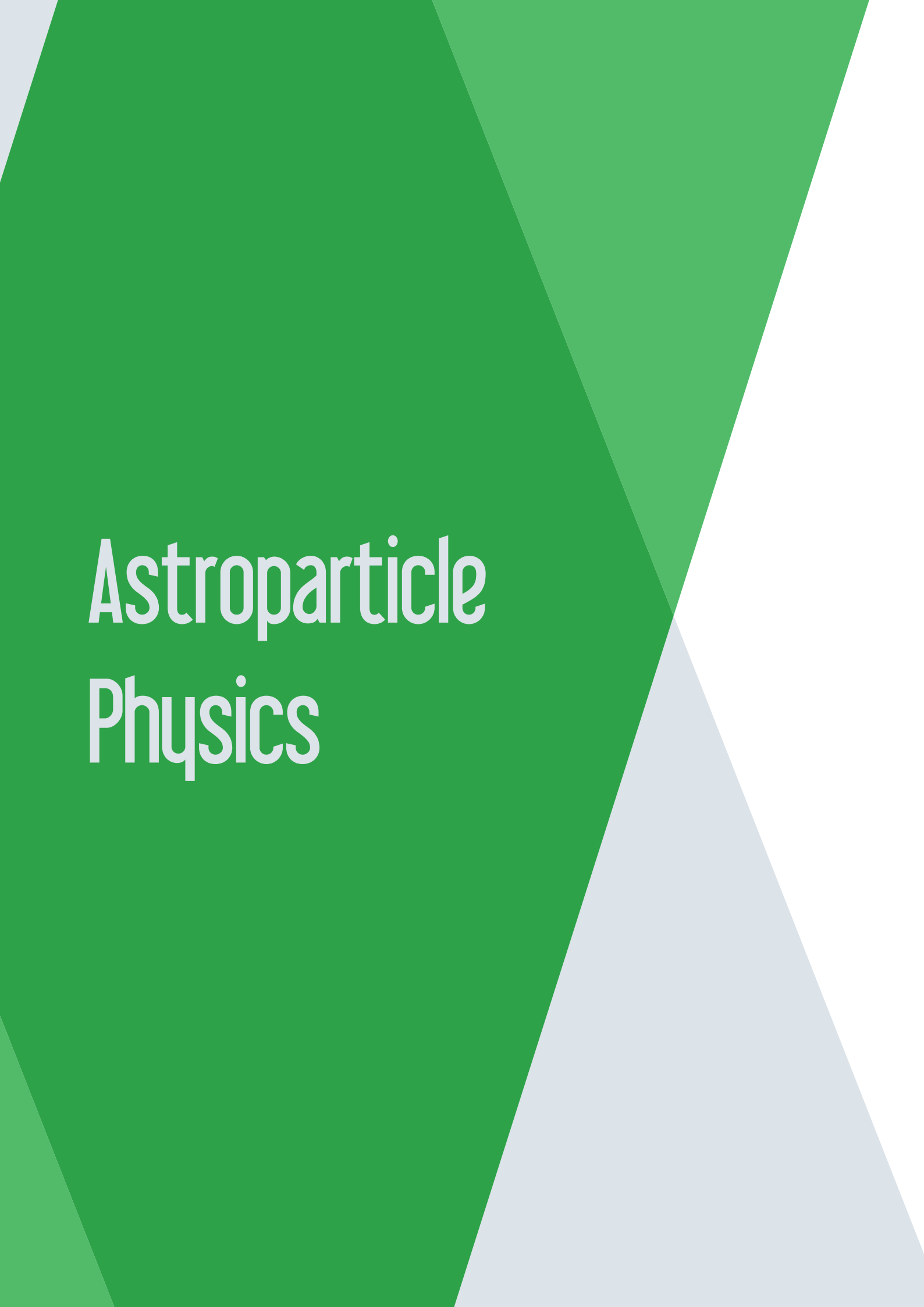


Figure 4: I-V curves of all RD53A sensors from wafer 5 of batch 4.

Selected Papers

Garcia-Alonso, A., Curras, E., Duarte-Campderros, J., Fernandez, M., Gomez, G., Gonzales, J., Silva, E., Vila, I., Jaramillo, R., Meschini, M., Ceccarelli, R., Dinardo, M., Gennai, S., Moroni, L., Zuolo, D., Demaria, L., Monteil, E., Gaioni, L., Messineo, A., Dalla Betta, G. F., Mendicino, R., Boscardin, M., Hidalgo, S., Merlos, A., Pellegrini, G., Quirion, D., and Manna, M. (2020). *Test beam characterization of irradiated 3D pixel sensors*. *Journal Instrum.* **15**. Art. no.: C03017.



Astroparticle Physics

ADHD

Francesco Dimiccoli, Roberto Iuppa, Francesco Nozzoli,[†] Ester Ricci, Paolo Zuccon

Low energy anti-deuterons in cosmic rays are considered a golden channel for the search of Dark matter annihilations in the galaxy. Anti Deuteron Helium Detector (ADHD) project is aiming to study the signatures offered by an high pressure He target for the identification of anti-deuterons in space. In particular exotic atoms are produced by stopping anti-protons/anti-deuterons in the gas and the captured particle can orbit the He nucleus for $\sim \mu\text{s}$ before the annihilation.

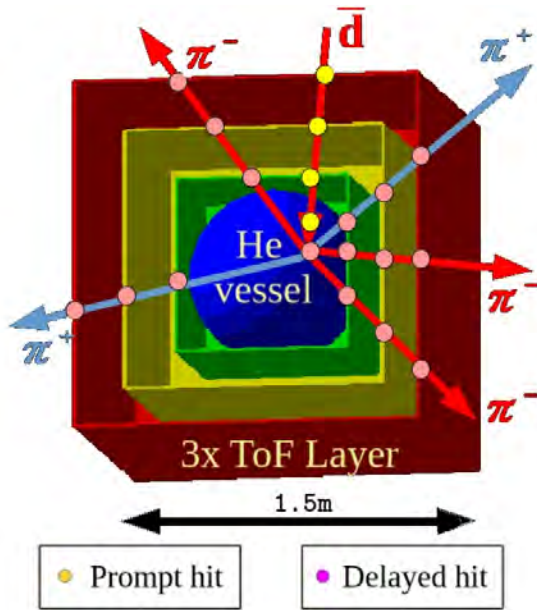


Figure 1: The ADHD detector is made of a 400 bar helium-gas calorimeter (HeCal) surrounded by a Time-of-Flight system with three scintillator layers. Antideuterons are detected as a single in-going prompt track (yellow points) followed by several out-going delayed pions (light-red points).

This meta-stability is a unique feature for the He target and the characteristic delayed annihilation is a distinctive signature to identify the antimatter nature of the stopping particle (Nozzoli et al. 2020; Dimiccoli et al. 2020c; Doetinchem et al. 2020).

A possible layout for ADHD is shown in Fig. 1. It is composed by a helium

calorimeter (HeCal) surrounded by a Time of Flight system. The sensitivity, evaluated by Geant4 simulations, would be similar to those provided by other \bar{d} searches in space/balloon (AMS/GAPS), exploring a complementary (lower) kinetic energy region (60-150 MeV/n).

A prototype of the pressurized calorimeter, with cylindrical geometry ($\varnothing 5 \times 47 \text{ cm}^2$ filled by 200 Bar He) has been tested in TIFPA laboratory with cosmic μ and proton beam during 2020.

During the test, the particles (vertical cosmic μ or horizontal proton beam) cross a plastic scintillator (CH3), cross the front ring of SiPM (CH2), cross 1 cm of optical Al_2O_3 window and produce scintillation light within the helium target detected by the front SiPM array and by the rear PMT (CH1). Finally if the energy is enough, the particles cross also the rear part of the detector and are detected by the plastic scintillator (CH4), see Fig. 2.

The HeCal prototype is based on the Arktis B470 (natural He) fast neutron detector that was originally equipped with two Hamamatsu R580 PMTs, each for side.

To allow a test of the B470 detector with ionizing particles, the front PMT was replaced by a SiPM ring array. The SiPM ring array (see Fig. 3) was designed and built at TIFPA using 8x SensL MisroFJ-SMTPA-60035.

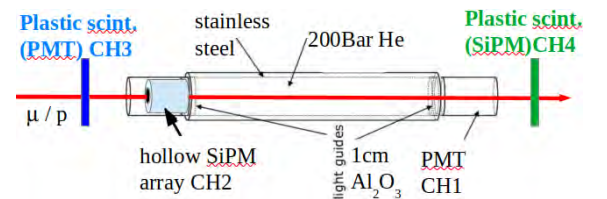


Figure 2: schema of the measurement set-up.

[†]Contact Author: francesco.nozzoli@unitn.it



Figure 3: 8xSiPM ring array developed at TIFPA to replace the front PMT. The particles can enter in the HeCal detector avoiding to cross the sensitive photodetector surface.

A passive iron shield (10 cm thickness) was

placed behind the SiPM array to stop secondary particles; a $\varnothing = 2.5$ cm hole at the center of the shield allows the particle beam to enter in the HeCal. Two plastic scintillators $40 \times 10 \times 5$ mm³ were placed at both sides of the detector, to provide the trigger for particles crossing the whole detector.

The COVID 2020 pandemic period was exploited for long duration data taking, with the detector placed vertically, to collect cosmic muons at the rate of $1.5 \mu/\text{d}$. The average energy of μ at ground is ~ 4 GeV therefore this allows the measurement of the detector response for minimum ionizing particles (MIPs). Analysis of muon events provides a time resolution of ~ 3 ns and an energy resolution of $\sim 15\%$ for MIPs.

At the end of 2020, the prototype was also tested with 70-240 MeV protons in the Trento Proton-therapy center (see Fig. 4). Analysis of proton events is ongoing.



Figure 4: The HeCal prototype at the Trento proton beam line (70-240 MeV).

Selected Papers

- Dimiccoli, F., Nozzoli, F., and Zuccon, P. (2020c). “Detectors for antideuteron search in cosmic rays: current status and new ideas”. Ed. by M. Nessi. Vol. 15. 06. Art. no.: C06033.
- Doetinchem, P. von et al. (2020). *Cosmic-ray antinuclei as messengers of new physics: status and outlook for the new decade*. JCAP **08**, p. 035.
- Nozzoli, F., Dimiccoli, F., and Zuccon, P. (2020). “Perspectives of dark matter indirect search with ADHD in space”. Vol. 1548. 1. Art. no.: 012035.

AMS

Roberto Battiston, William Jerome Burger, Cinzia Cernetti, Francesco Dimiccoli, Giuseppe Gebbia, Ignazio Lazzizzera, Francesco Nozzoli,[†] Paolo Zuccon.

AMS-02 is a state-of-the-art particle physics detector (see Fig. 1) designed to operate as an external module on the International Space Station (ISS).

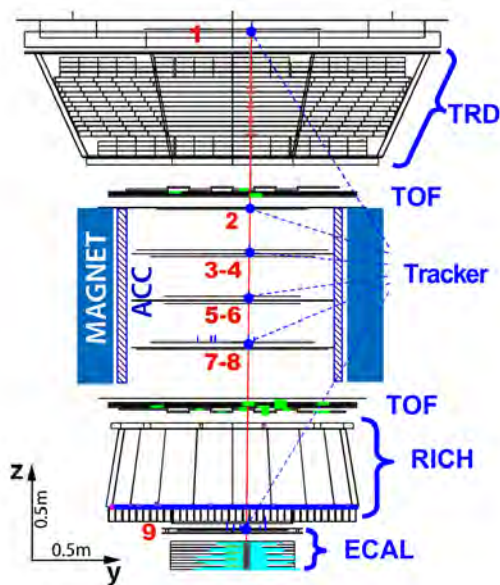


Figure 1: The AMS detector with an example of a measured 868 GeV positron event. Tracker planes 1-9 measure the particle charge, sign and momentum. The TRD identifies the particle as an electron/positron. The TOF measures the charge and ensures that the particle is downward-going. The RICH measures the charge and velocity. The ECAL independently identifies the particle as an electron/positron and measures its energy.

AMS-02 goal is to study the universe and its origin by searching for antimatter and dark matter, while performing precision measurements of cosmic ray composition and flux. The measurements high accuracy along with the large collected statistic allow to study cosmic ray component flux variations with rigidity and time. This is important to understand the origin, acceleration and propagation of cosmic rays in our galaxy.

In January 2020, after a series of 4 complex extra-vehicular activities, Luca Parmitano

(ESA) and Andrew Morgan (NASA) installed a new pump block for the cooling system of the AMS-02 Silicon Tracker (Fig. 2). This operation effectively extended the lifetime of AMS-02 up to the entire duration of the ISS mission, up to at least 2028.

During 2020 AMS published the flux of Neon, Magnesium, and Silicon Primary Cosmic Rays (Aguilar et al. 2020a). Unexpectedly, above 86.5 GV the rigidity dependence of Ne, Mg, and Si spectra is different from the rigidity dependence of primary cosmic rays He, C, and O, which have identical rigidity dependence above 60 GV and harden above 200 GV. Above 86.5 GV, the Ne/O, Mg/O, and Si/O ratios can be described by a simple power law, R^δ , with spectral index $\delta = -0.045 \pm 0.008$. This is the first evidence that the Ne, Mg, and Si and He, C, and O are two different classes of primary cosmic rays (Fig. 3).



Figure 2: L. Parmitano concluding the UTTPS replacement for AMS on 25/01/2020. The spacewalk was completed in 5 hours and 58 minutes.

Moreover, at the end of 2020 a review of the results obtained analyzing the first seven year of AMS-02 data has been published, it contains also some new results as the limits on the flux of strangelets or the measurement of inelastic nuclear cross sections of carbon at high energy (Aguilar et al. 2021a).

[†]Contact Author: francesco.nozzoli@tifpa.infn.it

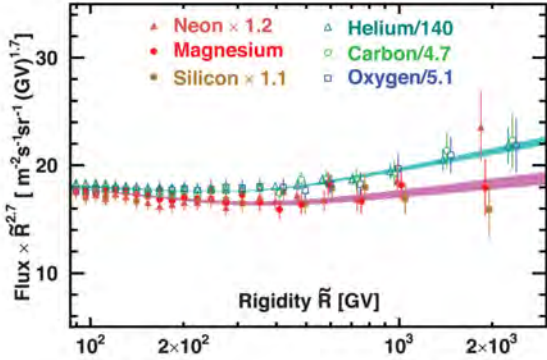


Figure 3: The rigidity dependence of the Ne, Mg, and Si fluxes compared to rigidity dependence of the He, C, and O fluxes above 86.5 GV. For display purposes the He, C, O, Ne, and Si fluxes were rescaled as indicated.

The AMS/TIFPA group is currently finalizing the measurement of Deuteron flux and flux ratio as a function of Rigidity and time (Dimiccoli et al. 2020a). Moreover, the analysis of $^{10}\text{Be}/^9\text{Be}/^7\text{Be}$ abundances in cosmic rays, is started as the next goal of the AMS/TIFPA group. In particular ^{10}Be is a β -radioactive nucleus ($T_{1/2} = 1.39 \times 10^6$ y) and acts as a cosmic-ray radioactive clock able to determine the average residence time of cosmic rays in the galaxy. The identification of Beryllium isotopes is performed in AMS02 with the combined measurement of charge Z , rigidity R and velocity β , which provide a mass reconstruction: $m = ZR/(\gamma\beta)$. Previous measurements of Be isotopes were scarce, affected by large uncertainties and limited to low energy. The large accep-

tance and exposure of AMS-02 allows to extend Be isotopic measurement up to ~ 10 GeV/n (Fig. 4). The comparison with theoretical expectation for $^{10}\text{Be}/^9\text{Be}$ flux ratio will provide a precise determination of halo half-thickness parameter H that is a fundamental parameter to model Cosmic Ray propagation in the Galaxy (and is currently known with large uncertainty $H = 5_{-2}^{+3}$ kpc).

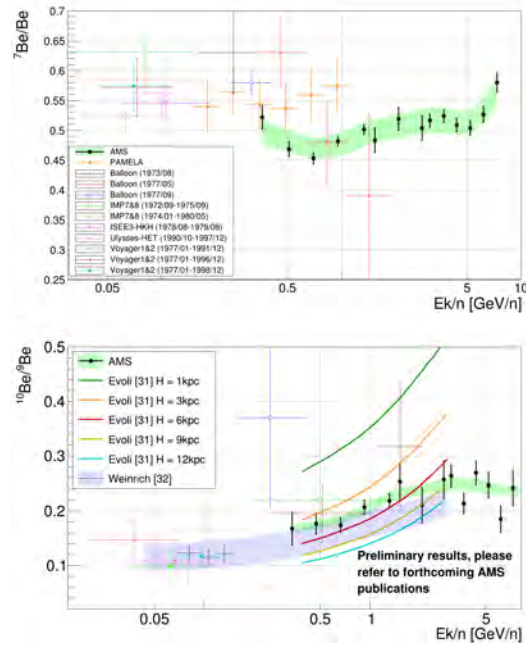


Figure 4: Preliminary measurement of $^{10}\text{Be}/^9\text{Be}$ and of the complementary $^7\text{Be}/\text{Be}$ flux ratios.

Selected Papers

- Aguilar, M. et al., AMS collaboration (2020a). *Properties of Neon, Magnesium, and Silicon Primary Cosmic Rays Results from the Alpha Magnetic Spectrometer*. Phys. Rev. Lett. **124**(21). Art. no.: 211102.
- AMS collaboration (2021a). *The Alpha Magnetic Spectrometer (AMS) on the international space station: Part II — Results from the first seven years*. Phys. Rept. **894**, pp. 1–116.
- Dimiccoli, F., Battiston, R., Kanishchev, K., Nozzoli, F., and Zuccon, P. (2020a). *Measurement of Cosmic Deuteron Flux with the AMS-02 Detector*. J. Phys. Conf. Ser. **1548**(1). Art. no.: 012034.

DarkSide

Alberto Mazzi,[†] Alberto Gola, Fabio Acerbi, Anna Rita Altamura, Stefano Merzi, Giovanni Paternoster

The existence of dark matter in the Universe is commonly accepted as the explanation of many phenomena, ranging from internal motions of galaxies to the large-scale inhomogeneities in the cosmic microwave background radiation and the dynamics of colliding galaxy clusters.

A favored hypothesis that explains these observations is that dark matter is made of weakly interacting massive particles (WIMPs). However, no such particles exist in the Standard Model and none has been observed directly at particle accelerators or elsewhere. Hence, the nature of the dark matter remains unknown.

DarkSide-20k experiment (DS-20k) is a direct dark matter detection experiment based on a shielded underground detector, with 20 tons of liquid argon (LAr) target mass. It will be based on a two-phase time projection chamber (TPC) filled with low-background, underground argon (UAr) and will be deployed in the underground Hall C at Gran Sasso National Laboratory (LNGS), inside a newly constructed, two-chamber veto, filled with atmospheric argon (AAr), and a cryostat, as shown in Fig. 1. DS-20k constitutes an expanded version of the DarkSide-50 experiment, which finished taking data at LNGS in October 2017.

DS-20k Time Projection Chamber In the TPC, events in the LAr result in electron or nuclear recoils that deposit energy in the argon, resulting in excitation and ionization. The direct excitation, and that due to recombining ions, results in a prompt scintillation signal, called S1. LAr scintillation has a wavelength of 128 nm, in the far UV, thus a wavelength shifter will cover all surfaces that the UV light hits. Ionization electrons escaping recombination drift under an applied electric field to the top of the LAr, where a stronger applied field extracts the electrons into the argon gas above the liquid. Here the strong field accelerates the electrons enough for them to excite (but not ionize) the argon gas, producing a secondary scintillation signal, S2, that is proportional to the initial ion-

ization. Photosensors at the top and bottom of the TPC read out both scintillation signals in each event.

S1 is used for energy determination and pulse-shape discrimination. S2 is used for energy and 3D position measurement of the event, obtaining the vertical coordinate from the drift time between S1 and S2, and the horizontal coordinates from the pattern of light in the top photosensors.

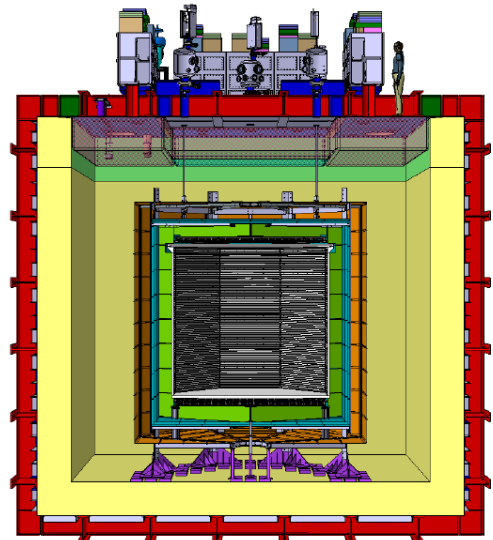


Figure 1: Cross-sectional view of the large AAr cryostat containing the LAr TPC and veto detectors.

Silicon Photomultipliers The use of Silicon Photomultipliers (SiPMs) instead of Photo Multiplier Tubes as photodetectors is one of the two main technological challenges of the experiment, the other being the purification of underground argon to produce ultra-low-background depleted argon. There are several advantages in using these detectors in DS-20k, among them: low bias voltage (30 — 45 V), efficient integration into tiles to cover large areas, customizable size and performance, excellent photon counting capabilities and high Photon Detection Efficiency (PDE). The most important one, however, is that SiPMs are virtually radioactivity free (silicon used in wafers is a very radio pure material). SiPMs will be grouped in

[†]Contact Author: mazzi@fbk.eu

tiles and integrated in several photo-detection modules, to cover a total area of more than 20 m².

DS-20k Activity at TIFPA TIFPA started the DS-20k activity in 2016, collaborating mainly with Fondazione Bruno Kessler (FBK), LNGS, Naples INFN section and Princeton University. The activity was focused on the cryogenic characterization of different SiPM technologies developed by FBK to verify and characterize their functionality at cryogenic temperatures and, in particular, at 87 K, to select the most suitable one for DS-20k, and to provide information to optimize the SiPM parameters and layout for the best possible performance in DS-20k.

In this context, the most important result was the development of NUV-HD-Cryo technology which demonstrated enabling features for DS-20k:

- (i) exceptionally low Dark Count Rate (DCR) at 87 K;
- (ii) suppression of the increase of the after-pulsing previously observed at cryogenic temperatures;
- (iii) increased temperature stability of SiPM quenching resistor.

The SiPMs feature a 1 cm² active area, 30 μm cell size, and show a PDE of 50% at 420 nm, DCR of 10 mHz/mm² at 77 K, after-pulsing probability lower than 8%, crosstalk probability lower than 25%, at 6 V of bias above breakdown.

Since 2019 the activities at TIFPA and FBK were focused on the technology transfer of the NUV-HD-Cryo technology to an external CMOS foundry (LFoundry), as needed for the mass production for DS-20k.

TIFPA commissioned to FBK the wafer level testing of SiPM lots produced by LFoundry for the assembly of DS-Proto, a prototype detector of intermediate size (~1 t), shown in Fig. 2. The functional characterization of SiPMs produced by LFoundry was also performed by FBK and LNGS, independently.

The device parameters measured at wafer level on the lots released by LFoundry showed a very accurate match with the design values and a high uniformity both wafer-to-wafer and batch-to-batch.



Figure 2: Concept design of the DS-Proto Detector.

On the other hand, a non-conformity emerged in these SiPM batches as regards the device series resistance. In particular, a parasitic resistance was present on the metallic backside of the devices which provides the cathode contact, showing a deterioration during thermal cycles.

This issue required an additional R&D activity that was carried out involving TIFPA, FBK, LFoundry and LNGS. Several process variations were proposed and studied, with a particular attention to technology reliability in view of the mass production planned for 2021.

Using cryogenic electronics developed at LNGS for the photodetector module (PDM) readout, remarkable few-photon counting capability was demonstrated at 77 K, with S/N in excess of 20, using a 24 cm² SiPM array coupled to a single analog readout channel (Fig. 3).

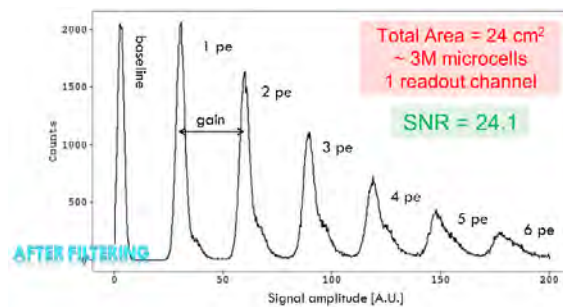


Figure 3: Few-photon spectrum recorded with a whole PDM, after optimized digital filtering. The spectrum demonstrates, among other things, the excellent gain uniformity of the 3M microcells composing the PDM.

FISH

Arturo Farolfi, Riccardo Cominotti, Carmelo Mordini, Arko Roy, Albert Gallemí, Iacopo Carusotto, Alessio Recati, Sandro Stringari, Alessandro Zenesini, Giacomo Lamporesi, Gabriele Ferrari[†]

FISH, Fundamental Interaction Simulations with quantum gases, focuses on the dynamics of quantum gases of ultracold atoms with the aim to model interactions and mechanisms at the basis of high energy physics. This research field belongs to the domain of quantum simulation, where physical systems difficult to address experimentally are studied through analogies with simpler systems. In particular we focus on the study of topological defects in a system made of two Rabi-coupled atomic Bose-Einstein condensates.

In the last year we focused on the particular situation where the strength of the Rabi coupling and the interaction energy of the atoms have comparable magnitude. This experimental condition, which is essential to the study of topological defects in the regime of relevance to the simulation, is possible thanks multilayer system developed in the last years of activities which protects the atomic sample from magnetic field noise. A side by side characterisation and calibration of our experimental apparatus and measurement parameters have been also performed.

Spinor system The basic ingredients of the planned investigation are two states of the hyperfine manifold of sodium and the microwave Rabi coupling in a low-noise magnetic field environments. The two states can be mapped into a spinor system and the physics of the cloud studied by mean of well known spin hamiltonians. In a first set of measurements we demonstrate the long coherent time in our mixtures and our capability to tune the different parameters of the coupling (intensity, detuning) within the ranges required for future investigations.

Breaking Interface We studied the atomic mixture in a very elongated trap which allows

us to neglect the dynamics along the transverse directions and to simulate the physics of a quasi-one-dimensional system. We were able to observe different dynamical regimes, spatially separated in different regions of the atomic cloud and the breakdown of the interface between them. The observed regimes originate from the local properties of the system and resemble magnetic material in presence of interface in solid state heterostructure. The dynamics of the interface and its breaking in a dissipationless system are unique phenomena so far predicted by theory but never observed in real

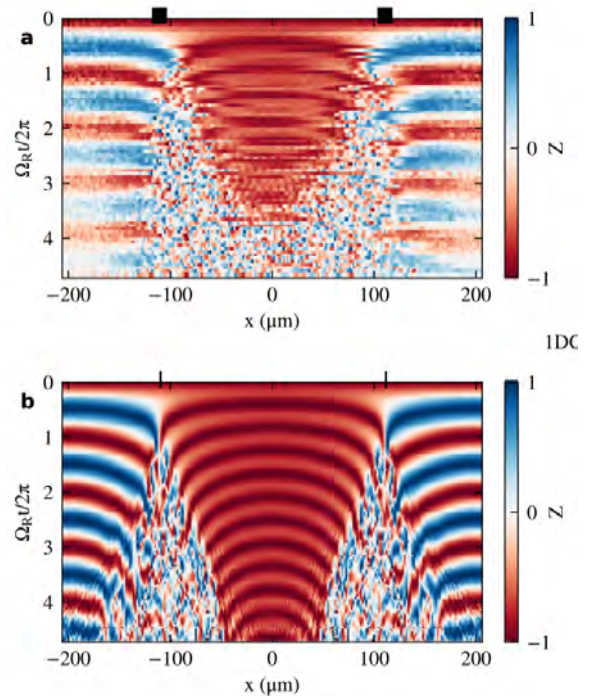


Figure 1: Experimental **a)** and numerical **b)** evidence of the breaking of the interface between two dynamical regime. The horizontal and vertical axes are the spatial and the temporal coordinates, respectively. The colour code refers to the population into the two states: Blue = State 1, White = Balanced mixtures, Red = State 2

[†]Contact Author: gabriele.ferrari@unitn.it

material. The comparison with numerical results demonstrates the validity of experimental system and the full understanding of the physical process (Farolfi et al. 2021). Additionally we found evidences of domain formation by observing the appearance of the typical spatial correlation.

Beyond one-dimensional system The measurements performed in a quasi-one-dimensional system were extended in three dimensions, revealing a richer dynamics where the interface breaking processes are mixed with the appearance of topological structure as vortices. This experimental campaign is still ongoing, with particular interest in the intermediate dynamics after the breaking of initial state and before the reaching of the final one.

Spin manipulation A spin system of many atoms is not only interesting in the context of simulating magnetic hamiltonians in spatially extended system, but also regarding the creation of magnetic solitons and domain walls. The mapping of this structures into high energy physics analogues requires the preparation of the system in particular initial conditions which are non trivial to prepare within the requested parameter range. We succeed to transfer the atoms from the initial state to a coherent superposition of two by mean of an adiabatic transfer

which appear to be robust and reliable in different experimental conditions and for the whole cloud (Farolfi et al. 2020b).

Current activity The current activity is focused on the study of a particular class of dynamical instabilities where the dynamic of the spin state of the system is coupled to the density one leading to novel phenomena, and on the stability of topological structures which mimic the quark confinement process.

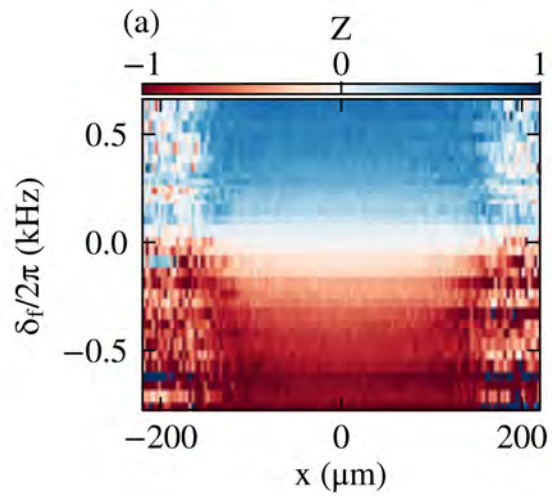


Figure 2: Adiabatic transfer. Different spin population across the cloud as function of the adiabatic passage detuning. Blue = State 1, White = Balanced mixtures, Red = State 2

Selected Papers

- Farolfi, A., Zenesini, A., Trypogeorgos, D., Recati, A., Lamporesi, G., and Ferrari, G. (2021). *Manipulation of an elongated internal Josephson junction of bosonic atoms*. arxiv. 2101.12643.
- Farolfi, A., Zenesini, A., Trypogeorgos, D., Mordini, C., Gallemì, A., Roy, A., Recati, A., Lamporesi, G., and Ferrari, G. (2020b). *Quantum-torque-induced breaking of magnetic domain walls in ultracold gases*. arxiv. 2011.04271.

HUMOR

Enrico Serra,[†] Michele Bonaldi,[†] Antonio Borrielli, Giovanni Andrea Prodi

A common feature of theories for Quantum Gravity (QG) is that the space-time changes nature, becoming *granular* at a very small length, called *Planck scale* ($L_p = \sqrt{\hbar G/c^3} = 10^{-35}$ m). The Heisenberg relation states that an arbitrarily precise measurement of only one of the two observables (position), is still possible at the cost of knowledge about the other (momentum), a fact which is incompatible with the existence of a minimal observable distance. This consideration motivates the introduction of generalized Heisenberg uncertainty principles (GUPs), such as $\Delta q \Delta p \geq \frac{\hbar}{2} \left(1 + \beta_0 \left(\frac{L_p \Delta p}{\hbar} \right)^2 \right)$. Therefore, to check QG effects is necessary to probe the uncertainty relation, to reveal any possible deviation from predictions of standard quantum mechanics. Quantum cavity optomechanics is a framework able to see these effects. Considering the joined roles of gravity and quantum physics, they should manifest themselves just on purely quantum objects. Based on this consideration, we propose experiments aiming to observe possible QG effects on macroscopic mechanical oscillators that are preliminarily prepared in a high purity state. The transition between a *classical* and a *quantum* state is not sharp, and its simplest and most immediate quantification uses the purity of the state. This indicator is defined as the trace of the square of the density matrix, which is equal to one for a pure state. Optical cooling is used to prepare high purity states and the goal is to reach a low occupation number \bar{n} , despite the relatively high background temperature. To this aim, we are working on two optomechanical state-of-the-art measurement protocols described in Bonaldi et al. (2020) and shown in Fig. 1.

The first scheme includes a preliminary state preparation by optical cooling, followed by an experimental cycle where the oscillator is firstly excited, then observed by a probe during the relaxation that follows the switching off

of the excitation signal. The second scheme implements a cycle in three steps: the optical cooling and the excitation are followed by the read-out with a weak probe after the complete shut-down of the laser system used for cooling and excitation, in a short period. In both schemes, we observe the most evident effect of the dynamics with a deformed commutator is a frequency shift having a quadratic dependence on the oscillation amplitude. In the first the shift is measured during the oscillator decay, exploiting the exponential decrease of the amplitude while in the second we explore the dynamics by varying the excitation strength, instead of relying on the decaying amplitude that would occur in a timescale longer than the re-thermalization time. Non-idealities can hide this effect because

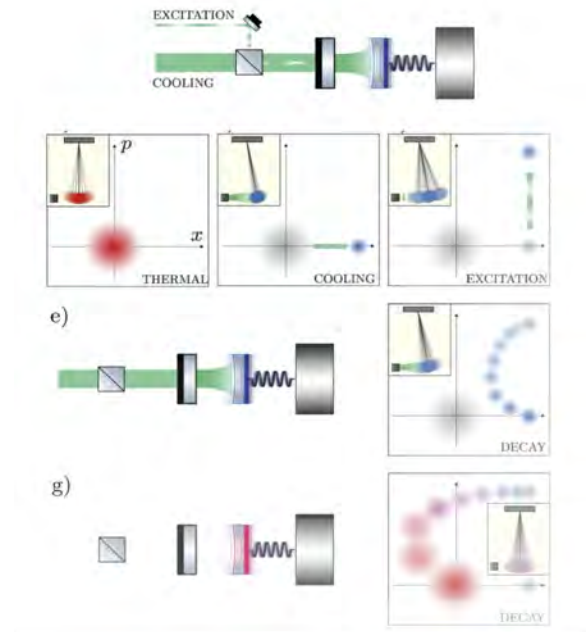


Figure 1: (e) Sketch of the first experimental proposal: the decay dynamics of the mechanical oscillator is detected once only the excitation beam is turned off. (g) Sketch of the second experimental proposal: the decay dynamics of the mechanical oscillator is detected once both the cooling and excitation beams are turned off.

[†]Contact Author: enrico.serra@tifpa.infn.it, michele.bonaldi@unitn.it

the decay time is much shorter than the natural oscillator relaxation time or can happen an uncontrolled optical spring effect with spurious and deleterious effects on the frequency stability and instabilities due to a strong intracavity field. Both schemes are investigated because one should find the optimal trade-off between strong coupling, and weak coupling.

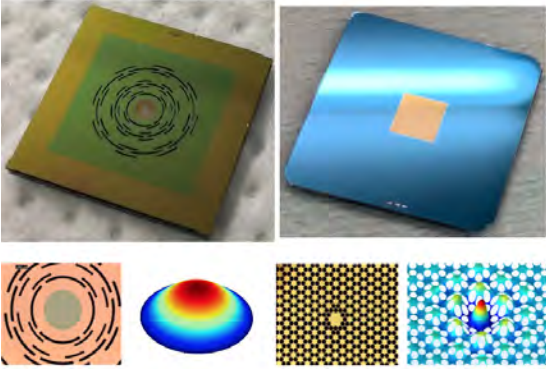


Figure 2: (left) round-shaped Si_3N_4 membrane with loss shield with its $(0,1)$ vibrational mode (right) softclamped membrane Si_3N_4 membrane with its bandgap vibrational mode A.

Our collaboration is working towards the implementation of the experimental schemes in two stages. The first is at cryogenic temperature (5-10 K), on a mechanical oscillator with a target phonon occupation number below 5 (thus, a purity above 0.1). For the second stage, we are preparing an ultra-cryogenic setup, achieving a base oscillator temperature below 1 K, with a target stationary mean phonon number below unity. The nanoresonators are free-standing silicon nitride (Si_3N_4) stressed membranes that

provide an ideal platform for realizing ultra-coherent harmonic oscillators. A first quantum signature of a quantum mechanical squeezed state was detected with devices in Fig. 2 and optical scheme described in the reference Chowdhury et al. (2020b). By exploiting the parametric modulation of the optical spring constant and observing the asymmetry of the stokes and anti-stokes peaks detected with a homodyne detection scheme it is possible to investigate the quantum behavior of the resonator. The sideband asymmetry in Fig. 3 is a footprint of the quantum motion of the oscillator, being originated by the non-commutativity between its ladder operators. A whole complete theoretical framework used to interpret the sideband asymmetry is reported in the reference Chowdhury et al. (2020a).

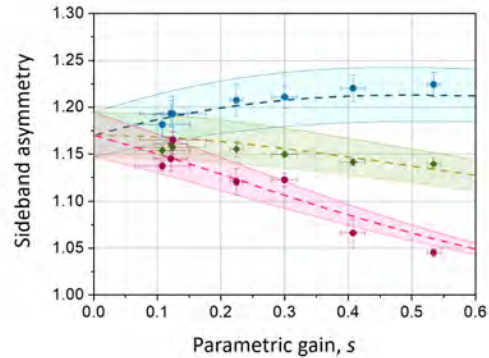


Figure 3: Sideband asymmetry in the absence of coherent parametric drive (green). (Blue) and (red) Lorentzian contributions in the two motional sidebands, with coherent parametric drive and dependence from parametric gain s .

Selected Papers

- Bonaldi, M., Borrielli, A., Chowdhury, A., Giuseppe, G. D., Li, W., Malossi, N., Marino, F., Morana, B., Natali, R., Piergentili, P., Prodi, G. A., Sarro, P. M., Serra, E., Vezio, P., Vitali, D., and Marin, F. (2020). *Probing quantum gravity effects with quantum mechanical oscillators*. THE EUROPEAN PHYSICAL JOURNAL D **74**, p. 178.
- Chowdhury, A., Vezio, P., Bonaldi, M., Borrielli, A., Marino, F., Morana, B., Prodi, G., Sarro, P., Serra, E., and Marin, F. (2020a). *Quantum motion of a squeezed mechanical oscillator attained via an optomechanical experiment*. PHYSICAL REVIEW A **102**. Art. no.: 053505.
- (2020b). *Quantum signature of a squeezed mechanical oscillator*. PHYSICAL REVIEW LETTERS **124**. Art. no.: 023601.

Limadou

Roberto Battiston, William Jerome Burger, Marco Cristoforetti, Francesco Maria Follega, Giuseppe Gebbia, Roberto Iuppa,[†] Ignazio Lazzizzera, Christian Manea, Coralie Neubuser, Francesco Nozzoli, Ester Ricci, Enrico Serra and Paolo Zuccon

The Limadou project made important steps ahead in 2020. Three years after the launch of CSES-01, the collaboration achieved the full control of the High Energy Particle Detector (HEPD) and started correlating data therefrom with inputs from the other payloads. The work package related to the analysis of transient phenomena, led by the Trento group, addressed the point of cross-calibrating data from the other CSES payloads and other space- and ground-based observatories. The event reconstruction of HEPD data is continuously improved by Trento's group, developing sophisticated Deep Learning models to make up for detector inefficiencies. But 2020 has been important also for the development of the HEPD-02 project. Trento is in charge of constructing the tracker with ALPIDE sensors, the most challenging innovation pertaining the second HEPD, as well as to develop the simulation of the whole apparatus.

Analysis of time transient phenomena.

Earth remote sensing provides new horizons for the study of the circumterrestrial medium. Using data from CSES payloads and including data from other satellites and observatories on ground, it is possible to identify phenomena correlated with seismic events of medium-to-large intensity and to establish direct connections for:

- co-seismic monitoring, i.e. identifying the occurrence of the seismic event;
- pre-seismic investigation, i.e. identifying possible precursor phenomena.

Detailed studies of atmospheric, ionospheric and magnetospheric data led to the development of the MILC model (Magnetospheric-Ionospheric-Litospheric Coupling), the first

quantitative description of the chain of co-seismic events associated to three earthquakes with magnitude $M > 5$, from the onset of a gravito-acoustic wave after the earthquake (Piersanti et al. 2020).

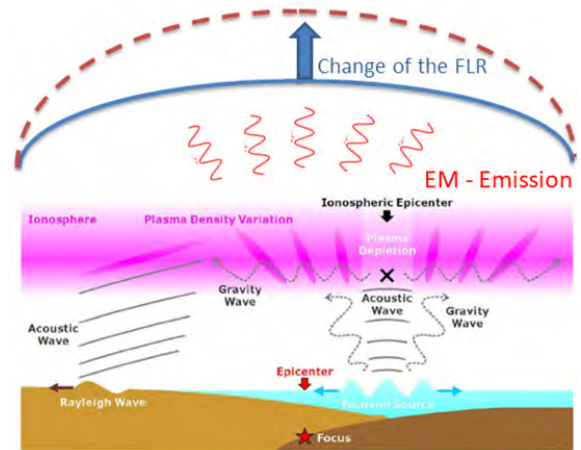


Figure 1: Cartoon view of the MILC model. From Piersanti et al. (2020)

Machine-learning-based event reconstruction for HEPD.

A Deep Learning based event reconstruction has been developed for electrons and protons measured with HEPD. The reconstruction chain is formed by a set of three deep neural networks taking as input the signals from the photomultipliers of HEPD. The networks distinguish electrons from protons and reconstruct the arrival direction and the kinetic energy of incoming particles. They have been trained with a dedicated Monte Carlo simulation of electrons and protons. The networks outperformed the standard methods and showed capable to correctly measure particles even not contained in the apparatus. They have been integrated in the official reconstruction software of the Limadou collaboration.

[†]Contact Author: roberto.iuppa@unitn.it

The tracker of HEPD-02. During 2020 the development of the HEPD-02 tracker focused on the engineering model (EM). A turret, the tracking unit of the detector, made of three sensitive layers hosting 10 ALPIDE detector each, has been realised. The EM turret successfully underwent vibration stress tests and was used to validate a prototype of the power supply unit of the HEPD-02. After these tests, the projects of (i) the power board and (ii) the electronic interface to the turret were frozen and got the approval of funding agencies. The DAQ system was also updated: besides data acquisition and transmission protocols, qualification and flight procedures were defined and implemented on a system of FPGAs. The production of tracker modules is taking place in the TIFPA clean room. The Qualification Model (QM) of the tracker will be ready for Fall 2021.

Monte Carlo Simulation of the HEPD-02. Trento's group is in charge of developing the GEANT4 Monte Carlo simulation of HEPD-02. This work is crucial for a full characterisation of the detector response to charged particles. It will provide important information to the collaboration, already during manufacturing, assembling and integration. The software package has been designed to take as in-

put the CAD model of the detector and to give as output the signals produced by all sensitive modules of HEPD-02. The simulation allowed to estimate the detector performance and to validate the project against the specifications. Among the most relevant parameters to reproduce: particle identification, energy threshold, angular and energy resolution for different particles such as electrons, protons and heavier nuclei. The Monte Carlo simulation will also be the base for the event reconstruction package of HEPD-02, that will be based on a Deep-Learning model, much like the one for HEPD-01.

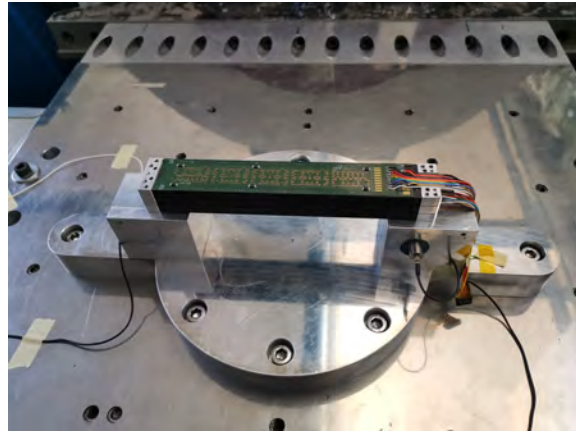


Figure 2: HEPD-02 tracker turret Engineering Model above the shaker for vibration tests.

Selected Papers

Piersanti, M., Materassi, M., Battiston, R., Carbone, V., Cicone, A., D'Angelo, G., Diego, P., and Ubertini, P. (2020). *Magnetospheric-Ionospheric-Lithospheric Coupling Model. 1: Observations during the 5 August 2018 Bayan Earthquake*. *Remote Sensing* **12**(20). Art. no.: 3299.

LISA Pathfinder e LISA

Daniele Bortoluzzi, Eleonora Castelli, Antonella Cavalleri, Davide Dalbosco, Edoardo Dalla Ricca, Rita Dolesi,[†] Valerio Ferroni, Renato Mezzena, Martina Muratore, Francisco Rivas Garcia, Giuliana Russano, Lorenzo Sala, Daniele Vetrugno, Davide Vignotto, Stefano Vitale, William Joseph Weber

Our current image of the Universe is essentially based on the observation of electromagnetic waves in a broad frequency spectrum. Much of the Universe, however, does not emit electromagnetic radiation, while everything interacts gravitationally. Despite being the weakest of the fundamental interactions, it is gravity that dominates the Universe on a large scale and regulates its expansion since the Big-Bang. As predicted by Einstein's General Relativity, gravity has its messenger: gravitational waves produced by massive accelerating bodies, such as coalescing black holes binaries or violent phenomena like stellar core collapse. Gravitational waves propagate at the speed of light, essentially undisturbed, bringing often not otherwise accessible information about events across all cosmic ages, from Cosmic Dawn to the present. The observation of gravitational waves promises to open new extraordinary perspectives for investigation of crucial issues like the nature of gravity in weak and in strong field regime, the nature of black holes, the formation and evolution of stellar binary system, the formation and evolution of cosmic structures since the earliest stages of the Universe.

The project of LISA (Laser Interferometry Space Antenna) is rapidly progressing toward the implementation of the first space-based observatory devoted to the low-frequency sources that can not be detected from ground. Einstein's theory describes gravity in terms of the curvature of space-time that is deformed by the passing of gravitational waves. These effect can be detected in space by measuring with great precision the relative acceleration of masses in free fall, i.e. reference masses subject to gravity field but well-isolated from other types of disturbing forces. The precursor space mission LISA Pathfinder measured the relative acceleration of two 2 kg test masses in near-perfect

geodesic motion, and its outstanding performance provided an experimental benchmark demonstrating the ability to realize the low-frequency science potential of the LISA mission. LISA consists of three identical satellite in a triangular constellation, with arms of several million km, orbiting around the Sun, shown in Fig. 1 with its strain sensitivity. It should allow for the observation of thousands of gravitational wave sources with high signal-to-noise, and in many cases very well characterized in terms of frequency, position in the sky, and luminosity distance. It targets massive sources emitting in the 0.1 mHz to 1 Hz band not accessible from ground due to the gravitationally noise terrestrial environment, ranging from stellar mass binaries in our own Galaxy to the merger of two galactic-core black holes, from 10^5 to 10^7 solar masses, from the recent Universe back to the epoch of the first galaxies.

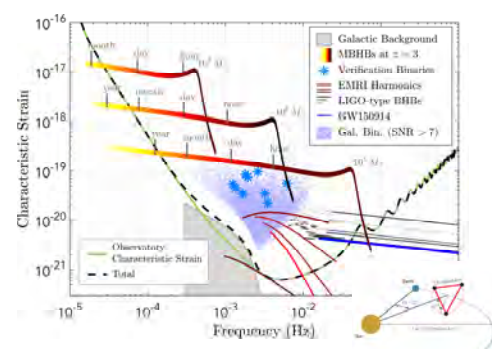


Figure 1: LISA's sensitivity curve plotted with the signal levels for several GW sources. In the insert a schematic of the LISA-concept.

The Trento Group, led by the Principal Investigator prof. Stefano Vitale, has contributed in a leadership role in all phases of the LISA PF mission, including hardware design and prototyping, laboratory torsion pendu-

[†]Contact Author: rita.dolesi@unitn.it

lum testing, scientific guidance of the industrial aerospace contractors, and finally to the design and operation of the flight measurement campaign.

LISA Pathfinder legacy consists in a LISA Gravitational Reference Sensor at TRL 9, a detailed physical model for parasitic forces close to quantitative demonstration at sub-femto-g level down to $20 \mu\text{Hz}$, a demonstration of local interferometry on free falling test-masses at tens of femto-m level down to mHz, the demonstration of drag-free satellite down to femto-g, the demonstration of gravitational balance, of test mass charge management system and of an in flight test mass releasing mechanism. Several papers documenting these performances has been published in 2020 (see p. 129) and others are still in preparation.

As internationally recognized leader in development and realization of systems of free-falling geodesic reference test masses for space based gravitational wave detector, the group TIFPA is currently working on the definition of the LISA instrument and guides the ASI development of the Gravitational Reference Sensor (GRS) system to guarantee the free fall of the geodetic reference masses that are at the heart of the instrument (for more information about LISA see <https://www.elisascience.org/>). The so called Phase A was extended until autumn 2021, aiming for the adoption of the mission by 2024 and launch around 2035. The progress of the activities was positively assessed by several progress meetings.

In addition, we are contributing on a number of other activities for LISA. We are playing a coordinating role in the simulation activities of the LISA space observatory, and the group is also working on the development of an alternative technique for calculating TDI (Time Delay interferometry) combinations. The group is involved in the activities of the INREP (Initial Noise Reduction Pipeline) group, in particular in the development of an independent verification pipeline for the construction of TDI variables. We are contributing to a catalog of instrumental artifacts (the “glitches” in the accelerating signal seen by LISA Pathfinder) that can be interfaced with the LISA simulator and to an

algorithm for inserting these artifacts into the phase signals of the simulator.

With regard to the issues related to the in-flight release of the test mass, the analysis of the tests carried out during the extended mission of Lisa Pathfinder continued, and the analysis of the dynamic response of the GPRM (Grabbing, Positioning, Release Mechanism) and of the effect of a collision between the test mass and the plunger.

Concerning the activities of the torsion pendulum facility, the verification campaign of the Test Mass discharge strategy with synchronized UV pulses continued, consolidating the results and the model that is guiding the definition and the verification strategies of the related requirements for LISA (see Fig. 2). Significant progress has also been made in simulating and modeling the behavior of the system in response to the distribution of UV light within the capacitive sensor as a function of several different operational conditions. As with LPF, the Trento torsion pendulum facility will be a vital instrument for targeted and representative tests that will validate the implementation of the LISA flight hardware from the design phase to the commissioning phases.

At the end of 2020, the three-year agreement for “Activities for phase A of the LISA mission” was signed between ASI, the Department of Physics of Trento and INFN, providing the core of the institutional context to which the Italian scientific community involved in LISA will refer.

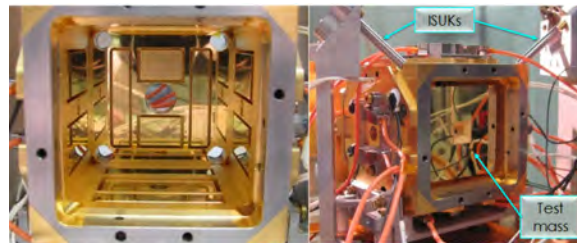


Figure 2: On the left, the capacitive sensor without one face to show its inner electrodes configuration (by OHB-Italy); on the right, a LISA-like test mass, which is part of the torsion pendulum inertial member, inside the capacitive sensor integrated with the UV ISUKs (Inertial Sensor UV Kit), that inject the UV light extracting photoelectrons needed to neutralize the Test Mass charged in space by cosmic rays

Quax

Paolo Falferi,[†] Renato Mezzena

The axion is a beyond-the-standard-model hypothetical particle predicted by S. Weinberg and F. Wilczek as a consequence of the mechanism introduced by R. D. Peccei and H. Quinn to solve the “strong CP problem”. Axions may have been produced in the early Universe by different mechanisms and may be the main constituents of galactic dark matter (DM) halos. Astrophysical and cosmological constraints, as well as lattice QCD calculations of the DM density, provide a preferred axion-mass window around tens of μeV . The experimental search of axions can be carried out with Earth-based instruments immersed in the Milky Way’s halo, which are therefore called “haloscopes” and rely on the inverse Primakoff effect to detect axion-induced excess photons inside a microwave cavity in a static magnetic field.

Differently from these, the QUAX experiment searches for DM axions through their coupling with the spin of the electron: the mode of a cylindrical cavity is coupled to spherical yttrium iron garnet (YIG, the best high-spin-density, narrow-linewidth material identified so far) samples placed on the axis of the cavity, where the rf magnetic field is uniform. The YIG samples are immersed in a static magnetic field to couple the axion field to the Kittel mode of uniform precession of the magnetization. The interaction yields a conversion rate of axions to magnons, which can be measured by searching for oscillations in the sample’s magnetization (Crescini et al. 2020).

Both of these experimental methods (with and without YIG spherical samples) need high quality factor cavities (the optimum value is approximately 10^6). The anomalous skin effect reduces the copper cavities quality factor at high frequencies (at 10 GHz $Q \leq 10^5$) while the “natural” solution represented by the superconducting cavity is hardly practical due to the presence of the strong magnetic fields.

A first solution to this problem is repre-

sented by the special type of hybrid superconducting cavity described in the 2019 TIFPA Activity Report in which the cavity is divided in two halves, each composed by a type II superconducting body (NbTi sputtered copper) and copper end caps. For $B = 2\text{T}$, the nominal field used in our axion search, we measured $Q = 4.5 \times 10^5$, a factor ≈ 5 better than a bulk copper cavity.

Another viable possibility is represented by the photonic cavities that is cavities in which a low-loss material with a high dielectric coefficient is inserted to shape and concentrate the mode, reducing the dissipation on the copper cavity walls and consequently increasing the quality factor.

Following this path (Alesini et al. 2020[c]), we designed a novel type of distributed Bragg reflector resonator working on the TM010-like mode at about 13.5 GHz in order to have the possibility of incorporating the resonator in the detection chain developed for the QUAX experiment.

The main idea was to design, using the code ANSYS Electronics for the electromagnetic calculations, a pseudocylindrical cavity realizing an interference pattern to confine the TM010 mode through long dielectric sapphire rods placed parallel to the cavity axis. Sapphire was chosen for its very low loss-tangent, going from about 10^{-5} , at room temperature, down to a fraction of 10^{-7} at cryogenic temperatures.

The distance among the 2 mm diameter sapphire rods was chosen to have the resonant frequency of the confined mode TM010 at around 13.5 GHz. The number of rods, 36, was chosen to have enough attenuation of the electromagnetic field toward the cavity outer wall.

To realize the cavity, two pieces of oxygen free high purity copper were machined to form two separate identical halves of the cavity (see Fig. 1). The inner surfaces were electro polished to reduce surface roughness. The two

[†]Contact Author: paolo.falferi@unitn.it

parts can then be joined together to form a closed cylinder.



Figure 1: The two halves of the copper cavity complete of sapphire rods.

Measurements have been performed at room temperature, liquid nitrogen temperature, and liquid helium temperature.

At room temperature we found, in agreement with the simulations, the resonance frequency of the TM₀₁₀ mode at 13495 MHz, linewidth 84 kHz, and unloaded quality factor 160000.

At liquid helium temperature the measured

resonance frequency is also in agreement with the simulations but the quality factor is considerably lower (290000 in comparison with 1100000). This discrepancy is due to a spurious peak that spoils the measured quality factor. In fact, the TM₀₁₁ mode, which does not have spurious peaks nearby, shows results in much closer agreement (520000 in comparison with the expected value of 770000), confirming the validity of the proposed scheme.

These cavities are ideal devices in the search for dark matter axions, where normal conducting ones are normally used. With the photonic cavity, an order of magnitude improvement of the quality factor is expected, while keeping the same detection volume. We are thus currently working to implement this new cavity type in our haloscope, and meanwhile, we are also studying other sapphire geometries that could boost the quality factor to even higher values.

Selected Papers

- Alesini, D., Braggio, C., Carugno, G., Crescini, N., D'Agostino, D., Di Gioacchino, D., Di Vora, R., Falferi, P., Gambardella, U., Gatti, C., Iannone, G., Ligi, C., Lombardi, A., Maccarrone, G., Ortolan, A., Pengo, R., Pira, C., Rettaroli, A., Ruoso, G., Taffarello, L., and Tocci, S. (2020[c]). *High quality factor photonic cavity for dark matter axion searches*. REVIEW OF SCIENTIFIC INSTRUMENTS **91**. Art. no.: 094701.
- Crescini, N., Alesini, D., Braggio, C., Carugno, G., D'Agostino, D., Di Gioacchino, D., Falferi, P., Gambardella, U., Gatti, C., Iannone, G., Ligi, C., Lombardi, A., Ortolan, A., Pengo, R., Ruoso, G., Taffarello, L., and Collaboration, Q. (2020). *Axion Search with a Quantum-Limited Ferromagnetic Haloscope*. PHYSICAL REVIEW LETTERS **124**. Art. no.: 171801.

Virgo

Albino Perego, Antonio Perreca, Giovanni A. Prodi,[†] Francesco Salemi, Sophie Bini, Andrea Grimaldi, Andrea Miani, Michele Valentini

During 2020 the LIGO Scientific Collaboration and Virgo Collaboration completed the third observing run (O3), a one calendar year long survey of the gravitational wave sky. The Virgo group at Trento focused on the upgrades planned for the next phase of Virgo detector, AdV+, and on the analysis and interpretation of O3 data.

INSTRUMENTAL SCIENCE

Trento is directly involved in two different upgrades of AdV+: the development of the new control strategy of the interferometer (required after the installation of the Signal Recycling mirror) and the upgrade of the quantum noise reduction strategies from a Frequency Independent to a Frequency Dependent injection of squeezed light.

Interferometer Sensing and Control (ISC) for AdV+. The activity of Trento group has been progressing in 2020 along the research line started in the previous year: we concluded the technical review of error signals for the longitudinal controls in dual recycled setup. Using the results of this review, we were able to start the analysis of longitudinal noise budget, i.e. the estimate of how the noises affecting the longitudinal control loops will affect the interferometer strain signal during the next observation run (O4). This requires the simulation of the couplings between different degrees of freedom in the new interferometer configuration and the design of new control loops to reduce these effects as much as possible. Moreover part of our team is directly involved with the on-site commissioning activities, focusing on the implementation of the new interferometer control strategy. This involves also the commissioning of the new Auxiliary Laser System using green light.

Frequency Dependent Squeezing (FDS) for AdV+. In 2020 the Quantum Noise Re-

duction group started all the preparatory work for the installation of the Frequency Dependent Squeezing system. In particular Trento is responsible for the design and installation of two optical benches that are used for the waveform sensing of the vacuum squeezed beam. These two subsystems will enable the measurement of the Mode Matching and the alignment of the squeezed light related to the main interferometer and to the optical Filter Cavity in AdV+. The measurement of the Mode Matching is based on a dedicated mode converter telescope and quadrants photodiodes, following a strategy developed with LIGO research groups. We have been testing and validating this technique for Virgo at the Laboratori Nazionali di Legnaro, INFN. In addition, we also started the design of an optical actuator for the active correction of optical mismatch of the squeezed light beam.

OBSERVATIONAL SCIENCE

Trento contributed to the successful completion of the observation run O3 (see www.gw-openscience.org) and to its scientific exploitation for what concerns the detection and interpretation of transient gravitational waves. The activities included methodological developments of the data analysis algorithms based on coherentWaveBurst (M. Drago et al. 2021) (see also [gwburst.gitlab.io](https://github.com/gwburst)).

Compact binary coalescences. Trento has been deeply involved in the analyses of the compact binary mergers detected in O3, when at least two detectors were in simultaneous observation. In particular, our main focus has been in the interpretation of the reconstructed waveforms of the gravitational waves, building on the data analysis methods of coherentWaveBurst (cWB).¹

A major LIGO-Virgo discovery based on cWB methods was the first observation of an intermediate mass black hole: a remnant

[†]Contact Author: giovanniandrea.prodi@unitn.it

¹Salemi, F. et al. (2019), Physical Review D **100**(4), Art. no.: 042003.

with mass $\sim 150M_{\odot}$ produced by the binary black hole merger GW190521 (R. Abbott et al. 2020c). Fig. 1 shows the reconstructed signal waveform: there are just a few observable signal cycles in the detectors' bandwidth and our minimally modeled data analysis methods did perform better than matched filter searches. GW190521 also provided the first experimental evidence of the existence of a black hole progenitor in the mass range $\sim 64\text{--}135M_{\odot}$, which is predicted not to be formed in collapse supernovae because of (pulsational) pair-instability.

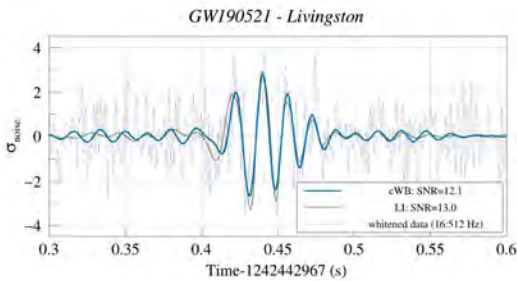


Figure 1: sample cWB reconstruction of GW190521, the first detection of an Intermediate Black Hole (from gwburst.gitlab.io).

In the case of GW190814, the merger event with the largest mass ratio between progenitors detected so far, cWB methods confirmed the detection of higher-order multipolar modes, on top of the dominant quadrupolar emission (R. Abbott et al. 2020d). Fig. 2 shows the coherent power in excess of at frequencies 1.5 larger than the main chirp, corresponding to the $l = 3$ and $m = 3$ mode.

Searches for gravitational wave bursts.

In 2020, the other main task of Trento has been

Selected Papers

- Abbott, R. et al., LIGO Scientific Collaboration and Virgo Collaboration (2020c). *GW190521: A Binary Black Hole Merger with a Total Mass of 150 M_{\odot}* . *Physical Review Letters* **125**(10). Art. no.: 101102.
- LIGO Scientific Collaboration and Virgo Collaboration (2020d). *GW190814: Gravitational Waves from the Coalescence of a 23 Solar Mass Black Hole with a 2.6 Solar Mass Compact Object*. *The Astrophysical Journal Letters* **896**(2). Art. no.: L44.
- Drago, M., Klimentko, S., Lazzaro, C., Milotti, E., Mitselmakher, G., Nacula, V., O'Brian, B., Prodi, G. A., Salemi, F., Szczepanczyk, M., Tiwari, S., Tiwari, V., V. G., Vedovato, G., and Yakushin, I. (2021). *coherent WaveBurst, a pipeline for unmodeled gravitational-wave data analysis*. *SoftwareX* **14**. Art. no.: 100678.

the analysis of O3 data searching for gravitational wave transients of short duration and unmodeled waveform. This search monitored the full bandwidth of sensitivity of the LIGO and Virgo detectors, from 24 Hz to 4 kHz and results will be presented in 2021.

In addition, Trento continued to develop new methods to search for possible weak features, associated to gravitational wave detections. In particular, we focused on methods to search for possible gravitational wave emissions following closely a binary black hole coalescence. Depending on their morphological properties, such weak signals would either hint to unexpected remnant properties, in violation of the no-hair theorem for black holes, or to the highly non-linear dynamics of asymmetric event horizons.

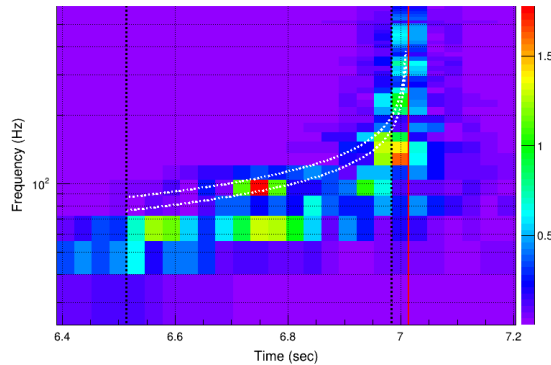


Figure 2: GW190814: reconstruction of time-frequency residuals by cWB after subtraction of the dominant quadrupolar emission. Higher order mode power is visible within the dotted white curves.

Activities starting in 2021

ET_ITALIA

Research outline High laser power is a critical point to achieve the expected sensitivity of Einstein Telescope (ET). However, the use of high power requires studies on the effect of the deformation of the optics caused by high temperatures. Deformations of optical surfaces reduce the couplings of the laser light with the optical cavities compromising the expected sensitivity. The experience gained with current gravitational wave detectors leads to the need of monitoring, sensing and correct for deformations of the optics.

The group in Trento is involved in modelling and optimizing the design of the detector. Starting from 2021, the group plans to extend the sensing of the mode-matching with the technique of the mode-converter, currently under development for Virgo (@ 1064 nm), at a wavelength of 1550 nm. The design and the realization of the technique will start by the end of the year. There will also be the design and development of an adaptive optics prototype for 1550 nm wavelength required for compensating deformations induced by laser light.

Furthermore, sensitivity for different configurations and topologies will be studied. In particular, the filtering cavities and strategies of mode-mismatch sensing will be the focus of a numerical simulation study.

The group will also focus its activities on the scientific case. In particular:

- Formation of neutron stars, binary systems and gravitational wave transients.
- Data analysis methods and tools for searching for gravitational wave bursts in an observatory, including ET.
- Feasibility of extending the methods used in the LIGO-Virgo-Kagra observatory.
- Characterization of the post-fusion signal of Neutron Star binary mergers.
- Multimessenger signals from near and far sources.

INFN groups Cagliari, GSGC, LNS, Napoli, Padova, Perugia, Pisa, Roma I, Salerno, Firenze, Genova, Roma II, Roma III, TIFPA

Principal Investigator Michele Punturo (Perugia)

TIFPA team Antonio Perreca (coordinator), Giovanni Prodi, Albino Perego, Francesco Salemi

XRO

Research outline The new XRO (X-Ray Observatories) project brings together the activities of the two projects IXPE Imaging (X-Ray Polarimetry Explorer) and eXTP (enhanced X-ray Timing and Polarimetry). The TIFPA group activity is focalised on the eXTP Mission.

The enhanced X-ray Timing and Polarimetry mission (eXTP) is a science mission designed to study the state of matter under extreme conditions of density, gravity and magnetism. Primary goals are the determination of the equation of state of matter at supra-nuclear density, the measurement of QED effects in highly magnetised star, and the study of accretion in the strong-field regime of gravity. Primary targets include isolated and binary neutron stars, strong magnetic field systems like magnetars, and stellar-mass and supermassive black holes

The mission carries a unique and unprecedented suite of state-of-the-art scientific instruments enabling for the first time ever the simultaneous spectral-timing-polarimetry studies of cosmic sources in the energy range from 0.5-30 keV (and beyond). Key elements of the payload are:

- the Spectroscopic Focusing Array (SFA): a set of 9 X-ray optics operating in the 0.5-10 keV energy band with a field-of-view (FoV) of 12 arc-min each and a total effective area of 0.8 m² and 0.5 m² at 2 keV and 6 keV respectively. The telescopes are equipped with Silicon Drift Detectors offering <180 eV spectral resolution.
- The Large Area Detector (LAD): a deployable set of 640 Silicon Drift Detectors, achieving a total effective area of 3.4 m² between 6 and 10 keV. The operational energy range is 2-30 keV and the achievable spectral resolution better than 250 eV. This is a non-imaging instrument, with the FoV limited to <1° FWHM by the usage of compact capillary plates.
- The Polarimetry Focusing Array (PFA): a set of 4 X-ray telescope, achieving a total effective area of 900 cm² at 2 keV, equipped with imaging gas pixel photoelectric polarimeters. The FoV of each telescope is 12 arcmin and the operating energy range is 2-10 keV.
- The Wide Field Monitor (WFM): a set of 3 coded mask wide field units, equipped with position-sensitive Silicon Drift Detectors, covering in total a FoV of 3.7 sr and operating in the energy range 2-50 keV.

The eXTP international consortium includes major institutions of the Chinese Academy of Sciences and Universities in China, as well as major institutions in several European countries and other International partners. The strong European participation has significantly enhanced the scientific capabilities of eXTP. The planned launch date of the mission is 2027.

The TIFPA group takes part in the development of the Large Area Detector (LAD), and the Wide Field Monitor (WFM). In particular, we are involved in:

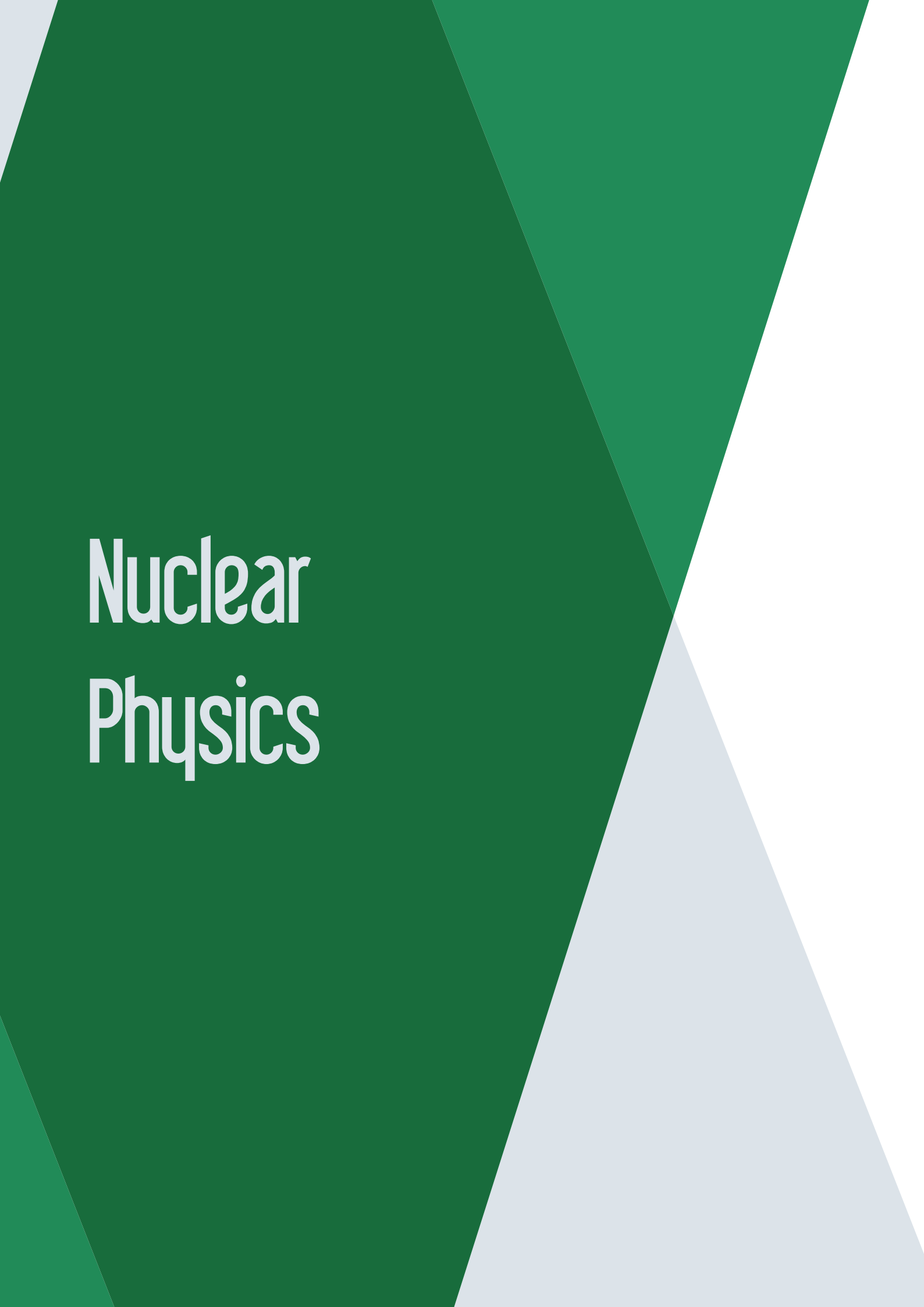
- Participation in the electrical characterisation of LAD sensors
- Optical inspection of LAD sensors
- Defect classification
- Definition of yield
- Definition of the acceptance parameters of the sensors
- Definition of process and material parameters through the characterisation of the test structures
- Contribution to the design of WFM
- Definition of the test procedure and electrical characterisation of WFM

involved external institutions ASI, FBK, INAF IASF-Milano, INAF/OAS-Bologna

INFN groups Trieste, Pisa, Torino, Milano, Pavia, Bologna, TIFPA, Perugia, Roma Tor Vergata.

Principal Investigator Walter Bonvicini (Trieste)

TIFPA team Irina Rashevskaya (coordinator), Antonino Picciotto, Giacomo Borghi, Francesco Ficorella, Nicola Zorzi



Nuclear Physics

AEGIS (Antimatter Experiment: gravity Interferometry Spectroscopy)

Sebastiano Mariazzi, Ruggero Caravita, Luca Povolo, Marco Volponi, Luca Penasa, Marco Bettonte, Roberto S. Brusa[†]

The main goal of the experiment AEGIS at CERN is the measure of the free fall of antihydrogen (\bar{H}) in the Earth gravitational field. The design of the experiment foresees:

- (i) the efficient pulsed production of antihydrogen atoms in Rydberg states by charge exchange between trapped antiprotons (\bar{p}) and positronium (Ps) excited in Rydberg states;
- (ii) the formation of an antiatom beam by acceleration of \bar{H} in Rydberg states by Stark acceleration and, in case, the optical de-excitation into their ground state;
- (iii) the horizontal launch of the beam through a moiré deflectometer consisting of two gratings and a high spatial resolution detector;
- (iv) the measurement of its vertical displacement.

The measurement of the free fall of antimatter atoms (\bar{H}) or of pure leptonic antimatter-matter system (Ps) would allow a test of the weak equivalent principle.

Results before the Long Shutdown 2 at CERN. In 2018 AEGIS has achieved the first pulsed production of antihydrogen by charge exchange and the data have been analysed, validated and recently published (Amsler et al. 2021), see Fig. 1. To reach this first important step towards the free fall measurement with a beam of antimatter, many new technical and scientific advances were necessary and obtained.

[†]Contact Author: robertosennen.brusa@unitn.it

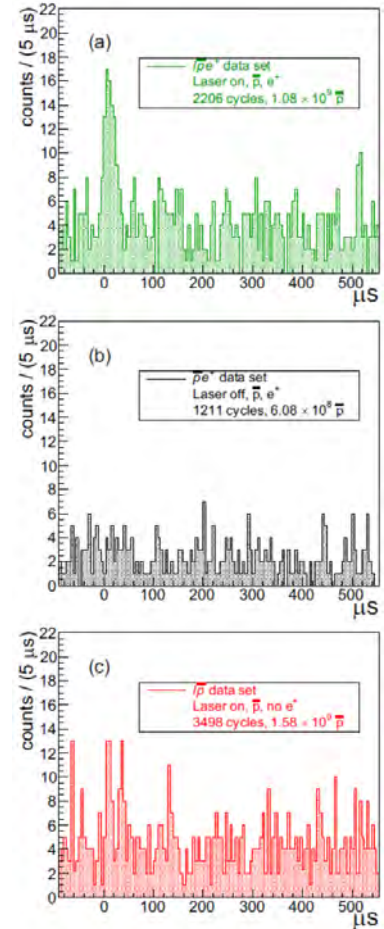


Figure 1: Time distribution of detected pulses in plastic detectors. a) excess of counts due to \bar{H} formation: laser on for Ps excitation, \bar{p} in the trap, e^+ on for Ps formation. Background: b) laser off, \bar{p} and e^+ on. c) laser on, \bar{p} on, e^+ off. Note that the counts must be normalized to the number of cycles: the counts in c) are reduced by a factor of ~ 1.5 and those in b) are increased by a factor of ~ 1.7 to respect counts in a). From Amsler et al. (2021).

The procedure for trapping and compression of antiprotons was optimized. Two new detectors were implemented: one based on optical fibers for detection of pions and ones for

high resolution diagnostic of the produced Ps in Rydberg states. A high yield nanostructured positron-positronium converter for the production of collisional cooled Ps in vacuum was developed and engineered. The first excitation of Ps with the two steps process, $1^3S \rightarrow 3^3P$ Ps and the $3^3P \rightarrow$ Rydberg, was demonstrated and implemented. Manipulation of Ps in electric and magnetic fields was experimentally performed by means of the production of Ps in the long lived 2^3S metastable level. The production of Ps, its excitation and its velocity distribution were fully characterized in the formation region of antihydrogen in the high 1T magnetic field (Antonello et al. 2020), Fig. 2.

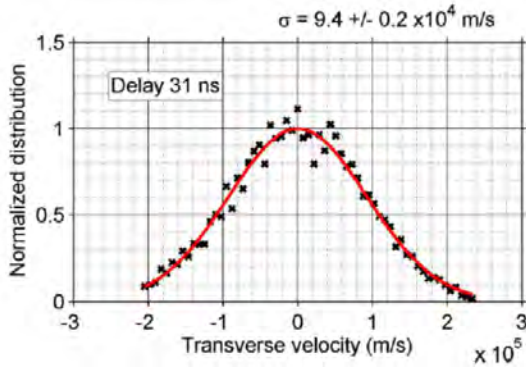


Figure 2: Doppler scan with the UV laser in the \bar{H} zone formation: plot of transverse Ps velocity. From Antonello et al. (2020).

AEgIS 2020. In Autumn 2021, the new decelerator ELENA at CERN will deliver antiprotons at 100 keV to the experiments allocated at the AD hall. AEgIS collaboration has updated the roadmap towards the \bar{H} free fall with an improved design of the experiment. The 2020 year was dedicated to the upgrading of the apparatus. The two main changes regarded the antiproton catching region and the antihydrogen formation region. The antiproton catching region was set in construction at the CERN

machine shop: due to the lower energy of the antiprotons delivered by ELENA, thin films are necessary to degrade antiprotons to an energy suitable (<10 keV) to be trapped by AEgIS. The choice for the thin films was Parylene (C_8H_8), a low Z material, assembled in two foils 1600 nm+300 nm, with the first foil metalized in four sector to allow monitoring the beam position. The new geometry design, chosen for the \bar{H} formation region, determined the primary technological changes. It allows to increase the overlap between the antiproton and the excited Ps clouds, to excite Ps in higher Rydberg states avoiding ionization due motional Stark effect because its velocity is mainly parallel to the magnetic field; to have the possibility to ionize the antihydrogen atoms near the formation zone for characterizing their Rydberg states; to simplify the design of the trapping electrodes gaining free volume for inserting a grating deflectometer in 1T homogeneous region. Some of these improvements go in the direction to increase the cross section of the charge-exchange reaction and consequently the number of formed antiatoms. The antiprotons trap has been designed with fine adjustments of the alignment using three cryogenic actuators which work in UHV and cryogenic (10 K) environment. The impulse signals to electrodes is given through filters compatible with cryogenic and UHV. Taking advantage of the long shutdown, many infrastructure interventions were started in the AEgIS experimental zone, as a new laser hut to allocate the four lasers for excitation and laser cooling of Ps. Because ELENA, when in full operation, will supply antiprotons twenty-four hours a day, a full automatization and remote control of the system is going to be achieved with a new software and with Sinara, an open-source hardware for quantum physics running the ARTIQ control software.

Selected Papers

- Amsler, C. et al., AEgIS collaboration (2021). *Pulsed production of antihydrogen*. *Comm. Phys.* **4**, p. 19.
- Antonello, M. et al., AEgIS collaboration (2020). *Rydberg-positronium velocity and self-ionization studies in a 1T magnetic field and cryogenic environment*. *Phys. Rev. A* **102**. Art. no.: 013101.

FOOT

Sofia Colombi and Francesco Tommasino,[†] on behalf of the FOOT collaboration

The FragmentatiOn Of Target (FOOT) project (Battistoni et al. 2021) is a nuclear physics experiment aiming to perform fragmentation studies of relevance for particle therapy and radioprotection in space. The FOOT experiment has been designed to measure with $\sim 5\%$ accuracy double differential fragmentation cross sections, i.e. with respect to the kinetic energy and the generation angle of the emitted fragments.^{1,2} FOOT is based on two complementary experimental setups: an electronic setup based on a magnetic spectrometer to identify fragments heavier than helium, and a setup exploiting the emulsion chamber capabilities to detect the light charged fragments ($Z \leq 4$). The electronic setup consists in a pre-target monitor region, a magnetic spectrometer, a scintillator detector with ΔE and Time-Of-Flight (*TOF*) capabilities and a calorimeter. The pre-target region is composed of a thin plastic scintillator Start Counter (SC) detector and a Beam Monitor (BM) drift chamber, which monitor the number of primary ions and the beam direction, respectively. The magnetic spectrometer provides instead production vertex and momentum (p) of the fragments. It consists in two cylindrical permanent magnets (PM), four pixel sensors of Vertex (VTX) detector placed between target and PM, two additional planes of pixel sensor detectors (ITR) placed in between the two PM and three layer of Microstrip Silicon Detector (MSD) placed beyond the second magnet. The downstream region is composed of two orthogonal planes of plastic Scintillator bars (i.e. the *TOF* Wall (TF)) and BGO calorimeter (CAL) to provide the stop signal for the *TOF* evaluation, the measurement of the fragments energy loss and kinetic energy (ΔE and E_{kin} , respectively). The TW and BGO are placed at about 1 m from the target center-of-mass rest frame in the case of a primary beam energy of 200 MeV/u, while at 700 MeV/u their position is moved downstream to about 3 m in order

to have the same angular acceptance. A detailed description of all the detectors involved in the electronic setup, as well as the emulsion spectrometer can be found in Battistoni et al. (2021).

The FOOT measurement campaigns will include beams of ^4He , ^{12}C , ^{16}O in the energy range spanning between 200 MeV/u and 700 MeV/u impinging on thin C, C_2H_4 and Al targets. A performances study of the electronic setup based on FLUKA Monte Carlo simulations and a preliminary analysis of experimental data collected in 2019 were the core activities of the TIFPA unit of the FOOT experiment during 2020.

The study of fragment reconstruction capability of the FOOT experiment has been performed based on the experimental-like data samples obtained by applying the experimental resolutions on *TOF*, ΔE , E_{kin} and p to the corresponding quantities produced by the FLUKA simulations. The charge identification and the mass evaluation through a χ^2 minimization procedure assure a complete isotopic identification of each fragment generated in the beam-target interaction. The present detectors performances (i.e., $\sigma(\text{TOF}) \simeq 70$ ps, $\sigma(p)/p \simeq 3.7\%$ and $\sigma(E_{kin})/E_{kin} \simeq 1.5\%$) allow identifying fragment charge with a precision spanning from $\sim 6\%$ for hydrogen to $\sim 2\%$ for oxygen and the fragment number of mass with a resolution ranging between $\sim 3.5\%$ and $\sim 4.5\%$, both for particles identified at primary beam energies of 200 MeV/u and 700 MeV/u. An example of mass number determination retrieved with a χ^2 minimization method is reported in Fig. 1 for the carbon fragments generated in the interaction of a 200 MeV/u oxygen beam with a polyethylene target. The isotopes separation is clearly visible. A fit with a superposition of several Gaussian functions is applied to the mass distribution, in order to evaluate each isotope yield, mass and relative resolution.

[†]Contact Author: francesco.tommasino@unitn.it

¹Battistoni, G. et al. (2017), PoS **BORMIO2017**, Art.no.: 023.

²Patera, V. et al. (2017), PoS **INPC2016**, p. 128.

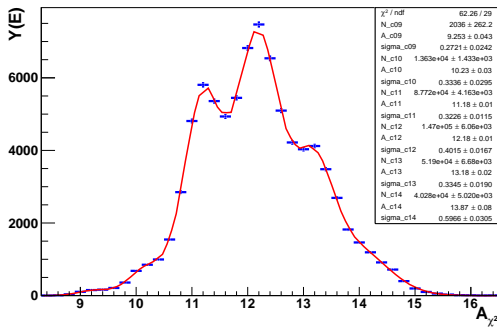


Figure 1: Example of mass number determination obtained through a χ^2 fit for the carbon fragments produced when a 200 MeV/u ^{16}O beam impinges on a 5 mm C_2H_4 target. The isotopes separation refers to the case of $\sigma(\text{TOF})=70$ ps, $\sigma(p)/p=3.7\%$, $\sigma(E_{kin})/E_{kin}=1.5\%$. In particular, peaks associated to ^{11}C , ^{12}C , ^{13}C are clearly visible. Blu dots represent the reconstructed values and the red line is the fitting function composed of the superposition of six Gaussian function.

A performance study has been performed by varying the resolution on TOF , p and E_{kin} , in order to understand which detectors mostly affect the precision on the mass number determination and the cross sections evaluation with respect to the MC prediction. The results show that the dependence on the TOF precision is much stronger than the influence of p and E_{kin} resolutions.

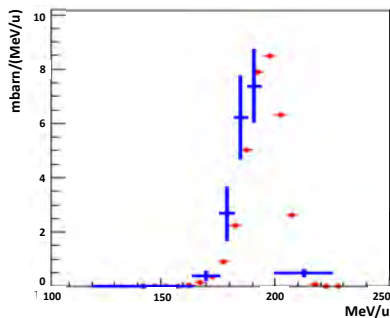


Figure 2: Example of comparison between the MC (red dots) and reconstructed (blue dots) differential cross sections as a function of the fragment kinetic energy for ^{12}C produced in the interaction of a 200 MeV/u ^{16}O beam with a 5 mm C_2H_4 target.

Selected Papers

Battistoni, G. et al. (2021). *Measuring the Impact of Nuclear Interaction in Particle Therapy and in Radio Protection in Space: the FOOT Experiment*. *Frontiers in Physics* **8**, p. 555.

A feasibility study of the differential cross sections with respect to the kinetic energy of each carbon isotope generated in the beam-target interaction have been evaluated with only MC data and afterwards compared with the MC prediction. Fig. 2 reports an example of comparison between the true and reconstructed cross section evaluated for ^{12}C fragments produced with only MC events in the interaction of a 200 MeV/u ^{16}O beam impinging on a polyethylene target. For all the targets and energies investigated, the results on the total cross section are compatible within the uncertainties with the MC predictions.

Experimental data collected in April 2019 at the GSI Helmholtz Center for Heavy Ion Research (GSI) with a 400 MeV/u ^{16}O beam impinging on a 5 mm graphite target have been analyzed to perform the first FOOT fragments charge separation based on real data. The plot reported in Fig. 3 shows that different charged fragments can be well discriminated, providing very encouraging results for future experimental campaigns foreseen in 2021.

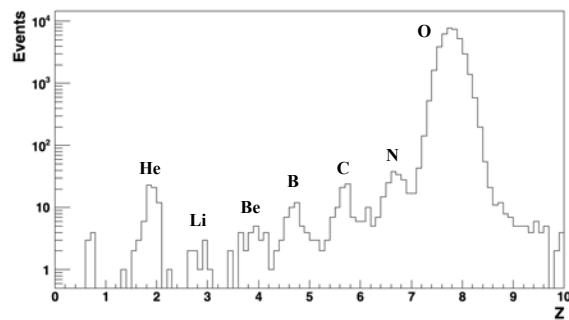


Figure 3: Charge spectra obtained from the fragmentation of 400 MeV/u ^{16}O ions beam on a graphite target. The Oxygen peak is due to not interacting beam nuclei.

In addition to the data analysis, the TIFPA unit of the FOOT experiment took part to the data acquisition at GSI in February 2020. Specifically, the BM and the SC have been employed to monitor the number of particles delivered to the emulsion spectrometer and to verify the irradiation pattern of Carbon ion beam at 700 MeV/u.

Activities starting in 2021

PANDORA_Gr3

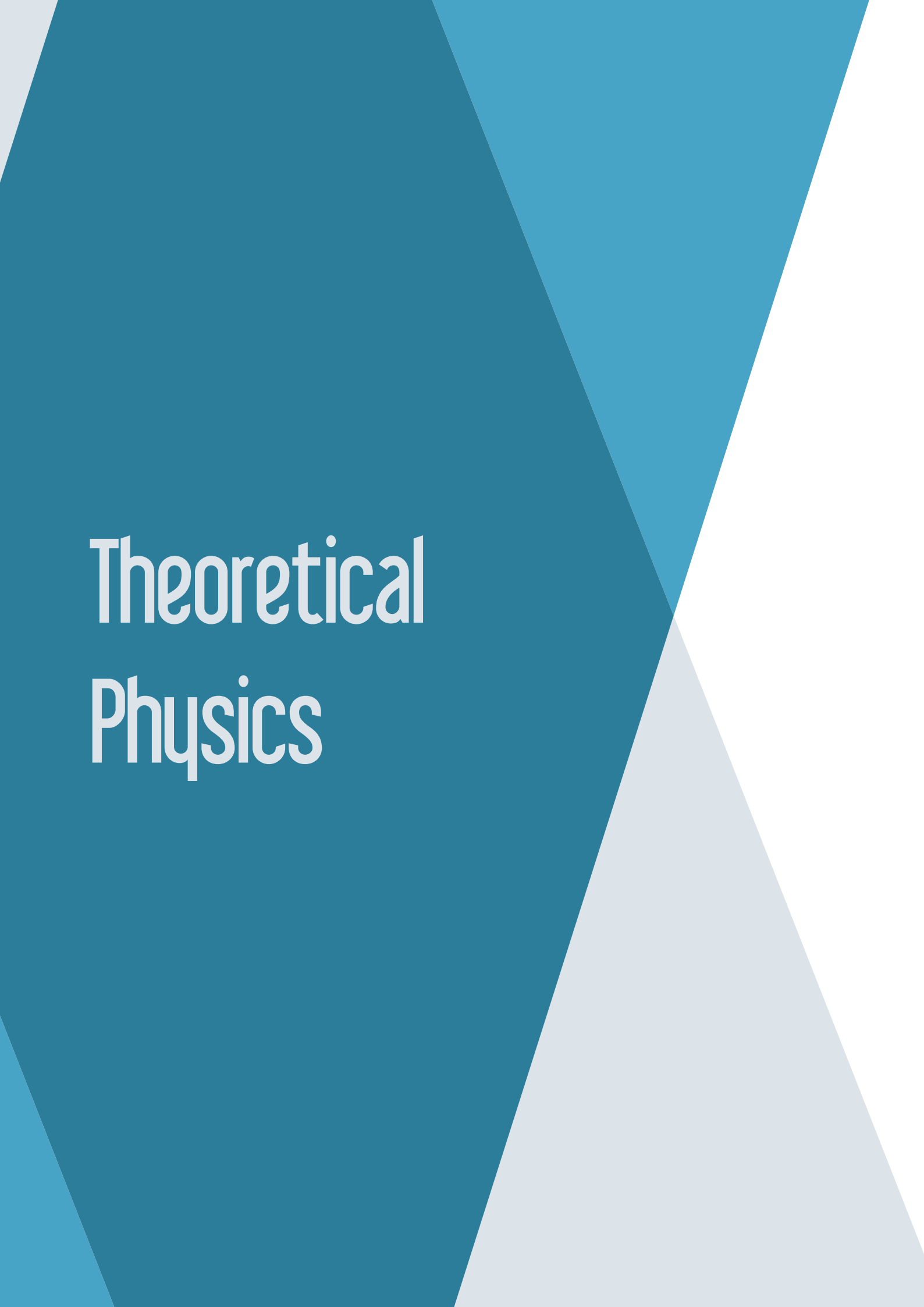
Research outline PANDORA_Gr3 aims to construct a new plasma trap designed to perform interdisciplinary research, equipped with a multidiagnostic setup to monitor plasma parameters and using an array of High purity Germanium (HPGe) detectors to measure in-plasma β -decays. The main goal is to carry out, for the first time in a magnetized plasma, beta decay rate measurements of nuclei relevant for astrophysics, as a function of the ionization state. The basic idea of PANDORA_Gr3 is that a compact plasma trap can be used to study the properties of radionuclides, undergoing β^\pm decay or electron capture, in an environment where plasma parameters (density, temperature and charge state distribution (CSD)) are fully under control. The CSD can be modulated according to the RF power sustaining the plasma, the magnetic field strength, the background pressure, etc. This will allow to characterize beta decay rates with respect to the CSD variation, i.e. versus the plasma density and temperature, in a stellar-like condition at least as it concerns the CSD (e.g. like in the stellar cores or resembling primordial nucleosynthesis conditions). Beta decay rates will be evaluated through the detection of the γ -rays emitted by the daughter nuclei in the plasma. An array of high efficiency HPGe detectors placed around the magnetic trap will be used to detect the γ -rays. Finally, theoretical simulations of β -decay and electron capture estimates via an ad-hoc implemented relativistic model will be compared against experimental measurements.

involved external institutions Fondazione Bruno Kessler (ECT*); Università di Perugia; CNR-IBAM; INAF; Hungarian Academy of Sciences; CNRS-LPSC, Grenoble (France); GANIL (France); Max Plank Institute IPP, Garching (Germany); Università di Camerino; ENEA Bologna.

INFN groups Laboratori Nazionali del Sud, Sezione di Perugia, Laboratori Nazionali di Legnaro, Sezione di Bologna, TIFPA

Principal Investigator David Mascali, Laboratori Nazionali del Sud, Catania

TIFPA team Simone Taioli (coordinator), Giovanni Garberoglio, Paolo Emilio Trevisanutto, Samuel Giuliani, Maurizio Dapor



Theoretical Physics

BELL

Valter Moretti,[†] Enrico Blanzieri, Nicolò Drago, Riccardo Ghiloni, Sonia Mazzucchi, Alessandro Perotti, Davide Pastorello, Daniele Volpe, Chris van de Ven

BELL research group at TIFPA studies various foundational, axiomatic and mathematical topics of Quantum Theories, also in relation with quantum field theory, quantum gravity, and quantum information and computing and associated technological problems. Mathematical advanced technologies are in particular exploited to solve difficult problems of theoretical physics or to construct physically significant, non-trivial, mathematical models, completely solvable which can be used as starting points for physical applications. During 2019-2020 we published several research papers on international research journals, two monographies and we also filed a patent on quantum technologies. Just to have a (not exhaustive) look of our intensive production we focus attention on four relevant papers about four corresponding topics of mathematical methods for physics.

Quantum Information and related technology In Pasini et al. (2020), by S. Pasini, N. Leone, S. Mazzucchi, V. Moretti, D. Pastorello, L. Pavesi, we studied an experiment (also performed) about the use of single-particle entanglement with an important technological impact. In single-particle or intraparticle entanglement, two degrees of freedom of a single particle, e.g., momentum and polarization of a single photon, are entangled. Single-particle entanglement (SPE) provides a source of non classical correlations which can be exploited both in quantum communication protocols and in experimental tests of noncontextuality based on the Kochen-Specker theorem. Furthermore, SPE is robust under decoherence phenomena. Here, we show that single-particle entangled states of single photons can be produced from attenuated sources of light, even classical ones. To experimentally certify the entanglement, we perform a Bell test, observing a violation of the Clauser, Horne, Shimony and Holt (CHSH) in-

equality. On the one hand, we show that this entanglement can be achieved even in a classical light beam, provided that first-order coherence is maintained between the degrees of freedom involved in the entanglement. On the other hand, we prove that filtered and attenuated light sources provide a flux of independent SPE photons that, from a statistical point of view, are indistinguishable from those generated by a single photon source. This has important consequences, since it demonstrates that cheap, compact, and low power entangled photon sources can be used for a range of quantum technology applications. The authors of this paper are also the owner of a patent regarding the involved technology “Device for the generation of single photon entangled states” (Priority Number 102020000005521, Priority Date 16/03/2020).

Foundational Aspects of Quantum Theories In N. Drago et al. (2020), by N. Drago, S. Mazzucchi, and V. Moretti, the existence of a real linear-space structure on the set of observables of a quantum system – i.e., the requirement that the linear combination of two generally non-commuting observables A, B is an observable as well – is a fundamental postulate of the quantum theory yet before introducing any structure of algebra. However, it is by no means clear how to choose the measuring instrument of the composed observable $aA + bB$ if such measuring instruments are given for the addends observables A and B when they are incompatible observables. A mathematical version of this dilemma is how to construct the spectral measure of $f(aA + bB)$ out of the spectral measures of A and B . The paper presents such a construction with a formula which is valid for generally unbounded selfadjoint operators A and B , whose spectral measures may not commute, and a wide class of real-valued functions f . We

[†]Contact Author: valter.moretti@unitn.it

proved that, in the bounded case the Jordan product of A and B can be constructed with the same procedure out of the spectral measures of A and B . The formula turns out to have an interesting operational interpretation and, in particular cases, a nice interplay with the theory of Feynman path integration and the Feynman-Kac formula.

In Pastorello (2020), D. Pastorello studied the link between fuzzy logic and the geometric formulation of Quantum Theories. Within the Hamiltonian framework, the propositions about a classical physical system are described in the Borel σ -algebra of a symplectic manifold (the phase space) where logical connectives are the standard set operations. Considering the

geometric formulation of quantum mechanics we give a description of quantum propositions in terms of fuzzy events in a complex projective space equipped with Kähler structure (the quantum phase space) obtaining a quantized version of a fuzzy logic by deformation of the product t -norm.

Another interesting paper is Moretti and van de Ven (2020) where V. Moretti and C.J.F. van de Ven studied some features of quantization maps related with the physically relevant Curie-Weiss model. This paper proves that there is a nice interplay between a pair of quantization maps dealing with coherent spin states. One model is constructed on the 3D unit sphere and the other on the boundary of that sphere.

Selected Papers

- Drago, N., Mazzucchi, S., and Moretti, V. (2020). *An operational construction of the sum of two non-commuting observables in quantum theory and related constructions*. Lett. Math. Phys **110**.
- Moretti, V. and van de Ven, C. (2020). *Bulk-boundary asymptotic equivalence of two strict deformation quantizations*. Lett. Math. Phys **110**, p. 303.
- Pasini, S., Leone, N., Mazzucchi, S., Moretti, V., Pastorello, D., and Pavesi, L. (2020). *Bell inequality violation by entangled single photon states generated from a laser, a LED or a Halogen lamp*. Phys. Rev. A **102**.
- Pastorello, D. (2020). *Geometric viewpoint on the quantization of a fuzzy logic*. Int J Geom Meth Modern Phys **17**(13).

BIOPHYS

Pietro Faccioli,[†] Gianluca Lattanzi, Raffaello Potestio, and Luca Tubiana

Exploration of the model space of a biomolecule (R. Potestio). The first step in the construction of a coarse-grained model of soft and biological matter systems consists in the definition of the mapping, that is, a function that transforms coordinates of atoms in the high-resolution representation of the molecule into those of the (fewer) effective interaction centres of the simpler model (Giulini et al. 2020).

A very simple choice of mapping is that of selecting, out of the n atoms, a subset of $N < n$ ones, and retain only those. This apparently innocent operation hides a tremendous statistical complexity: for a protein of 30 amino acids, the number of possible atom subsets is about 10^{162} . All these representations constitute the mapping space, that is, the space of all possible ways of selecting a subset of atoms in the molecule. To make sense of this immense wealth of models, we developed mathematical tools to explore the mapping space: specifically, we introduced a notion of distance between mappings in order to quantify their difference, and employed it to sample the space exhaustively. For this latter purpose, we developed a novel approach that combines an enhanced sampling technique - the Wang-Landau method - with deep neural networks. In this work we have thus shown that it is possible to “teach” a neural network to compute a function that takes as input a protein structure as a whole, thereby replacing complicated ensemble averages over a large amount of configurations; and we thoroughly characterized the mapping space, shedding new light on molecular structures and their functional implications.

Knotted (bio-)polymers (L. Tubiana) Much like shoelaces and strings, polymeric filaments such as DNA and proteins can self-entangle and become knotted, with measurable consequences on their physical properties and biological functions. In particular, knots are known

to hinder DNA transcription and replication, and are prevented, in vivo, by a class of enzymes which cut and reconnect DNA to keep it disentangled. Knots appear frequently in polymers subjected to compression, and have been observed in single-molecule experiments on DNA. Using coarse-grained approaches to model DNA both in vivo and in vitro, we are studying the relation between knots and DNA properties such as supercoiling, and the activity of topoisomerases. Particular attention is devoted to the interaction between knots and their consequences for single-molecule DNA sequencing experiments.

Supramolecular smart topological materials (L. Tubiana) Smart materials are designed materials whose properties can be controlled through external stimuli. A particularly fascinating line of research takes inspiration from naturally existing systems to develop them. A significant example is that of kinetoplast DNA, the mitochondrial genome of Trypanosomatids, which is constituted by a network of thousands of interlocked DNA minirings, and whose mechanical properties include a variation in size of a factor 100, as well as the possibility to actively control its elastic properties through the activity of topoisomerases. Using advanced molecular dynamics simulation schemes and analyses pipelines, we are working to characterize the effects of topology on the global properties of such systems. Recent results from our group show that, remarkably, in a closed system like a 2D sheet or a closed catenane of rings, local changes in the arrangement of the interlocked rings can completely reshape the global properties of the system, particularly its torsion and size. The implications of these results range from molecular biology to supramolecular chemistry and material science.

Target Search by Active Particles (P. Faccioli) Active particles are constantly out of equilibrium systems that can bring important in-

[†]Contact Author: pietro.faccioli@unitn.it

sight into many biological problems including, e.g., bacterial motion. In 2020 our unit completed a first project in this new research line. In this work, we demonstrated that, contrary to what was previously believed in the community, it is possible to develop an efficient and rigorous transition path sampling algorithm for active Brownian particles, in spite of the fact that the dynamics of these "micro-swimmers" is constantly out of equilibrium and violates detailed balance conditions. The analysis of the target search patterns obtained by simulations revealed intriguing counterintuitive behavior.

Investigating Rare Bio-molecular Transitions by Quantum Computing (P. Faccioli)

In 2020, we have started a new research line aiming at exploiting quantum technologies (in particular quantum annealers) to efficiently perform simulation of rare biomolecular transitions. The key element of our quantum algorithm is to represent the molecular transformation as a high-dimensional network. The molecular dynamics then becomes mapped to the task of finding the shortest path through this network. In a second step, we cast this problem into a form amenable for implementations in quantum annealers. Detailed numerics and first tests on a D-Wave quantum annealer have suggested that the path sampling problem can be efficiently solved using quantum technologies. Our approach represents a new paradigm and showcases the potential that modern quantum computers can have in the field of computational biophysics (Hauke et al. 2021).

Applications to Pharmacology and Drug Discovery (P. Faccioli)

Using the computational techniques developed in house, we can accurately reconstruct the folding mechanism of biologically relevant proteins. In previous years, this technological advancement enabled us to develop and patent an entirely new approach to Rational Drug Discovery denominated Pharmacological Protein Inactivation by Folding Intermediate Targeting (PPI-FIT). This scheme is based on identifying small molecules which can bind to folding intermediates, thus preventing the protein to reach its biologically active state. In 2020, we completed a large number of validation studies leading to a publication in a journal of Nature Publishing Group (Spagnolli

et al. 2021b). Furthermore, in response to the COVID-19 pandemic, we have joined forces with INFN and Sibylla Biotech SRL to use the PPI-FIT protocol for a drug repurposing campaign. This study led to the largest protein folding simulation ever performed and to identifying a drug capable of blocking the SARS-COV-2 viral infection in cell colonies.

Crystallization of Protein Folding Intermediates in Micro-Gravity Conditions (P. Faccioli)

The small molecules discovered with the PPI-FIT technology need to be optimized, for example to increase their efficiency or reduce their toxicity. A crucial piece of information that is required during this phase is the full atomistic structure of their interaction with the target protein. In conventional drug discovery schemes, this information can be obtained by standard experimental methods (X-ray crystallography and/or NMR experiments). Unfortunately, these conventional techniques cannot provide the structure of protein folding intermediates, even when they are stabilized by the interaction with a small molecule. However, a number of recent studies have highlighted striking advantages of performing protein crystallization in microgravity conditions, mostly due to the absence of convective motion. We began a new multidisciplinary research venture aiming at determining the structure of ligand binding architectures in protein folding intermediates, by exploiting several kinds of microgravity setups, including earth-based devices, parabolic flight microlabs and directly on the International Space Station. In particular, a proposal to the Ramon Foundation has been filed in partnership with private company Space Pharma, Universities of Santiago de Compostela and Tel Aviv to allocate part of astronaut time in a forthcoming Axiom1 mission, operated by Space-X. If the application will be successful, the first attempt of crystallizing protein folding intermediates will be performed in January 2022.

Biomolecular atomistic simulations of membrane proteins (G. Lattanzi)

Membrane proteins provide an excellent benchmark for biomolecular atomistic simulations. Indeed, they are difficult to crystallize and hence to be solved by standard X-ray or NMR techniques. However, they are involved in a number of

molecular mechanisms, including cell and host recognition, signal transduction and cellular response, to name a few. Atomistic molecular simulations provide the essential tool to investigate these proteins in motion in the realistic environment provided by a model membrane. We have constantly worked on membrane proteins, choosing systems for which experimental data are readily available in literature or in collaboration with experimental groups. In 2020, in particular, we have continued our previous work on the membrane proteins Recoverin and Prestin. In particular, we have analysed several mutants of the Recoverin protein, as a final project for the Computational Biophysics course. We have collected the results produced by our students and aim at finalizing a publication with all their names as authors. We have also started two new projects on proteins involved in serious diseases: in particular, we have worked in collaboration with CNR on the ribosome maturation protein SBDS, that is involved in the development of the rare Schwachman-Bodian-Diamond disease. In collaboration with the University of Milan, we have also started a new collaboration on the conformations of the intrinsically disordered protein alpha-synuclein.

Selected Papers

- Giulini, M. et al. (2020). *An Information-Theory-Based Approach for Optimal Model Reduction of Biomolecules*. *Journal of Chemical Theory and Computation* **16**(11), pp. 6795–6813.
- Hauke, P, Mattiotti, G., and Faccioli, P (2021). *Dominant Reaction Pathways by Quantum Computing*. *Physical Review Letters* **126**. Art. no.: 028104.
- Spagnolli, G., Massignan, T., Astolfi, A., Biggi, S., Brunelli, P., Libergoli, M., Ianeselli, A., Orioli, S., Boldrini, A., Terruzzi, L., Maietta, G., Rigoli, M., Lorenzo, N. L., Fernandez, L. C., Tosatto, L., Linsenmeier, L., Vignoli, B., Petris, G., Gasparotto, D., Pennuto, M., Guella, G., Canossa, M., Altmeppen, H. C., Lolli, G., Biressi, S., Pastor, M. M., Requena, J. R., Mancini, I., Barreca, M. L., Faccioli, P., and Biasini, E. (2021b). *Pharmacological inactivation of the prion protein by targeting a folding intermediate*. *Communication Biology* **4** (1), p. 62.

Photo-activated conformational changes of proteins (P Faccioli) In 2020, we have completed a project in which enhanced sampling simulations were used to clarify the molecular mechanism of the conformational changes involved in the Orange Carotenoid protein.

Combined MD/DFT protocol for the simulation of molecular materials for organic solar cells (G. Lattanzi) Theoretical physics methods and, in particular, molecular dynamics simulations combined with density functional theory have been successfully applied to the investigation of organic materials employed in the development of organic solar cells. Indeed, the molecular arrangement of organic molecules affect dramatically their transport properties: in addition, these materials can be successfully combined with biological molecules to enhance their performance. In this respect, theoretical physics methods offer a valuable insight not only on the organization of the bulk material, but also on the characterization of the interfaces and their transport properties. In 2020, we have carried out several calculations aimed at characterizing acceptor-donor dyads in organic photovoltaics.

FBS

Giuseppina Orlandini,[†] Winfried Leidemann, Ylenia Capitani, Elena Filandri

One of our long-term research lines is the study of relativistic effects in electroweak reactions of nuclei. Our starting point is a nonrelativistic treatment, where the nuclear dynamics is described by realistic nucleon-nucleon (NN) and 3N potential models with a subsequent solution of nonrelativistic wave equations (Schrödinger and LIT equations). Relativistic effects are then originated by different sources:

- (i) kinematical effects,
- (ii) higher order corrections to the nonrelativistic charge and current operators and
- (iii) boost corrections.

In our most recent study we were mainly concerned with the first item showing that also for the four-body nucleus of ${}^4\text{He}$ it is advantageous to carry out the calculation in the active nucleon Breit system (Orlandini et al. 2020a). Recently, concerning item (iii) we made a considerable progress. In collaboration with V. Efros, E. Tomusiak and L. Yuan we calculated the analytic form of the various contributions caused by a wave function boost and we were also able to code them in our numerical programs for the electrodisintegration of ${}^3\text{He}$. Thus we are confident to have interesting results in the near future.

We also have continued our work on cluster nuclei in Halo-EFT (Andreatta et al. 2020; Filandri et al. 2020). In the master thesis

of Francesca Bonaiti the photodisintegration of the ${}^9\text{Be}$ to the αn channel was studied via the LIT method in unretarded dipole approximation. Here it is important to note that our $\alpha\alpha$ and αn potentials are defined in momentum space, whereas the unretarded dipole approximation has its origin in coordinate space, thus proper Fourier transforms were necessary for the wave functions. The latter were expanded on a nonsymmetrized hyperspherical harmonics basis in momentum space. The thesis discusses results for the state $(1/2)^+$ of the final αn system. Since the ground state of ${}^9\text{Be}$ is $(3/2)^-$ state there are other possible E1 transitions to αn states with $(3/2)^+$ and $(5/2)^+$. In fact such transitions, as well as other important modifications, like, for example three-body force, will be taken into account in the doctoral thesis of Elena Filandri.

A further research project concerns hypernuclei. An interesting aspect in hypernuclear physics is the Λ - Σ coupling in the ΛN interaction. In our calculations of Λ -hypernuclei we use expansions on a hyperspherical harmonics basis. In such a calculation the mass difference of Λ and Σ hyperons leads to a certain freedom in the definition of the kinetic energy operator, which can be described by an additional free parameter. The optimal choice for this parameter is object of the study of the master thesis of Nicola Paracone, which started in October 2020.

Selected Papers

Andreatta, P., Manzata, C., Ji, C., Leidemann, W., and Orlandini, G. (2020). *Beryllium-9 in Cluster Effective Field Theory*. Springer Proc. Phys. **238**, pp. 191–194.

Filandri, E., Andreatta, P., Manzata, C., Ji, C., Leidemann, W., and Orlandini (2020). *Beryllium-9 in Cluster Effective Field Theory*. SciPost Phys. Proc. **3**, pp. 34.1–34.9.

Orlandini, G., Rocco, N., Lovato, A., and Leidemann, W. (2020a). *Relativistic Effects in Non-relativistic Calculations of Electroweak Cross Sections*. Springer Proc. Phys. **238**, pp. 663–667.

[†]Contact Author: giuseppina.orlandini@unitn.it

FLAG

Massimiliano Rinaldi,[†] Luciano Vanzo, Simon Boudet, Alessandro Casalino, Samuele Marco Silveravalle, Silvia Vicentini, Adolfo Cisterna Roa

The FLAG node in Trento is composed by two associated professors (M. Rinaldi and L. Vanzo), four PhD students (S. Boudet, A. Casalino, S. Silveravalle, S. Vicentini) and one postdoctoral researcher (A. Cisterna, since September 2020¹). In 2020 we have conducted research along the following lines.

Modified gravity We have studied a higher-derivative extension of general relativity that generalises the Lovelock model and allows for non-trivial contribution to the field equations also in four dimensions. We applied the model to cosmology and black hole physics and we showed that these terms can be thought as quantum corrections (Casalino et al. 2021). We also studied the cosmological perturbations in this theory. We studied the stability of black holes in quadratic gravity. In the literature it is claimed that in $f(R)$ gravity Kerr black holes have a curvature instability but we showed that when $f(R) = R^2$ such instability disappears (Dioguardi and Rinaldi 2020). We also considered an instability called “mass inflation” that affects the inner horizon of Kerr and Reissner-Nordstrom black holes in the context of $f(R)$ gravity. We showed that, as in General Relativity, this instability persists unless the black hole is regular and a certain limit is taken. We investigated the so-called mimetic model of gravity implemented by higher-derivative terms induced by quantum corrections, in the context of cosmology with non-flat spatial sections. One the main goal was to determine the solutions to the equations and also when bouncing solutions appear (Casalino et al. 2020a). A particular attention was devoted to non-singular solutions

to the theory.

Quantum gravity We considered a class of black holes inspired by Loop Quantum Gravity and where the Immirzi parameter becomes a field. We discussed in depth the properties of these black holes and, in particular, the thermodynamical properties. We found that the Immirzi field introduces modifications to the entropy area law and leads to a violation of the reverse isoperimetric inequality, giving rise to a so-called super-entropic black hole.

Semiclassical decay We studied the semiclassical decay of false vacuum configurations first introduced by Coleman and De Luccia. We proposed a new way to identify whether or not the decay occurs and also a new, faster numerical method to compute the decay rate. We first considered configurations with gravity and non-minimally coupled massless scalar fields. We then moved to modified gravity and showed that the presence of quadratic terms in the Ricci scalar prevents the decay.

Einstein-Higgs-Yang-Mills equations We studied various configurations of the Einstein-Higgs-Yang-Mills model applied to cosmology in connection with a possible mechanism to produce an effective dark energy term in the cosmological late time evolution. We studied what geometric configurations of the field are allowed and we concluded that the model can be feasible but with coupling parameters that are much different from the ones of the standard model of particle physics.

[†]Contact Author: massimiliano.rinaldi@unitn.it

¹The pandemic has prevented Dr. Cisterna to physically join our group.

Selected Papers

- Casalino, A., Colleaux, A., Rinaldi, M., and Vicentini, S. (2021). *Regularized Lovelock gravity*. Phys. Dark Univ. **31**. Art. no.: 100770.
- Casalino, A., Sebastiani, L., Vanzo, L., and Zerbini, S. (2020a). *Higher derivative and mimetic models on non flat FLRW space-times*. Phys. Dark Univ. **29**. Art. no.: 100594.
- Dioguardi, C. and Rinaldi, M. (2020). *A note on the linear stability of black holes in quadratic gravity*. Eur. Phys. J. Plus **135**(11), p. 920.

MANYBODY

Francesco Pederiva,[†] Alessandro Lovato, Maurizio Dapor, Simone Taioli, Hilla de Leon, Valentina Amitrano, Piero Luchi, Luca Riz, Francesco Turro

The TIFPA unit of the MANYBODY collaboration pursues development and applications of quantum many-body techniques to both systems of interest for nuclear physics and nuclear astrophysics (Lovato, Taioli, de Leon, Riz, Pederiva), applications to condensed matter physics and nuclear medicine (Dapor, Taioli), quantum simulations and quantum computing (Amitrano, Luchi, Turro, Pederiva). The methods toolbox is quite diverse, ranging from Quantum Monte Carlo and transport Monte Carlo to density functional theory and direct diagonalization of the Hamiltonian, quantum computing, and machine-learning methods for the solution of the quantum many-body problem

The proper interpretation of neutrino-oscillation experiments requires accurate theoretical calculations of neutrino-nucleus scattering cross sections. We carried out GFMC calculations of the charged-current response functions of ^{12}C , based on realistic treatments of nuclear interactions and currents, for momentum transfer ranging from $q = 100$ MeV to $q = 700$ MeV, utilizing ~ 100 million core-hours on Mira, a supercomputer hosted at Argonne National Laboratory, in the United States.

Our calculations are based on realistic treatments of nuclear interactions and currents, the latter including the axial, vector, and vector-axial interference terms crucial for determining the difference between neutrino and antineutrino scattering and the CP-violating phase. We find that the strength and energy dependence of two-nucleon processes induced by correlation effects and interaction currents are crucial in providing the most accurate description of neutrino-nucleus scattering in the quasi-elastic regime. Consistently with our results for the electromagnetic and neutral-current transitions, two-body contributions in the charge-current operator significantly en-

hance the transverse response functions. We take advantage of the scaling behavior of the response functions to interpolate and safely extrapolate them at large momentum transfers $q > 700$ MeV, that is, beyond the range of those calculated with GFMC methods. We then computed the flux-folded neutrino-nucleus scattering cross sections relevant for MiniBooNE and T2K experiments. A subset of our results for the flux-folded inclusive cross sections measured on ^{12}C by the MiniBooNE and T2K collaborations is shown in Fig. 1. Calculations with one-body only, and one- and two-body currents are shown by, respectively, dashed (green) and solid (blue) lines. The shaded areas result from combining statistical errors associated with the GFMC evaluation of the Euclidean response functions, uncertainties in the maximum-entropy inversion of them, and uncertainties due to extrapolation of the response functions outside the calculated range of momentum transfer. The large cancellation between the dominant terms proportional to the transverse and axial-vector responses in antineutrino cross sections leads to somewhat broader error bands than for the neutrino cross sections, for which those terms add up. Furthermore, the anti-neutrino cross section is a factor of about 2 to 10 smaller than for the neutrino data as the muon scattering angle increases from 0 to 90 degrees.

The MiniBooNE, and T2K data are in good agreement with theory, when including the contributions of two-body currents. This is especially noticeable in the case of the MiniBooNE neutrino data at forward scattering angles. However, the calculated cross sections underestimate somewhat the MiniBooNE neutrino data at progressively larger muon kinetic energy T_μ and backward scattering angles θ_μ , and the anti-neutrino data at forward θ_μ over the whole T_μ range. By contrast, the full theory

[†]Contact Author: francesco.pederiva@unitn.it

(with one- and two-body currents) appears to provide a good description of the T2K neutrino data over the whole measured region. A paper in this work has been published in Physical Review X (Lovato et al. 2020).

The GFMC calculations discussed above infer the nuclear electroweak response functions from their Laplace transforms. Inverting the Laplace transform is a notoriously ill-posed problem; and we use Bayesian techniques, such as maximum entropy, to reconstruct the original response functions in the quasi-elastic region. Recently, we introduced a physics-informed artificial neural network architecture suitable for approximating the inverse of the Laplace transform. Utilizing simulated, albeit realistic, electromagnetic response functions, we show that this physics-informed artificial neural network outperforms maximum entropy in both the low-energy transfer and the quasi-elastic regions, thereby allowing for robust calculations of electron scattering and neutrino scattering on nuclei and inclusive muon capture rates (Raghavan et al. 2021).

One of the important activities that have been ramping up in the MANYBODY group in the last year is related to the application of quantum computing techniques to study of nuclear reactions, in collaboration with LLNL (USA). In particular, in Trento we are pursuing two research lines. The first concerns the possibility to exploit unitary transformations to study the ground state of a many-body system (Turro, Amtrano, Pederiva). The second aims to find an efficient procedure, based on machine learning techniques, to implement the control pulses to generate arbitrary, parametrized unitary transformations (reconfigurable gates) used on the LLNL quantum testbed (Luchi, Turro, Pederiva).

Selected Papers

- Lovato, A., Carlson, J., Gandolfi, S., Rocco, N., and Schiavilla, R. (2020). *Ab initio study of (ν_ℓ, ℓ^-) and $(\bar{\nu}_\ell, \ell^+)$ inclusive scattering in ^{12}C : confronting the MiniBooNE and T2K CCQE data*. Phys. Rev. X **10**(3). Art. no.: 031068.
- Raghavan, K., Balaprakash, P., Lovato, A., Rocco, N., and Wild, S. M. (2021). *Machine learning-based inversion of nuclear responses*. Phys. Rev. C **103**(3). Art. no.: 035502.

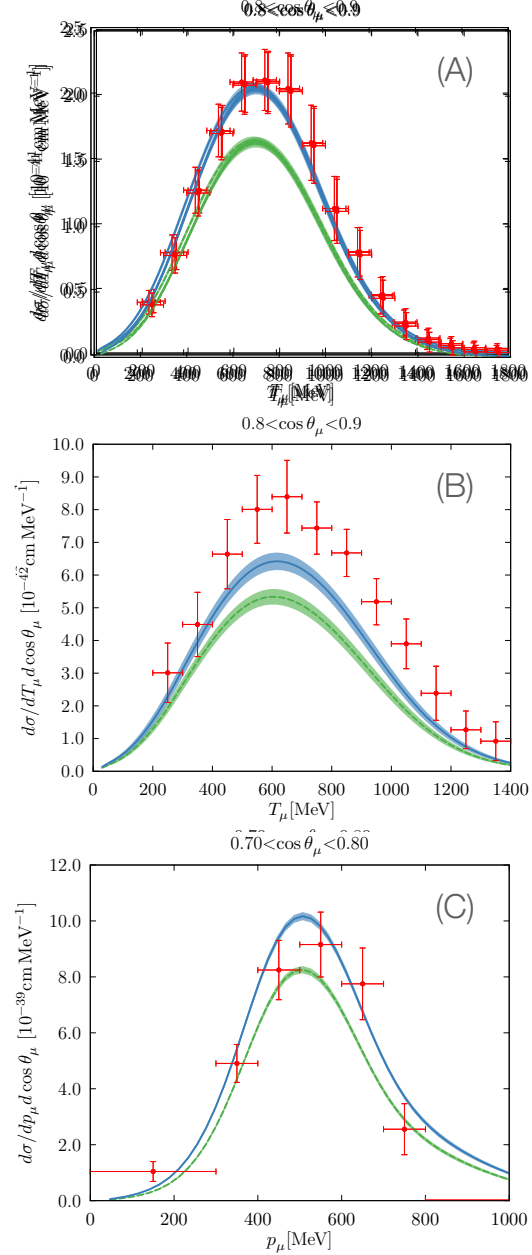


Figure 1: Flux-folded double differential cross sections per target neutron for neutrino and antineutrino scattering on ^{12}C , displayed as a function of the muon kinetic energy for different ranges of scattering angle. MiniBooNE neutrino and antineutrino data are displayed in panels (A), and (B), respectively. Panel (C) shows T2K neutrino scattering data.

NEMESYS

Simone Taioli,[†], Paolo E. Trevisanutto, Giovanni Garberoglio, Maurizio Dapor

Over the last year, our research focussed on four different areas.

First, using linear-response time-dependent density functional theory (TDDFT), we were able to calculate the energy loss function (ELF) of liquid water in excellent agreement with the experimental data (Taioli et al. 2020). The inelastic scattering cross-section obtained with this ELF, together with the elastic scattering cross-section derived considering the condensed state of water, have been used to simulate by Monte Carlo (MC) method the energy deposited in the medium by a beam of carbon ions and carried away by the generated secondary electrons, producing inelastic events such as ionizations, excitations and dissociative electron attachment (DEA). Cluster sizes of biological damage events have been calculated for a large number of carbon ion kinetic energies, from those relevant to hadrontherapy to cosmic rays. The MC code predicts with high statistical accuracy the nature and relative intensities of the main inelastic processes, finding that ionizations are the major source of biological damage.

We have also studied two different models, that are the Monte Carlo (MC) method and the Numerical Solution (NS) of the Ambartsumian-Chandrasekhar equations, to interpolate and predict Reflection Electron Energy Loss (REEL) spectra of metals as well as the emission of secondary electrons (Azzolini et al. 2020).

A third topic concerned the proposal of a solid state black-hole analogue (Morresi et al. 2020). In particular, the simulation of deformed graphene membranes has allowed us to study issues related to Hawking radiation in analogue systems. LISC researchers have developed a novel algorithm for generating microscopic Beltrami pseudospheres (≈ 100 nanometer radius), consisting of millions of carbon atoms, using graphene as a coating material of the negative curvature surface (see Fig. 1). The

latter is a non-Euclidean surface that, due to its conformation, creates the conditions for electrons to behave as if they were in the presence of a black hole-like event horizon, whose singularity leaves an indelible “signature” in the electronic density of states (DOS). Without curvature, the DOS would be completely symmetric, as in flat graphene. Instead, the presence of asymmetries in the DOS would suggest the existence of a solid-state analogue of the event horizon of a cosmological black hole. In particular, the DOS should show a “thermal” behavior, analogous to the Hawking radiation. The researchers have therefore focused on computing the DOS by a tight-binding method, finding such a bending. This study represents a significant step forward in demonstrating the possibility of studying in the laboratory, for the first time, certain phenomena that occur similarly near the event horizon. This study has received a fair amount of media coverage with publication in several national newspapers.

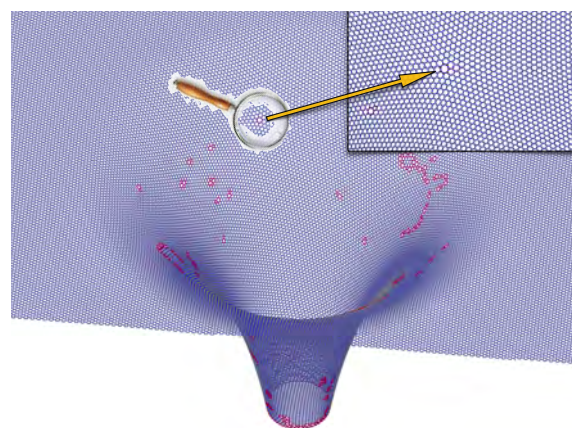


Figure 1: Graphene pseudosphere with highlight of Stone-Wales defects.

Finally, we developed a novel method for calculating dielectric virial coefficients (Garberoglio and Harvey 2020). The method has been applied to the calculation of the second dielectric virial coefficient using state-of-the-art potentials and polarizabilities for a number of noble gases of metrological interest.

[†]Contact Author: taioli@ectstar.eu

Selected Papers

- Azzolini, M., Ridzel, O. Y., Kaplya, P. S., Afanas'ev, V., Pugno, N. M., Taioli, S., and Dapor, M. (2020). *A comparison between Monte Carlo method and the numerical solution of the Ambartsumian-Chandrasekhar equations to unravel the dielectric response of metals*. Computational Materials Science **173**. Art. no.: 109420.
- Garberoglio, G. and Harvey, A. H. (2020). *Path-Integral Calculation of the Second Dielectric and Refractivity Virial Coefficients of Helium, Neon, and Argon*. Journal of Research of National Institute of Standards and Technology **125**. Art. no.: 125022.
- Morresi, T., Binosi, D., Simonucci, S., Piergallini, R., Roche, S., Pugno, N. M., and Taioli, S. (2020). *Exploring Event Horizons and Hawking Radiation through Deformed Graphene Membranes*. 2D Materials **7**. Art. no.: 041006.
- Taioli, S., Trevisanutto, P. E., Vera, P. de, Simonucci, S., Abril, I., Garcia-Molina, R., and Dapor, M. (2020). *Relative Role of Physical Mechanisms on Complex Biodamage Induced by Carbon Irradiation*. The Journal of Physical Chemistry Letters **12**, pp. 487–493.

Teongrav

Albino Perego,[†] Constantinos Constantinou, Federico Cipolletta

Teongrav is an INFN initiative whose goal is to model the sources of gravitational waves from a theoretical perspective. It is an initiative spread all over Italy, with 7 nodes, 21 staff members and about 50 additional participants, including postdocs and PhD students.

The Trento node is a small, but very active group whose scientific focus is on:

- modelling of binary neutron star mergers (BNSMs) through numerical simulations,
- study of nuclear matter and nuclear interactions in hot and dense matter,
- modelling of electromagnetic counterparts of compact binary mergers.

During 2020, the three members (A. Perego, assistant professor at Trento University), C. Constantinou (INFN postdoc since August and Fellini Fellow since December 2020) and F. Cipolletta (INFN postdoc until May 2020) published 7 Teongrav-related papers in peer-reviewed journals and additionally submitted 5 manuscripts. Despite the covid emergency, members of the group were invited to give 3 invited talks and gave 2 seminars at the ECT* Institute. In the following, we briefly summarize the major outcomes of the group in the three different areas outlined above.

TIFPA was the institute where a new fully general-relativistic magnetohydrodynamic code, named Spritz, was developed. This was a major achievement of the Teongrav local group, initiated by the former group members B. Giacomazzo and R. Ciolfi, and by F. Cipolletta. Fully general relativistic magnetohydrodynamic (GRMHD) simulations able to include the effects of a composition and temperature dependent equation of state describing NS matter as well as neutrino emission and reabsorption are necessary to understand the physical mechanisms involved in BNSMs. Spritz solves the GRMHD equations in 3D Cartesian coordinates and on a dynamical spacetime. The code can support tabulated equations of state,

taking into account finite temperature effects and allowing for the inclusion of neutrino radiation. With respect to other publicly available GRMHD codes, Spritz combines the robust approach of a staggered formulation of the vector potential, guaranteeing divergence-less magnetic field. The documentation of the code and its first benchmarks and tests was documented in a paper whose publication was led by F. Cipolletta (Cipolletta et al. 2020a), see Fig. 1.

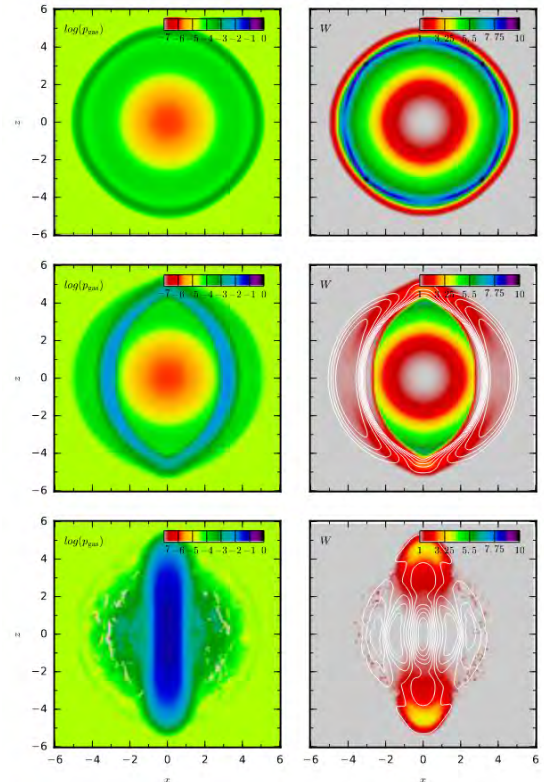


Figure 1: Spherical explosion test performed with the Spritz code. The three different rows correspond to different magnetization degrees. On the left (right) panels the logarithm of the gas pressure (Lorentz factor) is reported. See Cipolletta et al. (2020a).

The activity of A. Perego has mainly focused on the modelling of BNSMs and of their main observables, including neutrinos, photons and gravitational waves. Within an international collaboration, he has contributed in studying for the first time in a systematic way the dynam-

[†]Contact Author: albino.perego@tifpa.infn.it

ics of BNSMs in which the secondary star is significantly lighter than the primary (Bernuzzi et al. 2020). In this paper, new numerical relativity results of BNSMs with chirp mass $1.188 M_{\odot}$ and mass ratios $q = M_A/M_B = 1.67$ and 1.8 using finite-temperature equations of state, approximate neutrino transport, and a subgrid model for magnetohydrodynamics-induced turbulent viscosity were presented. The used equation of state were compatible with nuclear and astrophysical constraints and included a new microphysical model derived from ab initio calculations based on the Brueckner-Hartree-Fock approach. In these systems, the more extended, lighter NS is tidally disrupted by the companion. The resulting mass accretion process produces the gravitational collapse of the latter into a black hole (BH). As a result of the tidal disruption, an accretion disc of neutron-rich and cold matter forms with baryon masses $\sim 0.15M_{\odot}$, significantly heavier than the remnant discs in equal-masses prompt-collapse mergers see Fig. 2. Massive dynamical ejecta of the order of $0.01M_{\odot}$ also originate from the tidal disruption. They are neutron-rich and expand from the orbital plane with a crescent-like geometry. Consequently, bright, red, and temporally extended kilonova emission is predicted from these mergers. These results show that prompt BH mergers can power bright electromagnetic counterparts for high-mass-ratio binaries, and that the binary mass ratio can be, in principle, constrained from multimessenger observations. Within the same collaboration, A. Perego studied the thermodynamics conditions at which neutrinos decouple from matter in BNSM remnants by post-processing results of numerical relativity simu-

lations (A. Endrizzi et al. 2020b). In this work it was found that the matter density and the neutrino energies are the most relevant quantities in determining the decoupling surface location. In particular, for mean energy neutrinos ($E_{\nu} \sim 10 - 20$ MeV) the transition between diffusion and free-streaming conditions occurs around $10^{11} \text{ g cm}^{-3}$ for all neutrino species. Weak and thermal equilibrium freeze-out occurs deeper (several $10^{12} \text{ g cm}^{-3}$) for heavy-flavor neutrinos than for $\bar{\nu}_e$ and ν_e ($\gtrsim 10^{11} \text{ g cm}^{-3}$). The presence of a massive NS or a black hole influences the neutrino thermalization. While in the former case decoupling surfaces are present for all relevant energies, the lower maximum density ($\lesssim 10^{12} \text{ g cm}^{-3}$) in black hole-torus systems does not allow softer neutrinos to thermalize and diffuse.

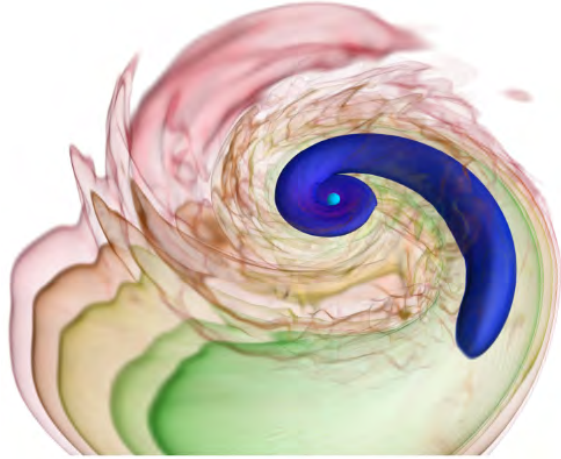


Figure 2: Volume rendering of the rest mass density as obtained by Numerical Relativity simulations modelling the tidal disruption of a light neutron star by a more massive one. The latter has collapsed to a black hole, whose horizon is visible as cyan sphere. See (Bernuzzi et al. 2020).

Selected Papers

- Bernuzzi, S., Breschi, M., Daszuta, B., Endrizzi, A., Logoteta, D., Nedora, V., Perego, A., Radice, D., Schianchi, F., Zappa, F., Bombaci, I., and Ortiz, N. (2020). *Accretion-induced prompt black hole formation in asymmetric neutron star mergers, dynamical ejecta, and kilonova signals*. Monthly Notices of the Royal Astronomical Society **497**(2), pp. 1488–1507.
- Cipolletta, F., Kalinani, J. V., Giacomazzo, B., and Ciolfi, R. (2020a). *Spritz: a new fully general-relativistic magnetohydrodynamic code*. Classical and Quantum Gravity **37**(13). Art. no.: 135010.
- Endrizzi, A., Perego, A., Fabbri, F. M., Branca, L., Radice, D., Bernuzzi, S., Giacomazzo, B., Pederiva, F., and Lovato, A. (2020b). *Thermodynamics conditions of matter in the neutrino decoupling region during neutron star mergers*. European Physical Journal A **56**(1), p. 15.

Activities starting in 2021

NUCSYS

Research outline The present project results from a partial merging of two previous INFN projects: Few-Body Systems (FBS) and Many-Body Systems (MANYBODY), both of them intended to describe particular aspects of atomic nuclei which are relevant for the progress in the knowledge of fundamental interactions. On the one hand, the ab-initio approach to few-nucleon systems offers a privileged laboratory to validate and constrain our modern understanding of the nuclear interaction, the nucleon-hyperon interaction, and the interaction of nuclei with external probes, based on the (chiral) effective field theory (EFT) paradigm. On the other hand, experiments probing fundamental interactions often involve medium and heavy nuclei, which makes it necessary to consider many-body effects and to bridge the two domains. Prominent examples are next-generation long-baseline neutrino experiments, aimed at the precise determination of the oscillation parameters. They will require accurate modeling of nuclear effects in medium and heavier nuclei at relativistic energies. Within this framework several aspects will be addressed, ranging from deeper studies of Effective Field Theory (EFT) potentials, to systematic studies of reactions relevant for nucleosynthesis, to fundamental issues, like identifying sources of CP violation beyond the Standard Model. In addition, theoretical support and guidance in nuclear processes for strategic INFN-Labs projects in fundamental research as well as in applications (such as the national programs for the production of innovative radionuclides and radiolabeled compounds for advanced medical therapies and diagnostics) will be provided.

involved external institutions Università di Pavia; Università di Pisa; Università del Salento; Università di Torino; Università di Trento.

INFN groups Lecce, Padova, Pisa, Torino, TIFPA

Principal Investigator Alejandro Kievsky, INFN Pisa

TIFPA team Winfried Leidemann (coordinator), Giuseppina Orlandini, Ylenia Capitani, Elena Filandri, Edna Carolina Pinilla Beltran



Technological Research

3D SIAM

Maurizio Boscardin,[†] Michele Crivellari

Hydrogenated amorphous silicon (a-Si:H) can be produced from growth by plasma-enhanced chemical vapor deposition (PECVD) of SiH₄. The resulting material has remarkable radiation resistance at high fluencies; planar diodes made with a-Si:H increase only a factor 2 in leakage current after an irradiation at 7×10^{15} p/cm² and after 24 hours of annealing their leakage current comes back at the original value before the irradiation. A-Si:H based particle detectors have been built since mid 80s as planar p-i-n or Schottky diode structures; the thickness of this detectors ranged from 1 to 50 μm . Planar a-Si:H detectors have been used also to detect different kind of radiation other than MIPs, namely: x-rays, neutron and ions as well as low energy protons and alphas. However, MIP detection using planar structures has always been problematic due to the poor S/N ratio due to high depletion field and consequently high leakage current and the charge collection efficiency around 50% for a 30 μm planar diode. In order to overcome these problems we propose to use a 3D detector geometry that allows to keep a small collection distance (the inter-electrode distance that may be kept around 20-30 μm) while having a larger detector space for charge generation since it is possible to grow the substrate up to about 100 μm in thickness. The de-

pletion voltage in this case can be kept as low as about 200 V-400 V reducing the leakage current (Menichelli et al. 2020a; Menichelli et al. 2020b).

The activity in 2020 has been focused on the realization of planar device on thins a-Si:H based on ion implantations. For this phase we have been defined a layout based on two main geometrical configuration: vertical diode and lateral. The difference on two options is illustrated in Fig. 1.

Vertical detectors are fabricated on a low resistivity p-doped crystal Silicon (c-Si) substrate where a 10 μm layer of intrinsic Hydrogenated amorphous silicon (a-Si:H) layer is deposited. On top of this layer a n-type layer is formed via ion implantation of Phosphorus, the resulting device is a n-i-p diode where the p-type electrode is made of c-Si. Lateral detectors are fabricated on a SiO₂ layer on the same low resistivity p-doped crystal Silicon (c-Si) substrate where a 10 μm layer of intrinsic Hydrogenated amorphous silicon (a-Si:H) layer is deposited, the electrodes are formed via ion implantation of layers of p and n type deposited on the upper surface. The batch has been completed (in Fig. 2 a picture of processed wafer is shown) and preliminary analysis based on IV measurements have been completed.

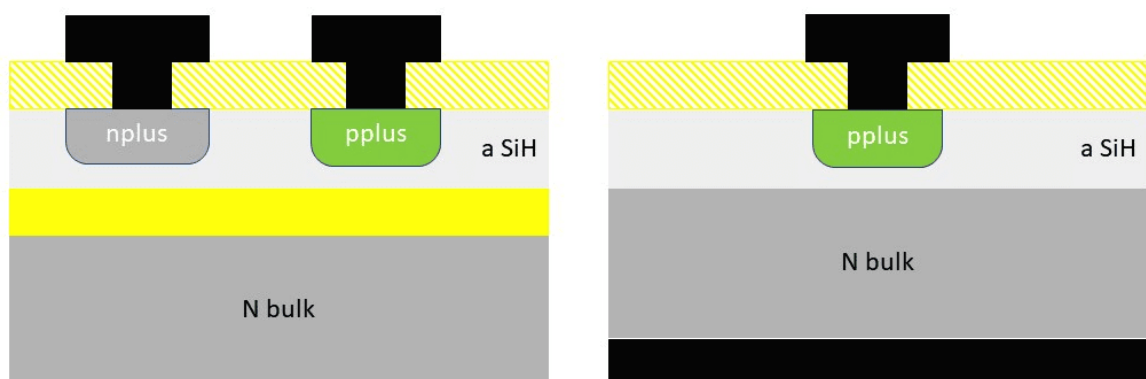


Figure 1: left: lateral diodes; right: vertical diodes

[†]Contact Author: boscardi@fbk.eu

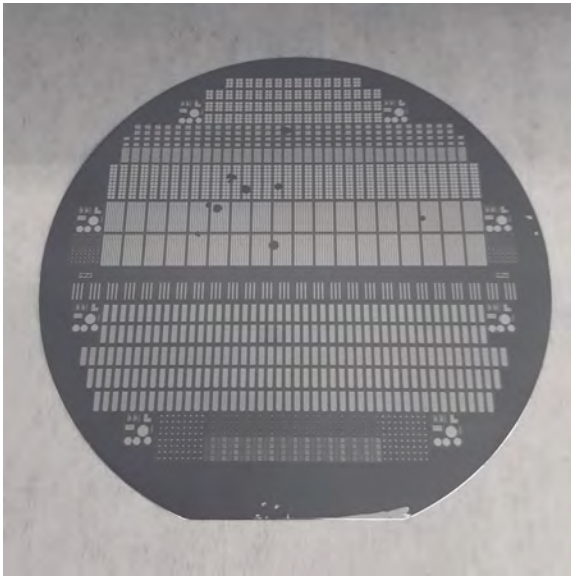


Figure 2: Wafers full processed at FBK

Leakage current versus Voltage have been measured and the results are under publication. Preliminary dosimetric tests with an electron beam from Wollongong University (Australia) have been performed with good results (under publication on *Frontiers in Physics*) as well as some total dose testing with x-rays up to 50Mrad (Davis et al. 2020). Other ongoing tests using phase I prototypes with results to be submitted for publication are:

- Leakage current versus temperature in lateral and vertical detector diodes
- Leakage current and x-ray sensitivity of option 1 detector diode.
- Radiation damage of vertical and lateral diodes irradiated up to $5 \times 10^{15} n_{eq}/cm^2$
- Radiation damage of lateral and vertical diodes irradiated with gamma rays (up to 1 Grad)
- Radiation damage with 5 MeV protons of

- lateral and vertical diodes (combined total dose and displacement damage)
- Dosimetric properties of a-Si:H detector diodes.

The layout of the phase II prototypes has been completed and presently these structures are under construction. Due to the COVID-19 emergency in order to save time the phase II prototype construction has been reduced to the essential purpose of validating and optimizing the DRIE process and the lithography for the doping process without building functional detectors.

The layout of the test structures was defined in order to test different hole geometry configurations corresponding to the electrodes of a 3D detector. Preliminary tests were carried out using c-Si substrates (Fig. 3), these tests show that by varying the diameter of the hole we can control the depth of the hole itself, so that we can with a single DRIE process define holes with different depths.

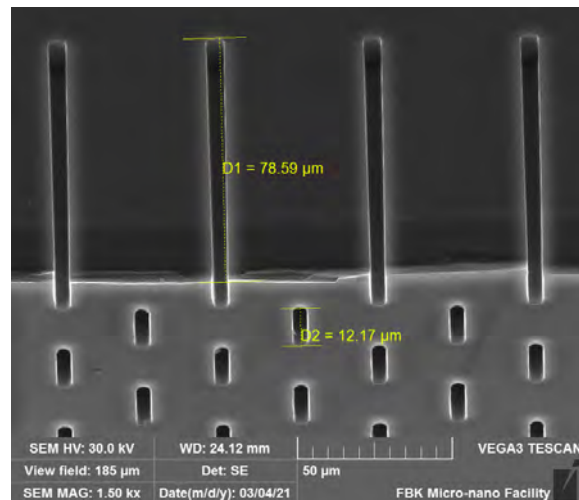


Figure 3: SEM pictures on DRIE etch test

Selected Papers

- Davis, J. A. et al. (2020). *Modeling a Thick Hydrogenated Amorphous Silicon Substrate for Ionizing Radiation Detectors*. *Frontiers in Physics* **8**, p. 158.
- Menichelli, M. et al. (2020a). *3D Detectors on Hydrogenated Amorphous Silicon for particle tracking in high radiation environment*. *J. Phys. Conf. Ser.* **1561**. Art. no.: 012016.
- (2020b). *Hydrogenated amorphous silicon detectors for particle detection, beam flux monitoring and dosimetry in high-dose radiation environment*. *Journal of Instrumentation* **15**. Art. no.: C04005.

ARCADIA

Lucio Pancheri,[†] Coralie Neubüser, Thomas Corradino, Gian-Franco Dalla Betta, Roberto Iuppa, Paolo Zuccon, Francesco Nozzoli, Benedetto Di Ruzza, Ester Ricci

The goal of ARCADIA project (Advanced Read-out CMOS Architectures with Depleted Integrated sensor Arrays) is to develop novel Fully-Depleted Monolithic Active Pixel Sensors (FD-MAPS) suitable for applications in the biomedical field, astro-particle detection and High-Energy Physics experiments.

The project was started in 2019, building on the experience acquired during INFN-funded project SEED, where the sensor structure and the CMOS-compatible fabrication process were first defined and patented, and a small proof of concept pixel sensor based on the proposed technology was fabricated together with a set of test structures (Fig. 1).

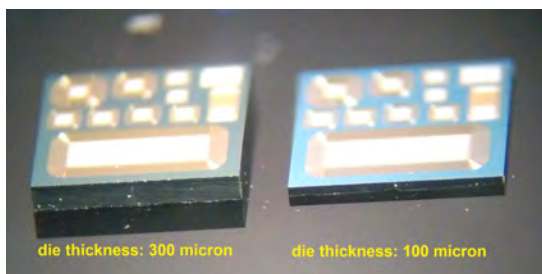


Figure 1: Test chips with different thickness produced in the SEED project.

A simplified cross-section of ARCADIA sensor is shown in Fig. 2. The sensor is based on a commercial 110-nm CMOS process flow, with the addition of dedicated processing steps (Pancheri et al. 2020). The high-resistivity substrate is n-type, and a p+ implant on the backside forms a junction that is used to deplete the substrate when a suitable backside bias is applied. This approach can be employed to realize thick sensors ($\geq 100 \mu\text{m}$), but is impractical for thinner active regions due to mechanical stability issues. An alternative approach, suitable for thin active volumes, exploits a p+ starting material with a double epitaxial n-/n layer. In this case, backside processing is not necessary, and the substrate can be thinned at the end of fabri-

cation until most of the p+ region is removed.

In the first year of the ARCADIA project, the process flow defined in SEED was extended in collaboration with the silicon foundry to make it compliant with the fabrication of thin sensors, having an active area in the 10s of μm range, while extensive tests and simulations based on the preliminary results obtained within SEED project were conducted. During 2019, the architecture of a cm^2 -sized demonstrator with characteristics suitable for Proton Computer Tomography and for particle tracking in space experiments was also defined, together with the requirements for the data acquisition system.

Most of the second year of the project has been devoted to the design of an engineering run including several monolithic active sensors with integrated electronics, as well as test structures for the characterization of the process. In addition to the main large-area demonstrator, other smaller active sensor designs, exploring different aspects of the technology, have also been included in the first fabrication run. The maskset of the engineering run was submitted in November 2020.

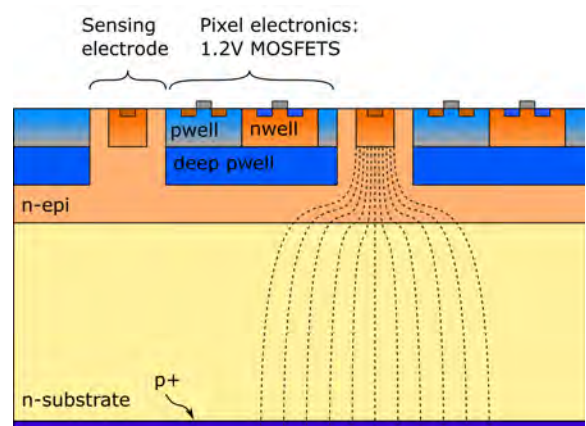


Figure 2: Simplified cross section of the ARCADIA monolithic sensors.

[†]Contact Author: lucio.pancheri@unitn.it

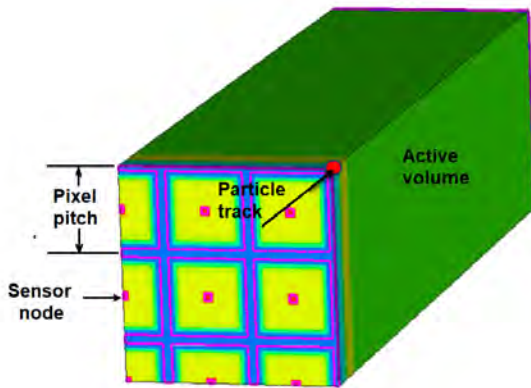


Figure 3: Example 3D simulation domain used for the TCAD simulation of charge collection dynamics and clustering with particles incident in the pixel corner.

During 2020, several simulation studies aimed at optimizing the detector layout have also been carried out (Fig. 3). In particular, the studies have been focused on the analysis of sensors with three different pixels pitches: $50\ \mu\text{m}$, allowing a readout channel with large area and functionality; $25\ \mu\text{m}$, used for the main demonstrator; and $10\ \mu\text{m}$, that is interesting for applications requiring fast timing and/or high granularity. The optimization of pixel layout has been mainly focused on two aspects: on one hand minimizing the detector capacitance, which is essential to maximize the sensor Signal-to-Noise ratio, and on the other hand improving the speed and uniformity of charge collection, which is important to improve both

the timing resolution of the sensors and their radiation hardness.

Together with the main active sensors with integrated electronics, a set of test structures have been included in the engineering run, in order to investigate process and sensor characteristics that would be more complex to address in the presence of integrated electronics. More specifically, small pixel arrays with different geometries and pixels connected in parallel have been laid out and will be used to characterize the sensor operation voltage, leakage currents and charge collection dynamics. In addition, using these structures, the radiation hardness characteristics of sensors can be analyzed independently from the degradation of electronics.

Irradiation studies on some of the devices produced within the SEED project have also been carried out in parallel. The characterization was done both using passive test structures and active pixel sensor featuring $50\ \mu\text{m}$ pixel pitch. A neutron irradiation campaign on these devices has been performed in 2020. The samples were irradiated with fluxes of neutrons up to $10^{14}\ \text{cm}^{-2}$ at the TRIGA reactor facility (RIC), “Jozef Stefan” Institute (JSI) - Ljubjana. The characterization of the irradiated sensors is still on-going.

The collaboration is currently preparing the boards and firmware required for the characterization of the devices produced in the first run, that will be delivered in May 2021.

Selected Papers

Pancheri, L., Giampaolo, R., Di Salvo, A., Mattiazzo, S., Corradino, T., Giubilato, P., Santoro, R., Caccia, M., Margutti, G., Olave, J., Rolo, M., and Rivetti, A. (2020). *Fully depleted MAPS in 110-nm CMOS process with 100-300- μm active substrate*. IEEE Transactions on Electron Devices **67**(6), pp. 2392–2399.

ASAP

Lucio Pancheri,[†] Gian-Franco Dalla Betta, Matteo Favaro, Matteo Perenzoni and Alberto Taffelli

The final goal of the ASAP (Array of Silicon Avalanche Pixels) project is to demonstrate a large-area pixel sensor based on the concept of 2-layer vertically-integrated avalanche pixels, using coincidence to reject thermally-generated spurious signals. This approach can be appealing for applications requiring fine detector segmentation and low material budget as, for instance, for tracking and vertex reconstruction in particle physics experiments and charged particle imaging in medicine and biology. A sensor based on this concept can have low power consumption, low noise and a good tolerance to electromagnetic interference. In addition, a timing resolution in the order of tens of picoseconds can be achieved without requiring a power-hungry analog front-end electronic channel, thanks to the intrinsic amplification and fast onset of avalanche multiplication in Geiger-mode regime.

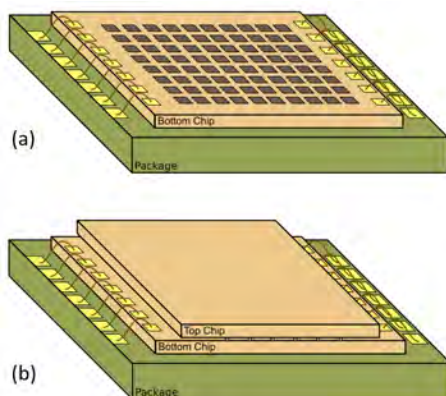


Figure 1: a) Schematic view of the single-layer sensor in package b) Schematic view of the 3D-integrated sensor assembly.

The 3D-integrated avalanche pixel concept, previously demonstrated on a small prototype in the APIX2 project, has been further developed in the ASAP project by building a module of larger area with improved efficiency and reduced sensor thickness. A pair of avalanche

sensor chips (bottom and top), designed for 3D integration and fabricated in $0.15\ \mu\text{m}$ CMOS process, were delivered and preliminarily characterized in 2019. The bottom and top chips have an area of $6\ \text{mm} \times 5\ \text{mm}$ and $5.4\ \text{mm} \times 5\ \text{mm}$, respectively, and contain several sub-arrays with pixel size of $50\ \mu\text{m} \times 50\ \mu\text{m}$ and $75\ \mu\text{m} \times 75\ \mu\text{m}$. The main array included in the design is made of 48×48 pixels, for a total size of $3.6\ \text{mm} \times 3.6\ \text{mm}$.

A few samples of top and bottom chips were glued and wire-bonded for testing before proceeding to vertical integration (Fig. 1a). After verifying the correct functionality of the single layers, several 3D-integrated assemblies were produced in 2020 using bump bonding technique, and bonded on a dedicated carrier (Fig. 1b). An extensive measurement campaign has been conducted to characterize the new demonstrators. More specifically, the following aspects have been analyzed in depth on single- and two-tier sensors:

- Dark Count Rate (DCR) as a function of bias voltage and coincidence time window. The coincidence DCR distribution measured on the 3D-integrated sensor shows an excellent agreement with the one expected from DCR of the single layers and is proportional to the width of the coincidence time window;
- variability of the breakdown voltage of the avalanche detectors in the same die and on different dies. While an excellent uniformity, of the order of 10s of mV, was observed between the pixels in the same die, the variation from die to die can be larger than 1V;
- cross-talk (Fig. 2) and optical coincidence with picosecond-pulsed laser source on the single layers.

[†]Contact Author: lucio.pancheri@unitn.it

An experimental assessment of the characteristics of the 3D-integrated assembly with different radiation sources is planned for 2021.

In 2019 and 2020, an extensive characterization of the radiation hardness of avalanche detectors fabricated by two different manufacturers has also been carried out, using both X-rays and neutrons. While a good tolerance to ionizing radiation up to 1 Mrad(SiO₂) was observed, the effect of NIEL strongly increases the DCR of the devices at fluences larger than 10⁹ 1MeV-n_{eq}/cm⁻². A predictive model for the damage probability of SPADs as a function of fluence was created and tuned on the experimental data (Ratti et al. 2020).

A preliminary investigation has also been carried out to explore the use of the sensors developed in ASAP for the imaging of radioactive β-sources, which have been recently demonstrated to be effective markers for radio-guided surgery. The collaboration has worked at the development of a hand-held probe, to be used for the real-time imaging of the spatial distribution of β-emitters in the cancerous tissue. Simulations based on GEANT4 have been conducted to estimate the efficiency of the proposed sensor in the detection of low-energy electrons from the emission spectrum of β-emitting radionuclides such as ⁹⁰Y or ¹⁰⁶Ru. A first version of the prototype of a hand-held

probe with a sensor head implemented using the APiX first sensor has been fabricated and tested, while an improved version of the probe based on the second sensor prototype, having larger active area, is currently under construction (Brogi et al. 2020). In view of this application, the sensor substrates were thinned down to 150 μm before dicing, resulting in a total thickness of 300 μm for the 3D-integrated sensors. The thickness was chosen as a compromise between the need for mechanical stability, required for die handling and assembly, and the need for a thinned substrate, required to increase the efficiency in the detection of low-energy β particles.

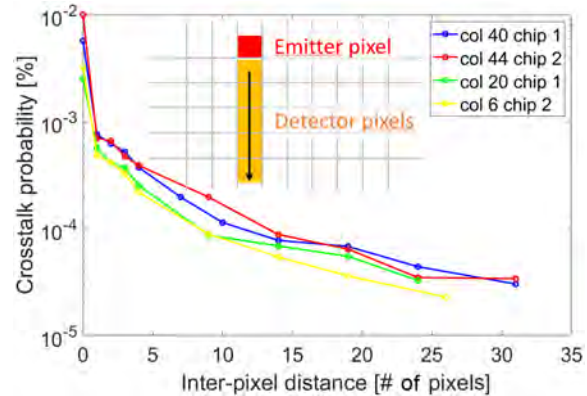


Figure 2: Optical cross-talk probability as a function of distance measured on the 75-μm pitch pixel array.

Selected Papers

- Brogi, P., Bigongiari, G., Checchia, C., Collazuol, G., Dalla Betta, G.-F., Ficorella, A., Marrocchesi, P., Morsani, F., Musacci, M., Torilla, G., Pancheri, L., Ratti, L., Savoy-Navarro, A., Silvestrin, L., Stolzi, F., Suh, J., Sulaj, A., Vacchi, C., and Zarghami, M. (2020). *APiX, a two-tier avalanche pixel sensor for digital charged particle detection*. Nuclear Instruments and Methods in Physics Research, Section A **958**. Art. no.: 162546.
- Ratti, L., Brogi, P., Collazuol, G., Dalla Betta, G.-F., Ficorella, A., Marrocchesi, P., Morsani, F., Pancheri, L., Torilla, G., and Vacchi, C. (2020). *DCR performance in neutron-irradiated CMOS SPADs from 150-to 180-nm technologies*. IEEE Transactions on Nuclear Science **67**(7), pp. 1293–1301.

DRAGoN

Davide Brunelli,[†] Lucio Pancheri

The goal of the DRAGoN project (Drone for Radiation detection of Gammas and Neutrons) is to develop a detection system, mounted on an Unmanned Aerial Vehicle (UAV), able to identify environmental radioactive contamination. The first neutron/gamma detector prototype in DRAGoN project has been made of a cylindrical scintillator crystal with 3" diameter, read out with a Hamamatsu photomultiplier tube (PMT) with 7 cm cathode diameter and 17 cm length. Although this readout system can provide a fast and low-noise output signal, its large size increases the overall weight and volume of the detection system. The total load to be carried by the UAV is further increased if a high-voltage supply board providing the detector bias is considered.

A parallel development has been carried on in the framework of DRAGoN project, with the goal of reducing the overall detector weight and size. For this development, Silicon Photomultiplier (SiPM) technology has been considered. SiPMs can be much more compact than PMTs and require a bias voltage in the order of a few 10s of volt, in contrast with the 1000V required by PMTs. On the other hand, separating neutron from gamma-generated events using Pulse-Shape Discrimination (PSD) technique requires a very fast readout, and obtaining ultra-fast signals from large-size single-channel SiPMs is a challenging task, due to the very large unit-area capacitance of these detectors. A feasible strategy to maintain a fast operation from large-area SiPM detectors is segmenting the overall sensitive area into smaller SiPM elements, and combine their outputs to deliver a single signal to the acquisition board. Several options have been considered for this purpose:

- Series combination of SiPMs: with this solution, the capacitance is reduced, but the required bias voltage is larger and the signal amplitude is also reduced.

- Parallel combination of SiPMs: this solution provides a current that is the sum of the currents from the single SiPMs, but the overall capacitance is the sum of the capacitance of the single SiPMs.
- Implementing a separate pre-amplification channel for each SiPM and combining the amplifier output signals using summing stages. This solution can provide large bandwidth and high Signal-to-Noise Ratio (SNR), but the number of required amplifiers, and thus the complexity of the system and the overall power consumption is increased.

In the final design, to balance the advantages and disadvantages of each approach, all the aforementioned techniques will be used to obtain a single large-area equivalent channel providing a fast signal to the acquisition board. Covering the overall detector area (3 inches in diameter) would require more than 250 SiPMs with an individual area of $4 \times 4 \text{ mm}^2$. Even if only a fraction of the scintillator area needs to be covered, a number of channels in the order of 100 - 200 would be needed for a reasonably good SNR. To better manage the complexity of the design, a modular solution, with each module providing a subset of the total number of SiPMs, can be adopted. As an intermediate step towards the implementation of the final detection system, a board for the operation of a 4x4 channel SiPM array (AdvanSiD) has been developed. The channels have been arranged in a 4 parallel of 4 series connection, to reduce the overall capacitance at the expense of a high bias voltage required for the operation of the SiPMs. A single amplifier in transimpedance configuration is used and a dedicated board providing the required bias and supply voltages has been designed and fabricated. A picture of the pre-amplifier and bias boards mounting the SiPM array is shown in Fig. 1. The system can be operated from a 9 - 14V battery, which is the one

[†]Contact Author: davide.brunelli@unitn.it

mounted on the UAV designed for this project, and provides a preamplified signal to the acquisition electronics through a 50-Ohm coaxial SMA connector.



Figure 1: Assembly of SiPM detector, amplifier and bias/supply board

A preliminary test with a 4-ns pulsed laser has confirmed the functionality of the detector, and the shape of the output signal is in line with simulations (Fig. 2). An in-depth characterization of the detector performance with different radiation sources, including the evaluation of gamma-neutron discrimination using PSD technique, is currently on-going. Field tests, with the detector mounted on the UAV to evaluate the effect of vibrations and electromagnetic interference, will also be held. The developed

UAV for this project is depicted in Fig. 3, and presented in Brunelli et al. (2020).

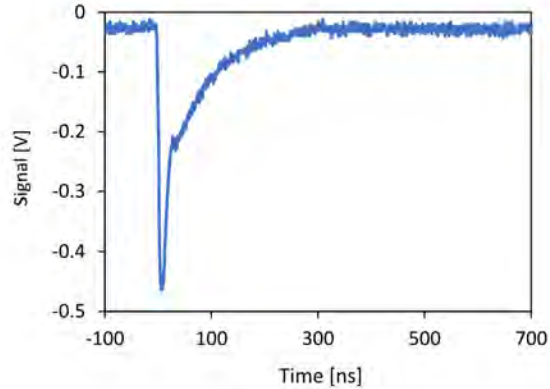


Figure 2: Output signal obtained with attenuated pulsed laser illumination

The characterization results will be used to define the possible improvements for the design of the final large-area SiPM-based modular readout system.



Figure 3: Tests with the assembled UAV

Selected Papers

Brunelli, D., Pino, F., Fontana, C. L., Pancheri, L., and Moretto, S. (2020). “DRAGoN: Drone for Radiation detection of Gammas and Neutrons”. *2020 IEEE SENSORS*, pp. 1–4.

FIRE

Alberto Quaranta,^{1†} Matteo Favaro,¹ Sara Carturan,² Laura Basiricò,³ Ilaria Fratelli,³ Andrea Ciavatti,³ Beatrice Fraboni³

During 2020, project FIRE (PI Beatrice Fraboni from Bologna) suffered a slowdown due to the covid emergency, especially regarding the runs for tests on scintillators and detectors. Nonetheless, some important achievements were obtained. In particular in this report we focus on the WP1, with responsible TIFPA unit, involving the development of flexible scintillators.

Flexible polysiloxane scintillators (PSS), synthesized owing to the LNL-TIFPA collaboration, were tested under low energy (5 MeV) and high energy (37 MeV) protons, giving a scintillation yield comparable and, in some case, superior to the best standard plastic scintillator (EJ-212 from Eljen Technology). Moreover, in order to compare the light yield with the organic photodetectors sensitivity, typically expressed in mA/W units, we also measured the scintillation light yield in W by coupling the scintillators with an optical power meter.

Tests under 5 MeV protons at LABEC facility, performed with different currents, allowed to verify the linearity of PSS performance. Moreover, the radiation hardness was tested by ir-

radiating the samples with doses of some Gy, comparable with therapy doses, and by re-measuring the light yield with a low beam current after the irradiation. We observed that the scintillation yield was preserved after different shots, thus outlining the stability of PSS under irradiation. Besides this activity, nanostructured flexible scintillators were obtained by dispersing ZnO:Zn powder into a surface layer of an undoped polysiloxane inert sample. Tests with X-rays and protons evidenced a radiation dependency of the light yield as a function of the powder composition. In particular, while for X-rays the radio luminescence intensity monotonically increases with ZnO reduction degree, following an exponential rule, under proton irradiation the maximum yield is reached for samples treated at 800 °C and performing a reduction degree of about 21%. These new recent results indicate that the defect distribution and concentration affect the response of the oxide powder to the different radiation fields. Further studies will be carried on with gamma rays and fast neutrons.

[†]Contact Author: alberto.quaranta@unitn.it

¹University of Trento and INFN TIFPA

²University of Padova and INFN LNL

³University of Bologna and INFN Bologna

GLARE-X

William Jerome Burger,[†] Alvise Bagolini, Roberto Battiston, Pietro Battocchio, Nicola Bazzanella, Massimo Cazzanelli, Claudio Cestari, Riccardo Checchetto, Roberto Iuppa, Christian Manea, Antonio Miotello, Michele Orlandi and Jacopo Terragni

The TIFPA participates in the INFN-CSN5 experiment GLARE-X (Geo-referencing via LAsER Ranging and LAsER debris Redirection from spaceE-X) on the applications of laser ablation for propulsion and debris mitigation. The group includes members with experience in the development and construction of instruments for fundamental research (AMS) and applications (active magnetic shielding) in space, and experience in the field of laser ablation, the Pulsed Laser Deposition (PLD) facility of the IdeA Laboratory devoted to the study of laser interactions in matter. A second vacuum chamber dedicated to the space application studies was installed at the PLD in 2019 (Battocchio et al. 2021). The KrF excimer laser and space applications vacuum chamber are shown in Fig. 1.

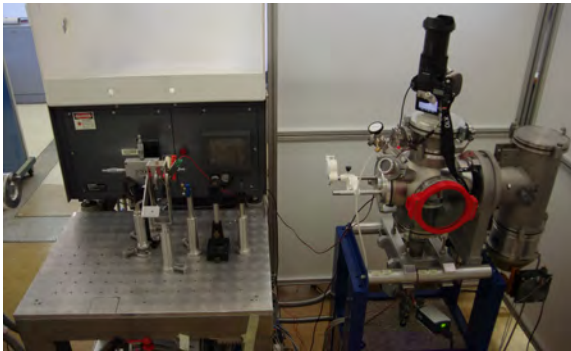


Figure 1: View of the KrF excimer laser and the components of the optical system mounted on the table (at the left), which deflects the beam to the ballistic pendulum located in the space applications vacuum chamber (at the right).

The fundamental parameter common to both space applications is the momentum-coupling coefficient C_m , which relates the impulse produced by the ablated mass to the energy density of the incident laser beam. The principle of the coupling coefficient measurement is shown in Fig. 2.

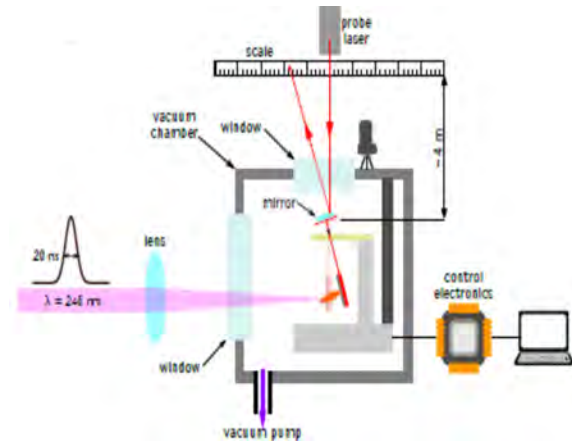


Figure 2: Schematic view of the ballistic pendulum used to measure the coupling coefficients at the PLD.

The vacuum chamber contains a ballistic pendulum mounted on a mechanical support which provides automated vertical and horizontal displacements with respect to the laser beam direction. The coupling coefficient is determined with a measurement of the angular deflection produced by the laser pulse ($\lambda = 248 \text{ nm}$, $\tau_{pulse} = 20 \text{ ns}$) in the target material attached to the pendulum. The deflection angle is measured with a second laser beam, reflected vertically from the top of the pendulum, to a graduated scale located at a distance of $\sim 4 \text{ m}$.

The published value of the aluminum C_m , relevant for space debris, $20.60 \pm 0.25 \mu\text{N/W}$ @ 70 J/cm^2 (Battocchio et al. 2021), and the results obtained to date with the new pendulum, are compared to preliminary results of a prototype pendulum in Fig. 3. The results of the prototype pendulum for two candidate propellants, Teflon and Vespel sp21, are also presented.

The estimated error of the C_m values of the preliminary aluminium, Teflon and Vespel sp21 measurements is 10%. The aluminium measurements are consistent with expected behavior of the aluminium coupling coefficient: a

[†]Contact Author: william.burger@tifpa.infn.it

Isolpharm_EIRA

Devid Maniglio,[†] Alessandra Bisio, Antonella Motta, Alberto Quaranta

As fundamental tool for nuclear medicine procedures, radiopharmaceuticals are unique medicinal formulations containing radionuclides, and are used in various clinical areas for diagnosis and/or therapy. Such radionuclides are bound to a ligand, which selectively accumulates into a target tissue allowing either a precise imaging or a focalized treatment. Therefore, progress in the research in the radiopharmaceutical field can be accomplished on one side by the discovery of the potential medical uses of innovative radionuclides on the other side by the development of new ligands. In targeted radiation therapy, a fundamental part of the radiopharmaceutical moiety is the targeting agent, i.e. the vector molecule. This portion is used for the molecular recognition between the drug and a biological entity, like a receptor, usually over-expressed on cancer cells. This moiety can be decorated with different chelators, opportunely spaced with a linker, depending on the radiometal to incorporate. Cholecystokinin 2 receptor (CCK2R) is a target extensively studied in nuclear medicine since it is over-expressed in different tumor types like pancreatic, medullary thyroid, lung, breast, ovarian, GI tract and colon. Either mAbs and peptides have been studied to target CCK2R and, recently, even a small molecule (Z-360) has been developed. The use of small molecules for tumor targeting has many advantages with respect to mAb and peptides: they undergo rapid extravasation, can rapidly penetrate into deep tissues, are not immunogenic and are amenable for chemical synthesis.

The IsolpharmEIRA project aims at developing a biologically compatible carrier molecule for ¹¹¹Ag capable of actively targeting CCK2R over expressed by humoral cells (Ballan et al. 2020).

The biology experiments performed in TIFPA (task 3) foresee in vitro and in vivo studies for the evaluation of the affinity of the de-

veloped drugs with the selected cellular target as well as the observation of their behavior in dynamic conditions. The affinity of new set of ligands for CCK2R have been evaluated through in vitro fluorescence studies on a model cell line expressing CCK2R. The biological studies started in standard 2D cell cultures, to move to more complex and more reliable 3D living systems.

This approach was accomplished following the typical tissue engineering approach, which includes the selection of a proper biomaterial on the base of parameters like bioactivity and biodegradability, and the adoption of a suitable technique to allow the fabrication of polymer-based scaffolds capable, after the cell seeding CCK2R over-expressing cells those cells and allow their proliferation and, thus, tissue maturation. To fulfill this objective, a photocrosslinkable semi-synthetic polymer, gelatin methacryloyl (GelMA), has been chosen thanks to its proven biomimetic properties. GelMA is obtained through the reaction between gelatin with methacrylic anhydride, which allows having the substitution of lysine and hydroxyl residues with methacrylamide and methacrylate side groups. The presence of these side groups endows the polymer with the possibility to undergo rapid polymerization when exposed to UV light in presence of a photoinitiator, giving the possibility to produce hydrogels. The produced hydrogels underwent to mechanical and rheological testing in order to understand the parameters that could influence the properties of the final construct.

Tissue-mimicking living constructs were realized by embedding cells into a GelMA solution, inducing gelation through 265 nm UV LED exposure. Drug targeting tests were performed evaluating accumulation of the targeting molecule in proximity of CCK2R over-expressing cells (A431-CCK2R+), compared to the accumulation on non expressing cells

[†]Contact Author: devid.maniglio@unitn.it

(A431-WT). Cell constructs were incubated with a CCK2R targeting molecule (Z-360-IP2-Rho), and a CCK2R target enabled liposome. The two molecular systems, developed in Padova (task 2), were rhodamine tagged, enabling fluorescence localization through confo-

cal microscopy. The results demonstrated that encapsulated chips preserve cell vitality, exhibiting an homogeneous distribution and permitting efficient CCK2R targeting both by Z-360-IP2-Rho molecules and liposomes (Fig. 1).

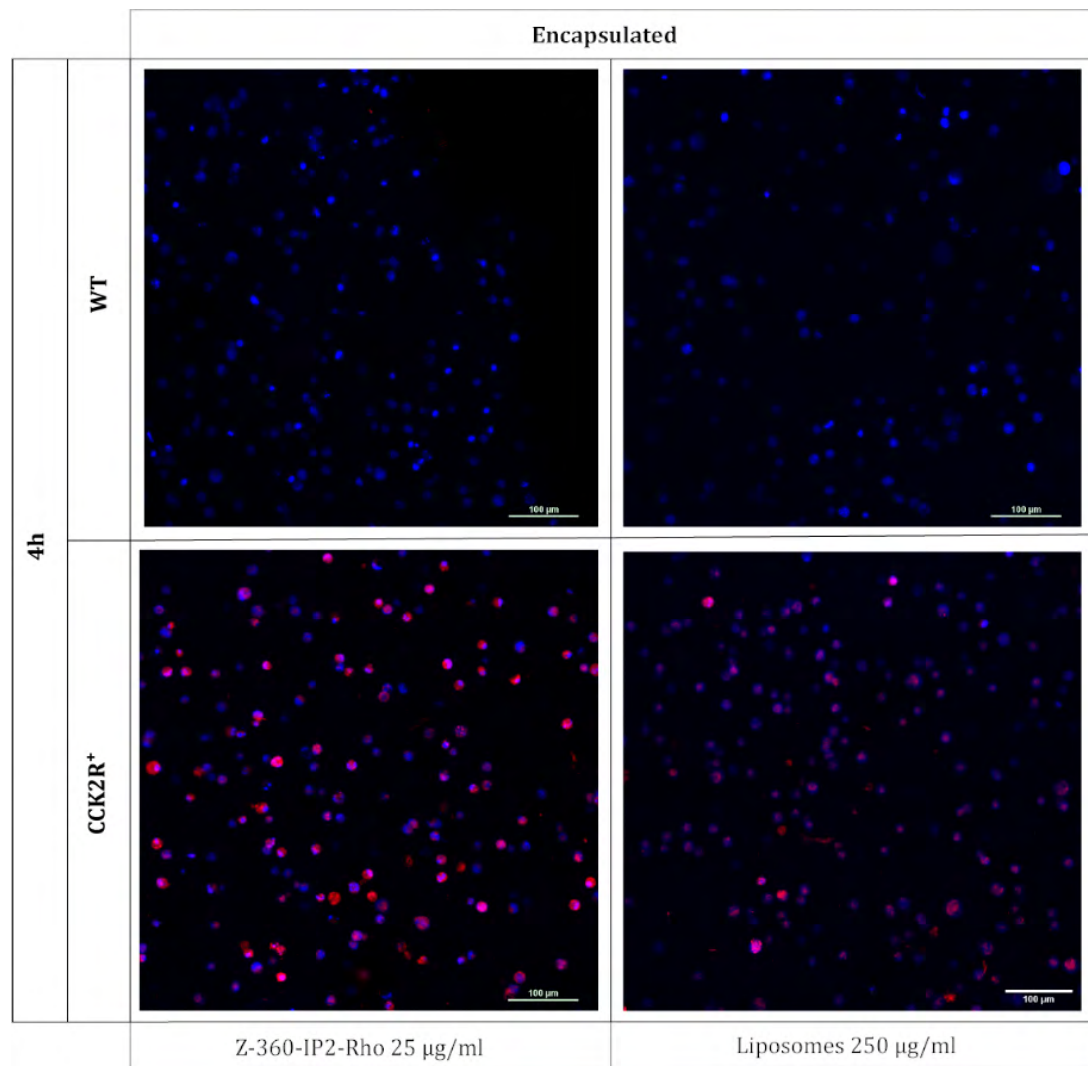


Figure 1: Confocal images of the cell constructs after 4 hours of incubation with the targeting molecular systems: Z-360-IP2-Rho and liposomes (in red). Cells nuclei are in blue.

Selected Papers

Ballan, M., Tosato, M., Verona, M., Caeran, M., Borgna, F., Vettorato, E., Corradetti, S., Zangrando, L., Sgaravatto, M., Verlato, M., Asti, M., Marzaro, G., Mastrotto, F., Di Marco, V., Maniglio, D., Bisio, A., Motta, A., Quaranta, A., Zenoni, A., Pastore, P., Realdon, N., and Andrighetto, A. (2020). Preliminary evaluation of the production of non-carrier added ^{111}Ag as core of a therapeutic radiopharmaceutical in the framework of ISOLPHARM_Ag experiment. Applied Radiation and Isotopes 164. Art. no.: 109258.

MADAM

Lorenzo Petrolli, Francesco Tommasino, Emanuele Scifoni and Gianluca Lattanzi[†]

The analysis of the radiation damage to DNA is an issue of paramount importance in radiation biophysics and a key ingredient to understand and optimize radiation based therapies, as well as radioprotection efforts. The detailed analysis of the initial occurrence of DNA damages, and their subsequent evolution, can be fundamental in unraveling and characterizing the differential effect of a specific type of radiation (such as the one delivered by particle beams, i.e., protons and heavy ions, at various energies) as compared to a reference standard radiation vector (usually X-rays). The present project, MADam (Multiscale Approach to the DNA Damage of particle radiation), is a joint initiative between the Computational Biophysics group and the BIMER (BioMedical Radiation physics) group operating at TIFPA and UniTN, at the frontier between projects in their respective fields (BIOPHYS, see p. 132, Theoretical Physics section, and MoVe IT, next report in this section). MADam attempts at advancing our understanding of the evolution of radiation-specific DNA damages, by combining the state of the art instruments of radiation biophysics and the powerful “computational microscopy” of advanced Molecular Dynamics, within a multiscale description.

Track Structure The first part of the work was dedicated to track structure simulations of the early DNA damage induced by particle beams on a tetranucleosome sample. This choice was motivated by the intent of taking a simplified, but significant, structural unit of a “chromatin-

like” framework, i.e., containing both linker and nucleosome-convoluted DNA. The simulations of the track structure of protons at different energies were performed via the Geant4-DNA Monte Carlo code; a tailored extension of the PDB4DNA tool was developed that allows the user to locate the position of the early DNA damage over an arbitrary target molecule, with base-pair resolution.

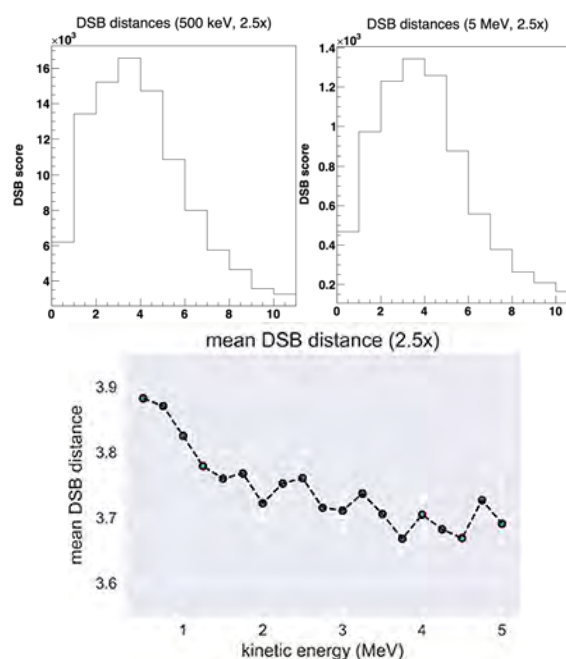


Figure 1: Double strand breaks distance distributions originated by protons at different energies on a tetranucleosome target molecule.

The results have been published on a topical issue of *Frontiers in Physics* on the “Biophysics of Particle Beams” (Petrolli et al. 2020b), and

[†]Contact Author: gianluca.lattanzi@unitn.it

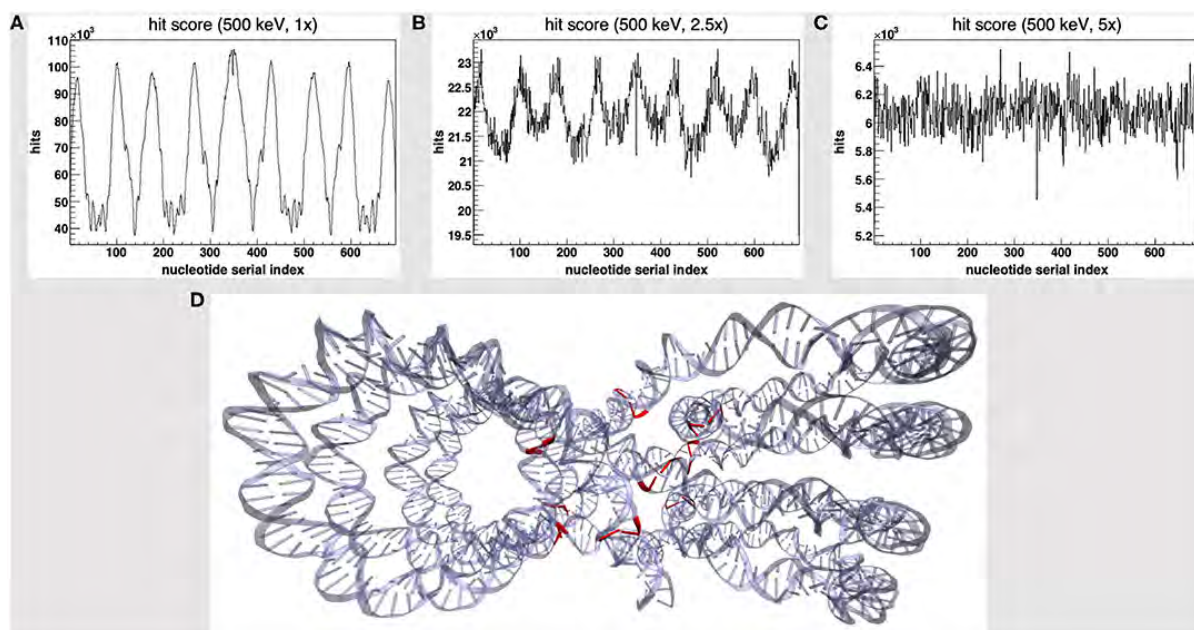


Figure 2: A,B,C: Hit score vs. the serial index of nucleotides, for a set of 500 keV-protons PDB4DNA runs at different expansion levels, and apparent hotspots on the tetranucleosome framework (D) used in this work - see Petrolli et al. (2020b) for details.

returned a distance distribution of the generated DSBs (Fig. 1); they also provided a critical scenario on the statistical significance of track structure simulations, when approaching the molecular scale (Fig. 2).

Molecular Dynamics In the second part of the work, Molecular Dynamics simulations at different resolution scales were performed on different DNA systems, ranging from single convolutions to entire nucleosomes (Fig. 3), in an attempt at describing the scales of radiation damage, from the molecular to the chromatin level. In this concern, an application of the OxDNA coarse grained force field was employed, to follow the subsequent evolution of a DNA filament after a DSB had occurred. The distance between damages has been correlated to the time scales over which the complete separation of the two broken DNA moieties oc-

curs. Such an information can be in principle “benchmarked” against novel experiments at the molecular level.

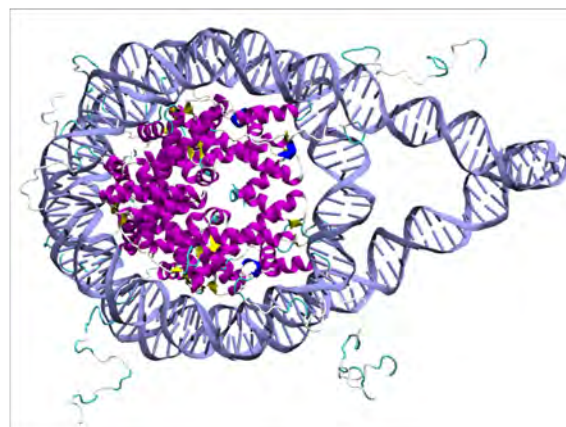


Figure 3: Structure of the nucleosome framework that was simulated at all-atom resolution via Molecular Dynamics.

Selected Papers

Petrolli, L., Tommasino, F., Scifoni, E., and Lattanzi, G. (2020b). *Can we assess early DNA damage at the molecular scale by radiation track structure simulations? A tetranucleosome scenario in Geant4-DNA*. *Frontiers in Physics* **8**. Art. no.: 576284.

MoVe IT

Elettra Bellinzona and Emanuele Scifoni[†] on behalf of the MoVe IT collaboration¹

In 2020, MoVe IT, Modeling and Verification for Ion beam Treatment planning, a CSNV-INFN Call project coordinated by TIFPA, started in 2017, and initially funded until 2019, got an extension for an additional year. The scope of MoVe IT is namely including in treatment planning systems (TPS) for hadron therapy new physical and biophysical properties of particle beams, and allowing their verification with advanced experimental methods and devices. The project completed most of its milestones, realized a large number of publications in the related activities (over 50 peer reviewed papers and 40 conference oral presentations) and got another extension for 2021. The TIFPA team, in the last year was involved not only in the national coordination (WPO), but also in first line, in collaboration with the other partners from Milan, Rome3, Turin, Naples and LNS, in all the scientific activities carried on in the Workpackages 1-4. A few notes on the latter are reported below.

WP1 - Radiobiological Modeling for Treatment Planning In this workpackage, led by E. Bellinzona, in strong collaboration with INFN-MI and INFN-RM3, as well as with the external partners, from GSI (Darmstadt) and IFJ-PAN (Krakow), the activities have been focused on the completion of the proton target fragmentation impact analysis on biologically weighted dose plans. The first approach was based on FLUKA simulations and dose averaged LET based biophysical modeling (Embriaco et al. 2020), while the second one, was employing full mixed field biological evaluation using TOPAS fragment spectra and TRiP98 TPS (Bellinzona et al. Cancers, *subm.* 2021), see Fig. 1.

[†]Contact Author: emanuele.scifoni@tifpa.infn.it

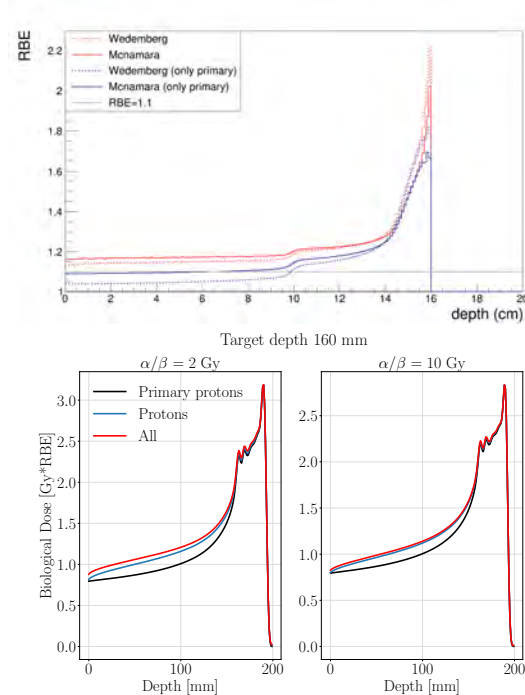


Figure 1: Impact on biologically weighted dose plans of proton fields computed with accounting target fragmentation. Top panel, fragmentation effect on the resulting dose averaged LET profile, and corresponding application of different related parametric models (see Embriaco et al. (2020) for details). Lower panels, results with a full mixed field approach for spread-out Bragg peaks optimized with constant RBE (Bellinzona et al., *subm.*).

An additional alternative study, using both the spectra computed with FLUKA and TOPAS, and a novel approach for evaluating the mixed field in microscopic cell-like volume elements have been recently realized (Attili et al., in prep. for Phys Med Biol).

WP2 - NTCP/TCP Modeling In this package, one of the focuses of TIFPA work was on the evaluation of secondary cancer induction on proton beam irradiation (Cartechini et al. 2020b). The evaluated results, demonstrated a strongly reduced probability of cancer induc-

¹for full list of contributors see www.tifpa.infn.it/projects/move-it/

tion in breast patients irradiated with protons as compared to two different advanced X-ray irradiation techniques.

Important advances, moreover, have been realized by the TIFPA team on the task of NTCP based optimization in TPS. In collaboration with GSI and APSS, the TRiP98 planning code was extended for allowing gEUD based optimization in the cost function. The new calculations allow large planning flexibility and an extremely advantageous coverage of the irradiated volume, with preserved target conformity and tremendously reduced organ at risk damage, modulated by the volume effect parameter in the most convenient way. The sparing effect, in terms of NTCP reduction, is up to a factor 3, for highly parallel organs.

WP3 -Biological Dosimetry In this workpackage an important advancement was the completion of the *in vivo* RBE experimental campaign guided by LNS team, and designed in cooperation with TIFPA, where a strong correlation was found with all the different levels of skin injury observed in proton irradiated mice, see Fig. 2 (Pisciotta et al. 2020).

The *in vitro* part, was instead focused on

the advancements on the devices for RBE and OER measurements. The prototype of the hypoxic chamber has been realized at TIFPA and shipped at the end of the year to GSI, where it was successfully tested for oxygen concentration stability and it is currently scheduled for experimental testing with the local ion beams.

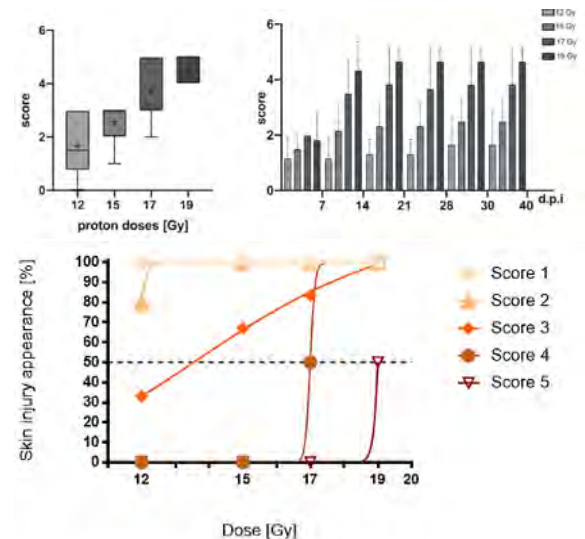


Figure 2: Measured tissue response to distal proton beams in mouse skin. The different grades refer to different level of skin injury, from normal conditions (0) to necrosis (5). See Pisciotta et al. (2020) for details.

Selected Papers

- Cartechini, G., Fracchiolla, F., Menegotti, L., Scifoni, E., La Tessa, C., Schwarz, M., Farace, P., and Tommasino, F. (2020b). *Proton pencil beam scanning reduces secondary cancer risk in breast cancer patients with internal mammary chain involvement compared to photon radiotherapy*. *Radiation Oncology* **15**(1), pp. 1–10.
- Embriaco, A., Attili, A., Bellinzona, E., Dong, Y., Grzanka, L., Mattei, I., Muraro, S., Scifoni, E., Tommasino, F., Valle, S., et al. (2020). *FLUKA simulation of target fragmentation in proton therapy*. *Physica Medica* **80**, pp. 342–346.
- Pisciotta, P., Costantino, A., Cammarata, F. P., Torrisi, F., Calabrese, G., Marchese, V., Cirrone, G. A. P., Petringa, G., Forte, G. I., Minafra, L., Bravatà, V., Gulisano, M., Scopelliti, F., Tommasino, F., Scifoni, E., Cuttone, G., Ippolito, M., Parenti, R., and Russo, G. (2020). *Evaluation of proton beam radiation-induced skin injury in a murine model using a clinical SOBP*. *Plos one* **15**(5). Art. no.: e0233258.

NEPTUNE

Emanuele Scifoni,[†] Francesco Tommasino, Elettra Bellinzona, Marta Missiaggia, Giorgio Cartechini, Francesco Giuseppe Cordoni, Christian Manea, Enrico Verroi, Enrico Pierobon, Antonino Picciotto, Chiara La Tessa

NEPTUNE - Nuclear process driven Enhancement of Proton Therapy Unraveled, is a INFN-CSN-V Call launched in 2019, dedicated to discover the origin of the radiosensitization observed in 11-Boron-compound enriched *in vitro* samples irradiated with proton beams.

The latter effect was attributed to short ranged α particles generated by the nuclear fusion process $p+^{11}\text{B}$, which, having a low energy around 4 MeV and thus an extremely high LET (linear energy transfer), are supposed to deliver a more dense ionization pattern and more lethal radiation damage to cells.

The projects aims then at exploring the possible experimental confirmation and mechanistic justification of the hypothesized process, through different workpackages, dedicated to Biophysical Modeling, Imaging, Microdosimetry and Radiobiology. The role of TIFPA team in the project was initially focused on WP5 - Coordination of Experimental Activities (WP Leader Chiara La Tessa), while in the last year it was extended also to WP1 - Modeling, with Emanuele Scifoni sharing WP leading with Andrea Attili (INFN-Roma3).

WP1- Modeling WP1 aims at providing a mechanistic based understanding of the potential radiosensitizing effect observed in the proton-Boron and proton-Fluoride nuclear reactions (see Fig. 1), i.e., analysing the radiobiological role of the alpha particles produced, as well as eventually other fragments produced in alternative channels, on different scales and modeling approaches. The 3 main approaches designed include

- (i) direct enhanced cell killing quantification modeling,
- (ii) radiation chemical track structure analysis,

(iii) non targeted effects.

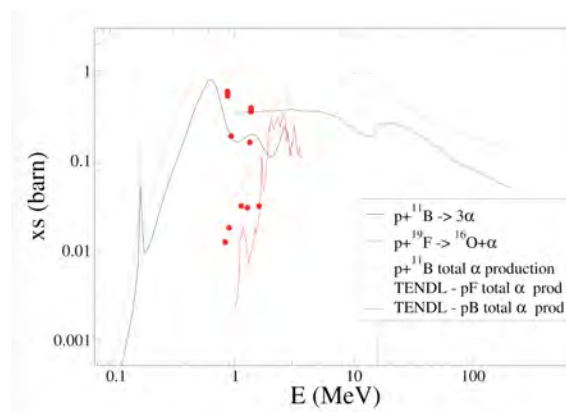


Figure 1: Total α production cross sections for Boron-11, Fluoride-19 and Oxygen-16 interaction with protons

In this second year, after the collection of the initial results, a remodulation of the package with a revised workflow, aiming at exploring in more detail the alpha production channel, and confirming the exclusion of the direct enhanced cell killing case, has been performed. In fact, despite the initial simulations it appears extremely unlikely a justification of the effect through this channel, an increasing experimental evidence of radiosensitization has been collected in WP4.

For this reason, in close collaboration with INFN-Roma3 and INFN-LNS, a new approach was based on MC simulations implementation and Radiobiological modeling (modified MKM and LEM models to account alpha short ranges) to carry on a simultaneous global fit of alpha production cross sections to every clonogenic assays, using all available reaction channel for alpha production, while the second approach (ii) was scheduled for the next year. The different flavours of the MKM model were employed (V. E. Bellinzona et al. 2021).

[†]Contact Author: emanuele.scifoni@tifpa.infn.it

The complete collection and systematic analysis of the experimental data performed in 2 facilities and at 6 different beam arrangements has been done, associated to the corresponding primary particle spectrum, and used as the input for the model, for a simultaneous optimization of a set of parameters.

Moreover, following an approach developed in MoVe IT (see in this report), the cross section variability is accounted for evaluating its impact on the biological effect, not only in terms of total total fragmentation yield, but also with a parameter defining the shape of the energy spectrum of the secondary particles. Moreover, the competitive source of alpha delivered by oxygen nuclei has been accounted for explicitly.

In the meantime the basis of the second approach, aiming at characterizing the “chemical signature” of the produced fragments has been laid, and the simulation setup for implementing a spectrum of alpha particles as a source phase space for microscopic scale simulations with TRAXCHEM and Geant4DNA has been designed.

WP5 - Coordination of Experimental Activities At the same time, TIFPA cared the coordination of all the experimental activities within the Call, both on the radiobiological side and on the microdosimetric side. These include, after the shutdown of LNS, beside the TIFPA facility, CNAO in Pavia, CN@LNL, CIRCE in Caserta, in order to scan the whole range of relevant ener-

gies useful for verifying the effect, comprising the low energies (<1 MeV) close to the resonance peak of the $p-^{11}\text{B}$ cross section.

At the same time, in order to prepare the TIFPA facility for the irradiation at distal end spread-out Bragg Peak positions, with high spatial resolution, a custom device for range shifting and modulation was designed and realized (by C. Manea et al.), see Fig. 2.



Figure 2: Customized binary range shifter developed for the high resolution microdosimetry and radiobiology measurements with the TIFPA proton beam, planned in the next year of the project.

Selected Papers

Bellinzona, V. E., Cordoni, F., Missiaggia, M., Tommasino, F., Scifoni, E., La Tessa, C., and Attili, A. (2021). *Linking microdosimetric measurements to biological effectiveness in ion beam therapy: a review of theoretical aspects of MKM and other models*. *Frontiers in Physics* **8**, p. 623.

Simp

Paolo Falferi,[†] Benno Margesin, Eugenio Monticone, Luca Oberto, Mauro Rajteri

The low-mass frontier of Dark Matter, the measurement of the neutrino mass, the search for new light bosons in laboratory experiments, all require detectors sensitive to excitations of meV or smaller. Faint and rare signals, such as those produced by vacuum photoemission or by an Axion in a magnetic field, could be efficiently detected only by a new class of sensors. An increasing number of experiments intend to exploit the conversion of Dark Matter axions by means of strong magnetic fields into microwave photons. These experiments would benefit from the development of ultrasensitive microwave photon detectors. Additionally, low dark-count is a key requirement, as the typical expected rate of the axion-to-photon conversion is around $10^{-2} - 10^{-3}$ Hz. This goal will be pursued by improving the sensitivity and the dark count rate of two types of photodetectors: Josephson Junctions and Transition Edge Sensors.

Here we will describe only some results regarding the development of the Transition Edge Sensors. For a detailed description of the Josephson Junction detector see Alesini et al. (2020). Transition Edge Sensors (TESs) are the most sensitive photon detectors available from THz to x-rays. The challenge of the Simp project is to extend their frequency (energy) sensitivity to the GHz range.

TESs are essentially thermometers based on

the steep resistive transition of a superconducting material: superconducting films are biased within the transition region where the high slope of the resistance vs temperature curve enhances the sensitivity to temperature variations and makes them thermometers suitable either as bolometers or as microcalorimeters.

The change of the TES resistance when heated by the incident radiation is read by a dc-Superconducting Quantum Interference Device (dc-SQUID). The dc-SQUID is a very sensitive flux-to-voltage converter, that allows to easily match the TES low impedance. In Fig. 1 is shown the principle of operation of a TES. A change of the current in the integrated input coil L_i of the SQUID is converted via the mutual inductance M_i in a change of magnetic flux through the SQUID loop resulting in a voltage output signal.

The Joule heating in a current-biased TES can lead the detector into the normal state (positive electrothermal feedback) making impossible a stable operation in the narrow superconducting transition region. This problem is solved by voltage-biasing the TES (negative electrothermal feedback, see Fig. 1). The voltage, determined by the resistance $R_{\text{bias}} \ll R_{\text{TES}}$, is chosen to put the TES in its so-called "self-biased region" where the power dissipated in the device is constant.

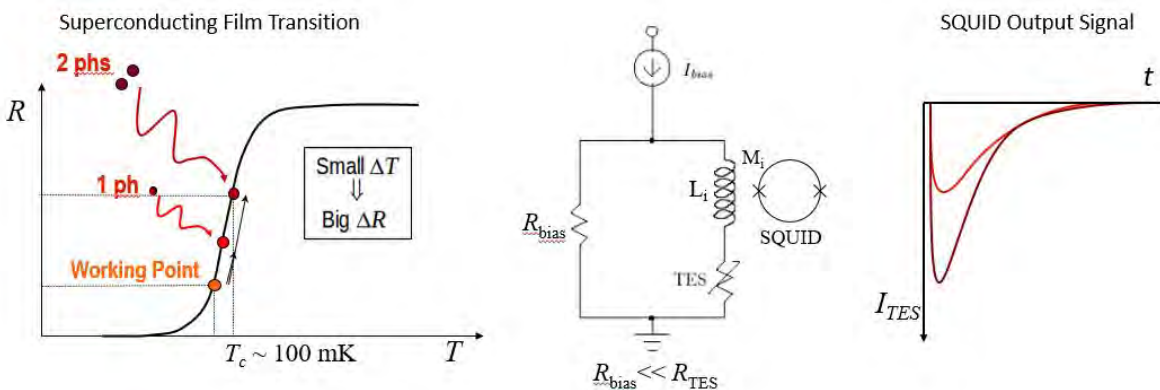


Figure 1: SQUID Detection principle of a TES.

[†]Contact Author: paolo.falferi@unitn.it

When the incident radiation is absorbed, the extra power increases the TES resistance, causing a drop in the TES current; then the Joule power drops, allowing the device to cool back to its equilibrium state in the self-biased region. As the TES is operated in series with the input coil of the SQUID, a change in the TES current produces a change in the flux to the SQUID loop, whose output is amplified and read by room-temperature electronics.

The TES sensitivity is basically determined by the Johnson noise of the TES resistance and thermodynamic fluctuations associated with its thermal impedance (phonon noise). In this case the TES energy resolution can be shown to scale with the critical temperature of the TES superconductor, and the square root of its heat capacitance. In addition, a critical parameter is the sharpness of the superconducting transition (higher is better). This suggests lowering the operation temperature and the sensor volume as much as possible in order to detect the low-energy microwave photons and suppress the dark count.

In order to finely tune the transition temperature in the range of tens of mK, we use of the proximity effect in the normal/superconductor bilayers made of Ti/Au or Al/Cu.

As an example we consider the nano-TES (Paolucci et al. 2020), highlighted by the dashed white box in Fig. 2, consisting in a $1.5\ \mu\text{m}$ -long, $100\ \text{nm}$ -wide, and $25\ \text{nm}$ -thick Al/Cu bilayer nanowire-like active region (red), which is sandwiched between the Al electrodes (blue). The critical temperature of the Al/Cu active region is $\approx 140\ \text{mK}$. Since the superconducting gap of the Al layer is higher than that of the Al/Cu bilayer (due to the inverse proximity effect), the Al electrodes act as heat barriers (the so-called Andreev mirrors) ensuring the optimal thermal efficiency of the devices.

Selected Papers

Alesini, D. et al. (2020). “Development of a Josephson junction based single photon microwave detector for axion detection experiments”. *14TH EUROPEAN CONFERENCE ON APPLIED SUPERCONDUCTIVITY (EUCAS2019)*. Ed. by E. Romans et al. Vol. 1559. Journal of Physics Conference Series. Art. no.: 012020.

Paolucci, F. et al. (2020). *Development of highly sensitive nanoscale transition edge sensors for gigahertz astronomy and dark matter search*. *JOURNAL OF APPLIED PHYSICS* **128**. Art. no.: 194502.

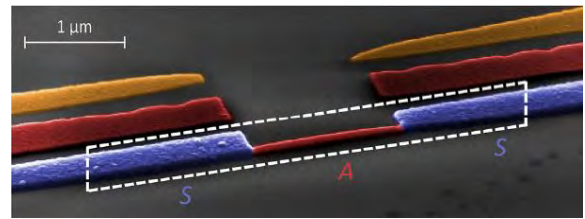


Figure 2: False-color SEM pictures of the nano-TES pointed out by the dashed white box. The two different layers are the active region Al/Cu bilayer A (red) and the Al electrodes S (blue).

To extract all the device parameters and determine the performance in both the bolometer and calorimeter operation, we performed a complete series of experiments. On the one hand, by characterizing electrically the nano-TES, we measured the critical current and the critical temperature of the active Al/Cu bilayer region. On the other hand, we fabricated and characterized a secondary device equipped with superconducting tunnel probes extracting the spectral and thermal properties of the active region. Starting from the experimental data, we calculated the performance of our device when operated as a nano-TES by employing widespread and well-known equations.

Thanks to the reduced dimensionality of the active region and the efficient heat confinement, our devices are predicted to reach state-of-the-art TES performance. In particular, as a bolometer the nano-TES is expected to have a noise equivalent power of $5 \times 10^{-20}\ \text{W}/\sqrt{\text{Hz}}$ and a relaxation time of $10\ \text{ns}$ for the sub-THz band, typical of cosmic microwave background studies. When operated as a single-photon sensor, the devices are expected to show a remarkable frequency resolution of $100\ \text{GHz}$, pointing toward the necessary energy sensitivity requested in laboratory axion search experiments.

THEEOM-RD

Enrico Serra,[†] Michele Bonaldi,[†] Antonio Borrielli, Giovanni Andrea Prodi

In Quantum Sensing and more generally in the Quantum Technologies context, High-Efficiency Electro-Optic Modulators (EOM) based on RF/Optic bi-directional conversion are gaining momentum because of their unique behavior of maintaining the coherence of quantum states in the two frequency domains. Efficient up-conversion/down-conversion of RF signals to an optical carrier would enable their transmission through optical fibers instead of through copper wires, drastically reducing losses, and would give access to the set of established quantum optical techniques that are used in quantum-limited signal detection.

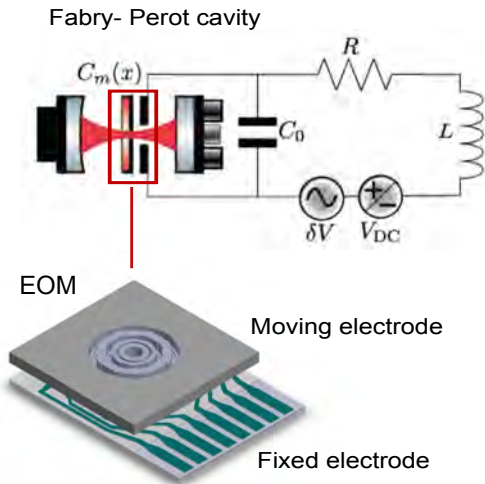


Figure 1: Schematic of a Fabry-Perot cavity with the EOM transducer used for rf/optical sensing used in a membrane-in-the-middle optomechanical setup.

This is of fundamental interest in quantum communications where qubits in a superconductive quantum computer in a cryogenic environment are transmitted to optical fibers networks at a great distance in a quantum network at room temperature. The relevance of these devices is foreseen also in other fields like

radio-astronomy, RF non-reciprocal switches, and medical imaging. EOM devices can efficiently work, in the classical domain, as ultra-low noise read-out systems for weak RF signals. For instance, in NMR (Nuclear Magnetic Resonance) a shot-noise limited read-out improves the image reconstruction process. The platform for the transduction consists of a high-quality nano-membrane resonator that can simultaneously be coupled to the electric and optical degrees of freedom and therefore they can transduce signals at disparate frequencies with high efficiency. This is done by adding a conductive layer to the membrane's surface realizing a capacitive coupling between the moving electrode and the fixed LC rf circuit. The fluctuations of the vibrating mode of the membrane link the rf-electromagnetic field to the optical field of a high finesse cavity as shown in Fig. 1. The EOM design in Fig. 1 consists of a membrane resonator with an on-chip shield for mechanical losses and the two electrodes separated by a micron-scale gap. The moving electrode is under the action of the fluctuation of the radiation pressure and the thermal noise coming from the environment. The coherence will be guaranteed by a high Q-factor of the membrane that is reachable applying advanced design techniques that reduce the mechanical dissipation and decouples the resonator from the thermal bath. To this aim, we have exploited a stress-engineering technique that reduces the dissipation by a selective tapering of the membrane's edge that makes the device Q-factor constant and reproducible in a wide operational band. From Fig. 2 the result derived with interferometric measurement of the Q-factor can be seen by comparing the original round-shaped membrane with the new version with clamp tapering. This result can be further improved by thinning down the edge to 25 nm with an estimated increase of the Q-factor up to 30 million.

[†]Contact Author: enrico.serra@tifpa.infn.it, michele.bonaldi@unitn.it

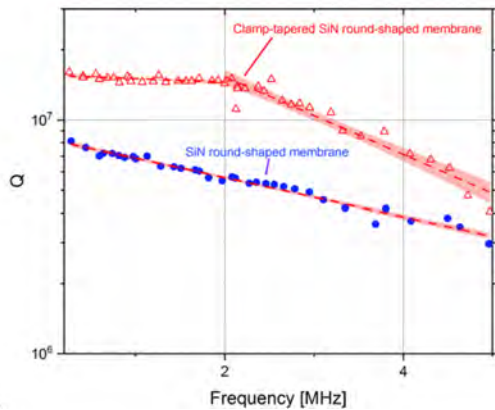


Figure 2: The measured quality factors of the membrane with (red triangles) and without the clamp tapering (blue circles).

On the other hand, the membrane's electrode design maximizes the overlapping function between electrodes improving the electro-optical coupling rate. A TiN (Titanium Nitride) layer is RF-sputtered and was chosen as a membrane's electrode, because it has a uniform thickness and resistivity, and shows the potential for yielding reproducible low-temperature devices with a transition temperature of 5.6 K. On the other hand, TiN films are widely used for coplanar resonators and microwave kinetic inductance detectors (MKID). The fabricated electrode is ultra-thin (25 nm) deposited over a tensile (1 GPa) with an ultra-high aspect ratio: 100 nm membrane's thickness and 1.5 mm in diameter for reducing the mechanical dissipation. The patterning of the electrode and the silicon structures was done by surface/bulk micromachining techniques used in M/N-MEMS processing. The result of the integration of the electrode can be seen in Fig. 3. The interferometric measurements show that the electrode does not affect the Q-factor of the membrane. There is only a frequency shift of the membrane's resonant modes.

In the experiment, the functionalized nano-

membrane will be embedded into a Fabry-Perot cavity and used to detect weak signals in the MHz bandwidth that are of interest in NMR imaging. Mapping the signal in the optical intracavity field with a shot-noise limited readout will give us the platform for understanding devices' behaviors and to study the electro-optomechanical interaction at room and cryogenic temperatures. Advanced measurement schemes based on quantum cavity optomechanics protocols will be used for observing state rf/Optical transfer when the resonator is at a low phonon occupation number. In fact, besides room temperature measurement and the demonstration of the transduction principle between an RF to optical conversion with an interferometric scheme developed a complete theory for laser cooling of a macroscopic radio-frequency LC electrical circuit using an opto-electromechanical system, consisting of an optical cavity dispersively coupled to a nanomechanical oscillator, which is in turn capacitively coupled to the LC circuit of interest. We determine the optimal parameter regime where the LC resonator can be cooled down to its quantum ground state, which requires large optomechanical cooperativity and larger electromechanical cooperativity. These requirements are fulfilled by our EOM design and the whole theory is reported in Malossi et al. (2021).



Figure 3: The TiN floating electrode on a Si_4N_3 membrane. (left) the whole device (right) detailed region of the electrode (optical microscope image).

Selected Papers

Malossi, N., Piergentili, P., Li, J., Serra, E., Natali, R., Di Giuseppe, G., and Vitali, D. (2021). *Sympathetic cooling of a radio-frequency LC circuit to its ground state in an optoelectromechanical system*. Phys. Rev. A **103**. Art. no.: 033516.

TIMESPOT

Gian-Franco Dalla Betta,[†] Maurizio Boscardin, Francesco Ficorella, Giulio Tiziano Forcolin, David Macii, Roberto Mendicino, Giovanni Paternoster, Giancarlo Pepponi, Sabina Ronchin, Giovanni Verzellesi, Nicola Zorzi

The project is aimed at the development and implementation of a complete integrated system for charged particle tracking having very high precision both in space (100 μm or less) and in time (100 ps or less) per pixel. The main use and scope is in High Energy Physics experiments at high luminosity (e.g., for the upgrade of the LHCb VELO), where the high density tracking, both in space and time, will be a major issue. The approach is based on 3D geometry Silicon and Diamond pixelated sensors, dedicated integrated front-end and pre-processing chip (time measurement electronics) in 28nm CMOS, and real-time processors for data elaboration both at front-end and back-end level (fast tracking algorithms). TIFPA is responsible for WP1: 3D Si sensors development and characterisation, and is also involved in WP6: System integration and tests.

In 2020 the activity was focused on the functional characterization of the first batch of sensors, produced at FBK in 2019 (Anderlini et al. 2020), and on the fabrication and preliminary characterization of the second batch of sensors.

The results of the first beam test carried out at PSI in 2019 were thoroughly analysed using different methods (Anderlini et al. 2020). As an example, Fig. 1 shows the distribution of the time difference between the signals of a 3D-trench silicon sensor and the pion arrival time with the result of the fit (gaussian + exponential tail) overlaid. From the standard deviation of the gaussian core ($\sigma_{core} \simeq 24$ ps) and keeping into account the uncertainty on the arrival time of the pions, the timing resolution of the sensor was found to be ~ 20 ps. This remarkably low value was confirmed and even surpassed by further functional measurements performed in the laboratories of the TIMESPOT Collaboration, using laser and radioactive sources. In

particular, position resolved laser tests allowed to explore the dependence of the timing resolution on the hit point, and confirmed a uniform response from most of the pixel area, in good agreement with simulations.

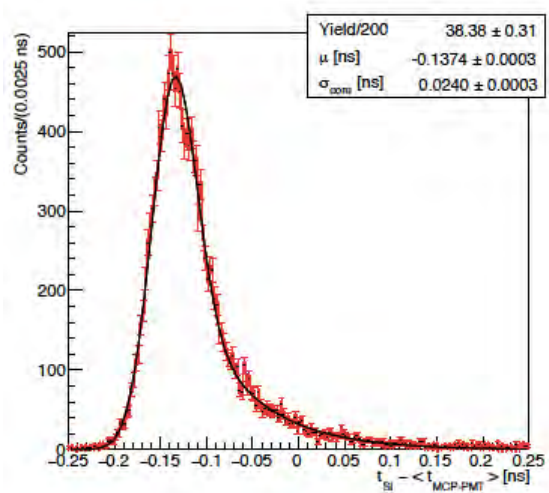


Figure 1: Distribution of the time difference between the 3D-trench silicon sensor and the pion arrival time with the result of the fit overlaid.

Simulations also allowed to explain the tail in the timing distribution observed in Fig. 1, that is to be ascribed to events taking place at the edge region in the test structure used in the beam test, where the electric field is very low, leading to a delay in the current pulses. It is worth stressing that this problem is specific to the test device and would not be present in a pixel sensor. From further tests using higher laser intensities it was possible to observe that 3D-trench sensors read-out with fast discrete electronics can reach a timing resolution below 1 ps !

Three sets of test samples from the first batch were irradiated with reactor neutrons at JSI (Ljubljana, Slovenia) up to three different fluences, the characterization of these devices

[†]Contact Author: gianfranco.dallabetta@unitn.it

is under way.

The layout of the second batch of sensors was completed at UniTN in February 2020 and

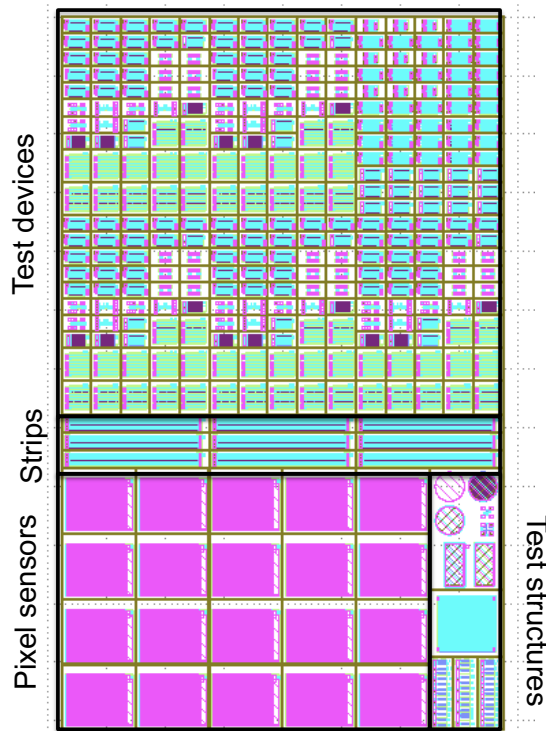


Figure 2: Reticle layout used for the fabrication of the second batch of sensors.

submitted for fabrication to FBK. The reticle layout is shown in Fig. 2: it contains twenty (5×4) pixel sensors, each consisting of an array of 32×37 pixels, compatible with the new TIMESPOT read-out chip, as well as nine strip sensors, a large number of test devices and a

few test structures for process monitoring. The fabrication of the batch was completed at FBK in November 2020, and a preliminary test of the current-voltage (I-V) characteristics in reverse bias was carried out on the pixels sensors using a temporary metal on the wafer. Fig. 3 shows the distribution of the total leakage currents measured at 30 V in all sensors compatible with the TIMESPOT1 read-out chip. Despite the large non uniformity in the values, a large fraction of the sensors is functional with low leakage current. In particular, $\approx 73\%$ of the sensors has leakage current lower than 100 nA that, after normalization to the number of pixels, corresponds to less than 100 pA/pixel. The breakdown voltage was found to be larger than the maximum voltage used in this automatic test (50 V) and will be measured on test structures after the removal of the temporary metal.

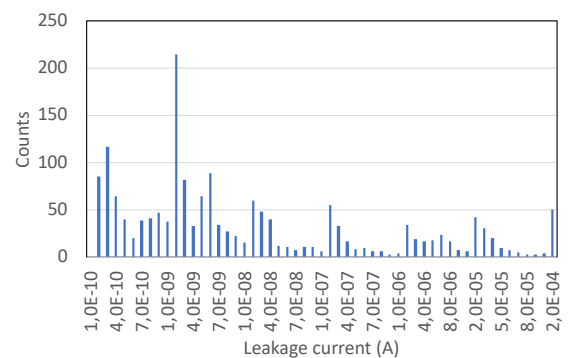


Figure 3: Distribution of total leakage current at 30 V in all arrays of 32×37 pixels from the second batch.

References

Anderlini, L., Aresti, M., Bizzeti, A., Boscardin, M., Cardini, A., Dalla Betta, G.-F., Ferrero, M., Forcolin, G. T., Garau, M., Lai, A., Lampis, A., Loi, A., Lucarelli, C., Mendicino, R., Mulargia, R., Obertino, M., Robutti, E., Ronchin, S., Ruspa, M., and Vecchi, S. (2020). *Intrinsic time resolution of 3D-trench silicon pixels for charged particle detection*. *Journal Instrum.* **15**. Art. no.: P09029.

Activities starting in 2021

DART WARS

Research outline The aim of the DART WARS project is to boost the sensitivity of INFN experiments based on low-noise superconducting detectors. This goal will be reached through the development of wideband superconducting amplifiers with noise at the quantum limit and the implementation of a quantum limited read out in different types of superconducting detectors. Noise at the quantum limit over a large bandwidth is a fundamental requirement for challenging future applications, like neutrino mass measurement, next-generation x-ray observatory, CMB measurement, and dark matter and axion detection, in which the INFN is deeply involved. The sensitivity and the bandwidth of microcalorimeter detectors such as Transition Edge Sensors (TESs) and Microwave Kinetic Inductance Detectors (MKIDs) using dissipative readout are limited by the noise temperature and bandwidth of the cryogenic amplifier. Likewise, resonant axion-detectors, such as haloscopes, must probe a range of frequencies of several GHz keeping the system noise to the lowest possible level. The need for a quantum limited microwave amplifier with large bandwidth operating at millikelvin temperatures is also particularly felt in many quantum technology applications, for example the rapid high-fidelity multiplexed readout of superconducting qubits. To this end, devices called traveling wave parametric amplifiers (TWPAs) are currently being developed. The nonlinear element of TWPAs is provided by Josephson junctions or by the kinetic inductance of a high-resistivity superconductor. The DART WARS project is a research effort to improve the performance and reliability of these amplifiers with the study of new materials and with improved microwave and thermal engineering. The long-term goal is to demonstrate, for the first time, the readout with different sensors (TESs, MKIDs, microwave cavities and qubits) opening the concrete possibility to increase the sensitivity of the next generation particle physics experiments.

involved external institutions Fondazione Bruno Kessler (FBK), Trento (Italy); Istituto Nazionale di Ricerca Metrologica (INRiM), Turin (Italy); Institute for Basic Science Center for Axion and Precision Physics Research (IBS-CAPP), Daejeon (South Korea).

INFN groups Milano Bicocca, Napoli — Gruppo Collegato di Salerno, TIFPA, LNF, Lecce

Principal Investigator Andrea Giachero (Milano Bicocca)

TIFPA team Benno Margesin (coordinator), Alessandro Cian, Paolo Falferi, Damiano Giubertoni, Renato Mezzena, Andrea Vinante, Emanuele Enrico, Mauro Rajteri

MICROBE_IT

Research outline The rationale for using ions in external beam radiotherapy is supported by both physical and radiobiological advantages. Although clinical results have been encouraging, numerous treatment uncertainties remain major obstacles to the full exploitation of charged particles. One of the key issues is understanding the link between the energy deposited by radiation and its biological effectiveness. The physical dose depends on the radiation field quality (particle species and LET) while RBE has a complex dependency on both physical and biological parameters of the irradiated system. Dose, LET and RBE represent the main ingredients of treatment planning, and

incorrect estimates can lead to both underdosing of the tumor or overdosing normal tissue. These effects can impact the treatment success and become exaggerated in hypofractionation schemes and reirradiation where error tolerances are even more limited.

The aim of MICROBE_IT (Microdosimetry-based assessment of Biological Effectiveness in Ion Therapy) is to improve the in- and out-of-field dose calculation and RBE quantification by developing a stochastic kinetic model based on a microdosimetric radiation quality characterization. Microdosimetry takes into account the stochastic nature of energy deposition and provides a description of the energy received by a cell that is superior to the standard dosimetry. The existing models for calculating RBE assume that all variables follow a Poisson distribution, and thus can be described by their mean. This assumption neglects stochastic fluctuations in energy deposition from cell to cell, and from dose fractionation (time variable), which can be especially significant in highly mixed radiation fields, that for example occur at the beam edges and in the distal region. The new model (GSM2 generalized stochastic microdosimetry model for radiobiological endpoints), will predict cell survival and RBE by considering stochastic fluctuations of both the energy imparted and the kinetics of cell inactivation, which lead to the final biological effect.

To achieve the project goals, energy deposition spectra will be measured with four existing (nano- and mini-TEPC, silicon telescope and Micro Plus Probe) and two under development (HDM- hybrid detector for microdosimetry and SiC-Silicon Carbide) detectors, whose finalization will be part of this project. A combination of the experimental spectra and Monte Carlo simulations will provide the energy deposited by each component of the mixed radiation field. Radiobiological experiments will provide DNA damage evolution and cell fate after exposure. GSM2 will model cellular responses to each component of the mixed field provided by the detectors. The central innovation of this methodology is that all probability distributions are derived from the data and not defined a priori (e.g. Poisson). Furthermore, non-standard microdosimetric and nanodosimetric spectra acquired by HDM and Nano-TEPC, respectively, will indicate possible new links between energy deposition and cell damage less dependent on particle type.

A more accurate RBE model will help improve ion therapy performance by increasing treatment effectiveness and reducing potential toxicity effects. We will focus on optimizing the methodology for protons and carbon ions, but GSM2 can be extended to any other ion radiation source and overcome major barriers to wide implementation of particle therapy.

involved external institutions Centre for Integrative Biology (CIBIO) — University of Trento (Italy); University of Verona (Italy); Politecnico of Milano (Italy); CNR IBFM (Italy); Bruno Kessler Foundation (FBK), Trento (Italy); Azienda Provinciale per i Servizi Sanitari (APSS), Trento (Italy); GSI Helmholtzzentrum für Schwerionenforschung GmbH, Darmstadt (Germany).

INFN groups TIFPA, LNS, Roma3, Milano, LNL

Principal Investigator Chiara La Tessa (TIFPA)

TIFPA team Chiara La Tessa (coordinator), Emanuele Scifoni, Francesco Tommasino, Enrico Verroi, Elettra Bellinzona, Marta Missiaggia, Francesco Cordoni, Enrico Pierobon, Leonardo Ricci, Michele Castelluzzo

NanoEnHanCeMent

Research outline NanoEnHanCeMent - Nanoparticle Enhanced Hadrontherapy: a Comprehensive Mechanistic Description, is a Marie Curie Individual Fellowship project awarded to Dr. Pablo

de Vera Gomis, with joint supervision of ECT* and TIFPA, started on November 2020. The project focuses on finding a comprehensive mechanistic understanding of the presently still largely unclear process of nanoparticle induced radiosensitization of particle beams in hadrontherapy, through the application of basic physics and chemistry methods and nanoscale based analysis. In fact, despite accumulating experimental evidence of high Z nanoparticles enhancing the biological effects of ion beams, with the perspective of promising clinical applications, also thanks to the possibility of the nanoparticles to be tuned to target tumor cells, several hypothesis for explaining the mechanisms have been shown inconsistent in the recent years. A proper exploitation of the nanoparticle radioenhancement in hadrontherapy depends on improving the understanding of the physico-chemical mechanisms underpinning it. In this project, thus, a theory and modelling approach is proposed, in which a series of semiempirical and ab initio methods will be extended and interfaced with Monte Carlo track-structure simulation tools, in order to advance the basic understanding of the nanoparticle enhanced hadron-therapy physical and chemical mechanisms.

involved external institutions ECT*, Trento; GSI, Darmstadt (Germany); University of Murcia (Spain); University of Ioannina (Greece); University of Alicante (Spain).

INFN groups TIFPA

Principal Investigator Pablo De Vera Gomis, ECT* and TIFPA

TIFPA team Pablo De Vera Gomis (coordinator), Simone Taioli, Maurizio Dapor, Emanuele Scifoni

XpCalib

Research outline The XpCalib experiment aims at exploiting the potential applications of the proton CT (pCT) system previously developed by INFN Firenze, by extending its potential towards clinic applications in the field of proton therapy. In particular, by applying the pCT on dedicated biological test phantoms developed in the framework of the project, the experiment aims at improving the accuracy of the x-CT calibration in producing the relative stopping power (RSP) maps for proton therapy treatment planning to finally outperform most advanced dual energy x-CT techniques. Final goal would be the incorporation of the new calibration into the treatment planning software, aiming at increasing treatment accuracy.

involved external institutions Trento Proton Therapy Center (APSS)

INFN groups Firenze, TIFPA

Principal Investigator Carlo Civinini (Firenze)

TIFPA team Francesco Tommasino (coordinator), Enrico Verroi, Marina Scarpa, Paolo Farace, Stefano Lorentini, Francesco Fracchiolla, Roberto Righetto

BOLAS_NEXT

Research outline BOLAS_NEXT is a new 2-years CSN5 project, starting on 2021 and involving the Units of INFN-Lecce (G. Quarta, A. Caricato), LNL-Padova (S. Carturan), LNS-Catania (P. Finocchiaro) and TIFPA-Trento (A. Quaranta) with Gianluca Quarta from Lecce as PI. The aim of BOLAS_NEXT is the development of new technological solutions for the detection of thermal neutrons based on ^{10}B -enriched thin films grown by Pulsed Laser Deposition (PLD). BOLAS_NEXT exploits the know-how acquired during the previous experiment, BoLAS, where the PLD set-up for the deposition of enriched films was developed. During BOLAS_NEXT the deposition technique will be used for the production of enriched coatings both on SI detectors and on organic scintillators in order to improve efficiency, sensitivity and discrimination against gamma background.

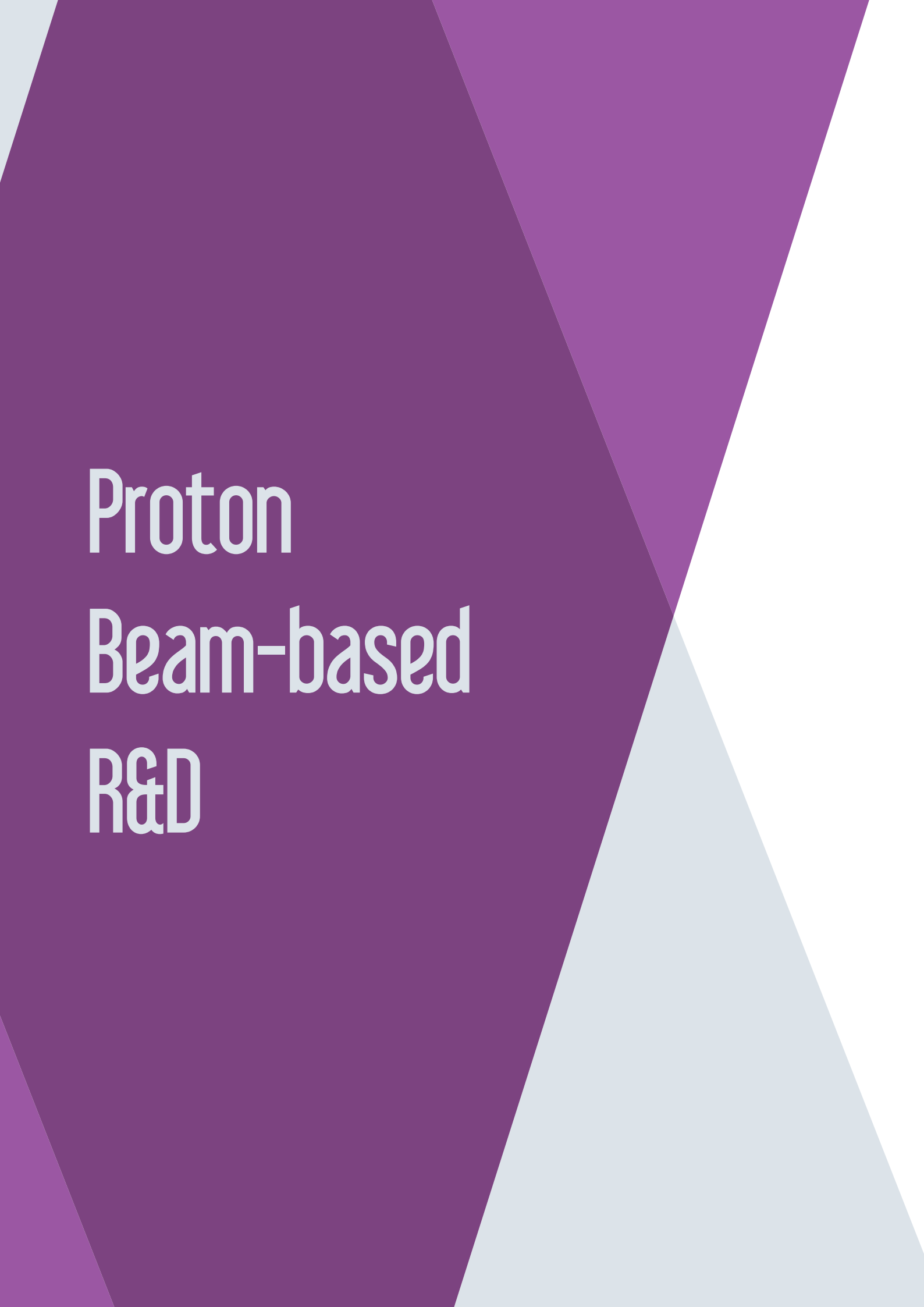
In applications involving solid state detectors the activity will provide new devices based on the combination of two detectors in order to get rid of the gamma background associated both to the neutron field and to the ^{10}B capture reaction. A comparison with alternative materials containing ^6Li will be also performed.

Following a different approach, thin enriched films will be coupled with polysiloxane scintillators (PSS) exploiting the possibility, already demonstrated, to grow thin films on flexible and soft substrates by PLD. In particular, PSS will allow to explore different geometries for the optimization of the detection of ^{10}B reaction products. By selected molding techniques different patterns will be realized on PSS surface before deposition, in order to increase the effective interaction surface between film and scintillator. Detection tests following traditional approaches, that is the coupling between the scintillator and a standard PMT, will be performed in order to verify the increase of detection efficiency with patterned structures. Then, the last step will consist in a further integration where both Is-detectors and PSS will be coupled in a single device in order to combine the advantages of both of them.

INFN groups Lecce, LNL, LNS, TIFPA

Principal Investigator Gianluca Quarta (Lecce)

TIFPA team Alberto Quaranta



Proton Beam-based R&D

Proton irradiation tests on FBK Silicon Photomultipliers

Fabio Acerbi,^{1,2†} Anna Rita Altamura,^{1,2,3} Alberto Mazzi,^{1,2} Alberto Gola,^{1,2} Enrico Verroi²

Silicon Photomultipliers (SiPMs) are arrays of many single-photon avalanche diodes (SPAD) connected in parallel to common anode and cathode, each with an integrated quenching resistor. Each pixel is sensitive to a single photon, working in Geiger-mode, with high internal electric fields to trigger self-sustaining avalanche multiplication processes. They are emerging as detector of choice in many applications (Acerbi and Gundacker 2019), such as in nuclear medicine, in high-energy and large physics experiments, in automotive LiDAR and in space applications.

In particular, when used in high-energy physics experiments (like CALICE Analog Hadron Calorimeter (AHCAL) or CMS-HCAL) or when used as part of the instrumentation for space-mission experiments, SiPMs are often exposed to a significant dose of radiations. Typical values of maximum radiation doses are in the order of $10^9 - 10^{10} n_{eq}/cm^2$ for space applications, or up to $10^{14} n_{eq}/cm^2$ (1 MeV neutron equivalent) for experiments in HEP.

To be able work properly, maintaining appropriate performance up to the end of the experiment, a good radiation tolerance (or radiation hardness) is required and the SiPMs have to be properly optimized, in particular reducing or mitigating their performance worsening. In FBK (Trento, Italy) we have been developing several SiPM technologies over the last years, optimized for different applications in terms of detection efficiency (for example with peak sensitivity in the blue-wavelength region or in the green-wavelength region) and performance characteristics in specific application conditions (e.g. working in liquid nitrogen). It is therefore very interesting to characterize and compare the main performance-parameters degradation, thus the radiation hardness of these dif-

ferent technologies.

As for the majority of the silicon-based photodetectors, the radiation damage can affect both the surface and the bulk region through ionizing energy loss (IEL) and non-ionizing energy loss (NIEL) respectively (Moll 2018), introducing defects and recombination centers. Depending on the energy and the particle type, either one type of damage or the other one is more relevant and likely to happen. However, differently from other type of radiation sensors, SiPMs work in Geiger mode, being possibly more sensitive to even small defects, particularly in the bulk.

Experimental setup and tests In September 2020 we performed some irradiation tests at the TIFPA Protontherapy Centre (Trento, Italy) on several Silicon Photomultipliers produced by FBK (Trento, Italy). Protons are heavy charged particles doing both ionizing and non-ionizing interactions. Moreover, in this experiment we used both the beam-lines of the research room. In particular we exploited the good dose-uniformity over large areas of the dual-ring double scattering system to irradiate many different silicon chips with the same nominal dose. Then, we used the Gaussian-shape beam line to achieve higher dose over a limited number of silicon chips. In the latter case we also repeated the irradiation (on different sets of silicon hips) at two different proton energies.

In our experiment we prepared different carriers to host bare silicon chips. The carriers are made by a 3D printed frame containing adhesive tape, where the chips are attached, and by a 3D printed base. We performed an irradiation with protons at 148 MeV, with a nominal beam current of 200nA, with the dual-ring double scattering system, reaching a dose on the

[†]Contact Author: acerbi@fbk.eu

¹FBK, Trento, Italy

²INFN TIFPA, Trento, Italy

³University of Udine, Italy

first set of silicon chips of $2.9 \cdot 10^7$ p/mm², on a second set of chips of $2.8 \cdot 10^8$ p/mm² and on a third set of chips of $2.6 \cdot 10^9$ p/mm². Then we switched on the gaussian-beam line, and we irradiated a different set of chips (reduced set, due to the smaller beam diameter), at 148 MeV, with a current of 300 nA, reaching an estimated dose of $2.9 \cdot 10^{10}$ p/mm² on a first set of chip and $2.3 \cdot 10^{11}$ p/mm² on another set of chips. We also irradiated another set of chip with proton at 70 MeV, reaching a dose of $1.5 \cdot 10^{10}$ p/mm². Dose values are calculated as the average of all

the test structures irradiated, considering a perfect centering of the beam on the sample carrier (see laser centering in Fig. 1).

Overall, the irradiation campaign was successful, but we found an unforeseen activation of chips irradiated with the highest doses. This prevented the measurements on some of the samples which, however, are planned and will be done soon. In the meanwhile the silicon chips have been placed in a fridge just after the irradiation to prevent room-temperature self-annealing of the irradiation damage.

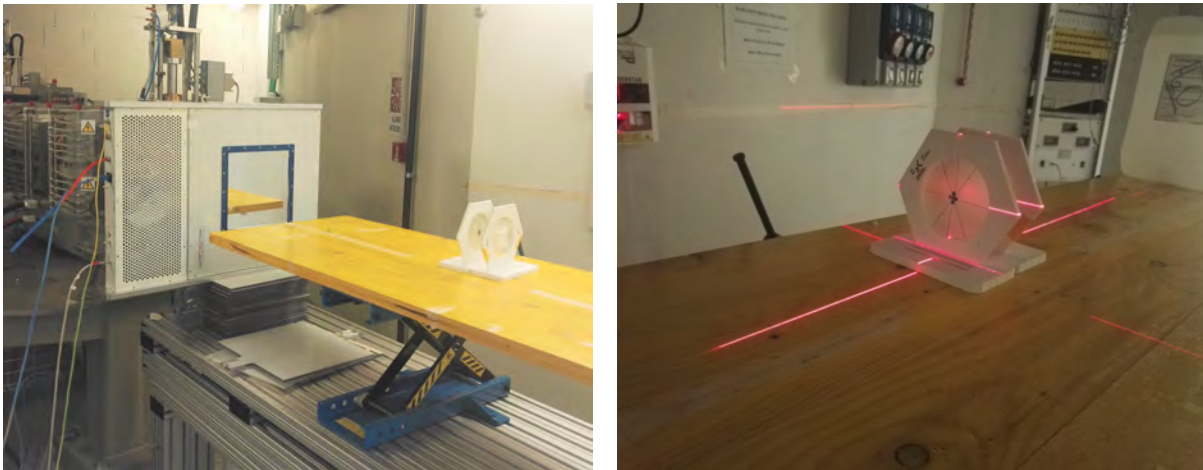


Figure 1: Pictures of two FBK chip carrier (containing SiPM chips) placed in front of the Gaussian beam line, aligned for irradiation.

References

- Acerbi, F. and Gundacker, S. (2019). *Understanding and simulating SiPMs*. Nuclear Instruments and Methods in Physics Research Section A: Accelerators, Spectrometers, Detectors and Associated Equipment **926**. Silicon Photomultipliers: Technology, Characterisation and Applications, pp. 16–35.
- Moll, M. (2018). *Displacement Damage in Silicon Detectors for High Energy Physics*. IEEE Transactions on Nuclear Science **65**(8), pp. 1561–1582.

Emulsion Cloud Chamber Exposure test at Proton Therapy Center in Trento in the framework of the FOOT experiment

Adele Lauria,^{1,2} Maria Cristina Montesi,^{1,2†} Francesco Tommasino³

Hadron therapy is based on the use of charged particle beams for the treatment of deep-seated tumour. The ions beam release a large dose in the tumour region and a smaller one in the surrounding healthy tissues. The fragments produced in the interaction with the human tissues are not well characterised and extensive studies are needed in order to improve the clinical treatment plans. The FOOT (FragmentatiOn Of Target) experiment aims to study the dose released by the tissues and particle beams fragmentation. The target (^{16}O , ^{12}C) fragmentation induced by 150-250 MeV/n proton beams will be studied via the inverse kinematic approach, where ^{16}O and ^{12}C therapeutic beams collide on graphite and hydrocarbons target to provide the cross section on hydrogen. The FOOT detector consists of an electronic setup for the identification of $Z \geq 3$ fragments and of an emulsion spectrometer to measure $Z \leq 3$ fragments.

The contribution of the TIFPA Unit was crucial for the calibration of the sub-detector units (both the electronic and the emulsion ones) forward looking the data taking performed at GSI (Darmstadt).

The first data taking has been performed in 2019 at the GSI facility by exposing the emulsion spectrometer to oxygen ion beams of 200-400 MeV/n. The emulsion spectrometers have been realised according the Emulsion Cloud Chamber (ECC) technique which consists of nuclear emulsion films alternated with passive material. Each emulsion spectrometer is composed of three sections:

- (i) a first section for vertexing composed by alternated emulsion films and passive layers of C or C_2H_4 acting as target in which

- secondary fragments are originated;
- (ii) a second section dedicated to ion charge separation consisting of emulsion films underwent to controlled fading treatments;
- (iii) a third section composed by emulsion films alternated with passive materials of increasing density (plastic, lead and tungsten) to measure the particle range and momentum.

Before the second FOOT experimental data acquisition at GSI in February 2020 to acquire data by exposing emulsion chambers to either a 200 or 700 MeV/u ^{12}C beam, in January 2020 an additional test was planned at TIFPA facilities to verify the response of a new emulsions batch to different energies of a proton beam.

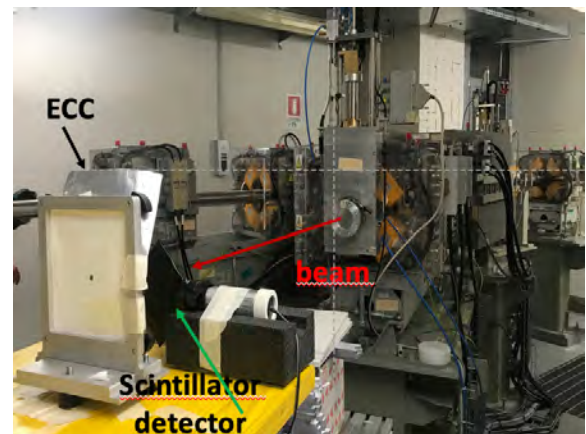


Figure 1: Experimental set-up of the ECC exposure.

To this aim, three emulsion cloud chambers were assembled for the test. Each chamber was composed by 20 emulsion films (5 cm x 4 cm) packed with a light tight aluminium envelope. Every ECC was exposed to the proton beam at 70, 90 and 200 MeV, respectively (Fig. 1). The

[†]Contact Author: montesi@unina.it

¹University of Naples Federico II, Italy

²INFN Naples, Italy

³University of Trento, Italy

particle fluence was set to be of the order of 1000 particle/cm² and it was monitored by a scintillator detector. After exposures, emulsions were thermally treated and developed in the dark room at Physics Department in Naples University. Different temperatures, ranging from 28°C up to 36°C, and timing, from 12 up to 48

hours, were tested. The optimal treatment conditions, in order to obtain the charge particle separation, were set at 28 °C, 32 °C and 34 °C for 24 hours.

The analysis of the emulsion data acquired at GSI in February 2020 is currently on-going.

GSM²: Generalized Stochastic Microdosimetric Model

Francesco G. Cordoni,^{1,2†} Marta Missiaggia,^{2,3} Andrea Attili,⁴ Emanuele Scifoni,² Chiara La Tessa^{2,3}

Currently, the only two radiobiological models used in clinical applications of cancer particle therapy are the Microdosimetric Kinetic Model (MKM) and the Local Effect Model (LEM). These models are used for predicting relative biological effectiveness (RBE) values, which are combined with the physical dose to calculate the biological dose. The main limitation shared by both models is the assumption that all physical and biological variables follow a Poisson distribution, thus can be described by mean values. This assumption neglects the stochastic fluctuations of energy deposition both from dose fractionation and from cell to cell which can be especially significant in highly mixed radiation fields that occur at the beam edges and in the distal region.

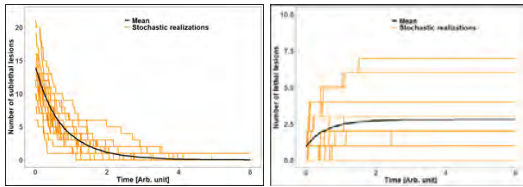


Figure 1: Comparison between average number (black line) of sub-lethal (left panel) and lethal (right panel) lesions, as postulated by the MKM and its generalization, and stochastic fluctuations around average values (orange), as predicted by GSM2.

Although some generalizations to overcome the Poissonian assumption have been made, (Hawkins 2003; Inaniwa et al. 2010; Sato and Furusawa 2012), a comprehensive stochastic description of the DNA damage formation accounting for both the spatial and temporal effects is missing. To overcome this limitation and improve the prediction of cell survival and RBE, we have developed a stochastic microdosimetry-based kinetic model

(GSM² Generalized Stochastic Microdosimetric Model), (Cordoni et al. 2021).

GSM² provides a general probabilistic framework to describe DNA damage kinetic, from which cell survival and RBE can be assessed.

Instead of relying on average values, the model is based on the joint probability distributions of lethal and sub-lethal damages, see Fig. 1. These two types of damages represent DNA double-strand break (DSB) of different severity, with the former being repairable DSB and the latter irreparable and clustered DSB. This change of paradigm has allowed us to incorporate into the model a true stochastic description of energy deposition with microdosimetric data either directly measured or simulated with a Monte Carlo code. From a rigorous point of view, the main mathematical object is the *microdosimetric master equation* (MME) describing the time-evolution of the joint probability distribution $p(t, x, y)$ of sublethal lesions (x) and lethal lesions (y),

$$\partial_t p(t, y, x) = \mathcal{E}^{-1,2} [x(x-1)bp(t, y, x)] + \mathcal{E}^{-1,1} [xap(t, y, x)] + \mathcal{E}^{0,1} [xrp(t, y, x)],$$

where $\mathcal{E}^{i,j}$ are suitable creation and annihilation operators. In particular, the rate r accounts for the repair rate at which a sublethal lesion recovers, a accounts for the rate at which a sublethal lesion is converted into a lethal one and b is the rate of pairwise interaction of sublethal lesions to create a single lethal lesion, Fig. 2.

In Cordoni et al. (2021), GSM² mathematical framework has been introduced, showing how besides spatial stochasticity, also temporal stochastic effects can be included in

[†]Contact Author: francescogiuseppe.cordoni@univr.it

¹University of Verona, Italy

²INFN TIFPA, Trento, Italy

³University of Trento, Italy

⁴INFN Roma3, Italy

the model. GSM² formalism allows to efficiently treat acute, split or protracted irradiations, as well as pave the way to model ultra-high dose rate regimes. Furthermore, it has been shown how GSM² encompasses standard linear-quadratic formulation, to provide

in addition a better ground for a mechanistic interpretation. As a relevant consequence, GSM² offers a generalization to the *multi-hit model*, (Vassiliev 2012), that accounts for non-Poissonian effects and damage repair.

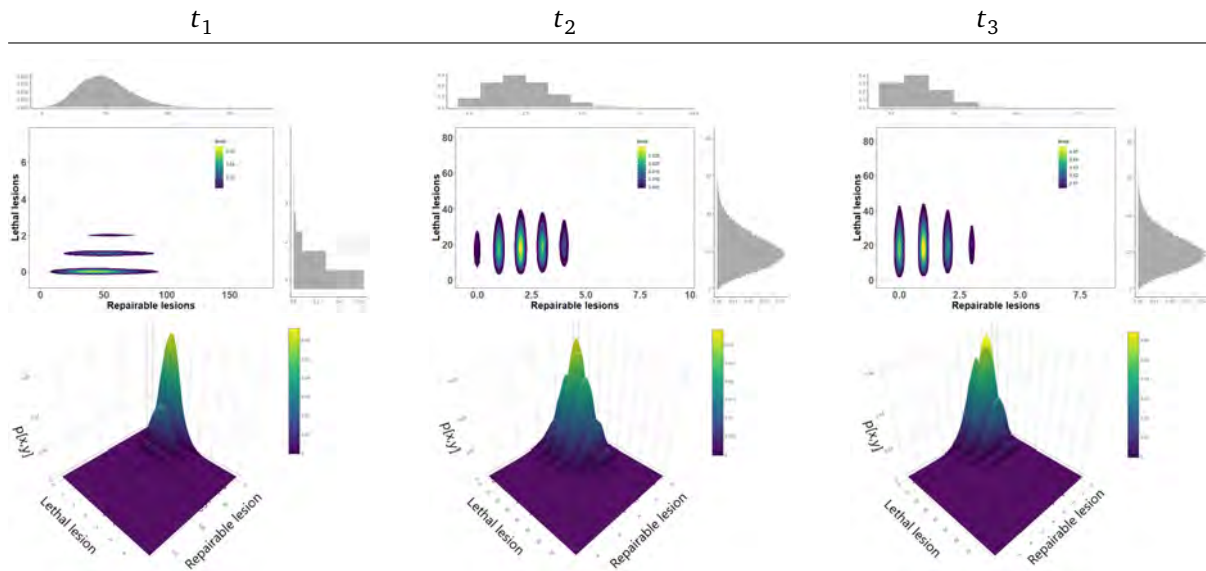


Figure 2: Master equation solution at time $t_1 = 1$ arb. unit (left panels), $t_2 = 100$ arb. unit (middle panels) and $t_3 = 150$ (right panels) arb. unit. GSM² parameters were set to $r = 1$, $a = 0.2$ and $b = 0.1$.

References

- Cordoni, F., Missiaggia, M., Attili, A., Welford, S., Scifoni, E., and La Tessa, C. (2021). *Generalized stochastic microdosimetric model: The main formulation*. Physical Review E **103**(1), p. 012412.
- Hawkins, R. B. (2003). *A microdosimetric-kinetic model for the effect of non-Poisson distribution of lethal lesions on the variation of RBE with LET*. Radiation research **160**(1), pp. 61–69.
- Inaniwa, T., Furukawa, T., Kase, Y., Matsufuji, N., Toshito, T., Matsumoto, Y., Furusawa, Y., and Noda, K. (2010). *Treatment planning for a scanned carbon beam with a modified microdosimetric kinetic model*. Physics in Medicine & Biology **55**(22), p. 6721.
- Sato, T. and Furusawa, Y. (2012). *Cell survival fraction estimation based on the probability densities of domain and cell nucleus specific energies using improved microdosimetric kinetic models*. Radiation research **178**(4), pp. 341–356.
- Vassiliev, O. N. (2012). *Formulation of the multi-hit model with a non-Poisson distribution of hits*. International Journal of Radiation Oncology* Biology* Physics **83**(4), pp. 1311–1316.

MoVe IT-TLD: Thermoluminescent dosimetry in high-energy proton beam line

Vittoria D'Avino,^{1,2†} Mariagabriella Pugliese,^{1,2} Emanuele Scifoni³

The performance of thermoluminescent dosimeters, LiF:Mg, Ti (TLDs-100) were checked in the context of Move IT (Modeling and Verification for Ion beam Treatment planning) project. Thermoluminescent experiments were performed in WP3, dedicated to the biological dosimetry analysis. Pure physical dosimetry combined with biological effects measurements served to provide an insight in the radiation induced damage to living cells. Prior to use the TLD-chips as dosimeters, three batches of TLDs-100 (Harshaw Chemical Company), provided by the team of the Radioactivity Laboratory (LaRa) of the Physics Department of University of Naples Federico II, were characterized with TIFPA proton beam line (D'Avino et al. 2020).

The physical and dose-response properties of the TLD met the requirements for in vivo dosimetry resulting easy to handle and peaceable in small inserts thanks to characteristics such as close tissue equivalent (effective atomic number 8.2, compared to 7.4 for tissue), low signal fading (5%-10% per year), wide linear response range (0.01 – 10 Gy), spatial resolution of 2 mm and high sensitivity.

At now several experiments have been performed to optimize the setup and the procedures from both the biological and physical point of view.

The cells and two arrays of TLDs, accommodated in the same biophantom developed by the biological dosimetry team, were irradiated with the proton beam which was orthogonal to the surface. In Fig. 1 was reported a picture of the biophantom with TLDs and cells fixed in 20% Gelatin Methacrylate (GelMA). While the initial energy of the monoenergetic beam was

equal to 150 MeV (about 80 MeV on the phantom entrance) for all the experimental sessions, the dose in the Bragg peak ranged from 0.9 up to 1.7 Gy.

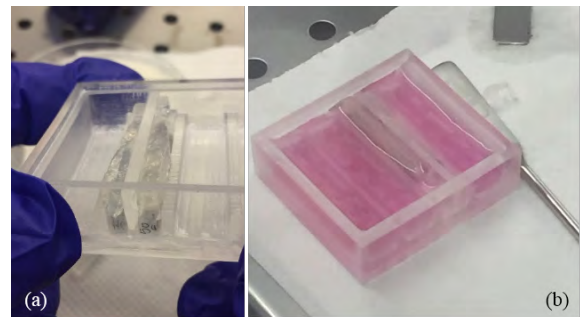


Figure 1: (a): Placement of two TLDs arrays; (b): biological phantom with TLDs and cells fixed in Gelatin Methacrylate (GelMA).

Before each irradiation TLDs were annealed in air at 10 °C for 1 hour, followed by 2 hours annealing at 100 °C/s (Rudén 1976). After irradiation, the readout of TLDs was performed by a Harshaw model 3500 manual TLD reader. The TLDs have been read at 300 °C/s using a heating rate of 10 °C/s to optimize the TL signal-to-background ratio in the high temperature region. A continuous nitrogen flow was used to reduce chemiluminescence and spurious signals not related to the irradiation (Massillon-Jl et al. 2006). Afterwards, dose values were calculated through the calibration factor, which was previously obtained from the slope of the calibration curve and it was determined for each TLDs batch. In the analysed range (0–10 Gy) this curve resulted linear as for the conventional photon beam. Conversely, as observed in high dose-per-pulse electron beams, the quadratic model resulted the best fit in the dose region above 10 Gy (Liuzzi

[†]Contact Author: vittoria.davino@na.infn.it

¹INFN Naples, Italy

²University of Naples Federico II, Italy

³INFN TIFPA, Trento, Italy

et al. 2015; Liuzzi et al. 2020). The calculated calibration factors resulted equal to $4.6 \pm 0.2 \mu\text{C}/\text{Gy}$, $4.9 \pm 0.1 \mu\text{C}/\text{Gy}$ and $5.4 \pm 0.1 \mu\text{C}/\text{Gy}$ for each batch.

The calculated doses were plotted as function of the distance between the entrance point of the biophantom and the TLD position. A typical dose profile is reported in Fig. 2. The biological dosimetry allowed to verify the delivered dose and to assess the correlation between the effective absorbed dose and the radiation induced damage.

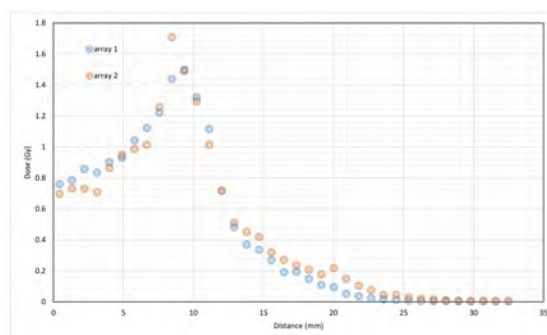


Figure 2: Typical depth-dose curves obtained from the readout of two arrays of TLD.

References

- D'Avino, V., Caruso, M., Arrichiello, C., Ametrano, G., La Verde, G., Muto, P., Scifoni, E., Tommasino, F., and Pugliese, M. (2020). *Thermoluminescent dosimeters (TLDs-100) calibration for dose verification in photon and proton radiation therapy*. *IL NUOVO CIMENTO* **43**(6), pp. 1–11.
- Liuzzi, R., Piccolo, C., D'Avino, V., Clemente, S., Oliviero, C., Cella, L., and Pugliese, M. (2020). *Dose-Response of TLD-100 in the Dose Range Useful for Hypofractionated Radiotherapy*. *Dose-Response* **18**(1), pp. 1–8.
- Liuzzi, R., Savino, F., D'Avino, V., Pugliese, M., and Cella, L. (2015). *Evaluation of LiF: Mg, Ti (TLD-100) for intraoperative electron radiation therapy quality assurance*. *PloS one* **10**(10). Art. no.: e0139287.
- Massillon-Jl, G., Gamboa-deBuen, I., and Brandan, M. (2006). *Onset of supralinear response in TLD-100 exposed to ^{60}Co gamma-rays*. *Journal of Physics D: Applied Physics* **39**(2), p. 262.
- Rudén, B.-I. (1976). *Evaluation of the clinical use of TLD*. *Acta radiologica: therapy, physics, biology* **15**(5), pp. 447–464.

Oxygen depletion measurements for different media with energetic proton beams

Daria Boscolo,^{1†} Martina Fuss,¹ Felix Horst,¹ Christoph Schuy,¹ Enrico Verroi,² Francesco Tommasino,² Emanuele Scifoni,² and Uli Weber¹

The radiosensitivity of biological systems is strongly affected by the system oxygenation: poorly oxygenated tissues result to be up to a factor three more radioresistant compared to well oxygenated ones. On the molecular level, this effect is considered to relate with the indirect damage of radiation. Additionally to the oxygen fixation hypothesis, which is so far the most accepted theory (Hirayama et al. 2013), recent studies open up another possible pathway which can also take part in the oxygenation induced radio sensitivity. In oxygenated media, the solvated electrons, e_{aq}^- , and hydrogen atoms, H^\bullet produced during the irradiation can react with the molecular oxygen dissolved in the target and lead to an enhanced production of highly toxic reactive oxygen species including the superoxide anion, $O_2^{\bullet-}$, and its protonated form HO_2^\bullet (Boscolo et al. 2020a). Both these species have been identified as possible responsible of the oxygen driven sensitization effect. For low LET radiation, an oxygen depletion rate of $0.33 \mu\text{M}/\text{Gy}$ has been measured previously in PBS (Whillans and Rauth 1980), and in cell culture medium it showed an increased value (of a factor around 4/3) (Palcic and Skarsgard 1984). To our best knowledge however, no experimental data for proton or ion radiation is available. In this context, oxygen depletion measurements can aid the basic understanding of the principles of the oxygen effect providing basic quantitative measurements fundamental for studying both the radiolytic oxygen consumption and the production yield of cytotoxic species such as $O_2^{\bullet-}$ and HO_2^\bullet . Additionally they provide a basic dataset suitable for

benchmarking radiation chemical Monte Carlo track structure codes (Boscolo et al. 2020a).

Oxygen consumption curves have been measured at the TIFPA proton beam lab in the Trento proton therapy center for three different target materials: de-ionized water, PBS and cell culture media. To that end, an online optical oxygen sensor (OXY-1 SMA-RS232-AO by Pre-Sens, Regensburg), able to measure variation in the oxygen concentration with a time resolution of 100 ms, was used. For a contact-less measurement of the sealed sample volume, a sensor sticker (SP-PSt3-SA23-D5-OIW-US, Pre-Sens) containing a fluorophore was placed inside the samples (see Fig. 1) and read out with an optical cable from outside.

A series of 0.5 cm^3 sealed targets at initially ambient oxygenation were then irradiated in the "Physics" narrow beam line, with proton doses of approximately 80 Gy delivered with a

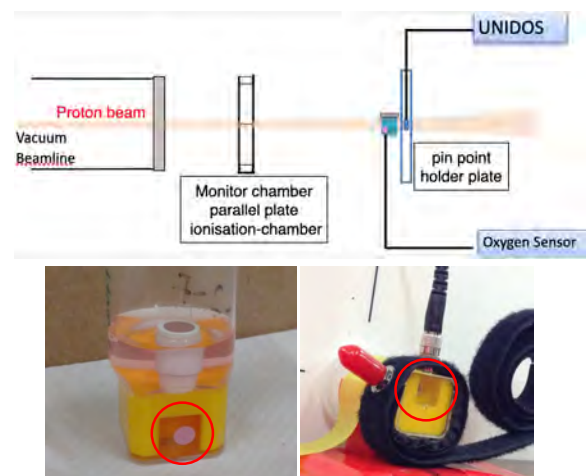


Figure 1: Sample container with sensor spot before and during irradiation

¹GSI Helmholtz Center for Heavy Ion Research, Germany

²INFN TIFPA, Trento, Italy

[†]Contact Author: d.boscolo@gsi.de

125 MeV and 70 MeV pencil beams, with respectively 11.6 and 16.2 mm FWHM size at isocenter, ranging from 30 to 220 nA extraction current. This corresponds to an average dose rate over the target, from 40 to 285 Gy/min. The particle number was monitored for all irradiations with a parallel plate ionization chamber customly designed from De.Tec.Tor. These readings were correlated with dose in the sample by an initial no target calibration with a pin point chamber (PTW 31009).

Fig. 2 depicts a typical oxygen depletion curve for cell culture medium: the initial relatively stable oxygen concentration decreases during the irradiation and reaches a new stable level after the beam application. The concentration difference divided by the total dose gives the oxygen consumption yield for the specific target and radiation quality. A summary of the measured yields for the different media is presented in Table 1. Values here presented are obtained averaging between three to five irradiation repetitions. The largest and lower oxygen consumption has been observed in cell medium and in the water target respectively. The measured depletion yields are significantly lower compared to the predicted ones, however the non-uniform radiation field across the target

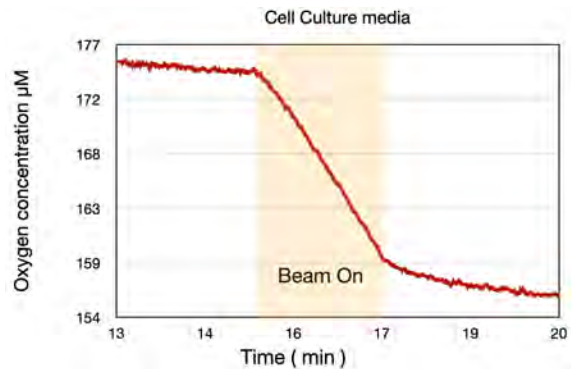


Figure 2: Example oxygen measurement in cell culture medium for irradiation with $1.39 \cdot 10^{11}$ particles (approximately 73 Gy).

(pencil beam) can be responsible for an inhomogeneous oxygen depletion over the sample: larger consumption in the target center and a reduced one closer to the side where the sensor's pellet is attached. Thus the measured values are first underestimated and a subsequent slow oxygen depletion component is expected at longer timescales due to re-diffusion.

Table 1: Measured oxygen depletion yields.

Target	Oxygen consumption ($\mu\text{M}/\text{Gy}$)
Water	0.16 +/- 0.02
PBS	0.20 +/- 0.01
Cell Culture Medium	0.22 +/- 0.01

References

- Boscolo, D., Krämer, M., Fuss, M. C., Durante, M., and Scifoni, E. (2020a). *Impact of target oxygenation on the chemical track evolution of ion and electron radiation*. International journal of molecular sciences.
- Hirayama, R., Ito, A., Noguchi, M., Matsumoto, Y., Uzawa, A., Kobashi, G., Okayasu, R., and Furu-sawa, Y. (2013). *OH• radicals from the indirect actions of X-rays induce cell lethality and mediate the majority of the oxygen enhancement effect*. Radiation Research.
- Palcic, B. and Skarsgard, L. (1984). *Reduced oxygen enhancement ratio at low doses of ionizing radiation*. Radiation research.
- Whillans, D. and Rauth, A. (1980). *An experimental and analytical study of oxygen depletion in stirred cell suspensions*. Radiation research.

A Timepix-based small animal proton imaging setup for the SIRMIO project

Matthias Würfl,^{1†} Katrin Schnürle,¹ Jonathan Bortfeldt,¹ Cristina Oancea,² Carlos Granja,² Enrico Verroi,³ Francesco Tommasino,^{3,4} Katia Parodi^{1†}

The precision of preclinical small animal proton irradiation can benefit from image guidance and beam properties adapted to the small animal model. The **SIRMIO** (Small Animal Proton Irradiator for Research in Molecular Image-guided Radiation-Oncology) (Parodi et al. 2019) project aims at developing a solution for precise preclinical proton irradiation. The design of this portable platform will allow for temporal or permanent installation at experimental beamlines of existing proton therapy centres. Clinical beam properties will be actively adjusted to match requirements of small animal irradiation using an energy degradation and focussing system (S. Gerlach et al. 2020b). Besides pre-treatment ultra-sound imaging for tumor localization, a novel in-beam positron emission tomography scanner and ionoacoustic measurements for proton range verification, proton imaging will be a fundamental part of image-guidance within the SIRMIO project.

Although proton imaging typically exhibits inferior spatial resolution than X-ray imaging, it can offer several advantages. With proton computed tomography (pCT) the proton stopping power relative to water can be directly measured. Since this quantity is required for treatment planning in proton therapy, planning uncertainties caused by the conversion from Hounsfield Units obtained in X-ray CT can be reduced. Secondly, imaging in our foreseen treatment workflow will be performed immediately before treatment. Hence, positioning errors can be eliminated since the small animal will already be set up in treatment position.

single particle tracking (SPT), where the trajectory of individual protons through the imaged object is estimated by measuring their position and direction upstream and downstream of the object, using dedicated tracking detectors. Additionally, the residual range/energy of each particle is determined with a suitable device. Within the SIRMIO project, we are developing a SPT pCT system composed of low material budget floating strip Micromegas detectors as trackers and a segmented time projection chamber as residual range telescope (Meyer et al. 2020). At synchrocyclotron-based proton therapy facilities, however, the high instantaneous particle flux during the few- μ s short beam pulses exceeds the detection capabilities of contemporary SPT systems. For compatibility with such facilities, we are in parallel developing a compact proton imaging setup based on the hybrid semiconductor pixel detector Timepix.

First experiments to explore potential and limitations of this Timepix-based small animal proton imaging setup were performed at the physics beamline of the experimental room of the Trento Proton Therapy facility (Fig. 1).

We used the miniaturized radiation camera MiniPIX-Timepix (Granja et al. 2018) to detect the position-dependent energy loss in the 300 μ m thick silicon sensor for individual protons after traversing a μ CT calibration phantom (*SmART Scientific Solutions, Netherlands*). The detector high granularity (14 \times 14 mm² sensitive area, matrix of 256 \times 256 energy sensitive pixels) and per-pixel signal electronics allow simultaneous detection of up to a few hundred protons with sub-pixel position resolution and spectral sensitivity. Since the phantom dimen-

The common approach for pCT is based on

[†]Contact Author:

matthias.wuerfl@physik.uni-muenchen.de

katia.parodi@physik.uni-muenchen.de

¹Ludwig-Maximilians-Universität München, Germany

²ADVACAM s.r.o, Czech Republic

³INFN TIFPA, Italy

⁴University of Trento, Italy

sions exceeded the sensor size, it was mounted on a motorized translation stage. Lateral movement w.r.t. the beam allowed to create a radiographic image of the entire phantom by combining 6 scan positions. For quantitative imaging, the energy loss in the sensor chip was converted to water-equivalent thickness (WET) of the phantom using a Monte Carlo based and experimentally tuned calibration curve.

Good agreement of the retrieved WET values with ground truth (differences $< 3\%$) and sub-mm spatial resolution for air gaps between phantom and sensor up to 5 cm was found (Würl et al. 2021). Encouraged by the promising results, we are currently refining the imaging setup for future studies. Among other changes, this includes using the fast Timepix3 ASIC, which will considerably reduce imaging time from 15 – 20 min to less than 10 s per ra-

diography.

Acknowledgements The authors acknowledge financial support from the European Research Council (grant number 725539).

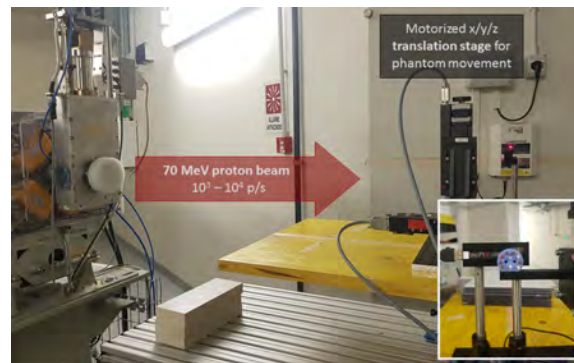


Figure 1: Experimental setup. The inset shows phantom and detector in beam's eye view (Würl et al. 2021)

References

- Gerlach, S., Pinto, M., Kurichyanil, N., Grau, C., Herault, J., Hillbrand, M., Poulsen, P., Safai, S., Schippers, J. M., Schwarz, M., Søndergaard, C., Tommasino, F., Verroi, E., Vidal, M., Yohannes, I., Schreiber, J., and Parodi, K. (2020b). *Beam characterization and feasibility study for a small animal irradiation platform at clinical proton therapy facilities*. *Physics in Medicine & Biology*.
- Granja, C., Kudela, K., Jakubek, J., Krist, P., Chvatil, D., Stursa, J., and Polansky, S. (2018). *Directional detection of charged particles and cosmic rays with the miniaturized radiation camera MiniPIX Timepix*. *Nuclear Instruments and Methods in Physics Research Section A* **911**, pp. 142–152.
- Meyer, S., Bortfeldt, J., Lämmer, P., Englbrecht, F., Pinto, M., Schnürle, K., Würl, M., and Parodi, K. (2020). *Optimization and performance study of a proton CT system for pre-clinical small animal imaging*. *Physics in Medicine & Biology* **65**(15). Art. no.: 155008.
- Parodi, K., Assmann, W., Belka, C., Bortfeldt, J., Clevert, D.-A., Dedes, G., Kalunga, R., Kundel, S., Kurichyanil, N., Lämmer, P., Lascaud, J., Lauber, K., Lovatti, G., Meyer, S., Nitta, M., Pinto, M., Safari, M. J., Schnürle, K., Schreiber, J., Thirolf, P. G., Wieser, H.-P., and Würl, M. (2019). *Towards a novel small animal proton irradiation platform: the SIRMIO project*. *Acta Oncologica* **58**(10), pp. 1470–1475.
- Würl, M., Schnürle, K., Bortfeldt, J., Oancea, C., Granja, C., Verroi, E., Tommasino, F., and Parodi, K. (2021). *Proton Radiography for a Small-Animal Irradiation Platform based on a Miniaturized Timepix Detector*. IEEE (submitted).

SPYRO - Stable Prompt- γ enhanceR for prOtontherapy

Giorgio Cartechini,^{1,2} Luna Pellegrini,^{3,4} Michela Maraffini,^{5,6} Franco Camera,⁷ Francesco Tommasino,^{1,2} Emanuele Scifoni,² Chiara La Tessa^{1,2†}

Particle therapy is an emerging technology in radiotherapy, whose benefits stem from both physical and biological properties. Ions deposit the maximum dose in a localized region close to the end of range called Bragg peak (BP). The combination of a favourable depth-dose profile with advanced delivery techniques, like pencil beam scanning, translates into a high dose conformality as well as into a superior normal tissue sparing. These features lead to a better preservation the organs at risk, and have the potential to decrease toxicity effects, especially in the tissue surrounding the tumor where the dose is still relatively high.

Although clinical results have been encouraging, numerous treatment uncertainties remain major obstacles to the full exploitation of particle therapy. One of the major challenges is monitoring the dose delivered during the treatment, both in terms of absolute value and spatial distribution inside the body.¹ Decreasing these uncertainties would reduce the safety margins, i.e. the treatment volume, and decrease the dose delivered to the healthy tissue.

Several techniques have been proposed to address the issue of verifying in real-time the treatment planning system. Most of the existing methods exploit nuclear interactions that occur in the tissue along the primary beam path towards the tumor and produce de-excitation (prompt) or annihilation (delayed) photons, secondary ions or neutrons energetic enough

to emerge from the patient's body.^{2,3,4} The detection of high energetic prompt gammas (PGs) is considered a direct and real-time method for monitoring the BP position. A limiting factor of this methodology is the low statistics of PGs collected during an irradiation because of the limited detection efficiency and of the large contribution of the background radiation.

We are investigating a novel approach for real-time range verification based on enhancing the production of prompt gammas in the tumor. We propose to achieve this goal by loading the tumor with a drug-delivered stable element, whose nuclei emit characteristic de-excitation PG following nuclear interactions with the primary beam. By detecting and tracking the PGs produced, it is possible to reconstruct the tumor position at the time of irradiation. At the moment the investigation is focused on proton beam both due to the absence of projectile fragmentation and due to the presence of an experimental room at Trento protontherapy center. One of the keys for the applicability of the proposed technique is to find an element that can be carried inside the tumor with a high selectivity and concentration, without causing toxicity, and that emits characteristic de-excitation gammas different from the background created by the normal tissue. Following these criteria, we identified four possible candidates: 19-Fluorine, 45-Scandium, 63-Copper and 89-Yttrium. The choice of these elements was driven also by the existence of a carrier al-

[†]Contact Author: chiara.latessa@unitn.it

¹University of Trento, Italy

²INFN TIFPA, Trento, Italy

³iThemba LABS, Cape Town, South Africa

⁴University of the Witwatersrand, South Africa

⁵Museo Storico della Fisica e Centro Studi e Ricerche

E. Fermi, Roma, Italy

⁶Sapienza Università di Roma, Italy

⁷University of Milan La Statale, Italy

¹Paganetti, H. (2012), *Physics in Medicine & Biology* **57**(11), R99.

²Zhu, X. et al. (2011), *Physics in Medicine & Biology* **56**(13), p. 4041.

³Krimmer, J. et al. (2018), *Nuclear Instruments and Methods in Physics Research Section A* **878**, pp. 58–73.

⁴Traini, G. et al. (2019), *Physica Medica* **65**, pp. 84–93.

ready used in the clinics. To study the feasibility of this approach, we performed Monte Carlo simulations, using Geant4 toolkit. Using the geometry shown in Fig. 1, we characterized the photon-evaporation energy spectra from the interaction of 20 MeV proton beam with the four

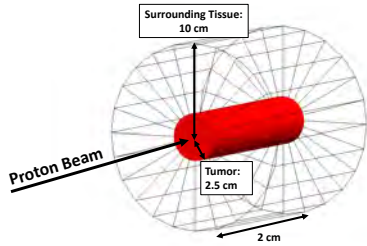


Figure 1: Sketch of the phantom geometry used for all Monte Carlo simulations (not to scale). The outer cylinder is made of G4_BRAIN_ICRP material while the inner cylinder is made of the four candidate materials (Fluorine, Scandium, Copper and Yttrium), in addition to brain tissue.

tumor-tag elements. Although 20 MeV is not a clinical energy, it is the energy of protons close to the Bragg peak region and therefore interacting with tumor volume. Fig. 2 shows the comparison between photon-evaporation spectra from brain tissue and the four selected elements. Brain tissue is characterized by the de-excitation peaks of Carbon and Oxygen nuclei which are the most abundant components. The peak at 4.44 MeV is the product of three different reactions: $^{12}\text{C}(p, p')^{12}\text{C}^*$, $^{12}\text{C}(p, 2p)^{11}\text{B}^*$ and $^{16}\text{O}(p, p\alpha)^{12}\text{C}^*$, while the peaks at 6.13 MeV, 6.9 MeV and 7.1 MeV are the first three excited states of Oxygen.⁵ Only ^{63}Cu and ^{89}Y shows signature PG peaks above 8 MeV, where the background emission is negligible. In particular, Copper emits well-defined peaks within 9 MeV and 11 MeV; Yttrium shows de-excitation peaks at 12 MeV and 13 MeV.

Fluorine and Scandium did not show a signature energy spectrum at high gamma energies. For Fluorine, the most probable reaction is the proton capture forming ^{20}Ne which decays by alpha emission to ^{16}O , one of the most

abundant elements in the human body.

The ultimate goal of the proposed methodology is the integration in the clinical workflow as treatment verification system. One of the crucial and most challenging limitations is the amount of the non-radioactive element that can be delivered inside the tumor to obtain a detectable PGs enhancement. To study a more reasonable case, we estimated the minimum element concentration required to collect 10^3 gammas (statistically significant to detect the enhancement) on a signature peak (e.g. 13 MeV from ^{89}Y). Assuming that in a single fraction, around 10^{11} protons are delivered for each beam energy, and that the reaction yield of 13 MeV PG peak is around 10^{-5} counts per proton, the material density inside the tumor should be of the order of 0.1 g cm^{-3} .

This study also highlighted the need of an experimental verification of Geant4 predictions. For not well studied materials, partial or not existing experimental data are available for the photon evaporation models implemented in the code. This fact leads to results with evident artifacts due to low accuracy in the prediction of gammas. Therefore, we are carrying out an experimental campaign at the experimental room of Trento protontherapy center for measuring the prompt gamma emission of ^{63}Cu and ^{89}Y targets.

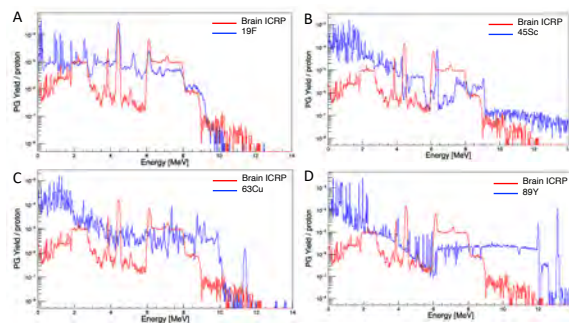


Figure 2: PG energy spectra scored at production point and normalized to the number of protons incident on the target for Fluorine (A), Scandium (B), Copper (C) and Yttrium (D). The results for the G4_BRAIN_ICRP material are reported in all plots as representative of the background spectrum.

⁵Verburg, J. M. et al. (2012), Physics in Medicine & Biology 57(17), p. 5459.

SUN_MEYER

Iacopo Sardi,¹ Giacomo Casati,^{1†} Anna Lisa Iorio,¹ Laura Giunti,¹ Arianna Marturano¹

We investigated the feasibility of a novel therapeutic approach involving the administration of Doxorubicin (DOX), a drug belonging to the anthracycline family, and Temozolomide (TMZ), the most used chemotherapy for glioblastoma (GBM), in combination with Proton therapy (PT). We used two GBM cell lines: the A172 cell line, sensitive to DOX, and the T98G cell line, resistant to chemotherapy drugs. Through first experiments we have shown that the A172 cell line is sensitive to the combined treatment PT (8 Gy and 16 Gy) -DOX (0.5 $\mu\text{g}/\text{ml}$), since a significant reduction in cell viability is observed. The T98G resistant cell line shows a slight but not significant sensitivity to treatment. Therefore, we analyzed the resistance of T98G cell line to the combined treatment. In particular, the molecular mechanisms that regulate the resistance to PT and antineoplastic agents. Our goal was to evaluate whether the Hippo Pathway, an oncogenic molecular pathway active on GBM cell lines, could negatively influence the combined PT-chemotherapy treatment.

METHODS

Cell lines The human glioblastoma (GBM) cell lines used in this study were T98G and A172. The cells were purchased from the American Type Culture Collection (ATCC, Manassas, Virginia, USA) and grown in a humidified atmosphere at 37 °C with 5% CO₂. The culture conditions are different depending on the cell type. The T98G cell line was grown in Eagle's Minimum Essential Medium (EMEM) (Cell Biology, Manassas, Virginia, USA) while the A172 cell line was grown in Dulbecco's Modified Eagle Medium (DMEM) (Cell Biology, Manassas, Virginia, USA). The mediums were added with 10% fetal bovine serum (FBS, Euroclone S.P.A., Italy) and 1% penicillin-streptomycin (Euroclone S.P.A., Italy), by instructions of the supplier company.

Experimental design of the combined Proton Therapy-Doxorubicin treatment

The two GBM cell lines were seeded in small flasks (T25 Culture Flask, Corning Incorporated, New York, USA) 24h before treatment with PT. Two flasks were prepared for each cell line, one of them was the control (0 Gy) and the second was irradiated (16 Gy). 5×10^5 cells per flask of T98G and 7×10^5 cells per flask of A172 were seeded, to obtain their sub-confluence at 24h from seeding. The cells, once irradiated, remained in the incubator overnight to allow the decay of the residual radiation. Next day, the cells were seeded in 6-well plates (Corning Incorporated, New York, USA): 2×10^5 cells for both lines. After 24h the two cell lines underwent pharmacological treatment with DOX at a concentration of 0.5 $\mu\text{g}/\text{ml}$ and with TMZ at a concentration of 200 μM . 24h after drug administration, the cells were lysed, measured and Western Blotting (WB) experiments were performed to evaluate the apoptotic rate and key proteins of the Hippo Pathway.

RESULTS

Evaluation of apoptosis rate after combined PT-chemotherapy treatment (DOX-TMZ)

After having subjected the cells to PT, DOX and TMZ treatment, we evaluated, by Western Blotting, the expression levels of cleaved PARP, a protein involved in DNA damage that is cut by caspase 3 when active. The results, obtained on the T98G cell line, show an increase of apoptosis following treatment with PT (see Fig. 1).



Figure 1: Modulation of the expression levels of cleaved PARP

[†]Contact Author: giacomo_casati@libero.it

¹Azienda Osped. Univers. Meyer, Florence, Italy

It is noteworthy how the PT-DOX combination increments the expression of cleaved PARP compared to the single administration of DOX, demonstrating how this treatment can rise cellular apoptosis. TMZ treatment shows levels of cleaved PARP similar to the combined PT-TMZ treatment; furthermore, co-treatment DOX+TMZ irradiated at 16 Gy increases the level of apoptosis compared to DOX+TMZ 0 Gy treatment.

Evaluation of the expression of the main effectors of the Hippo Pathway (MST-1 and YAP) after combined PT-chemotherapy treatment (DOX-TMZ) The Hippo Pathway is a molecular way consisting of a series of kinases. They activate or deactivate, through a cascade phosphorylation based on various conditions including external stimuli, cell density and oxidative stress, the transcription factor YAP, the main effector of the pathway. If YAP is phosphorylated it is retained in the cytoplasm, conversely the lack of phosphorylation causes its transfer to nuclear level. Here, it induces the transcription of its main targets involved in proliferation and resistance to apoptosis.

One of the main kinases belonging to the pathway is MST-1 which if it remains dephosphorylated, and therefore inactive, allows the nuclear translocation of YAP, conversely in the presence of phosphorylation. We evaluated on the T98G cell line, by Western Blotting, the modulation of MST-1 expression following treatment with PT and chemotherapy (DOX-TMZ). The results (see Fig. 2) show an increase in the expression of MST-1 after irradiation at 16 Gy both in the control and in the treated with DOX, TMZ and DOX+TMZ.



Figure 2: Modulation of MST-1 kinase expression levels.

We also analyzed nuclear YAP expression levels on the T98G cell line. Through Western Blotting experiments, we observed a modulation of expression similar to the MST-1 kinase;

YAP increases after PT both in control and in treated (see Fig. 3).



Figure 3: Modulation of YAP expression levels.

CONCLUSIONS

In the first place, preliminary data obtained after the WB demonstrate that the T98G cell line shows an increase in apoptosis after treatment with PT at 16 Gy. In particular, the expression of PARP-cleaved increases after combined PT-chemotherapy treatment (DOX and TMZ). The Hippo Pathway is a molecular pathway active in GBM with an oncogenic role as it causes a proliferation growth and resistance to apoptosis. The main effector of the Pathway is YAP which, when phosphorylated by a cascade of upstream kinases, is retained in the cytoplasm and degraded through ubiquitination. Conversely, when YAP is not phosphorylated, it moves into the nucleus where, by binding to TEAD factors, it promotes the transcription of numerous targets, including C-MYC, CYR61 and CTGF, involved in proliferation, invasion and resistance to apoptosis. These experiments show that the T98G cell line expresses higher levels of both MST-1 kinase and nuclear YAP after PT than the untreated control. The greatest expression of both effectors of the pathway was observed especially after the combined treatment of PT plus chemotherapy (DOX and TMZ). We hypothesized that the increase of MST-1 and YAP observed after the combined treatment is due to the cell suffering by DNA damage and that the Hippo Pathway can play a protective role over-expressing YAP in the nucleus to favor the transcription of its oncogenic targets. These results, although promising, are preliminary and have to be evaluated by in vitro experiments confirming the increase of apoptosis and the expression of YAP targets after combined PT-chemotherapy treatment. These data have to be further confirmed by Western Blotting experiments that analyze the levels of phosphorylated YAP and MST-1.



TIFPA
publications

TIFPA Publications

Particle Physics

ATLAS

- Aad, G. et al., ATLAS (2021a). *A search for the dimuon decay of the Standard Model Higgs boson with the ATLAS detector*. Phys. Lett. B **812**, p. 135980.
- ATLAS (2020a). *A search for the $Z\gamma$ decay mode of the Higgs boson in pp collisions at $\sqrt{s} = 13$ TeV with the ATLAS detector*. Phys. Lett. B **809**, p. 135754.
- ATLAS (2020b). *Alignment of the ATLAS Inner Detector in Run-2*. Eur. Phys. J. C **80**(12), p. 1194.
- ATLAS (2020c). *Charged-lepton-flavour violation at the LHC: a search for $Z \rightarrow e\tau/\mu\tau$ decays with the ATLAS detector*.
- CMS, ATLAS (2020d). *Combination of the W boson polarization measurements in top quark decays using ATLAS and CMS data at $\sqrt{s} = 8$ TeV*. JHEP **08**(08), p. 051.
- ATLAS (2020e). *CP Properties of Higgs Boson Interactions with Top Quarks in the $t\bar{t}H$ and tH Processes Using $H \rightarrow \gamma\gamma$ with the ATLAS Detector*. Phys. Rev. Lett. **125**(6), p. 061802.
- ATLAS (2021b). *Differential cross-section measurements for the electroweak production of dijets in association with a Z boson in proton–proton collisions at ATLAS*. Eur. Phys. J. C **81**(2), p. 163.
- ATLAS (2020f). *Dijet resonance search with weak supervision using $\sqrt{s} = 13$ TeV pp collisions in the ATLAS detector*. Phys. Rev. Lett. **125**(13), p. 131801.
- ATLAS (2020g). *Evidence for $t\bar{t}t\bar{t}$ production in the multilepton final state in proton–proton collisions at $\sqrt{s} = 13$ TeV with the ATLAS detector*. Eur. Phys. J. C **80**(11), p. 1085.
- ATLAS (2020h). *Exclusive dimuon production in ultraperipheral $Pb+Pb$ collisions at $\sqrt{s_{NN}} = 5.02$ TeV with ATLAS*.
- ATLAS (2020i). *Higgs boson production cross-section measurements and their EFT interpretation in the 4ℓ decay channel at $\sqrt{s} = 13$ TeV with the ATLAS detector*. Eur. Phys. J. C **80**(10). [Erratum: Eur.Phys.J.C 81, 29 (2021), Erratum: Eur.Phys.J.C 81, 398 (2021)], p. 957.
- ATLAS (2020j). *Jet energy scale and resolution measured in proton-proton collisions at $\sqrt{s} = 13$ TeV with the ATLAS detector*.
- ATLAS (2021c). *Longitudinal Flow Decorrelations in $Xe+Xe$ Collisions at $\sqrt{s_{NN}} = 5.44$ TeV with the ATLAS Detector*. Phys. Rev. Lett. **126**(12), p. 122301.
- ATLAS (2020k). *Measurement of azimuthal anisotropy of muons from charm and bottom hadrons in $Pb+Pb$ collisions at $\sqrt{s_{NN}} = 5.02$ TeV with the ATLAS detector*. Phys. Lett. B **807**, p. 135595.
- ATLAS (2021d). *Measurement of hadronic event shapes in high- p_T multijet final states at $\sqrt{s} = 13$ TeV with the ATLAS detector*. JHEP **01**, p. 188.
- ATLAS (2021e). *Measurement of light-by-light scattering and search for axion-like particles with 2.2 nb^{-1} of $Pb+Pb$ data with the ATLAS detector*. JHEP **03**, p. 243.
- ATLAS (2020l). *Measurement of single top-quark production in association with a W boson in the single-lepton channel at $\sqrt{s} = 8$ TeV with the ATLAS detector*.
- ATLAS (2021f). *Measurement of the associated production of a Higgs boson decaying into b -quarks with a vector boson at high transverse momentum in pp collisions at $\sqrt{s} = 13$ TeV with the ATLAS detector*. Phys. Lett. B **816**, p. 136204.
- ATLAS (2021g). *Measurement of the CP -violating phase ϕ_s in $B_s^0 \rightarrow J/\psi\phi$ decays in ATLAS at 13 TeV*. Eur. Phys. J. C **81**(4), p. 342.
- ATLAS (2020m). *Measurement of the Lund Jet Plane Using Charged Particles in 13 TeV Proton-Proton Collisions with the ATLAS Detector*. Phys. Rev. Lett. **124**(22), p. 222002.

- Aad, G. et al., ATLAS (2020n). *Measurement of the $t\bar{t}$ production cross-section in the lepton+jets channel at $\sqrt{s} = 13$ TeV with the ATLAS experiment.* Phys. Lett. B **810**, p. 135797.
- ATLAS (2020o). *Measurements of Higgs Bosons Decaying to Bottom Quarks from Vector Boson Fusion Production with the ATLAS Experiment at $\sqrt{s} = 13$ TeV.*
- ATLAS (2020p). *Measurements of inclusive and differential cross-sections of combined $t\bar{t}\gamma$ and $tW\gamma$ production in the $e\mu$ channel at 13 TeV with the ATLAS detector.* JHEP **09**, p. 049.
- ATLAS (2020q). *Measurements of the Higgs boson inclusive and differential fiducial cross sections in the 4ℓ decay channel at $\sqrt{s} = 13$ TeV.* Eur. Phys. J. C **80**(10), p. 942.
- ATLAS (2020r). *Measurements of the production cross-section for a Z boson in association with b-jets in proton-proton collisions at $\sqrt{s} = 13$ TeV with the ATLAS detector.* JHEP **07**, p. 044.
- ATLAS (2021h). *Measurements of top-quark pair single- and double-differential cross-sections in the all-hadronic channel in pp collisions at $\sqrt{s} = 13$ TeV using the ATLAS detector.* JHEP **01**, p. 033.
- ATLAS (2021i). *Measurements of WH and ZH production in the $H \rightarrow b\bar{b}$ decay channel in pp collisions at 13 TeV with the ATLAS detector.* Eur. Phys. J. C **81**(2), p. 178.
- ATLAS (2021j). *Medium-Induced Modification of Z-Tagged Charged Particle Yields in Pb + Pb Collisions at 5.02 TeV with the ATLAS Detector.* Phys. Rev. Lett. **126**(7), p. 072301.
- ATLAS (2020s). *Muon reconstruction and identification efficiency in ATLAS using the full Run 2 pp collision data set at $\sqrt{s} = 13$ TeV.*
- ATLAS (2020t). *Observation and Measurement of Forward Proton Scattering in Association with Lepton Pairs Produced via the Photon Fusion Mechanism at ATLAS.* Phys. Rev. Lett. **125**(26), p. 261801.
- ATLAS (2020u). *Observation of electroweak production of two jets and a Z-boson pair with the ATLAS detector at the LHC.*
- ATLAS (2021k). *Observation of photon-induced W^+W^- production in pp collisions at $\sqrt{s} = 13$ TeV using the ATLAS detector.* Phys. Lett. B **816**, p. 136190.
- ATLAS (2020v). *Observation of the associated production of a top quark and a Z boson in pp collisions at $\sqrt{s} = 13$ TeV with the ATLAS detector.* JHEP **07**, p. 124.
- ATLAS (2020w). *Operation of the ATLAS trigger system in Run 2.* JINST **15**(10), P10004.
- ATLAS (2021l). *Optimisation of large-radius jet reconstruction for the ATLAS detector in 13 TeV proton-proton collisions.* Eur. Phys. J. C **81**(4), p. 334.
- ATLAS (2020x). *Performance of the ATLAS muon triggers in Run 2.* JINST **15**(09), P09015.
- ATLAS (2020y). *Performance of the missing transverse momentum triggers for the ATLAS detector during Run-2 data taking.* JHEP **08**, p. 080.
- ATLAS (2020z). *Performance of the upgraded PreProcessor of the ATLAS Level-1 Calorimeter Trigger.* JINST **15**(11), P11016.
- ATLAS (2020aa). *Reconstruction and identification of boosted di- τ systems in a search for Higgs boson pairs using 13 TeV proton-proton collision data in ATLAS.* JHEP **11**, p. 163.
- ATLAS (2021m). *Search for a heavy Higgs boson decaying into a Z boson and another heavy Higgs boson in the $\ell\ell b\bar{b}$ and $\ell\ell WW$ final states in pp collisions at $\sqrt{s} = 13$ TeV with the ATLAS detector.* Eur. Phys. J. C **81**(5), p. 396.
- ATLAS (2020ab). *Search for a scalar partner of the top quark in the all-hadronic $t\bar{t}$ plus missing transverse momentum final state at $\sqrt{s} = 13$ TeV with the ATLAS detector.* Eur. Phys. J. C **80**(8), p. 737.
- ATLAS (2021n). *Search for dark matter in association with an energetic photon in pp collisions at $\sqrt{s} = 13$ TeV with the ATLAS detector.* JHEP **02**, p. 226.
- ATLAS (2021o). *Search for Dark Matter Produced in Association with a Dark Higgs Boson Decaying into $W^\pm W^\mp$ or ZZ in Fully Hadronic Final States from $\sqrt{s} = 13$ TeV pp Collisions Recorded with the ATLAS Detector.* Phys. Rev. Lett. **126**(12), p. 121802.

- ATLAS (2020ac). *Search for dark matter produced in association with a single top quark in $\sqrt{s} = 13$ TeV pp collisions with the ATLAS detector.*
- ATLAS (2020ad). *Search for dijet resonances in events with an isolated charged lepton using $\sqrt{s} = 13$ TeV proton-proton collision data collected by the ATLAS detector.* JHEP **06**, p. 151.
- ATLAS (2020ae). *Search for direct production of electroweakinos in final states with missing transverse momentum and a Higgs boson decaying into photons in pp collisions at $\sqrt{s} = 13$ TeV with the ATLAS detector.* JHEP **10**, p. 005.
- ATLAS (2020af). *Search for direct production of electroweakinos in final states with one lepton, missing transverse momentum and a Higgs boson decaying into two b -jets in pp collisions at $\sqrt{s} = 13$ TeV with the ATLAS detector.* Eur. Phys. J. C **80**(8), p. 691.
- ATLAS (2020ag). *Search for displaced leptons in $\sqrt{s} = 13$ TeV pp collisions with the ATLAS detector.*
- ATLAS (2020ah). *Search for heavy diboson resonances in semileptonic final states in pp collisions at $\sqrt{s} = 13$ TeV with the ATLAS detector.* Eur. Phys. J. C **80**(12), p. 1165.
- ATLAS (2020ai). *Search for heavy Higgs bosons decaying into two tau leptons with the ATLAS detector using pp collisions at $\sqrt{s} = 13$ TeV.* Phys. Rev. Lett. **125**(5), p. 051801.
- ATLAS (2021p). *Search for heavy resonances decaying into a pair of Z bosons in the $\ell^+\ell^-\ell'^+\ell'^-$ and $\ell^+\ell^-\nu\bar{\nu}$ final states using 139 fb^{-1} of proton-proton collisions at $\sqrt{s} = 13$ TeV with the ATLAS detector.* Eur. Phys. J. C **81**(4), p. 332.
- ATLAS (2020aj). *Search for heavy resonances decaying into a photon and a hadronically decaying Higgs boson in pp collisions at $\sqrt{s} = 13$ TeV with the ATLAS detector.* Phys. Rev. Lett. **125**, p. 251802.
- ATLAS (2020ak). *Search for Higgs Boson Decays into a Z Boson and a Light Hadronically Decaying Resonance Using 13 TeV pp Collision Data from the ATLAS Detector.* Phys. Rev. Lett. **125**(22), p. 221802.
- ATLAS (2020al). *Search for Higgs boson decays into two new low-mass spin-0 particles in the $4b$ channel with the ATLAS detector using pp collisions at $\sqrt{s} = 13$ TeV.* Phys. Rev. D **102**, p. 112006.
- ATLAS (2021q). *Search for Higgs boson production in association with a high-energy photon via vector-boson fusion with decay into bottom quark pairs at $\sqrt{s}=13$ TeV with the ATLAS detector.* JHEP **03**, p. 268.
- ATLAS (2020am). *Search for long-lived, massive particles in events with a displaced vertex and a muon with large impact parameter in pp collisions at $\sqrt{s} = 13$ TeV with the ATLAS detector.* Phys. Rev. D **102**(3), p. 032006.
- ATLAS (2020an). *Search for new non-resonant phenomena in high-mass dilepton final states with the ATLAS detector.* JHEP **11**. [Erratum: JHEP 04, 142 (2021)], p. 005.
- ATLAS (2020ao). *Search for new phenomena in final states with large jet multiplicities and missing transverse momentum using $\sqrt{s} = 13$ TeV proton-proton collisions recorded by ATLAS in Run 2 of the LHC.* JHEP **10**, p. 062.
- ATLAS (2021r). *Search for new phenomena with top quark pairs in final states with one lepton, jets, and missing transverse momentum in pp collisions at $\sqrt{s} = 13$ TeV with the ATLAS detector.* JHEP **04**, p. 174.
- ATLAS (2021s). *Search for pair production of scalar leptoquarks decaying into first- or second-generation leptons and top quarks in proton-proton collisions at $\sqrt{s} = 13$ TeV with the ATLAS detector.* Eur. Phys. J. C **81**(4), p. 313.
- ATLAS (2020ap). *Search for pairs of scalar leptoquarks decaying into quarks and electrons or muons in $\sqrt{s} = 13$ TeV pp collisions with the ATLAS detector.* JHEP **10**, p. 112.
- ATLAS (2021t). *Search for phenomena beyond the Standard Model in events with large b -jet multiplicity using the ATLAS detector at the LHC.* Eur. Phys. J. C **81**(1). [Erratum: Eur.Phys.J.C 81, 249 (2021)], p. 11.

- Aad, G. et al., ATLAS (2020aq). *Search for resonances decaying into a weak vector boson and a Higgs boson in the fully hadronic final state produced in proton–proton collisions at $\sqrt{s} = 13$ TeV with the ATLAS detector.* Phys. Rev. D **102**(11), p. 112008.
- ATLAS (2021u). *Search for squarks and gluinos in final states with jets and missing transverse momentum using 139 fb^{-1} of $\sqrt{s} = 13$ TeV pp collision data with the ATLAS detector.* JHEP **02**, p. 143.
- ATLAS (2020ar). *Search for the $HH \rightarrow b\bar{b}b\bar{b}$ process via vector-boson fusion production using proton-proton collisions at $\sqrt{s} = 13$ TeV with the ATLAS detector.* JHEP **07**. [Erratum: JHEP **01**, 145 (2021)], p. 108.
- ATLAS (2020as). *Search for top squarks in events with a Higgs or Z boson using 139 fb^{-1} of pp collision data at $\sqrt{s} = 13$ TeV with the ATLAS detector.* Eur. Phys. J. C **80**(11), p. 1080.
- ATLAS (2020at). *Search for trilepton resonances from chargino and neutralino pair production in $\sqrt{s} = 13$ TeV pp collisions with the ATLAS detector.*
- ATLAS (2020au). *Search for $t\bar{t}$ resonances in fully hadronic final states in pp collisions at $\sqrt{s} = 13$ TeV with the ATLAS detector.* JHEP **10**, p. 061.
- ATLAS (2021v). *Search for type-III seesaw heavy leptons in dilepton final states in pp collisions at $\sqrt{s} = 13$ TeV with the ATLAS detector.* Eur. Phys. J. C **81**(3), p. 218.
- ATLAS (2020av). *Test of CP invariance in vector-boson fusion production of the Higgs boson in the $H \rightarrow \tau\tau$ channel in proton–proton collisions at $\sqrt{s} = 13$ TeV with the ATLAS detector.* Phys. Lett. B **805**, p. 135426.
- ATLAS (2020aw). *Test of the universality of τ and μ lepton couplings in W-boson decays from $t\bar{t}$ events with the ATLAS detector.*
- Abbot, B., ATLAS (2020). *Heavy flavour production in ATLAS: Charmonium production in $p - p$ at 13 TeV and in $Pb - Pb$ collisions. Associated charmonium and vector bosons production.* PoS **Beauty2019**, p. 023.
- Abraham, N., ATLAS (2020). *The design and performance of the ATLAS Inner Detector trigger in high pile-up collisions at 13 TeV at the Large Hadron Collider.* J. Phys. Conf. Ser. **1525**(1), p. 012034.
- Agapopoulou, C., ATLAS (2020). *Search for squarks and gluinos in final states with jets and missing transverse momentum with the ATLAS detector.* PoS **EPS-HEP2019**, p. 605.
- Agaras, M. N., ATLAS (2021). *Recent $t\bar{t}H$ measurements with ATLAS.* PoS **LHCP2020**. Ed. by B. Mansoulie, G. Marchiori, R. Salern, and T. Bos, p. 179.
- Aggarwal, A., ATLAS (2021). *Higgs Boson measurements in the $H \rightarrow WW \rightarrow \ell \nu \ell \nu$ decay channel.* PoS **ICHEP2020**, p. 093.
- Al Khoury, K., ATLAS (2021). *Measurement of the Standard Model Higgs boson produced in association with a vector boson and decaying to a pair of b-quarks in p-p collisions at 13 TeV using the ATLAS detector.* PoS **LHCP2020**. Ed. by B. Mansoulie, G. Marchiori, R. Salern, and T. Bos, p. 241.
- Alhroob, M., ATLAS (2021). *ATLAS Virtual Visits - Take part from anywhere in the world.* PoS **LHCP2020**. Ed. by B. Mansoulie, G. Marchiori, R. Salern, and T. Bos, p. 230.
- Amoroso, S., ATLAS, CMS (2020). *Precision measurements at the LHC.* PoS **RADCOR2019**, p. 001.
- Aparo, M., ATLAS (2021). *The ATLAS Inner Detector Trigger performance in pp collisions at 13 TeV during LHC Run 2.* PoS **LHCP2020**. Ed. by B. Mansoulie, G. Marchiori, R. Salern, and T. Bos, p. 248.
- Arcangeletti, C., ATLAS (2020). *Measurement of the Higgs boson properties using the ATLAS detector.* J. Phys. Conf. Ser. **1690**(1). Ed. by P. Teterin, p. 012154.
- ATLAS Collaboration (2021). *Study of Higgs-boson production with large transverse momentum using the $H \rightarrow b\bar{b}$ decay with the ATLAS detector.* All figures including auxiliary figures are available at <https://atlas.web.cern.ch/Atlas/GROUPS/PHYSICS/CONFNOTES/ATLAS-CONF-2021-010>.
- ATLAS HL-LHC Computing Conceptual Design Report (2020).

- Bailey, A., ATLAS, CMS (2021). *Searches for BSM Higgs bosons at ATLAS and CMS*. PoS **LHCP2020**. Ed. by B. Mansoulie, G. Marchiori, R. Salern, and T. Bos, p. 011.
- Bartolini, G., ATLAS (2021). *Measurement of the combined online and offline b-jet identification efficiency with $t\bar{t}$ events using a likelihood method in the ATLAS detector*. PoS **LHCP2020**. Ed. by B. Mansoulie, G. Marchiori, R. Salern, and T. Bos, p. 240.
- BasalaeV, A., ATLAS (2021). *Search for the Higgs boson in the final state with two leptons and a photon produced in pp collisions at $\sqrt{s} = 13$ TeV with the ATLAS detector*. PoS **ICHEP2020**, p. 094.
- Belyaev, N., ATLAS, CMS (2021). *Interpretation of ATLAS and CMS Higgs measurements in STXS and EFT*. PoS **LHCP2020**. Ed. by B. Mansoulie, G. Marchiori, R. Salern, and T. Bos, p. 137.
- Bergmann, B., Billoud, T., Burian, P., Leroy, C., Mánek, P., Meduna, L., Pospíšil, S., and Suk, M., ATLAS (2020). *Particle tracking and radiation field characterization with Timepix3 in ATLAS*. Nucl. Instrum. Meth. A **978**, p. 164401.
- Bhattacharya, S., ATLAS, CMS (2021). *Multiboson measurements in CMS and ATLAS*. PoS **LHCP2020**. Ed. by B. Mansoulie, G. Marchiori, R. Salern, and T. Bos, p. 164.
- Bielski, R., ATLAS (2020). *ATLAS High Level Trigger within the multi-threaded software framework AthenaMT*. J. Phys. Conf. Ser. **1525**(1), p. 012031.
- Biglietti, M., ATLAS (2020). *Measurements of the Higgs Boson Properties at the ATLAS Experiment*. J. Phys. Conf. Ser. **1586**(1). Ed. by E. Widmann, J. Marton, A. Pichler, M. Simon, and D. Murtagh, p. 012028.
- Bold, T., ATLAS (2020). *Azimuthal anisotropy in Pb+Pb, Xe+Xe and p+Pb collisions and v_n-p_t correlations in Pb+Pb and p+Pb collisions with the ATLAS experiment*. PoS **EPS-HEP2019**, p. 314.
- Boosted hadronic vector boson and top quark tagging with ATLAS using Run 2 data* (2020).
- Borecka-Bielska, H. M., ATLAS (2021). *Search for rare and lepton-flavour-violating decays of the Higgs boson with the ATLAS detector*. PoS **ICHEP2020**, p. 050.
- Boumediene, D., ATLAS (2020). *ATLAS Tile calorimeter calibration and PMT response*. JINST **15**(04), p. C04051.
- Boumediene, D. E., ATLAS (2021). *Timing for the ATLAS Phase-II Upgrade*. PoS **LHCP2020**. Ed. by B. Mansoulie, G. Marchiori, R. Salern, and T. Bos, p. 080.
- Bruscino, N., ATLAS (2020). *Top quark physics with the ATLAS detector: recent highlights*. Phys. Scripta **95**(9). Ed. by L. Bravina, S. Kabana, V. Volkova, and V. I. Zakharov, p. 094005.
- Buckland, M. D., ATLAS (2020). *Series Production and Test of Hybrid Modules for the ALICE ITS Upgrade*. PoS **Vertex2019**, p. 063.
- Burger, A. M., ATLAS (2021). *Efficiency calibrations for ATLAS b-jet identification algorithms*. PoS **ICHEP2020**, p. 799.
- Bussey, P. J., ATLAS (2021). *Soft-QCD and diffractive processes in ATLAS*. PoS **LHCP2020**. Ed. by B. Mansoulie, G. Marchiori, R. Salern, and T. Bos, p. 148.
- Calfayan, P., ATLAS (2020). *Measurements of inclusive WW and WZ production with ATLAS*. PoS **EPS-HEP2019**, p. 663.
- Callea, G., ATLAS (2020). *Recent Tests of QCD with the ATLAS Detector*. Acta Phys. Polon. Supp. **13**, pp. 9–15.
- Camarero, D., ATLAS (2020). *Measurement of photon production at ATLAS*. Nucl. Part. Phys. Proc. **309-311**, pp. 37–42.
- Carratta, G., ATLAS (2020). *Search for Type-III SeeSaw heavy lepton with the ATLAS Detector at the LHC using $\sqrt{s} = 13$ TeV up to 140 fb^{-1}* . J. Phys. Conf. Ser. **1548**(1), p. 012032.
- Carratta, G., ATLAS (2021). *Search for Type-III SeeSaw heavy leptons in dileptonic final states using 139 fb^{-1} of pp collision at $\sqrt{s} = 13$ TeV with the ATLAS detector*. PoS **ICHEP2020**, p. 297.
- Carter, J. W., ATLAS (2021). *Luminosity measurement with the ATLAS experiment at the LHC*. PoS **ICHEP2020**, p. 726.

- Casado, M. P., ATLAS (2020). *HL-LHC physics with the ATLAS detector*. Nucl. Part. Phys. Proc. **309-311**, pp. 43–48.
- Cerny, K., ATLAS (2020). *Performance study of the ATLAS Forward Proton Time-of-Flight Detector System*. PoS **Vertex2019**, p. 055.
- Chapman, J. et al., ATLAS (2020). *Fast simulation methods in ATLAS: from classical to generative models*. EPJ Web Conf. **245**. Ed. by C. Doglioni, D. Kim, G. A. Stewart, L. Silvestris, P. Jackson, and W. Kamleh, p. 02035.
- Chen, Y.-H., ATLAS (2020). *Searches for new resonances decaying to heavy-flavour quarks with the ATLAS detector at $\sqrt{s} = 13$ TeV*. Nucl. Part. Phys. Proc. **309-311**, pp. 55–62.
- Cieri, D., ATLAS (2020). *Hardware Demonstrator Of The Phase-II ATLAS MDT Trigger Processor*. PoS **TWEPP2019**, p. 141.
- Daneri, F. M., ATLAS (2020). *FCNC in top quark transitions in ATLAS*. PoS **Beauty2019**, p. 021.
- Deep Learning for Pion Identification and Energy Calibration with the ATLAS Detector* (2020).
- Di Gregorio, G., ATLAS (2020). *Measurement of the associated production of the Higgs boson with a vector boson in 13 TeV pp collisions with the ATLAS detector*. Nuovo Cim. C **43**(4-5), p. 106.
- Dong, B., ATLAS (2020). *SEARCH FOR A NEW HEAVY RESONANCE IN FINAL STATES WITH DI-JET OR DI-b-JETS WITH THE ATLAS DETECTOR**. Acta Phys. Polon. B **51**(6). Ed. by J. Bohm, M. Chrzęszcz, S. Sapeta, and A. Siódsmok, pp. 1327–1332.
- Drobac, A. S., ATLAS (2021). *The ATLAS Muon Trigger Design and Performance*. PoS **LHCP2020**. Ed. by B. Mansoulie, G. Marchiori, R. Salern, and T. Bos, p. 249.
- El Jarrari, H., ATLAS (2021). *Dark photon searches with the ATLAS detector at the LHC*. PoS **LHCP2020**. Ed. by B. Mansoulie, G. Marchiori, R. Salern, and T. Bos, p. 220.
- Ermoline, Y., ATLAS (2020). *The Phase-I upgrade of the ATLAS Level-1 calorimeter trigger*. JINST **15**(06), p. C06040.
- Evans, M. O., ATLAS (2021a). *ATLAS Open Data: Data visualisation and educational physics analysis to re-discover the Higgs boson*. PoS **LHCP2020**. Ed. by B. Mansoulie, G. Marchiori, R. Salern, and T. Bos, p. 228.
- ALICE, ATLAS, CMS, LHCb (2021b). *LHC Open Data for the world to see*. PoS **LHCP2020**. Ed. by B. Mansoulie, G. Marchiori, R. Salern, and T. Bos, p. 199.
- ATLAS (2021c). *The ATLAS public website - Evolution to Drupal 8*. PoS **ICHEP2020**, p. 941.
- Falke, S., ATLAS (2020). *Measurement of differential cross sections in Higgs boson decays to bosons using the ATLAS detector*. Nucl. Part. Phys. Proc. **309-311**, pp. 31–36.
- Fiorini, L., ATLAS, CMS (2021). *What we learned about the Higgs boson*. PoS **LHCP2020**. Ed. by B. Mansoulie, G. Marchiori, R. Salern, and T. Bos, p. 159.
- Flick, T., ATLAS (2020). *Module and system test development for the Phase-2 ATLAS ITk Pixel upgrade*. Nucl. Instrum. Meth. A **958**. Ed. by M. Krammer, T. Bergauer, M. Dragicevic, M. Friedl, M. Jeitler, J. Schieck, and C. Schwanda, p. 162054.
- Franchino, S., ATLAS (2021). *The Phase-I upgrade of the ATLAS Level-1 Calorimeter Trigger*. PoS **LHCP2020**. Ed. by B. Mansoulie, G. Marchiori, R. Salern, and T. Bos, p. 253.
- Freeman, P. M., ATLAS (2020). *MALTA: a Monolithic Active Pixel Sensor for tracking in ATLAS*. JINST **15**(03), p. C03019.
- Freeman, P. M. et al., ATLAS (2020). *Recent measurements on MiniMALTA, a radiation hard CMOS sensor with small collection electrodes for ATLAS*. PoS **Vertex2019**, p. 020.
- Geanta, A. A., ATLAS (2020). *Search for the strong pair production of squarks and gluinos in events with an isolated lepton, jets and missing transverse momentum at $\sqrt{s} = 13$ TeV with the ATLAS detector*. PoS **EPS-HEP2019**, p. 602.
- Gerlach, L., ATLAS (2020). *Experimental Results in the Extended Higgs Sector*. Acta Phys. Polon. B **51**(6). Ed. by J. Bohm, M. Chrzęszcz, S. Sapeta, and A. Siódsmok, pp. 1333–1343.

- Ghosh, A., ATLAS (2020). *Deep generative models for fast shower simulation in ATLAS*. J. Phys. Conf. Ser. **1525**(1), p. 012077.
- Giagu, S., ATLAS (2020). *Fast and resource-efficient Deep Neural Network on FPGA for the Phase-II Level-0 muon barrel trigger of the ATLAS experiment*. EPJ Web Conf. **245**. Ed. by C. Doglioni, D. Kim, G. A. Stewart, L. Silvestris, P. Jackson, and W. Kamleh, p. 01021.
- Gololo, M. G. D., ATLAS (2020). *Performance for the ATLAS Tile Calorimeter*. JINST **15**(08), p. C08020.
- Gonzalez Fernandez, S., ATLAS (2021). *Search for new phenomena in mono-X final states using pp collision data collected in Run-2 by the ATLAS experiment at the LHC*. PoS **ICHEP2020**, p. 658.
- Gonzalez Lopez, O., ATLAS, CMS (2021). *Searches for heavy resonances at ATLAS and CMS*. PoS **LHCP2020**. Ed. by B. Mansoulie, G. Marchiori, R. Salern, and T. Bos, p. 015.
- Gonzalez, B. A., ATLAS, CMS (2021). *Inclusive and differential single-top cross sections from ATLAS and CMS*. PoS **LHCP2020**. Ed. by B. Mansoulie, G. Marchiori, R. Salern, and T. Bos, p. 069.
- Graziani, G., LHCb, ATLAS, CMS (2020). *Heavy ion and fixed-target physics at ATLAS, CMS and LHCb*. Nuovo Cim. C **42**(6), p. 248.
- Grigorieva, M. A., Alekseev, A. A., Galkin, T. P., Klimentov, A. A., Korchuganova, T. A., Milman, I. E., Padolski, S. V., Pilyugin, V. V., and Titov, M. A., ATLAS (2020). *A New Visual Analytics Toolkit for ATLAS Computing Metadata*. J. Phys. Conf. Ser. **1525**(1), p. 012086.
- Grummer, A., ATLAS, CMS (2021). *Leptonic decays of light hadronic states and rare B decays*. PoS **LHCP2020**. Ed. by B. Mansoulie, G. Marchiori, R. Salern, and T. Bos, p. 113.
- Guerrero, D., ATLAS, CMS (2021). *Recent results on HH production from ATLAS and CMS*. PoS **LHCP2020**. Ed. by B. Mansoulie, G. Marchiori, R. Salern, and T. Bos, p. 132.
- Guescini, F., ATLAS (2020). *Searches for new phenomena with the ATLAS detector*. Int. J. Mod. Phys. A **35**(34n35), p. 2044005.
- Han, K., ATLAS (2021). *Performance of the ATLAS RPC detector and Level 1 Muon Barrel trigger at $\sqrt{s} = 13$ TeV*. PoS **ICHEP2020**, p. 737.
- Hatzifotiadou, D., ALICE, ATLAS, CMS, LHCb (2021). *Report on outreach activities at LHC*. PoS **LHCP2020**. Ed. by B. Mansoulie, G. Marchiori, R. Salern, and T. Bos, p. 203.
- Helling, C. et al., ATLAS (2020). *Strip sensor performance in prototype modules built for ATLAS ITk*. Nucl. Instrum. Meth. A **978**, p. 164402.
- Hinterkeuser, F., ATLAS (2021). *Development and evaluation of prototypes for the ATLAS ITk pixel detector*. PoS **ICHEP2020**, p. 891.
- Hoang Dai Nghia, N., ATLAS (2021). *Search for phenomena beyond the Standard Model in events with large b-jet multiplicity using the ATLAS detector at the LHC*. PoS **LHCP2020**. Ed. by B. Mansoulie, G. Marchiori, R. Salern, and T. Bos, p. 218.
- Hodgkinson, M., ATLAS, CMS (2021). *Third-generation SUSY Searches at ATLAS and CMS*. PoS **LHCP2020**. Ed. by B. Mansoulie, G. Marchiori, R. Salern, and T. Bos, p. 008.
- Hoz, S. G. de la et al., ATLAS (2020). *Computing activities at the Spanish Tier-1 and Tier-2s for the ATLAS experiment towards the LHC Run3 and High-Luminosity periods*. EPJ Web Conf. **245**. Ed. by C. Doglioni, D. Kim, G. A. Stewart, L. Silvestris, P. Jackson, and W. Kamleh, p. 07027.
- Ilic, N., ATLAS (2020). *Searching for Dark Matter with the ATLAS detector*. J. Phys. Conf. Ser. **1690**(1). Ed. by P. Teterin, p. 012153.
- Izzo, V., ATLAS (2021). *ATLAS upgrades*. PoS **LHCP2020**. Ed. by B. Mansoulie, G. Marchiori, R. Salern, and T. Bos, p. 094.
- Jacka, P., ATLAS (2021). *Inclusive and differential $t\bar{t}$ cross sections in ATLAS experiment*. PoS **LHCP2020**. Ed. by B. Mansoulie, G. Marchiori, R. Salern, and T. Bos, p. 067.
- Jakoubek, T., ATLAS (2020). *Measurement of CP violation and mixing in $B_s^0 \rightarrow J/\psi \phi$ in ATLAS*. Nucl. Part. Phys. Proc. **309-311**, pp. 148–151.

- Jiggins, S., ATLAS, CMS (2021). *Higgs boson measurements in third generation decay channels (excluding ttH) with ATLAS and CMS*. PoS **LHCP2020**. Ed. by B. Mansoulie, G. Marchiori, R. Salern, and T. Bos, p. 130.
- Kalogeropoulos, A., ATLAS, CMS (2021). *Experimental SUSY overview*. PoS **LHCP2020**. Ed. by B. Mansoulie, G. Marchiori, R. Salern, and T. Bos, p. 166.
- Kaneda, M., ATLAS (2020). *External Resources: Clouds and HPCs for the expansion of the ATLAS production system at the Tokyo regional analysis center*. EPJ Web Conf. **245**. Ed. by C. Doglioni, D. Kim, G. A. Stewart, L. Silvestris, P. Jackson, and W. Kamleh, p. 07034.
- Kano, Y., ATLAS (2020). *ATLAS Level-0 Endcap Muon Trigger for HL-LHC*. PoS **TWEPP2019**, p. 139.
- Kaur, A., ATLAS, CMS (2020). *Exotic searches by ATLAS and CMS*. J. Phys. Conf. Ser. **1690**(1). Ed. by P. Teterin, p. 012169.
- Keller, J. S., ATLAS (2020). *The ATLAS ITk strip detector system for the High Luminosity LHC upgrade*. Nucl. Instrum. Meth. A **958**. Ed. by M. Krammer, T. Bergauer, M. Dragicevic, M. Friedl, M. Jeitler, J. Schieck, and C. Schwanda, p. 162053.
- Kendrick, J., ATLAS (2020). *Measurement of differential cross sections for Single Diffractive Dissociation in $\sqrt{s} = 8$ TeV pp collisions using the ATLAS detector*. Nucl. Part. Phys. Proc. **309-311**, pp. 9–14.
- Ketabchi Haghigha, S., ATLAS (2021). *ATLAS Liquid Argon Calorimeter Commissioning for LHC Run-3*. PoS **LHCP2020**. Ed. by B. Mansoulie, G. Marchiori, R. Salern, and T. Bos, p. 226.
- Khandoga, M., ATLAS, CMS (2021). *EWK physics prospects for the HL-LHC*. PoS **LHCP2020**. Ed. by B. Mansoulie, G. Marchiori, R. Salern, and T. Bos, p. 029.
- Klein, M. H., ATLAS (2021). *Combined Higgs boson measurements at the ATLAS experiment*. PoS **ICHEP2020**, p. 064.
- Klimentov, A. et al., ATLAS (2020). *Enabling Data Intensive Science on Supercomputers for High Energy Physics R&D Projects in HL-LHC Era*. EPJ Web Conf. **226**. Ed. by G. Adam, J. Buša, and M. Hnatič, p. 01007.
- Klimpel, F., ATLAS (2020). *Track propagation for different detector and magnetic field setups in Acts*. J. Phys. Conf. Ser. **1525**(1), p. 012080.
- Köck, D. M., ATLAS (2020). *The ATLAS electron and photon trigger performance in Run 2*. Int. J. Mod. Phys. A **35**(34n35), p. 2044007.
- Kontaxakis, P., ATLAS, CMS (2021). *Boosted object identification in searches in ATLAS and CMS*. PoS **LHCP2020**. Ed. by B. Mansoulie, G. Marchiori, R. Salern, and T. Bos, p. 017.
- Krzysiak, J., ATLAS (2020). *SEARCHING FOR BSM HIGGS AND GAUGE BOSONS DECAYING TO TWO TAU LEPTONS USING 36 fb^{-1} OF DATA COLLECTED AT $\sqrt{s} = 13$ TeV WITH THE ATLAS DETECTOR* ***. Acta Phys. Polon. B **51**(6). Ed. by J. Bohm, M. Chrzęszcz, S. Sapeta, and A. Siódmok, pp. 1405–1410.
- Kulchitsky, Y., ATLAS, CMS (2020). *Soft QCD at ATLAS and CMS*. Acta Phys. Polon. B **51**(6). Ed. by J. Bohm, M. Chrzęszcz, S. Sapeta, and A. Siódmok, pp. 1411–1423.
- Langford, J. M., ATLAS, CMS (2021). *Combination of Higgs measurements from ATLAS and CMS : couplings and $||$ - framework*. PoS **LHCP2020**. Ed. by B. Mansoulie, G. Marchiori, R. Salern, and T. Bos, p. 136.
- Lapertosa, A., ATLAS (2020). *The ATLAS tracking system for HL-LHC*. Nuovo Cim. C **43**(2-3). Ed. by G. D’Ambrosio and G. De Nardo, p. 33.
- Lari, T., ATLAS (2020a). *Modeling radiation damage in the pixel sensors of the ATLAS detector*. JINST **15**(02). Ed. by M. Nessi, p. C02034.
- ATLAS, CMS (2020b). *Searches for SUSY at the LHC*. Nuovo Cim. C **42**(6), p. 256.
- Latonova, V., ATLAS (2021). *Radiation-Hard Silicon Strip Sensors for the ATLAS Phase-2 Upgrade*. PoS **ICHEP2020**, p. 892.
- Laudrain, A., ATLAS (2021). *Measurement of differential cross sections and the Higgs mass in Higgs boson decays to bosons using the ATLAS detector*. PoS **ICHEP2020**, p. 066.

- LeBlanc, M., ATLAS (2021). *Measurements of event shapes and jet substructure with ATLAS Run 2 data*. PoS **LHCP2020**. Ed. by B. Mansoulie, G. Marchiori, R. Salern, and T. Bos, p. 144.
- Lefebvre, B., ATLAS (2020). *Precision survey of the readout strips of small-strip Thin Gap Chambers using X-rays for the muon spectrometer upgrade of the ATLAS experiment*. JINST **15**(07), p. C07013.
- Lenz, T., ATLAS (2020). *Measurement of jet substructure observables and jet fragmentation properties using the ATLAS detector*. Nucl. Part. Phys. Proc. **309-311**, pp. 1–8.
- Leontsinis, S., ATLAS, CMS (2021). *Quarkonia production in ATLAS and CMS experiments*. PoS **LHCP2020**. Ed. by B. Mansoulie, G. Marchiori, R. Salern, and T. Bos, p. 185.
- Li, K., ATLAS, CMS (2021). *Searches for heavy resonances decaying to Higgs bosons at ATLAS & CMS*. PoS **LHCP2020**. Ed. by B. Mansoulie, G. Marchiori, R. Salern, and T. Bos, p. 013.
- Loch, P., ATLAS (2021a). *Inclusive jet measurements with the ATLAS experiment at the LHC*. PoS **ICHEP2020**, p. 482.
- ATLAS (2021b). *Jet and missing transverse momentum reconstruction in ATLAS at the LHC*. PoS **LHCP2020**. Ed. by B. Mansoulie, G. Marchiori, R. Salern, and T. Bos, p. 049.
- Lorenz, J. M., ATLAS (2021). *Searches for additional Higgs bosons in the ATLAS detector*. PoS **ICHEP2020**, p. 067.
- Lykasov, G., Brodsky, S. J., Bednyakov, V. A., Lipatov, A. V., Smiesko, J., and Tokar, S., ATLAS (2020). *Constraints on the Intrinsic Charm Content of the Proton from Recent ATLAS Data*. PoS **LC2019**, p. 060.
- Lyubushkina, T., ATLAS (2020). *ATLAS results on quarkonia and heavy flavor production*. Int. J. Mod. Phys. A **35**(34n35), p. 2044003.
- Macchiolo, A., ATLAS (2020). *The Phase-2 ATLAS ITk pixel upgrade*. Nucl. Instrum. Meth. A **962**, p. 162261.
- Mahon, D. J., ATLAS (2020). *ATLAS LAr calorimeter performance in LHC Run 2*. JINST **15**(06), p. C06045.
- Majerský, O., ATLAS (2020a). *Highlights of top-quark properties measurements at the ATLAS experiment*. Nucl. Part. Phys. Proc. **309-311**, pp. 22–29.
- Majerský, O., ATLAS (2020b). *Identifying hadronically-decaying vector bosons and top quarks in ATLAS*. J. Phys. Conf. Ser. **1525**(1), p. 012118.
- Megino, F. H. B. et al., ATLAS (2020). *Using Kubernetes as an ATLAS computing site*. EPJ Web Conf. **245**. Ed. by C. Doglioni, D. Kim, G. A. Stewart, L. Silvestris, P. Jackson, and W. Kamleh, p. 07025.
- Mehlhase, S., ATLAS (2021). *ATLAS, Play! – Teaching particle physics through educational games*. PoS **ICHEP2020**, p. 950.
- Mejia Guisao, J. A., ATLAS, CMS, LHCb (2020). “Experimental status of CPV in B_s^0 mixing”. *18th Conference on Flavor Physics and CP Violation*.
- Meloni, F., ATLAS, CMS (2020). *Collider physics at the intensity and energy frontier – the HL-LHC and beyond*. J. Phys. Conf. Ser. **1586**(1). Ed. by E. Widmann, J. Marton, A. Pichler, M. Simon, and D. Murtagh, p. 012038.
- Meng, L., ATLAS (2020). *Module and System Test Development for the Phase-2 ATLAS ITk Pixel Upgrade*. PoS **TWEPP2019**, p. 122.
- Meshreki, J. K. R., ATLAS (2021). *Top-quark-antiquark production in association with a photon in the electron-muon channel at a centre-of-mass energy of 13 TeV with the ATLAS detector*. PoS **ICHEP2020**, p. 355.
- Mijović, L., ATLAS (2021). *Measurement of production mode cross sections of the Higgs boson in decays to bosons with the ATLAS detector*. PoS **ICHEP2020**, p. 069.
- Milic, A., ATLAS (2020). *Searches for new phenomena in final states involving leptons and jets using the ATLAS detector*. PoS **EPS-HEP2019**, p. 548.
- Mitsou, V. A., ATLAS, CMS (2020). *SUSY searches in ATLAS and CMS*. PoS **CORFU2019**, p. 050.

- Mizukami, A., ATLAS (2020). *ATLAS Level-1 Endcap Muon Trigger for Run 3*. EPJ Web Conf. **245**. Ed. by C. Doglioni, D. Kim, G. A. Stewart, L. Silvestris, P. Jackson, and W. Kamleh, p. 01002.
- Mlynáriková, M., ATLAS (2020). *Search for rare and lepton-flavor violating decays of the Higgs boson with the ATLAS detector*. Int. J. Mod. Phys. A **35**(34n35), p. 2044001.
- Mondal, S., ATLAS (2021). *Tau-lepton Fake-Rate determination for the ttH coupling measurement using the ATLAS detector at the LHC*. PoS **ICHEP2020**, p. 100.
- Moreira De Carvalho, A. L., ATLAS (2021). *The ATLAS Hardware Track Trigger performance studies for the HL-LHC*. PoS **LHCP2020**. Ed. by B. Mansoulie, G. Marchiori, R. Salern, and T. Bos, p. 247.
- Moser, B., ATLAS (2021). *Measurement of Higgs boson production at high transverse momentum in the $VH, H \rightarrow b\bar{b}$ channel with the ATLAS detector*. PoS **ICHEP2020**, p. 101.
- Muškinja, M., Calafiura, P., Leggett, C., Shapoval, I., and Tsulaia, V., ATLAS (2020a). *Raythena: a vertically integrated scheduler for ATLAS applications on heterogeneous distributed resources*. EPJ Web Conf. **245**. Ed. by C. Doglioni, D. Kim, G. A. Stewart, L. Silvestris, P. Jackson, and W. Kamleh, p. 05042.
- Muškinja, M., Chapman, J. D., and Gray, H., ATLAS (2020b). *Geant4 performance optimization in the ATLAS experiment*. EPJ Web Conf. **245**. Ed. by C. Doglioni, D. Kim, G. A. Stewart, L. Silvestris, P. Jackson, and W. Kamleh, p. 02036.
- Negrini, M., ATLAS, CMS (2021). *Top mass and width from CMS and ATLAS*. PoS **LHCP2020**. Ed. by B. Mansoulie, G. Marchiori, R. Salern, and T. Bos, p. 073.
- Neutelings, I., ATLAS, CMS (2021). *Hadronic tau reconstruction and identification performance in ATLAS and CMS*. PoS **LHCP2020**. Ed. by B. Mansoulie, G. Marchiori, R. Salern, and T. Bos, p. 045.
- Nibigira, E., ATLAS (2020). *Search for vector-boson resonances decaying to a top quark and a bottom quark with the ATLAS experiment at LHC*. Nuovo Cim. C **42**(6), p. 258.
- Nielsen, J., ATLAS (2020). *Physics prospects for ATLAS at the HL-LHC*. J. Phys. Conf. Ser. **1690**(1). Ed. by P. Teterin, p. 012156.
- Nikolaenko, V., ATLAS (2020). *Measurement of the weak mixing phase ϕ_s through time-dependent CP violation in $B_s^0 \rightarrow J/\psi\phi$ decays in the ATLAS detector*. Int. J. Mod. Phys. A **35**(34n35), p. 2044006.
- Nobe, T., ATLAS (2021a). *ATLAS Level-1 Endcap Muon Trigger from Run 2 to Run 3*. PoS **LHCP2020**. Ed. by B. Mansoulie, G. Marchiori, R. Salern, and T. Bos, p. 227.
- ATLAS (2021b). *Observations of weak boson scattering with the ATLAS detector*. PoS **ICHEP2020**, p. 336.
- Novak, T., ATLAS (2020). *Searches for new phenomena in final states involving leptons and jets using the ATLAS detector*. Int. J. Mod. Phys. A **35**(34n35), p. 2044004.
- Novotny, R., ATLAS (2020a). *ATLAS measurements of production, decays and spectroscopy of heavy flavour hadrons*. J. Phys. Conf. Ser. **1690**(1). Ed. by P. Teterin, p. 012152.
- ATLAS (2020b). *CP violation in $B_s^0 \rightarrow J/\psi\phi$ in the ATLAS experiment*. PoS **Beauty2019**, p. 003.
- Okumura, Y., ATLAS (2021). *Search for leptoquarks using the ATLAS detector*. PoS **ICHEP2020**, p. 268.
- Oliveira Gonçalves, D., ATLAS (2020). *Energy reconstruction of the ATLAS Tile Calorimeter under high pile-up conditions using the Wiener filter*. J. Phys. Conf. Ser. **1525**(1), p. 012092.
- O'Neill, A. P., ATLAS (2021). *When jets MET SUSY: ATLAS searches for squarks and gluinos*. PoS **ICHEP2020**, p. 269.
- Ördek, S., ATLAS (2020). *Investigation of the CP Properties of VBF Higgs Production Using the Decay to a Pair of tau Leptons with the ATLAS Detector*. Acta Phys. Polon. B **51**(6). Ed. by J. Bohm, M. Chrzęszcz, S. Sapeta, and A. Siódsmok, pp. 1497–1502.
- Orellana, G. E., ATLAS (2021). *Projected ATLAS Electron and Photon Trigger Performance in Run 3*. PoS **LHCP2020**. Ed. by B. Mansoulie, G. Marchiori, R. Salern, and T. Bos, p. 244.

- Ould-Saada, F., ATLAS (2020). *ATLAS Open Data – Development of a simple-but-real HEP data analysis framework*. EPJ Web Conf. **245**. Ed. by C. Doglioni, D. Kim, G. A. Stewart, L. Silvestris, P Jackson, and W. Kamleh, p. 08023.
- Pardos, C. D., ATLAS (2020). *Recent highlights of top-quark physics with the ATLAS detector*. J. Phys. Conf. Ser. **1690**(1). Ed. by P. Teterin, p. 012155.
- Pásztor, G., ATLAS, CMS, LHCb (2020). “Hard QCD Measurements at the LHC”. *Proceedings, 28th International Symposium on Lepton Photon Interactions at High Energies (LP17): Guangzhou (Guangdong), China, August 7-12, 2017*. Ed. by W. Wang and Z.-z. Xing. Singapore: WSP.
- Pater, J., ATLAS (2020). *The ATLAS Pixel Detector upgrade at High Luminosity LHC*. PoS **Vertex2019**, p. 011.
- Pedro, R., ATLAS (2020). *Operation and Performance of the ATLAS Tile Calorimeter*. J. Phys. Conf. Ser. **1690**(1). Ed. by P. Teterin, p. 012045.
- Peixoto, A., ATLAS (2021). *ATLAS Public Engagement : The CERN Open Days Experience*. PoS **LHCP2020**. Ed. by B. Mansoulie, G. Marchiori, R. Salern, and T. Bos, p. 229.
- Peixoto, A., Bianchi, R. M., Vukotic, I., Potter, C., and Adam Bourdarios, C., ATLAS (2021). *Getting the public closer to the experimental facilities: How Virtual Reality helps High Energy Physics experiments engage public interest*. PoS **ICHEP2020**, p. 954.
- Penc, O., ATLAS (2020a). *Observation and measurements of vector-boson scattering with the ATLAS detector*. Int. J. Mod. Phys. A **35**(34n35), p. 2044002.
- ATLAS (2020b). *Observation and measurements of vector-boson scattering with the ATLAS detector*. Phys. Scripta **95**(8). Ed. by L. Bravina, S. Kabana, V. Volkova, and V. I. Zakharov, p. 084014.
- Pereira Sanchez, L., ATLAS (2020). *Search for supersymmetric partners of third-generation quarks in 139 fb^{-1} of pp collisions at $\sqrt{s} = 13\text{ TeV}$ with the ATLAS detector*. PoS **EPS-HEP2019**, p. 611.
- Pereira, B., ATLAS (2020). *Radiation hardness of the ATLAS Tile Calorimeter optical components*. J. Phys. Conf. Ser. **1690**(1). Ed. by P. Teterin, p. 012053.
- Petruciani, G., ATLAS, CMS (2021). *Higgs sector: What we would like to know*. PoS **LHCP2020**. Ed. by B. Mansoulie, G. Marchiori, R. Salern, and T. Bos, p. 161.
- Pizzimento, L., ATLAS (2020). *Performance of the BIS78 RPC detectors: a new concept of electronics and detector integration for high-rate and fast timing large size RPCs*. JINST **15**(11). Ed. by B. Liberti, A. Paoloni, and P. Camarri, p. C11010.
- Poley, L. et al., ATLAS (2020). *The ABC130 barrel module prototyping programme for the ATLAS strip tracker*. JINST **15**(09), P09004.
- Przybycien, M., ATLAS (2021). *Recent results on hard and rare probes from ATLAS*. PoS **LHCP2020**. Ed. by B. Mansoulie, G. Marchiori, R. Salern, and T. Bos, p. 031.
- Queitsch-Maitland, M., ATLAS, CMS (2021). *Dark sector searches with the ATLAS and CMS experiments*. PoS **LHCP2020**. Ed. by B. Mansoulie, G. Marchiori, R. Salern, and T. Bos, p. 111.
- Ran, K., ATLAS (2021). *Constraints on the Higgs boson self-coupling from the combination of single-Higgs and double-Higgs production analyses performed with the ATLAS experiment*. PoS **ICHEP2020**, p. 104.
- Richter, R., ATLAS (2020). *Upgrade of the ATLAS MDT Readout and Trigger for the HL-LHC*. PoS **TWEPP2019**, p. 146.
- Richter, S., ATLAS (2020). *Measurements of inclusive neutral diboson production with ATLAS*. PoS **EPS-HEP2019**, p. 669.
- Rieck, P., ATLAS (2020). *Design, construction and test of small-diameter Muon Drift Tube chambers (sMDT) for the Phase-1 upgrade of the ATLAS muon spectrometer*. Nucl. Instrum. Meth. A **958**. Ed. by M. Krammer, T. Bergauer, M. Dragicevic, M. Friedl, M. Jeitler, J. Schieck, and C. Schwanda, p. 162791.
- Rizzi, C., ATLAS (2021). *A High-Granularity Timing Detector for the ATLAS Phase-II upgrade*. PoS **ICHEP2020**, p. 868.

- Rosser, B. J., ATLAS (2021). *Searches for invisible Higgs boson decays at the ATLAS experiment*. PoS **ICHEP2020**, p. 078.
- Rossi, E., ATLAS (2020). *Constraining the Higgs boson self-coupling via single-Higgs production measurements*. PoS **EPS-HEP2019**, p. 366.
- Sabatini, P., ATLAS (2020). *Operational experience and performance with the ATLAS Pixel detector at the Large Hadron Collider at CERN*. JINST **15**(02). Ed. by M. Nessi, p. C02039.
- ATLAS (2021). *Rare top quark production in ATLAS ($t\bar{t}\bar{t}$, tqZ , $tq\gamma$)*. PoS **LHCP2020**. Ed. by B. Mansoulie, G. Marchiori, R. Salern, and T. Bos, p. 076.
- Saito, M., ATLAS (2021). *Searches for long-lived particles in ATLAS*. PoS **LHCP2020**. Ed. by B. Mansoulie, G. Marchiori, R. Salern, and T. Bos, p. 107.
- Salvador Salas, A., ATLAS (2021). *New results of the $H^+ \rightarrow tb$ search using full Run-2 data with the ATLAS detector*. PoS **ICHEP2020**, p. 105.
- Sano, Y., ATLAS (2020). *ATLAS searches for di-Higgs production at 13 TeV and prospects for HL-LHC*. Phys. Scripta **95**(8). Ed. by L. Bravina, S. Kabana, V. Volkova, and V. I. Zakharov, p. 084008.
- Santra, A., ATLAS (2020). *QCD Issues in Searches for Supersymmetry with the ATLAS Detector*. Nucl. Part. Phys. Proc. **309-311**, pp. 49–54.
- Sauerburger, F., ATLAS (2021). *Measurement of the Higgs boson coupling to τ -leptons in proton–proton collisions at $\sqrt{s} = 13$ TeV with the ATLAS detector at the LHC*. PoS **ICHEP2020**, p. 106.
- Savina, M., ATLAS, CMS (2021). *DM interpretations of heavy resonances and BSM-Higgs searches in ATLAS and CMS*. PoS **LHCP2020**. Ed. by B. Mansoulie, G. Marchiori, R. Salern, and T. Bos, p. 176.
- Schramm, S., ATLAS (2021). *Fully Hadronic Diboson searches in ATLAS*. PoS **ICHEP2020**, p. 284.
- Sciacca, F. G., ATLAS (2020). *Enabling ATLAS big data processing on Piz Daint at CSCS*. EPJ Web Conf. **245**. Ed. by C. Doglioni, D. Kim, G. A. Stewart, L. Silvestris, P. Jackson, and W. Kamleh, p. 09005.
- Scutti, F., ATLAS (2020). *Search for heavy neutrinos with the ATLAS detector*. PoS **NuFact2019**, p. 094.
- ATLAS (2021). *Searches for heavy particles with leptons at ATLAS*. PoS **ICHEP2020**, p. 279.
- Seidel, S., ATLAS (2021). *ATLAS Results on Heavy Flavor Production and Decays*. PoS **ICHEP2020**, p. 419.
- Serkin, L., ATLAS (2020). *The release of the 13 TeV ATLAS Open Data: using open education resources effectively*. EPJ Web Conf. **245**. Ed. by C. Doglioni, D. Kim, G. A. Stewart, L. Silvestris, P. Jackson, and W. Kamleh, p. 08026.
- Sessa, M., ATLAS (2020). *Performance of the ATLAS RPC detector and Level-1 muon barrel trigger at $\sqrt{s} = 13$ TeV*. Phys. Scripta **95**(8). Ed. by L. Bravina, S. Kabana, V. Volkova, and V. I. Zakharov, p. 084005.
- Shope, D. R., ATLAS Collaboration (2021). *Higgs Simplified Template and Differential Cross Sections*. <https://cds.cern.ch/record/2759461>.
- Skovpen, K., ATLAS, CMS (2021). *Search for new phenomena in top quark interactions*. PoS **LHCP2020**. Ed. by B. Mansoulie, G. Marchiori, R. Salern, and T. Bos, p. 075.
- Smirnov, Y., Chakraborty, D., Solodkov, A., and Harkusha, S., ATLAS (2020). *ATLAS Tile Calorimeter Conditions Database architecture and operations in Run 2*. EPJ Web Conf. **245**. Ed. by C. Doglioni, D. Kim, G. A. Stewart, L. Silvestris, P. Jackson, and W. Kamleh, p. 02006.
- Snyder, S., ATLAS (2020). *Concurrent data structures in the ATLAS offline software*. EPJ Web Conf. **245**. Ed. by C. Doglioni, D. Kim, G. A. Stewart, L. Silvestris, P. Jackson, and W. Kamleh, p. 05007.
- Søgaard, A., ATLAS (2020). *Constructing mass-decorrelated hadronic decay taggers in ATLAS*. J. Phys. Conf. Ser. **1525**(1), p. 012117.
- Sohns, F., ATLAS (2020). *Operational Experience and Performance with the ATLAS Pixel detector at the Large Hadron Collider at CERN*. JINST **15**(05). Ed. by M. Nessi, p. C05010.
- Solans Sanchez, C. A., ATLAS (2020). *The FELIX detector interface for the ATLAS TDAQ upgrades and its deployment in the ITk demonstrator setup*. J. Phys. Conf. Ser. **1525**(1), p. 012033.

- Sopczak, A., ATLAS, CMS (2020a). *Precision measurements in Higgs sector at ATLAS and CMS*. PoS **FFK2019**, p. 006.
- ATLAS (2020b). *Timepix3 Luminosity Determination of 13 TeV Proton-Proton Collisions at the ATLAS Experiment*. EPJ Web Conf. **225**. Ed. by A. Lyoussi, M. Giot, M. Carette, I. Jenčič, C. Reynard-Carette, L. Vermeeren, L. Snoj, and P. Le Dû, p. 01002.
- ATLAS (2020c). *Timepix3 Luminosity Determination of 13-TeV Proton-Proton Collisions at the ATLAS Experiment*. IEEE Trans. Nucl. Sci. **67**(4), pp. 609–616.
- Spolidoro Freund, W., ATLAS (2020). *An Ensemble of Neural Networks for Online Electron Filtering at the ATLAS Experiment*. J. Phys. Conf. Ser. **1525**(1), p. 012076.
- Spousta, M., ATLAS (2020). *Recent Results from ATLAS: Onia, Heavy-Flavor, and More*. Springer Proc. Phys. **250**. Ed. by D. Elia, G. E. Bruno, P. Colangelo, and L. Cosmai, pp. 55–60.
- Steinhebel, A. L., ATLAS (2021). *Search for Invisibly Decaying Vector Boson Fusion Produced Higgs Bosons with $139/\text{fb}^{-1}$ of pp collisions with the ATLAS Detector*. PoS **ICHEP2020**, p. 107.
- Sykora, T., ATLAS (2020). *ATLAS Forward Proton Time-of-Flight Detector: LHC Run2 performance and experiences*. JINST **15**(10), p. C10004.
- Terzo, S., ATLAS (2021). *ATLAS ITk pixel detector overview*. PoS **ICHEP2020**, p. 878.
- Todome, K., ATLAS (2020a). *Search for chargino neutralino production in final states with a W boson and Higgs boson*. Nuovo Cim. C **43**(2-3). Ed. by G. D’Ambrosio and G. De Nardo, p. 102.
- ATLAS (2020b). *Searches for squarks and gluinos with the ATLAS detector*. Phys. Scripta **95**(9). Ed. by L. Bravina, S. Kabana, V. Volkova, and V. I. Zakharov, p. 094003.
- Tsuno, S., ATLAS, CMS (2020). “Search for Beyond SM Higgs Bosons”. *Proceedings, 28th International Symposium on Lepton Photon Interactions at High Energies (LP17): Guangzhou (Guangdong), China, August 7-12, 2017*. Ed. by W. Wang and Z.-z. Xing. Singapur: WSP.
- Turchikhin, S., ATLAS (2021). *ATLAS studies of Spectroscopy and exotics*. PoS **ICHEP2020**, p. 433.
- ATLAS (2020). *Spectroscopy and production of quarkonia and heavy flavour at ATLAS*. Nucl. Part. Phys. Proc. **309-311**, pp. 162–167.
- Tzani, P., ATLAS (2020). *Electronics performance of the ATLAS New Small Wheel Micromegas wedges at CERN*. JINST **15**(07), p. C07002.
- Varni, C., ATLAS (2020). *Real-time selection using flavour-tagging algorithms in ATLAS*. Nuovo Cim. C **43**(2-3). Ed. by G. D’Ambrosio and G. De Nardo, p. 105.
- Ventura, A., ATLAS (2020a). *Recent results from SUSY searches with ATLAS and prospects for the HL-LHC*. J. Phys. Conf. Ser. **1586**(1). Ed. by E. Widmann, J. Marton, A. Pichler, M. Simon, and D. Murtagh, p. 012029.
- Ventura, A., ATLAS (2020b). *ATLAS muon trigger performance*. Phys. Scripta **95**(7). Ed. by L. Bravina, S. Kabana, V. Volkova, and V. I. Zakharov, p. 074004.
- Vittori, C., ATLAS (2020). *Observation of $H \rightarrow bb$ in ATLAS*. Nuovo Cim. C **43**(2-3). Ed. by G. D’Ambrosio and G. De Nardo, p. 40.
- Vittori, C., ATLAS (2021). *Measurements of W/Z boson production in association with jets at ATLAS*. PoS **ICHEP2020**, p. 517.
- Walkowiak, W., ATLAS (2020). *Rare and Semi-rare Decays of Beauty Mesons in ATLAS*. PoS **Beauty2019**, p. 017.
- Wang, Y., ATLAS (2021). *Search for new resonances in high-mass diphoton final states using proton-proton collision data collected with the ATLAS detector*. PoS **ICHEP2020**, p. 109.
- Wiglesworth, C., ATLAS (2020). “Overview of Recent Results from ATLAS”. *12th International Workshop on Top Quark Physics*.
- Wong, V. W. S., ATLAS (2021). *Search for Scalar Leptoquark Pair Production Decaying into Top-Quarks and Leptons at $\sqrt{s} = 13$ TeV with ATLAS detector*. PoS **ICHEP2020**, p. 313.
- Wonsak, S., ATLAS (2020). *The ATLAS ITk Strip Detector System for the Phase-II LHC Upgrade*. PoS **Vertex2019**, p. 017.

- Yamazaki, Y., ATLAS, CMS, LHCb (2020). “Determination of Top-Quark Properties”. *Proceedings, 28th International Symposium on Lepton Photon Interactions at High Energies (LP17): Guangzhou (Guangdong), China, August 7-12, 2017*. Ed. by W. Wang and Z.-z. Xing. Singapur: WSP.
- Yazgan, E., ATLAS, CMS (2021). *Measurements of top quark properties at the LHC*. PoS **LHCP2020**. Ed. by B. Mansoulie, G. Marchiori, R. Salern, and T. Bos, p. 099.
- Yeletsikh, I., ATLAS (2020). *Search for exotic states in ATLAS: pentaquarks*. PoS **Beauty2019**, p. 010.
- Young, C., ATLAS (2021). *Top Quark Properties from ATLAS*. PoS **LHCP2020**. Ed. by B. Mansoulie, G. Marchiori, R. Salern, and T. Bos, p. 071.
- Yuan, L., ATLAS, CMS (2020). *Exotics and BSM in ATLAS and CMS (Non dark matter searches)*. PoS **CORFU2019**, p. 051.
- Zakareishvili, T., ATLAS (2020a). *Associated quarkonium production at ATLAS*. Ed. by F.-K. Guo and W.-H. Liang.
- ATLAS (2020b). *Upgrade of the ATLAS Hadronic Tile Calorimeter for the High Luminosity LHC*. JINST **15**(09), p. C09003.
- Zakareishvili, T., ATLAS (2020c). *Measurement of the production cross-section of J/ψ and $\psi(2S)$ mesons at high transverse momentum in pp collisions at $\sqrt{s} = 13$ TeV with the ATLAS detector*. J. Phys. Conf. Ser. **1690**(1). Ed. by P. Teterin, p. 012160.
- Zarucki, M., ATLAS, CMS (2021). *Soft Supersymmetry Searches at ATLAS and CMS*. PoS **LHCP2020**. Ed. by B. Mansoulie, G. Marchiori, R. Salern, and T. Bos, p. 009.
- Zhang, L., ATLAS (2020). “Muon Reconstruction Performance of the ATLAS Detector at the LHC at $\sqrt{s} = 13$ TeV”. *Proceedings, 28th International Symposium on Lepton Photon Interactions at High Energies (LP17): Guangzhou (Guangdong), China, August 7-12, 2017*. Ed. by W. Wang and Z.-z. Xing.
- Zheng, D., Aukerman, A., and Hong, T. M., ATLAS (2020). “Commissioning and Validation of the ATLAS Level-1 Topological Trigger in Run 2”. *Proceedings, 28th International Symposium on Lepton Photon Interactions at High Energies (LP17): Guangzhou (Guangdong), China, August 7-12, 2017*. Ed. by W. Wang and Z.-z. Xing. Singapur: WSP.

FASE2_ATLAS

- Boscardin, M., Ceccarelli, R., Dalla Betta, G. F., Darbo, G., Dinardo, M., Giacomini, G., Menasce, D., Mendicino, R., Meschini, M., Messineo, A., Moroni, L., Rivera, R., Ronchin, S., Sultan, D., Uplegger, L., Viliani, L., Zoi, I., and Zuolo, D. (2020). *Performance of new radiation-tolerant thin planar and 3D columnar $n+$ on p silicon pixel sensors up to a maximum fluence of $5 \times 10^{15} n_{eq} cm^{-2}$* . Nuclear Instrum. Methods A **953**. Art. no.: 163222.
- Boughedda, A., Lakhdara, M., Latreche, S., and Dalla Betta, G.-F. (2020). *Compact border termination for active-edge planar radiation detectors with enhanced breakdown voltage*. Micro and Nano Letters **15**, pp. 969–971.
- Cassese, A., Ceccarelli, R., Meschini, M., Viliani, L., Dinardo, M., Gennai, S., Moroni, L., Zuolo, D., Messineo, A., Dalla Betta, G.-F., Boscardin, and M. (2020). *Performances of highly irradiated 3d and planar pixel sensors interconnected to the RD53A readout chip*. Journal Instrum. **15**. Art. no.: C02016.
- Ceccarelli, R., Meschini, M., Viliani, L., Dinardo, M., Gennai, S., Menasce, D., Moroni, L., Zuolo, D., Demaria, L., Monteil, E., Gaioni, L., Messineo, A., Curras, E., Duarte, J., Fernandez, M., Gomez, G., Garcia, A., Gonzales, J., Silva, E., Vila, I., Dalla Betta, G.-F., Mendicino, R., and Boscardin, M. (2020). “Characterization of planar and 3D Silicon pixel sensors for the high luminosity phase of the CMS experiment at LHC”. *Proceedings of Science - EPS HEP 2019*. Trieste, Italy: Sissa, p. 117.
- Garcia-Alonso, A., Curras, E., Duarte-Campderros, J., Fernandez, M., Gomez, G., Gonzales, J., Silva, E., Vila, I., Jaramillo, R., Meschini, M., Ceccarelli, R., Dinardo, M., Gennai, S., Moroni, L., Zuolo,

- D., Demaria, L., Monteil, E., Gaioni, L., Messineo, A., Dalla Betta, G. F., Mendicino, R., Boscardin, M., Hidalgo, S., Merlos, A., Pellegrini, G., Quirion, D., and Manna, M. (2020). *Test beam characterization of irradiated 3D pixel sensors*. *Journal Instrum.* **15**. Art. no.: C03017.
- Meschini, M., Cassese, A., Ceccarelli, R., Viliani, I., Dinardo, M., Gennai, S., Zuolo, D., Messineo, A., Parolia, S., Ebrahimi, A., Pitzl, D., Steinbrück, G., Dalla Betta, G. F., Mendicino, R., Alimonti, A., Gemme, C., Boscardin, M., and Ronchin, S. (2020). *Radiation resistant innovative 3D pixel sensors for the CMS upgrade at the High Luminosity LHC*. *Nuclear Instrum. Methods A* **978**. Art. no.: 164429.
- Moscattelli, F., Morozzi, A., Passeri, D., Mattiazzo, S., Dalla Betta, G. F., Bergauer, T., Dragicevic, M., Hinger, V., and Bilei, G. (2020). *Measurements and simulations of surface radiation damage effects on IFX and HPK test structures*. *Nuclear Instrum. Methods A* **958**. Art. no.: 162974.

Astroparticle Physics

- Abbrescia, M. et al. (2020a). *New high precision measurements of the cosmic charged particle rate beyond the Arctic Circle with the PolarquEEEst experiment*. *Eur. Phys. J. C* **80**(7), p. 665.
- (2020b). *Results from the PolarquEEEst missions*. *J. Phys. Conf. Ser.* **1561**(1). Ed. by A. Trifiró, G. Mandaglio, and M. Trimarchi. Art. no.: 012001.

ADHD

- Dimiccoli, F., Nozzoli, F., and Zuccon, P. (2020c). “Detectors for antideuteron search in cosmic rays: current status and new ideas”. Ed. by M. Nessi. Vol. 15. 06. Art. no.: C06033.
- Doetinchem, P. von et al. (2020). *Cosmic-ray antinuclei as messengers of new physics: status and outlook for the new decade*. *JCAP* **08**, p. 035.
- Nozzoli, F., Dimiccoli, F., and Zuccon, P. (2020). “Perspectives of dark matter indirect search with ADHD in space”. Vol. 1548. 1. Art. no.: 012035.

AMS

- Aguilar, M. et al., AMS collaboration (2020a). *Properties of Neon, Magnesium, and Silicon Primary Cosmic Rays Results from the Alpha Magnetic Spectrometer*. *Phys. Rev. Lett.* **124**(21). Art. no.: 211102.
- AMS collaboration (2020b). *Properties of Neon, Magnesium, and Silicon Primary Cosmic Rays Results from the Alpha Magnetic Spectrometer*. *Phys. Rev. Lett.* **124**(21). Art. no.: 211102.
- AMS collaboration (2021a). *The Alpha Magnetic Spectrometer (AMS) on the international space station: Part II — Results from the first seven years*. *Phys. Rept.* **894**, pp. 1–116.
- AMS collaboration (2021b). *The Alpha Magnetic Spectrometer (AMS) on the international space station: Part II — Results from the first seven years*. *Phys. Rept.* **894**, pp. 1–116.
- Battiston, R. (2020a). *High precision cosmic ray physics with AMS-02 on the International Space Station*. *Riv. Nuovo Cim.* **43**(7), pp. 319–384.
- Battiston, R. (2020b). “Spaceborne Experiments”, pp. 823–870.
- Dimiccoli, F., Battiston, R., Kanishchev, K., Nozzoli, F., and Zuccon, P. (2020a). *Measurement of Cosmic Deuteron Flux with the AMS-02 Detector*. *J. Phys. Conf. Ser.* **1548**(1). Art. no.: 012034.
- (2020b). *Measurement of Cosmic Deuteron Flux with the AMS-02 Detector*. *J. Phys. Conf. Ser.* **1548**(1). Art. no.: 012034.

DarkSide

- Aalseth, C. et al. (2020). *Design and construction of a new detector to measure ultra-low radioactive isotope contamination of argon*. *J. Instrum.* **15**. Art. no.: P02024.

FISH

- Caleffi, F., Capone, M., Menotti, C., Carusotto, I., and Recati, A. (2020). *Quantum fluctuations beyond the Gutzwiller approximation in the Bose-Hubbard model*. Phys. Rev. Research **2** (3). Art. no.: 033276.
- Farolfi, A., Trypogeorgos, D., Mordini, C., Lamporesi, G., and Ferrari, G. (2020a). *Observation of Magnetic Solitons in Two-Component Bose-Einstein Condensates*. Phys. Rev. Lett. **125** (3). Art. no.: 030401.
- Gallemí, A., Rocuzzo, S. M., Stringari, S., and Recati, A. (2020). *Quantized vortices in dipolar supersolid Bose-Einstein-condensed gases*. Phys. Rev. A **102** (2). Art. no.: 023322.
- Martone, G. I., Recati, A., and Pavloff, N. (2021). *Supersolidity of cnoidal waves in an ultracold Bose gas*. Phys. Rev. Research **3** (1). Art. no.: 013143.
- Mordini, C., Trypogeorgos, D., Farolfi, A., Wolswijk, L., Stringari, S., Lamporesi, G., and Ferrari, G. (2020a). *Measurement of the Canonical Equation of State of a Weakly Interacting 3D Bose Gas*. Phys. Rev. Lett. **125** (15). Art. no.: 150404.
- Mordini, C., Trypogeorgos, D., Wolswijk, L., Lamporesi, G., and Ferrari, G. (2020b). *Single-shot reconstruction of the density profile of a dense atomic gas*. Opt. Express **28**(20), pp. 29408–29418.
- Tajima, H., Recati, A., and Ohashi, Y. (2020). *Spin-dipole mode in a trapped Fermi gas near unitarity*. Phys. Rev. A **101** (1). Art. no.: 013610.

HUMOR

- Bonaldi, M., Borrielli, A., Chowdhury, A., Giuseppe, G. D., Li, W., Malossi, N., Marino, F., Morana, B., Natali, R., Piergentili, P., Prodi, G. A., Sarro, P. M., Serra, E., Vezio, P., Vitali, D., and Marin, F. (2020). *Probing quantum gravity effects with quantum mechanical oscillators*. THE EUROPEAN PHYSICAL JOURNAL D **74**, p. 178.
- Chowdhury, A., Vezio, P., Bonaldi, M., Borrielli, A., Marino, F., Morana, B., Prodi, G., Sarro, P., Serra, E., and Marin, F. (2020a). *Quantum motion of a squeezed mechanical oscillator attained via an optomechanical experiment*. PHYSICAL REVIEW A **102**. Art. no.: 053505.
- (2020b). *Quantum signature of a squeezed mechanical oscillator*. PHYSICAL REVIEW LETTERS **124**. Art. no.: 023601.

LIMADOU

- Ambrosi, G., Bartocci, S., Basara, L., Battiston, R., Burger, W., Campana, D., Carfora, L., Castellini, G., Cipollone, P., Conti, L., et al. (2020). *Beam test calibrations of the HEPD detector on board the China Seismo-Electromagnetic Satellite*. Nuclear instruments and methods in physics research section a: accelerators, spectrometers, detectors and associated equipment **974**. Art. no.: 164170.
- Bartocci, S., Battiston, R., Burger, W., Campana, D., Carfora, L., Castellini, G., Conti, L., Contin, A., De Donato, C., De Persio, F., et al. (2020b). *Galactic Cosmic-Ray Hydrogen Spectra in the 40–250 MeV Range Measured by the High-energy Particle Detector (HEPD) on board the CSES-01 Satellite between 2018 and 2020*. The Astrophysical Journal **901**(1), p. 8.
- Gebbia, G., Ricci, E., Di Ruzza, B., Iuppa, R., Nozzoli, F., and Zuccon, P. (2020). *Development of a particle tracker for space applications*. Il nuovo cimento C **43**(2-3), pp. 1–3.
- Panico, B., Osteria, G., Perfetto, F., Scotti, V., Cipollone, P., De Donato, C., De Santis, C., Marcelli, L., Masciantonio, G., Mergè, M., et al. (2020b). “The HEPD apparatus for the CSES mission”. *Journal of Physics: Conference Series*. Vol. 1342. 1. IOP Publishing. Art. no.: 012125.
- Piersanti, M., Materassi, M., Battiston, R., Carbone, V., Cicone, A., D’Angelo, G., Diego, P., and Ubertini, P. (2020). *Magnetospheric-Ionospheric-Lithospheric Coupling Model. 1: Observations during the 5 August 2018 Bayan Earthquake*. Remote Sensing **12**(20). Art. no.: 3299.

Sotgiu, A., De Donato, C., Fornaro, C., Tassa, S., Scannavini, M., Iannaccio, D., Ambrosi, G., Bartocci, S., Basara, L., Battiston, R., et al. (2020b). *Control and data acquisition software of the high-energy particle detector on board the China Seismo-Electromagnetic Satellite space mission*. Software: Practice and Experience.

LISA and LISA Pathfinder

Armano, M., Audley, H., Baird, J., Born, M., Bortoluzzi, D., Cardines, N., Castelli, E., Cavalleri, A., Cesarini, A., Cruise, A., et al. (2020a). *Analysis of the accuracy of actuation electronics in the laser interferometer space antenna pathfinder*. Review of Scientific Instruments **91**(4). Art. no.: 045003.

Armano, M., Audley, H., Baird, J., Binetruy, P., Born, M., Bortoluzzi, D., Castelli, E., Cavalleri, A., Cesarini, A., Cruise, A. M., et al. (2020b). *Spacecraft and interplanetary contributions to the magnetic environment on-board LISA Pathfinder*. Monthly Notices of the Royal Astronomical Society **494**(2), pp. 3014–3027.

Muratore, M., Vetrugno, D., and Vitale, S. (2020). *Revisitation of time delay interferometry combinations that suppress laser noise in LISA*. Classical and Quantum Gravity **37**(18). Art. no.: 185019.

QUAX

Alesini, D., Braggio, C., Carugno, G., Crescini, N., D’Agostino, D., Di Gioacchino, D., Di Vora, R., Falferi, P., Gambardella, U., Gatti, C., Iannone, G., Ligi, C., Lombardi, A., Maccarrone, G., Ortolan, A., Pengo, R., Pira, C., Rettaroli, A., Ruoso, G., Taffarello, L., and Tocci, S. (2020[c]). *High quality factor photonic cavity for dark matter axion searches*. REVIEW OF SCIENTIFIC INSTRUMENTS **91**. Art. no.: 094701.

Crescini, N., Alesini, D., Braggio, C., Carugno, G., D’Agostino, D., Di Gioacchino, D., Falferi, P., Gambardella, U., Gatti, C., Iannone, G., Ligi, C., Lombardi, A., Ortolan, A., Pengo, R., Ruoso, G., Taffarello, L., and Collaboration, Q. (2020). *Axion Search with a Quantum-Limited Ferromagnetic Haloscope*. PHYSICAL REVIEW LETTERS **124**. Art. no.: 171801.

VIRGO

Abbott, B. P. et al., LIGO Scientific Collaboration and Virgo Collaboration (2020a). *GW190425: Observation of a Compact Binary Coalescence with Total Mass $\sim 3.4 M_{\odot}$* . The Astrophysical Journal **892**(1). Art. no.: L3.

— LIGO Scientific Collaboration and Virgo Collaboration (2020b). *Model comparison from LIGO-Virgo data on GW170817’s binary components and consequences for the merger remnant*. Classical and Quantum Gravity **37**(4). Art. no.: 045006.

— LIGO Scientific Collaboration and Virgo Collaboration (2020c). *Optically targeted search for gravitational waves emitted by core-collapse supernovae during the first and second observing runs of advanced LIGO and advanced Virgo*. Physical Review D **101**(8). Art. no.: 084002.

Abbott, R. et al., LIGO Scientific Collaboration and Virgo Collaboration (2020a). *Gravitational-wave Constraints on the Equatorial Ellipticity of Millisecond Pulsars*. The Astrophysical Journal Letters **902**(1). Art. no.: L21.

— LIGO Scientific Collaboration and Virgo Collaboration (2020b). *GW190412: Observation of a binary-black-hole coalescence with asymmetric masses*. Physical Review D **102**(4). Art. no.: 043015.

— LIGO Scientific Collaboration and Virgo Collaboration (2020c). *GW190521: A Binary Black Hole Merger with a Total Mass of 150 M_{\odot}* . Physical Review Letters **125**(10). Art. no.: 101102.

— LIGO Scientific Collaboration and Virgo Collaboration (2020d). *GW190814: Gravitational Waves from the Coalescence of a 23 Solar Mass Black Hole with a 2.6 Solar Mass Compact Object*. The Astrophysical Journal Letters **896**(2). Art. no.: L44.

- Abbott, R. et al., LIGO Scientific Collaboration and Virgo Collaboration (2020e). *Properties and Astrophysical Implications of the 150 M Binary Black Hole Merger GW190521*. The Astrophysical Journal Letters **900**(1). Art. no.: L13.
- Acernese, F. et al., Virgo Collaboration (2020a). *Quantum Backaction on Kg-Scale Mirrors: Observation of Radiation Pressure Noise in the Advanced Virgo Detector*. Physical Review Letters **125**(13). Art. no.: 131101.
- Virgo Collaboration (2020b). *The advanced Virgo longitudinal control system for the O2 observing run*. Astroparticle Physics **116**. Art. no.: 102386.
- Drago, M., Klimentko, S., Lazzaro, C., Milotti, E., Mitselmakher, G., Necula, V., O'Brien, B., Prodi, G. A., Salemi, F., Szczepanczyk, M., Tiwari, S., Tiwari, V., V. G., Vedovato, G., and Yakushin, I. (2021). *coherent WaveBurst, a pipeline for unmodeled gravitational-wave data analysis*. SoftwareX **14**. Art. no.: 100678.
- Hamburg, R. et al., LIGO Scientific Collaboration and Virgo Collaboration (2020). *A Joint Fermi-GBM and LIGO/Virgo Analysis of Compact Binary Mergers from the First and Second Gravitational-wave Observing Runs*. The Astrophysical Journal **893**(2). Art. no.: 100.
- Prodi, G. A., Vedovato, G., Drago, M., Klimentko, S., Lazzaro, C., Miani, A., Milotti, E., Salemi, F., Tiwari, S., Szczepanczyk, M., V. G., and O'Brien, B. (2020). *Technical note on the measurement of inspiral higher order modes on GW190814 by coherentWaveBurst*. LIGO DCC. <https://dcc.ligo.org/LIGO-T2000124>.
- Szczepańczyk, M., Klimentko, S., O'Brien, B., Bartos, I., Gayathri, V., Mitselmakher, G., Prodi, G., Vedovato, G., Lazzaro, C., Milotti, E., Salemi, F., Drago, M., and Tiwari, S. (2021). *Observing an intermediate-mass black hole GW190521 with minimal assumptions*. Phys. Rev. D **103** (8). Art. no.: 082002.

Nuclear Physics

- Di Ruzza, B. (2021b). *Proton and x-ray irradiation of silicon devices at the TIFPA-INFN facilities in Trento*. PoS ICHEP2020, p. 685.

AEGIS

- Amsler, C. et al., AEGIS collaboration (2021). *Pulsed production of antihydrogen*. Comm. Phys. **4**, p. 19.
- Amsler, C., Antonello, M., Belov, A., Bonomi, G., Brusa, R., Caccia, M., Camper, A., Caravita, R., Castelli, F., Comparat, D., Consolati, G., Demetrio, A., Di Noto, L., Doser, M., Ekman, P., Fani, M., Ferragut, R., Gerber, S., Giammarchi, M., Gligorova, A., Guatieri, F., Hackstock, P., Haider, D., Haider, S., Hinterberger, A., Kellerbauer, A., Khalidova, O., Krasnický, D., Lagomarsino, V., Malbrunot, C., Mariazzi, S., Matveev, V., Müller, S., Nebbia, G., Nedelec, P., Nowak, L., Oberthaler, M., Oswald, E., Pagano, D., Penasa, L., Petracek, V., Prelz, F., Prevedelli, M., Rienaecker, B., Robert, J., Röhne, O., Rotondi, A., Sandaker, H., Santoro, R., Storey, J., Testera, G., Tietje, I., Toso, V., Wolz, T., Wuethrich, J., Yzombard, P., Zimmer, C., and Zurlo, N. (2020). *A cryogenic tracking detector for antihydrogen detection in the AEGIS experiment*. Nuclear Instruments and Methods in Physics Research Section A: Accelerators, Spectrometers, Detectors and Associated Equipment **960**. Art. no.: 163637.
- Antonello, M. et al., AEGIS collaboration (2020). *Rydberg-positronium velocity and self-ionization studies in a 1T magnetic field and cryogenic environment*. Phys. Rev. A **102**. Art. no.: 013101.

- Caravita, R., Antonello, M., Belov, A., Bonomi, G., Brusa, R., Caccia, M., Camper, A., Castelli, F., Comparat, D., Consolati, G., Demetrio, A., Di Noto, L., Doser, M., Fanì, M., Ferragut, Gerber, S., Giammarchi, M., Gligorova, A., Glöggler, L., Guatieri, F., Haider, S., Hinterberger, A., Kellerbauer, A., Khalidova, O., Krasnický, D., Lagomarsino, V., Malbrunot, C., Mariazzi, S., Matveev, V., Müller, S., Nebbia, G., Nedelec, P., Oberthaler, M., Oswald, E., Pagano, D., Penasa, L., Petracek, V., Prelz, F., Prevedelli, M., Rienaecker, B., Røhne, O., Rotondi, A., Sandaker, H., Santoro, R., Testera, G., Tietje, I., Toso, V., Wolz, T., Zimmer, C., and Zurlo, N. (2020). “Hybrid Imaging and Timing Ps Laser Excitation Diagnostics for Pulsed Antihydrogen Production”. Vol. 137. Art. no.: 96.
- Fanì, M., Antonello, M., Belov, A., Bonomi, G., Brusa, R., Caccia, M., Camper, A., Caravita, R., Castelli, F., G., Comparat, D., Cheinet, P., Consolati, G., Demetrio, A., Di Noto, L., Doser, M., Ferragut, R., Fesel, J., Gerber, S., Giammarchi, M., Gligorova, A., Glöggler, L., Guatieri, F., Haider, S., Hinterberger, A., Kellerbauer, A., Khalidova, O., Krasnický, D., Lagomarsino, V., Malbrunot, C., Nowak, L., Mariazzi, S., Matveev, V., Müller, S., Nebbia, G., Nedelec, P., Oberthaler, M., Pagano, D., Penasa, L., Petracek, V., Povolo, L., Prelz, F., Prevedelli, M., Rienaecker, B., Robert, J., Røhne, O., Rotondi, A., Sandaker, H., Santoro, R., Testera, G., Tietje, I., Toso, V., Wolz, T., Zimmer, C., and Zurlo, N. (2020). “Developments for pulsed antihydrogen production towards direct gravitational measurement on antimatter”. Vol. 95. 1. Art. no.: 114001.
- Guatieri, F., Mariazzi, S., and Brusa, R. (2020). “Simulating Positron to Positronium Conversion in Nanostructured Materials”. Vol. 137.
- Mariazzi, S., Caravita, R., Doser, M., Nebbia, G., and Brusa, R. (2020a). *Toward inertial sensing with a 2^3S positronium*. European Physics Journal D **74**. Art. no.: 79.
- Mariazzi, S., Vespertini, A., Caravita, R., Antonello, M., Belov, A., Bonomi, G., Brusa, R., Caccia, M., Camper, A., Castelli, F., Comparat, D., Consolati, G., Demetrio, A., Di Noto, L., Doser, M., Fanì, M., Ferragut, Gerber, S., Giammarchi, M., Gligorova, A., Glöggler, L. T. and Guatieri, F., Haider, S., Hinterberger, A., Kellerbauer, A., Khalidova, O., Krasnický, D., Lagomarsino, V., Malbrunot, C., Matveev, V., Müller, S., Nebbia, G., Nedelec, P., Oberthaler, M., Oswald, E., Pagano, D., Penasa, L., Petracek, V., Prelz, F., Prevedelli, M., Rienaecker, B., Røhne, O., Rotondi, A., Sandaker, H., Santoro, R., Testera, G., Tietje, I., Toso, V., Wolz, T., Zimmer, C., and Zurlo, N. (2020b). “Techniques for Production and Detection of $2(3)\text{S}$ Positronium”. Vol. 137. Art. no.: 91.
- Tietje, I. C., Amsler, C., Antonello, M., Belov, A., Bonomi, G., Brusa, R. S., Caccia, M., Camper, A., Caravita, R., Castelli, F., Cheinet, P., Comparat, D., Consolati, G., Demetrio, A., Noto, L. D., Doser, M., Fanì, M., Ferragut, R., Fesel, J., Gerber, S., Giammarchi, M., Gligorova, A., Glöggler, L. T., Guatieri, F., Haider, S., Hinterberger, A., Kellerbauer, A., Khalidova, O., Krasnický, D., Lagomarsino, V., Malbrunot, C., Nowak, L., Mariazzi, S., Matveev, V., Müller, S. R., Nebbia, G., Nedelec, P., Oberthaler, M., Oswald, E., Pagano, D., Penasa, L., Petracek, V., Povolo, L., Prelz, F., Prevedelli, M., Rienaecker, B., Røhne, O. M., Rotondi, A., Sandaker, H., Santoro, R., Testera, G., Toso, V., Wolz, T., Yzombard, P., Zimmer, C., and Zurlo, N. (2020). Vol. 1612. 012025.
- Zurlo, N., Amsler, C., Antonello, M., Belov, A., Bonomi, G., Brusa, R., Caccia, M., Camper, A., Caravita, R., Castelli, F., Cerchiari, G., Comparat, D., Consolati, G., Demetrio, A., Di Noto, L., Doser, M., Fanì, M., Ferragut, Gerber, S., Giammarchi, M., Gligorova, A., Guatieri, F., Haider, S., Hinterberger, A., Kellerbauer, A., Khalidova, O., Krasnický, D., Lagomarsino, V., Malbrunot, C., Mariazzi, S., Matveev, V., Müller, S., Nebbia, G., Nedelec, P., Oberthaler, M., Oswald, E., Pagano, D., Penasa, L., Petracek, V., Prelz, F., Prevedelli, M., Rienaecker, B., Røhne, O., Rotondi, A., Sandaker, H., Santoro, R., Testera, G., Tietje, I., Toso, V., Wolz, T., and Yzombard, P. (2020). *Calibration and Equalisation of Plastic Scintillator Detectors for Antiproton Annihilation Identification over Positron/Positronium Background*. Acta Physica Polonica B **51**. Art. no.: 213.

FOOT

- Battistoni, G. et al. (2021). *Measuring the Impact of Nuclear Interaction in Particle Therapy and in Radio Protection in Space: the FOOT Experiment*. *Frontiers in Physics* **8**, p. 555.
- Mattei, I., Alexandrov, A., Alunni Solestizi, L., Ambrosi, G., Argirò, S., Bartosik, N., Battistoni, G., Belcari, N., Biondi, S., Bisogni, M. G., Bruni, G., Camarlinghi, N., Carra, P., Catanzani, E., Ciarracchi, E., Cerello, P., Clozza, A., Colombi, S., De Lellis, G., Del Guerra, A., De Simoni, M., Di Crescenzo, A., Donetti, M., Dong, Y., Durante, M., Embriaco, A., Emde, M., Faccini, R., Ferrero, V., Ferroni, F., Fiandrini, E., Finck, C., Fiorina, E., Fischetti, M., Francesconi, M., Franchini, M., Galli, L., Gentile, V., Hetzel, R., Hild, S., Iarocci, E., Ionica, M., Kanxheri, K., Kraan, A. C., Lante, V., Lauria, A., La Tessa, C., Lopez Torres, E., Massimi, C., Marafini, M., Mengarelli, A., Mirabelli, R., Montesi, M. C., Morone, M. C., Morrocchi, M., Muraro, S., Narici, L., Pastore, A., Pastrone, N., Patera, V., Pennazio, F., Placidi, P., Pullia, M., Ramello, L., Ridolfi, R., Rosso, V., Rovituso, M., Sanelli, C., Sartorelli, G., Sato, O., Savazzi, S., Scavarda, L., Schiavi, A., Schuy, C., Scifoni, E., Sciubba, A., Sécher, A., Selvi, M., Servoli, L., Silvestre, G., Sitta, M., Spighi, R., Spiriti, E., Sportelli, G., Stahl, A., Tomassini, S., Tommasino, F., Traini, G., Toppi, M., Valeri, T., Valle, S. M., Vanstalle, M., Villa, M., Weber, U., Zoccoli, A., and Sarti, A. (2020). *Measurement of ^{12}C Fragmentation Cross Sections on C, O, and H in the Energy Range of Interest for Particle Therapy Applications*. *IEEE Transactions on Radiation and Plasma Medical Sciences* **4**(2), pp. 269–282.
- Traini, G. et al. (2020). *Performance of the ToF detectors in the FOOT experiment*. *Nuovo Cimento della Società Italiana di Fisica C* **43**. Art. no.: A16.

Theoretical Physics

BELL

- Drago, N., Mazzucchi, S., and Moretti, V. (2020). *An operational construction of the sum of two non-commuting observables in quantum theory and related constructions*. *Lett. Math. Phys* **110**.
- Moretti, V. and van de Ven, C. (2020). *Bulk-boundary asymptotic equivalence of two strict deformation quantizations*. *Lett. Math. Phys* **110**, p. 303.
- Pasini, S., Leone, N., Mazzucchi, S., Moretti, V., Pastorello, D., and Pavesi, L. (2020). *Bell inequality violation by entangled single photon states generated from a laser, a LED or a Halogen lamp*. *Phys. Rev. A* **102**.
- Pastorello, D. (2020). *Geometric viewpoint on the quantization of a fuzzy logic*. *Int J Geom Meth Modern Phys* **17**(13).

BIOPHYS

- Baptista, L. A., Dutta, R. C., Sevilla, M., Heidari, M., Potestio, R., Kremer, K., and Cortes-Huerta, R. (2021). *Density-Functional-Theory Approach to the Hamiltonian Adaptive Resolution Simulation Method*. *Journal of Physics: Condensed Matter*.
- Bondanza, M., Cupellini, L., Faccioli, P., and Mennucci, B. (2021). *The Molecular Mechanisms of Photoactivation of Orange Carotenoid Protein Revealed by Molecular Dynamics*. *J. Am. Chem. Soc.* **142**. Art. no.: 21829.
- Errica, F., Giulini, M., Bacciu, D., Menichetti, R., Micheli, A., and Potestio, R. (2021). *A deep graph network-enhanced sampling approach to efficiently explore the space of reduced representations of proteins*. *Front. Mol. Biosci.*
- Fiorentini, R., Kremer, K., and Potestio, R. (2020). *Ligand-protein interactions in lysozyme investigated through a dual-resolution model*. *Proteins: Structure, Function, and Bioinformatics*.

- Gershenson, A., Gosavi, S., Faccioli, P., and Wintrode, P. (2020). *Successes and Challenges in Simulating the Folding of Large Proteins*. *J. Biol. Chem* **295**, p. 15.
- Giulini, M. et al. (2020). *An Information-Theory-Based Approach for Optimal Model Reduction of Biomolecules*. *Journal of Chemical Theory and Computation* **16**(11), pp. 6795–6813.
- Hauke, P., Mattiotti, G., and Faccioli, P. (2021). *Dominant Reaction Pathways by Quantum Computing*. *Physical Review Letters* **126**. Art. no.: 028104.
- Petrolli, L., Tommasino, F., Scifoni, E., and Lattanzi, G. (2020b). *Can we assess early DNA damage at the molecular scale by radiation track structure simulations? A tetranucleosome scenario in Geant4-DNA*. *Frontiers in Physics* **8**. Art. no.: 576284.
- Potestio, R., Heidari, M., Kremer, K., Golestanian, R., Potestio, R., and Cortes-Huerto, R. (2020). *Open-boundary Hamiltonian adaptive resolution. From grand canonical to non-equilibrium molecular dynamics simulations*. *The Journal of Chemical Physics*.
- Spagnolli, G. et al. (2021a). *Pharmacological Inactivation of the Prion Protein by Targeting a Folding Intermediate*. *Comms. Biol. Nature* **4**, p. 62.
- Spagnolli, G., Massignan, T., Astolfi, A., Biggi, S., Brunelli, P., Libergoli, M., Ianeselli, A., Orioli, S., Boldrini, A., Terruzzi, L., Maietta, G., Rigoli, M., Lorenzo, N. L., Fernandez, L. C., Tosatto, L., Linsenmeier, L., Vignoli, B., Petris, G., Gasparotto, D., Pennuto, M., Guella, G., Canossa, M., Altmeppen, H. C., Lolli, G., Biressi, S., Pastor, M. M., Requena, J. R., Mancini, I., Barreca, M. L., Faccioli, P., and Biasini, E. (2021b). *Pharmacological inactivation of the prion protein by targeting a folding intermediate*. *Communication Biology* **4** (1), p. 62.
- Terruzzi, L., Spagnolli, G., Boldrini, A., Requena, J., Biasini, E., and Faccioli, P. (2020). *All-Atom Simulation of HET-s Prion Replication*. *PLoS Comput. Biol* **16** (9). Art. no.: e1007922.
- Turelli, M., Alberga, D., Lattanzi, G., Ciofini, I., and Adamo, C. (2020). *Theoretical insights on acceptor-donor dyads for organic photovoltaics*. *Physical Chemistry Chemical Physics* **22**, pp. 27413–27424.
- Zanovello, L., Caraglio, M., Franosh, T., and Faccioli, P. (2021). *Target Search of Active Agents Crossing High Energy Barriers*. *Physical Review Letters* **126**. Art. no.: 018001.

FBS

- Andreatta, P., Manzata, C., Ji, C., Leidemann, W., and Orlandini, G. (2020). *Beryllium-9 in Cluster Effective Field Theory*. *Springer Proc. Phys.* **238**, pp. 191–194.
- Filandri, E., Andreatta, P., Manzata, C., Ji, C., Leidemann, W., and Orlandini (2020). *Beryllium-9 in Cluster Effective Field Theory*. *SciPost Phys. Proc.* **3**, pp. 34.1–34.9.
- Orlandini, G., Rocco, N., Lovato, A., and Leidemann, W. (2020a). *Relativistic Effects in Non-relativistic Calculations of Electroweak Cross Sections*. *Springer Proc. Phys.* **238**, pp. 663–667.

FLAG

- Casalino, A., Colleaux, A., Rinaldi, M., and Vicentini, S. (2021). *Regularized Lovelock gravity*. *Phys. Dark Univ.* **31**. Art. no.: 100770.
- Casalino, A. and Sebastiani, L. (2021). *Perturbations in Regularized Lovelock Gravity*. *Phys. Dark Univ.* **31**. Art. no.: 100771.
- Casalino, A., Sebastiani, L., Vanzo, L., and Zerbini, S. (2020a). *Higher derivative and mimetic models on non flat FLRW space-times*. *Phys. Dark Univ.* **29**. Art. no.: 100594.
- Casalino, A., Sebastiani, L., and Zerbini, S. (2020b). *Note on nonsingular Einstein-Aether cosmologies*. *Phys. Rev. D* **101**(10). Art. no.: 104059.
- Dioguardi, C. and Rinaldi, M. (2020). *A note on the linear stability of black holes in quadratic gravity*. *Eur. Phys. J. Plus* **135**(11), p. 920.

MANYBODY

- Endrizzi, A., Perego, A., Fabbri, F. M., Branca, L., Radice, D., Bernuzzi, S., Giacomazzo, B., Pederiva, F., and Lovato, A. (2020a). *Thermodynamics conditions of matter in the neutrino decoupling region during neutron star mergers*. THE EUROPEAN PHYSICAL JOURNAL. A, HADRONS AND NUCLEI **56**, p. 15.
- Gandolfi, S., Lonardoni, D., Lovato, A., and Piarulli, M. (2020). *Atomic nuclei from quantum Monte Carlo calculations with chiral EFT interactions*. Front. in Phys. **8**, p. 117.
- Holland, E. T., Wendt, K. A., Kravvaris, K., Wu, X., Ormand, W. E., Dubois, J. L., Quaglioni, S., Pederiva, F., and Pederiva, F. (2020). *Optimal control for the quantum simulation of nuclear dynamics*. PHYSICAL REVIEW A **101**. Art. no.: 062307.
- Isaacson, J., Jay, W. I., Lovato, A., Machado, P. A. N., and Rocco, N. (2021). *New approach to intranuclear cascades with quantum Monte Carlo configurations*. Phys. Rev. C **103**(1). Art. no.: 015502.
- De-Leon, H. and Pederiva, F. (2020). *Particle modeling of the spreading of coronavirus disease (COVID-19)*. PHYSICS OF FLUIDS **32**. Art. no.: 087113.
- Lovato, A., Carlson, J., Gandolfi, S., Rocco, N., and Schiavilla, R. (2020). *Ab initio study of (ν_ℓ, ℓ^-) and $(\bar{\nu}_\ell, \ell^+)$ inclusive scattering in ^{12}C : confronting the MiniBooNE and T2K CCQE data*. Phys. Rev. X **10**(3). Art. no.: 031068.
- Massella, P., Barranco, F., Lonardoni, D., Lovato, A., Pederiva, F., and Vigezzi, E. (2020). *Exact restoration of Galilei invariance in density functional calculations with quantum Monte Carlo*. JOURNAL OF PHYSICS. G, NUCLEAR AND PARTICLE PHYSICS **47**. Art. no.: 035105.
- Orlandini, G., Rocco, N., Lovato, A., and Leidemann, W. (2020b). *Relativistic Effects in Non-relativistic Calculations of Electroweak Cross Sections*. Springer Proc. Phys. **238**, pp. 663–667.
- Raghavan, K., Balaprakash, P., Lovato, A., Rocco, N., and Wild, S. M. (2021). *Machine learning-based inversion of nuclear responses*. Phys. Rev. C **103**(3). Art. no.: 035502.
- Riz, L., Gandolfi, S., and Pederiva, F. (2020a). *Spin response and neutrino mean free path in neutron matter*. JOURNAL OF PHYSICS. G, NUCLEAR AND PARTICLE PHYSICS **47**. Art. no.: 045106.
- Riz, L., Pederiva, F., Lonardoni, D., and Gandolfi, S. (2020b). *Spin Susceptibility in Neutron Matter from Quantum Monte Carlo Calculations*. PARTICLES **3**, pp. 706–718.

NEMESYS

- Azzolini, M., Ridzel, O. Y., Kaplya, P. S., Afanas'ev, V., Pugno, N. M., Taioli, S., and Dapor, M. (2020). *A comparison between Monte Carlo method and the numerical solution of the Ambartsumian-Chandrasekhar equations to unravel the dielectric response of metals*. Computational Materials Science **173**. Art. no.: 109420.
- Dapor, M. (2020). *Transport of Energetic Electrons in Solids. Computer Simulation with Applications to Materials Analysis and Characterization, 3rd ed.* Springer Springer Nature Switzerland AG.
- Garberoglio, G. and Harvey, A. H. (2020). *Path-Integral Calculation of the Second Dielectric and Refractivity Virial Coefficients of Helium, Neon, and Argon*. Journal of Research of National Institute of Standards and Technology **125**. Art. no.: 125022.
- Morresi, T., Binosi, D., Simonucci, S., Piergallini, R., Roche, S., Pugno, N. M., and Taioli, S. (2020). *Exploring Event Horizons and Hawking Radiation through Deformed Graphene Membranes*. 2D Materials **7**. Art. no.: 041006.
- Taioli, S., Trevisanutto, P. E., Vera, P. de, Simonucci, S., Abril, I., Garcia-Molina, R., and Dapor, M. (2020). *Relative Role of Physical Mechanisms on Complex Biodamage Induced by Carbon Irradiation*. The Journal of Physical Chemistry Letters **12**, pp. 487–493.

TEONGRAV

- Bernuzzi, S., Breschi, M., Daszuta, B., Endrizzi, A., Logoteta, D., Nedora, V., Perego, A., Radice, D., Schianchi, F., Zappa, F., Bombaci, I., and Ortiz, N. (2020). *Accretion-induced prompt black hole formation in asymmetric neutron star mergers, dynamical ejecta, and kilonova signals*. Monthly Notices of the Royal Astronomical Society **497**(2), pp. 1488–1507.
- Cipolletta, F., Kalinani, J. V., Giacomazzo, B., and Ciolfi, R. (2020a). *Spritz: a new fully general-relativistic magnetohydrodynamic code*. Classical and Quantum Gravity **37**(13). Art. no.: 135010.
- Cipolletta, F., Vijay Kalinani, J., Giangrandi, E., Giacomazzo, B., Ciolfi, R., Sala, L., and Giudici, B. (2020b). *Spritz: General Relativistic Magnetohydrodynamics with Neutrinos*. arXiv e-prints, arXiv:2012.10174.
- Endrizzi, A., Perego, A., Fabbri, F. M., Branca, L., Radice, D., Bernuzzi, S., Giacomazzo, B., Pederiva, F., and Lovato, A. (2020b). *Thermodynamics conditions of matter in the neutrino decoupling region during neutron star mergers*. European Physical Journal A **56**(1), p. 15.
- Mewes, V., Zlochower, Y., Campanelli, M., Baumgarte, T. W., Etienne, Z. B., Armengol, F. G. L., and Cipolletta, F. (2020). *Numerical relativity in spherical coordinates: A new dynamical spacetime and general relativistic MHD evolution framework for the Einstein Toolkit*. Physical Review D **101**(10). Art. no.: 104007.
- Radice, D., Bernuzzi, S., and Perego, A. (2020). *The Dynamics of Binary Neutron Star Mergers and GW170817*. Annual Review of Nuclear and Particle Science **70**, pp. 95–119.
- Rossi, A., Stratta, G., Maiorano, E., Spighi, D., Masetti, N., Palazzi, E., Gardini, A., Melandri, A., Nicastro, L., Pian, E., Branchesi, M., Dadina, M., Testa, V., Brocato, E., Benetti, S., Ciolfi, R., Covino, S., D’Elia, V., Grado, A., Izzo, L., Perego, A., Piranomonte, S., Salvaterra, R., Selsing, J., Tomasella, L., Yang, S., Vergani, D., Amati, L., and Stephen, J. B. (2020). *A comparison between short GRB afterglows and kilonova AT2017gfo: shedding light on kilonovae properties*. Monthly Notices of the Royal Astronomical Society **493**(3), pp. 3379–3397.

Technological and Interdisciplinary Physics

- Arcidiacono, R., Borghi, G., Boscardin, M., Cartiglia, N., Costa, M., Dalla Betta, G. F., Fausti, F., Ferrero, M., Ficorella, F., Mandurrino, M., Mazza, S., Olave, J., Pancheri, L., Paternoster, G., Sadrozinski, H. F. W., Sola, V., Staiano, A., Seiden, A., Siviero, F., Tornago, M., and Zhao, Y. (2020). *State-of-the-art and evolution of UFSO sensors design at FBK*. Nuclear Instrum. Methods A **978**. Art. no.: 164375.
- Ferrero, M., Arcidiacono, R., Borghi, G., Boscardin, M., Cartiglia, N., Costa, M., Dalla Betta, G. F., Ficorella, F., Mandurrino, M., Obertino, M., Pancheri, L., Paternoster, G., Siviero, F., Sola, V., Staiano, A., Vignati, A., and Centis Vignali, M. (2020). *Evolution of the design of ultra fast silicon detector to cope with high irradiation fluences and fine segmentation*. Journal Instrum. **15**. Art. no.: C04027.
- Mandurrino, M., Arcidiacono, R., Boscardin, M., Cartiglia, N., Dalla Betta, G. F., Ferrero, M., Ficorella, F., Pancheri, L., Paternoster, G., Siviero, F., Sola, V., Staiano, A., and Vignati, A. (2020a). *Analysis and numerical design of Resistive AC-Coupled Silicon Detectors (RSD) for 4D particle tracking*. Nuclear Instrum. Methods A **959**. Art. no.: 163479.
- Mandurrino, M., Arcidiacono, R., Boscardin, M., Cartiglia, N., Dalla Betta, G.-F., Ferrero, M., Ficorella, F., Pancheri, L., Paternoster, G., Siviero, F., and Tornago, M. (2020b). “First Production of 50- μ m-thick Resistive AC-Coupled Silicon Detectors (RSD) at FBK”. *2019 IEEE NSS-MIC Conference Record*. Piscataway, NJ, USA: IEEE.
- Mazza, S., Estrada, E., Galloway, Z., Gee, C., Goto, A., Luce, Z., McKinney Martinez, F., Rodriguez, R., Sadrozinski, H.-W., Seiden, A., Zhao, Y., Cindro, V., Kramberger, G., Mandic, I., Mikuz, M., Za-

- vrtanik, M., Arcidiacono, R., Cartiglia, N., Ferrero, M., Mandurrino, M., Sola, V. S., A., Boscardin, M., Dalla Betta, G.-F., Ficorella, F., Pancheri, L., and Patetnoster, G. (2020). *Properties of FBK UFSDs after neutron and proton irradiation up to 6×10^{15} neq/cm²*. *Journal Instrum.* **15**. Art. no.: T04008.
- Boscolo, D., Scognamiglio, D., Horst, F., Weber, U., Schuy, C., Durante, M., La Tessa, C., Kozlova, E., Sokolov, A., Dinescu, I., Radon, T., Radeck, D., and Zbořil, M. (2020b). *Characterization of the Secondary Neutron Field Produced in a Thick Aluminum Shield by 1 GeV/u ⁵⁶Fe Ions Using TLD-Based Ambient Dosimeters*. *Frontiers in Physics* **8**, p. 365.
- Cartechini, G., Fracchiolla, F., Menegotti, L., Scifoni, E., La Tessa, C., Schwarz, M., Farace, P., and Tommasino, F. (2020a). *Proton pencil beam scanning reduces secondary cancer risk in breast cancer patients with internal mammary chain involvement compared to photon radiotherapy*. *Radiation Oncology* **15**, p. 228.
- Norbury, J. W., Battistoni, G., Besuglow, J., Bocchini, L., Boscolo, D., Botvina, A., Cloudsley, M., de Wet, W., Durante, M., Giraud, M., Haberer, T., Heilbronn, L., Horst, F., Krämer, M., La Tessa, C., Luoni, F., Mairani, A., Muraro, S., Norman, R. B., Patera, V., Santin, G., Schuy, C., Sihver, L., Slaba, T. C., Sobolevsky, N., Topi, A., Weber, U., Werneth, C. M., and Zeitlin, C. (2020). *Are Further Cross Section Measurements Necessary for Space Radiation Protection or Ion Therapy Applications? Helium Projectiles*. *Frontiers in Physics* **8**, p. 409.
- Patel, R., Zhang, L., Desai, A., Hoenerhoff, M. J., Kennedy, L. H., Radivoyevitch, T., La Tessa, C., Gerson, S. L., and Welford, S. M. (2020). *Protons and high-linear energy transfer radiation induce genetically similar lymphomas with high penetrance in a mouse model of the aging human hematopoietic system*. *IJROBP* **108**, p. 1091.
- Civinini, C., Scaringella, M., Brianzi, M., Intravaia, M., Randazzo, N., Sipala, V., Rovituso, M., Tommasino, F., Schwarz, M., and Bruzzi, M. (2020). *Relative stopping power measurements and prosthesis artifacts reduction in proton CT*. *Physics in Medicine and Biology* **65**. Art. no.: 225012.
- Gerlach, S., Pinto, M., Kurichiyanil, N., Grau, C., Héroult, J., Hillbrand, M., Poulsen, P., Safai, S., Schiippers, J., Schwarz, M., Sondergaard, C., Tommasino, F., Verroi, E., Vidal, M., Yohannes, I., Schreiber, J., and Parodi, K. (2020a). *Beam characterization and feasibility study for a small animal irradiation platform at clinical proton therapy facilities*. *Physics in Medicine and Biology* **65**. Art. no.: 245045.
- Missiaggia, M., Cartechini, G., Scifoni, E., Rovituso, M., Tommasino, F., Verroi, E., Durante, M., and La Tessa, C. (2020). *Microdosimetric measurements as a tool to assess potential in-field and out-of-field toxicity regions in proton therapy*. *Physics in Medicine and Biology* **65**. Art. no.: 245024.
- Petrolli, L., Tommasino, F., Scifoni, E., and Lattanzi, G. (2020a). *Can We Assess Early DNA Damage at the Molecular Scale by Radiation Track Structure Simulations? A Tetranucleosome Scenario in Geant4-DNA*. *Frontiers in Physics* **8**. Art. no.: 576284.
- Righetto, R., Clemens, L., Lorentini, S., Fracchiolla, F., Algranati, C., Tommasino, F., Dionisi, F., Cianchetti, M., Schwarz, M., and Farace, P. (2020). *Accurate proton treatment planning for pencil beam crossing titanium fixation implants*. *Physica Medica* **70**, pp. 28–38.
- Rucinski, A. et al. (2020). *Investigations on physical and biological range uncertainties in Krakow proton beam therapy centre*. *Acta Physica Polonica B* **51**, pp. 9–16.
- Widesott, L., Dionisi, F., Fracchiolla, F., Tommasino, F., Centonze, M., Amichetti, M., and Greco, D. (2020). *Proton or photon radiosurgery for cardiac ablation of ventricular tachycardia? Breath and ECG gated robust optimization*. *Physica Medica* **78**, pp. 15–31.

3DSIAM

- Davis, J. A. et al. (2020). *Modeling a Thick Hydrogenated Amorphous Silicon Substrate for Ionizing Radiation Detectors*. *Frontiers in Physics* **8**, p. 158.

- Menichelli, M. et al. (2020a). *3D Detectors on Hydrogenated Amorphous Silicon for particle tracking in high radiation environment*. J. Phys. Conf. Ser. **1561**. Art. no.: 012016.
- (2020b). *Hydrogenated amorphous silicon detectors for particle detection, beam flux monitoring and dosimetry in high-dose radiation environment*. Journal of Instrumentation **15**. Art. no.: C04005.

ARCADIA

- Pancheri, L., Giampaolo, R., Di Salvo, A., Mattiazzo, S., Corradino, T., Giubilato, P., Santoro, R., Caccia, M., Margutti, G., Olave, J., Rolo, M., and Rivetti, A. (2020). *Fully depleted MAPS in 110-nm CMOS process with 100-300- μ m active substrate*. IEEE Transactions on Electron Devices **67**(6), pp. 2392–2399.

ASAP

- Brogi, P., Bigongiari, G., Checchia, C., Collazuol, G., Dalla Betta, G.-F., Ficorella, A., Marrocchesi, P., Morsani, F., Musacci, M., Torilla, G., Pancheri, L., Ratti, L., Savoy-Navarro, A., Silvestrin, L., Stolzi, F., Suh, J., Sulaj, A., Vacchi, C., and Zarghami, M. (2020). *APiX, a two-tier avalanche pixel sensor for digital charged particle detection*. Nuclear Instruments and Methods in Physics Research, Section A **958**. Art. no.: 162546.
- Ratti, L., Brogi, P., Collazuol, G., Dalla Betta, G.-F., Ficorella, A., Marrocchesi, P., Morsani, F., Pancheri, L., Torilla, G., and Vacchi, C. (2020). *DCR performance in neutron-irradiated CMOS SPADs from 150-to 180-nm technologies*. IEEE Transactions on Nuclear Science **67**(7), pp. 1293–1301.

DRAGoN

- Brunelli, D., Pino, F., Fontana, C. L., Pancheri, L., and Moretto, S. (2020). “DRAGoN: Drone for Radiation detection of Gammas and Neutrons”. *2020 IEEE SENSORS*, pp. 1–4.

GLARE-X

- Battocchio, P. et al. (2021). *Ballistic measurements of laser ablation generated impulse*. Meas. Sci. Technol. **32**, 15pp. Art. no.: 015901.
- Bazzanella, N. et al. (2018). “A Systematic Study of Laser Ablation for Space Debris Mitigation”. *Proceedings 21st International Workshop on Laser Ranging*. (Canberra, Australia). <https://cddis.nasa.gov/lw21/Program/index.html>.

ISOLPHARM_EIRA

- Ballan, M., Tosato, M., Verona, M., Caeran, M., Borgna, F., Vettorato, E., Corradetti, S., Zangrando, L., Sgaravatto, M., Verlato, M., Asti, M., Marzaro, G., Mastrotto, F., Di Marco, V., Maniglio, D., Bisio, A., Motta, A., Quaranta, A., Zenoni, A., Pastore, P., Realdon, N., and Andrighetto, A. (2020). *Preliminary evaluation of the production of non-carrier added ¹¹¹Ag as core of a therapeutic radiopharmaceutical in the framework of ISOLPHARM_Ag experiment*. Applied Radiation and Isotopes **164**. Art. no.: 109258.

MoVe IT

- Cartechini, G., Fracchiolla, F., Menegotti, L., Scifoni, E., La Tessa, C., Schwarz, M., Farace, P., and Tommasino, F. (2020b). *Proton pencil beam scanning reduces secondary cancer risk in breast cancer patients with internal mammary chain involvement compared to photon radiotherapy*. Radiation Oncology **15**(1), pp. 1–10.

- Catalano, R., Petringa, G., Cuttone, G., Bonanno, V., Chiappara, D., Musumeci, M., Pugli, S., Stella, G., Scifoni, E., Tommasino, F., and Cirrone, G. (2020). *Transversal dose profile reconstruction for clinical proton beams: A detectors inter-comparison*. *Physica Medica* **70**, pp. 133–8.
- Embriaco, A., Attili, A., Bellinzona, E., Dong, Y., Grzanka, L., Mattei, I., Muraro, S., Scifoni, E., Tommasino, F., Valle, S., et al. (2020). *FLUKA simulation of target fragmentation in proton therapy*. *Physica Medica* **80**, pp. 342–346.
- Palma, G., Taffelli, A., Fellin, F., D'Avino, V., Scartoni, D., Tommasino, F., Scifoni, E., Durante, M., Amichetti, M., Schwarz, M., Amelio, D., and Cella, L. (2020). *Modelling the risk of radiation induced alopecia in brain tumor patients treated with scanned proton beams*. *Radiotherapy and Oncology* **144**, pp. 127–34.
- Pisciotta, P., Costantino, A., Cammarata, F. P., Torrisi, F., Calabrese, G., Marchese, V., Cirrone, G. A. P., Petringa, G., Forte, G. I., Minafra, L., Bravatà, V., Gulisano, M., Scopelliti, F., Tommasino, F., Scifoni, E., Cuttone, G., Ippolito, M., Parenti, R., and Russo, G. (2020). *Evaluation of proton beam radiation-induced skin injury in a murine model using a clinical SOBP*. *Plos one* **15**(5). Art. no.: e0233258.
- Tommasino, F., Widesott, L., Fracchiolla, F., Lorentini, S., Righetto, R., Algranati, C., Scifoni, E., Dionisi, F., Scartoni, D., Amelio, D., Cianchetti, M., Schwarz, M., Amichetti, M., and Farace, P. (2020). *Clinical implementation in proton therapy of multi-field optimization by a hybrid method combining conventional PTV with robust optimization*. *Physics in Medicine and Biology* **65**. Art. no.: 045002.

NEPTUNE

- Bellinzona, V. E., Cordini, F., Missiaggia, M., Tommasino, F., Scifoni, E., La Tessa, C., and Attili, A. (2021). *Linking microdosimetric measurements to biological effectiveness in ion beam therapy: a review of theoretical aspects of MKM and other models*. *Frontiers in Physics* **8**, p. 623.

Redsox2

- Bartocci, S. et al. (2020a). *Galactic Cosmic-Ray Hydrogen Spectra in the 40–250 MeV Range Measured by the High-energy Particle Detector (HEPD) on board the CSES-01 Satellite between 2018 and 2020*. *Astrophys. J.* **901**(1), p. 8.
- Casarosa, G. et al., Belle-IISVD (2020). *Commissioning of the Belle II Silicon Vertex Detector*. *Nucl. Instrum. Meth. A* **958**. Ed. by M. Krammer, T. Bergauer, M. Dragicevic, M. Friedl, M. Jeitler, J. Schieck, and C. Schwanda. Art. no.: 162184.
- Dilillo, G. et al. (2020). *A summary on an investigation of GAGG:Ce afterglow emission in the context of future space applications within the HERMES nanosatellite mission*.
- Grassi, M. et al. (2020). “X-/ γ -Ray Detection Instrument for the HERMES Nano-Satellites Based on SDDs Read-Out by the LYRA Mixed-Signal ASIC Chipset”. *IEEE International Instrumentation and Measurement Technology Conference*.
- Irmeler, C. et al., Belle-IISVD (2020). *Run and slow control system of the Belle II silicon vertex detector*. *Nucl. Instrum. Meth. A* **958**. Ed. by M. Krammer, T. Bergauer, M. Dragicevic, M. Friedl, M. Jeitler, J. Schieck, and C. Schwanda. Art. no.: 162706.
- Martucci, M. et al. (2020). *Space-Weather capabilities and preliminary results of the High Energy Particle Detector (HEPD) on-board the CSES-01 satellite*. *PoS ICRC2019*, p. 1118.
- Panico, B. et al. (2020a). *The HEPD apparatus for the CSES mission*. *J. Phys. Conf. Ser.* **1342**(1). Ed. by K. Clark, C. Jillings, C. Kraus, J. Saffin, and S. Scorza. Art. no.: 012125.
- Sammartini, M. et al. (2020). *Pixel Drift Detector (PixDD) – SIRIO: an X-ray spectroscopic system with high energy resolution at room temperature*. *Nucl. Instrum. Meth. A* **953**. Art. no.: 163114.
- Sotgiu, A. et al. (2020a). *Status and performance of the High Energy Particle Detector (HEPD) on-board the CSES-01 satellite*. *PoS ICRC2019*, p. 1155.

Thalmeier, R. et al., Belle-IISVD (2020). *Series production testing and commissioning of the Belle II SVD readout system*. Nucl. Instrum. Meth. A **958**. Ed. by M. Krammer, T. Bergauer, M. Dragicevic, M. Friedl, M. Jeitler, J. Schieck, and C. Schwanda. Art. no.: 162942.

SIMP

Alesini, D., Babusci, D., Barone, C., Buonomo, B., Beretta, M. M., Bianchini, L., Castellano, G., Chiarello, F., Di Gioacchino, D., Falferi, P., Felici, G., Filatrella, G., Foggetta, L. G., Gallo, A., Gatti, C., Giazotto, F., Lamanna, G., Ligabue, F., Ligato, N., Ligi, C., Maccarrone, G., Margesin, B., Mattioli, F., Monticone, E., Oberto, L., Pagano, S., Paolucci, F., Rajteri, M., Rettaroli, A., Rolandi, L., Spagnolo, P., Toncelli, A., and Torrioli, G. (2020[a]). “Development of a Josephson junction based single photon microwave detector for axion detection experiments”. *14TH EUROPEAN CONFERENCE ON APPLIED SUPERCONDUCTIVITY (EUCAS2019)*. Ed. by Romans, E and Ainslie, M and Berger, K and Bykovskiy, N and Kennedy, O and Palau, A and Pegrum, C and Queval, L and Sotelo, GG and DeSousa, WTB and Zhang, M. Vol. 1559. Journal of Physics Conference Series. 14th European Conference on Applied Superconductivity (EUCAS), Glasgow, SCOTLAND, SEP 01-05, 2019. Art. no.: 012020.

— (2020[b]). *Status of the SIMP Project: Toward the Single Microwave Photon Detection*. JOURNAL OF LOW TEMPERATURE PHYSICS **199**(1-2, SI), 348–354.

Paolucci, F., Buccheri, V., Germanese, G., Ligato, N., Paoletti, R., Signorelli, G., Bitossi, M., Spagnolo, P., Falferi, P., Rajteri, M., Gatti, C., and Giazotto, F. (2020). *Development of highly sensitive nanoscale transition edge sensors for gigahertz astronomy and dark matter search*. JOURNAL OF APPLIED PHYSICS **128**(19). Art. no.: 194502.

THEEOM-RD

Malossi, N., Piergentili, P., Li, J., Serra, E., Natali, R., Di Giuseppe, G., and Vitali, D. (2020). *Ground state cooling of a radio-frequency LC circuit in an optoelectromechanical system*. Published in 2021 in Phys. Rev. A (preprint available at arXiv:2009.04421).

— (2021). *Sympathetic cooling of a radio-frequency LC circuit to its ground state in an optoelectromechanical system*. Phys. Rev. A **103**. Art. no.: 033516.

TIMESPOT

Anderlini, L., Aresti, M., Bizzeti, A., Boscardin, M., Cardini, A., Dalla Betta, G.-F., Ferrero, M., Forcolin, G. T., Garau, M., Lai, A., Lampis, A., Loi, A., Lucarelli, C., Mendicino, R., Mulargia, R., Obertino, M., Robutti, E., Ronchin, S., Ruspa, M., and Vecchi, S. (2020). *Intrinsic time resolution of 3D-trench silicon pixels for charged particle detection*. Journal Instrum. **15**. Art. no.: P09029.

Forcolin, G., Boscardin, M., Ficorella, F., Lai, A., Loi, A., Mendicino, R., Ronchin, S., and Dalla Betta, G.-F. (2020). *3D trenched-electrode pixel sensors: Design, technology and initial results*. Nuclear Instrum. Methods A **981**. Art. no.: 164437.

Lai, A., Anderlini, L., Aresti, M., Bizzeti, A., Cardini, A., Dalla Betta, G.-F., Forcolin, G. T., Garau, M., Lampis, A., Loi, A., Lucarelli, C., Mendicino, R., Mulargia, R., Obertino, M., Robutti, E., and S., V. (2020). *First results of the TIMESPOT project on developments on fast sensors for future vertex detectors*. Nuclear Instrum. Methods A **981**. Art. no.: 164491.

Loi, A., Contu, A., Mendicino, R., Forcolin, G., Lai, A., Dalla Betta, G.-F., Boscardin, M., and Vecchi, S. (2020). *Timing optimization for 3D Silicon sensors*. Nuclear Instrum. Methods A **958**. Art. no.: 162491.

Mendicino, R., Kok, A., Koybasi, O., Povoli, M., Summanwar, A., and Dalla Betta, G.-F. (2020). *Characterization of SINTEF 3D diodes with trenched-electrode geometry before and after neutron irradiation*. *Journal Instrum.* **15**. Art. no.: C02023.

Outreach

Di Ruzza, B. (2021a). *Education initiatives in the Trento Proton Therapy Center experimental area*. *PoS ICHEP2020*, p. 939.

Seminars

As a consequence of the outbreak of the COVID-19 pandemic, many events were cancelled and, apart those organised in January and February, very few could be held in presence. Therefore this list of seminars and talks is regrettably much smaller than what it was in previous years. Talks given remotely are marked as “on-line event”. A series of internal cross-talks was organised by Roberto Iuppa during the lockdown period in the first part of 2020. Roberto and all contributors are warmly acknowledged for their effort under such difficult circumstances.

TIFPA Guest Seminars

- Omar Tibolla, Polytechnic University of Pachuca, Pachuca de Soto, Mexico, *The origin of cosmic rays: the possible role of unidentified high energy sources*, Jan. 16, 2020.
- Shuang-Nan Zhang, Institute of High Energy Physics, Chinese Academy of Sciences, China, *Introduction to Space High Energy Astronomy Missions of China*, Jan. 31, 2020.
- Pedro José Pompeia, Aeronautics Institute of Technology, Sao José dos Campos, Brazil, *High order derivative theories: theoretical aspects and applications*, Feb. 5, 2020.

TIFPA Cross-talks

- Francesco Nozzoli, INFN-TIFPA, *Dark matter indirect search with Anti-Deuterons in space*, Apr. 29, 2020. (on-line event).
- Chiara La Tessa, University of Trento and INFN-TIFPA, *The magic of nuclear physics in particle therapy applications*, May 6, 2020. (on-line event).
- Sebastiano Mariuzzi, University of Trento and INFN-TIFPA, *Positronium production and laser excitation for antimatter experiments*, May 13, 2020. (on-line event).
- Pietro Faccioli, University of Trento and INFN-TIFPA, *Can Nuclear Theory help find an anti-viral drug for COVID 19*, May 20, 2020. (on-line event).
- Paolo Zuccon, University of Trento and INFN-TIFPA, *Dark Matter and Anti-Matter searches with AMS-02*, May 27, 2020. (on-line event).
- Irina Rashevskaya, INFN-TIFPA, *Electric characterisation and test of double sided silicon strip detector, silicon drift detector and silicon drift detector of large area*, June 3, 2020. (on-line event).
- William Burger, Centro Fermi and INFN-TIFPA, *Observation of Seismic Phenomena in Space*, June 10, 2020. (on-line event).
- Albino Perego, University of Trento and INFN-TIFPA, *Modelling of binary neutron star mergers in the multimessenger Astrophysics era*, June 17, 2020. (on-line event).
- Antonino Picciotto, FBK and INFN-TIFPA, *Advanced Target for Laser Driven Nuclear Fusion*, June 24, 2020. (on-line event).
- Roberto Battiston, University of Trento and INFN-TIFPA, *From nanosatellites to megacostellations*, July 1, 2020. (on-line event).
- Daniele Vetrugno, University of Trento and INFN-TIFPA, *LISA, the gravitational wave observatory from space*, July 8, 2020. (on-line event).
- Giacomo Borghi, FBK and INFN-TIFPA, *Low Gain Avalanche Diodes — A novel type of silicon detectors for 4-D tracking and x-ray detection*, July 22, 2020. (on-line event).
- Francesco Pederiva, University of Trento and INFN-TIFPA, *Optimal control based quantum computation of nuclear reactions*, July 29, 2020. (on-line event).

Astroparticle Physics

AMS

- Cinzia Cernetti, *Misura della frazione isotopica di ^{10}Be nei raggi cosmici*. At: 106^o Congresso Nazionale Società Italiana di Fisica, on-line event, Sept. 2020.
- Francesco Dimiccoli, *Measurements of the Deuteron flux and of the Deuteron to proton flux ratio in Cosmic Rays with AMS on the ISS*, At: ICHEP2020, on-line event, July 2020.
- Francesco Dimiccoli, *Measurements of the Deuteron flux and of the Deuteron to proton flux ratio in Cosmic Rays with AMS on the ISS*, At: COSPAR2020, on-line event, Jan. 2020.

LISA Pathfinder

- Eleonora Castelli, *Low frequency noise disturbances in LISA: discussion of experimental results from LISA PF*, At: XIII LISA Symposium, USA-online, Sept. 2020.
- Davide Dalbosco, *Torsion-pendulum testing of LISA charge management with a replica LPF GRS*, At: XIII LISA Symposium, USA-online, Sept. 2020.
- Edoardo Dalla Ricca, *Latest development in the analysis of the grabbing positioning and release mechanism performance*, At: XIII LISA Symposium, USA-online, Sept. 2020.
- Valerio Ferroni, *Limitations on LISA sensitivity to gravitational waves from local spacecraft gravitational field*, At: XIII LISA Symposium, USA-online, Sept. 2020.
- Lorenzo Sala, *Sub-pN force glitches on LISA Pathfinder as outgassing events: ongoing analysis and simulations*, At: XIII LISA Symposium, USA-online, Sept. 2020.
- Daniele Vetrugno, *Experimental challenges in unveiling the sub-mHz gravitational wave universe*, At: XIII LISA Symposium, USA-online, Sept. 2020.
- Davide Vignotto, *A challenging technological problem: the injection of the LISA Pathfinder TM*, At: 43rd COSPAR Scientific Assembly, Australia-online, Jan. 2020.
- Stefano Vitale, invited talk: *LISA Pathfinder ad LISA*, At: EAS2020. European Astronomical Society Annual Symposium, online, July 2020.

Nuclear Physics

- Benedetto Di Ruzza, *Proton and x-ray irradiation of silicon devices at the TIFPA-INFN facilities in Trento (Italy)*, At: ICHEP 2020, 40th International Conference on High Energy Physics, The International Union of Pure and Applied Physics (IUPAP), on-line event, July 2020.
- Benedetto Di Ruzza, *4DPhantom: An innovative device for oncological proton treatment uncertainties minimization*, At: SIF 2020, Annual National Congress of the Italian Physical Society, Italian Physical Society, on-line event, Sept. 2020.

Theoretical Physics

BIOPHYS

- Gianluca Lattanzi, invited talk: *Membrane Proteins: In & Out*, At: 6th Workshop on Physics of Biomolecules: Structure, Dynamics and Function, University of Padua, Bressanone, Italy, Feb. 2020.
- Raffaello Potestio, invited talk: *Simple, but not simpler - In search of the optimal level of coarse-graining*, At: 6th Workshop on Physics of Biomolecules: Structure, Dynamics and Function, University of Padua, Bressanone, Italy, Feb. 2020.
- Raffaello Potestio, invited talk: *On the algorithmic identification of optimal coarse-grained representations of biomolecules*, At: Biophysical Society Meeting, San Diego, California, USA, Feb. 2020.

Raffaello Potestio, invited talk: *Exploring the crossroad between information theory, statistical mechanics, and biology*, GSSI, l'Aquila, Italy, on-line event, June 2020.

MANYBODY

Alessandro Lovato, *An overview of nuclear quantum Monte Carlo*, At: Physics Seminar, Roma 3 University, Rome, Italy, Feb. 2020.

Alessandro Lovato, *Recent progress in nuclear Quantum Monte Carlo*, At: Physics Seminar, Colorado State University, Fort Collins, CO (remotely), United States, Mar. 2020.

Alessandro Lovato, invited talk: *Neutrino-Nucleus Scattering From Quantum Monte Carlo*, At: NUCLEI collaboration meeting, Argonne National Laboratory, Lemont, IL (remotely), United States, June 2020.

Alessandro Lovato, *An overview of nuclear Quantum Monte Carlo*, At: Cyclotron Institute Colloquium, Texas A&M, College Station, TX (remotely), United States, Sept. 2020.

Alessandro Lovato, *Progress in nuclear quantum Monte Carlo*, At: INT S@INT Seminar, Institute for Nuclear Theory, Seattle, WA (remotely), United States, Sept. 2020.

Alessandro Lovato, invited talk: *Neural network quantum states for atomic nuclei*, At: ECT* program â Advances in Many-Body Theories: from First Principle Methods to Quantum Computing and Machine Learning, Trento (remotely), Italy, Nov. 2020.

Alessandro Lovato, *Nuclear theory for neutrino scattering*, At: Review Talk, HEP Division, Argonne National Laboratory, Lemont, IL (remotely), United States, Nov. 2020.

Alessandro Lovato, *Recent progress in nuclear quantum Monte Carlo*, At: Physics Seminar, HEP Division, Argonne National Laboratory, College Park, MD, United States, Nov. 2020.

Alessandro Lovato, invited talk: *Nuclear structure with chiral forces*, At: Theoretical aspects of Hadron Spectroscopy and Phenomenology, University of Valencia, Valencia (remotely), Spain, Dec. 2020.

Francesco Pederiva, invited talk: *Accurate estimation of magnetic effects in neutron matter by Quantum Monte Carlo*, At: 5th Topical Workshop on Modern Aspects in Nuclear Structure, Bormio, Italy, Feb. 2020.

Francesco Pederiva, invited talk: *Optimal control based quantum computation of nuclear reactions*. At: NSCL/FRIB Summer Virtual Seminars (MSU, USA), East Lansing, MI (remotely), USA, May 2020.

TEONGRAV

Constantinos Constantinou, *Hot Equation of State: Astrophysical Applications*, At: ECT* Seminars, ECT*, on-line event, Nov. 2020.

Albino Perego, invited talk: *Modeling of Binary Neutron Star Mergers: from Simulations to Multimessenger Astrophysics*, At: Colloquium, APC Laboratory, Paris, France, Jan. 2020.

Albino Perego, *Compact binary mergers: linking the strong field dynamics to multimessenger observables*, At: GW Physics and Astrophysics: Genesis 2020 Symposium, Konan University, Kobe, Japan, Feb. 2020.

Albino Perego, *Compact Binary Mergers: New Opportunities for Nuclear and Fundamental Physics*, At: Nuclear Physics and Related Areas at Trento, ECT*, Trento, Italy, Feb. 2020.

Albino Perego, invited talk: *Modeling of Binary Neutron Star Mergers: from Strong Field Dynamics to Electromagnetic Counterparts*, At: Annual Meeting of the European Astronomical Society, Leiden University, The Netherlands, on-line event, July 2020.

Technological and Interdisciplinary Physics

ARCADIA

Lucio Pancheri, invited talk: *Timing detectors*, At: ALICE 3: First workshop on physics and detector, CERN, on-line event, Oct. 2020.

Outreach

Benedetto Di Ruzza, *Education initiatives in the experimental area of the Trento Proton Therapy Center (Italy)*, At: ICHEP 2020, 40th International Conference on High Energy Physics, The International Union of Pure and Applied Physics (IUPAP), on-line event, July 2020.



Trento Institute for
Fundamental Physics
and Applications

TIFPA - INFN

c/o Dipartimento di Fisica
Università di Trento
Via Sommarive, 14
38123 Povo (Trento), Italy
tel.: +39 0461 281500
fax: +39 0461 282000
email: info@tifpa.infn.it
www.tifpa.infn.it